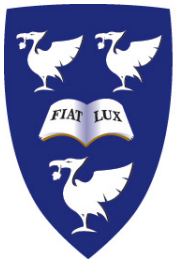

UNIVERSITY OF LIVERPOOL

Photoresponsive Gelators

Thesis submitted in accordance with the requirements of the University of Liverpool for the degree of Doctor in Philosophy by Emily Rose Draper

January 2016

ABSTRACT

We describe the synthesis of new low molecular weight gelators based on three different photoresponsive molecules functionalised with amino acids or dipeptides. Photoresponsive gels are interesting from the perspective of patterning. The gelation ability of the new gelators is explored using different methods two different methods of changing the pH. The photoresponse of these gels is investigated and the rheological properties measured to determine how the gel has changed.

A coumarin based dipeptide gel is formed electrochemically and by GdL. By using UV light, the dimer of the coumarin is formed in the gel and in solution, which is then investigated. Interestingly, this gel is an extremely rare example where the strength of the gel increases on irradiation. Most others examples become a solution when irradiated.

The gelation of a stilbene-based gelator is carried out using GdL. Upon UV irradiation, stilbene isomerises from *trans* to *cis*. This is examined in both the gel and the solution. The stilbene molecule is then used as part of a multi-component system to investigate self-assembly or co-assembly of different molecules upon gelation. This system allows us to prove that the second network is completely independent of the self-assembled stilbene network, which is the first time that this has been proven.

A series of gelators based on perylene bisimides are synthesised and the assembly of the gelators in solution and the gel are investigated. The two systems are dried down between two electrodes to monitor the change in electronic properties when irradiated with light. We have then aligned these materials to give better conductive properties. The perylene thin films are further examined with the properties of the films being measured in the presence of different hole scavengers. The perylene and stilbene gelators are then used in a multi-component gelator systems, and again the self-assembly or co-assembly is explored. The two-components are gelled in different ratios to each other and the conductive response under light again is investigated to see whether they could be used as a p-n heterojunction material. We show that the stilbene is able to act as a hole scavenger and affect the wavelength at which the photoconductivity is most effective. This provides evidence that we have managed to prepare two networks that are able to interact with one another, and hence are likely to effective as a bulk heterojunction.

ACKNOWLEDGEMENTS

Firstly, I would like to express my gratitude to The University of Liverpool for all of the opportunities offered to me over the last seven and bit years. My thanks also go to all the technical staff, analytical staff and workshop staff at the Department of Chemistry. Thank you also to the CMD for the use of their equipment and training.

I would like to thank my family who have always supported me in every decision I have made and have been more excited than me for every achievement and milestone I have reached. I am forever thankful for my Nan's Sunday roast and my family's amazing baking skills for keeping me going.

I thank my all my close friends in the department even though a lot of them have now moved on to bigger and better things. Thanks for all the Costa runs and Fancy Food Fridays. Their ridiculous conversations and Photoshop skills have kept me entertained and have made me enjoy coming into the department everyday.

My thanks go to the members of the Adams group past and present for all their help and support. I am especially thankful to Jaclyn and Lin who have guided and helped me throughout my PhD. I am very proud to call them my good friends. They have both made working in the group interesting and enjoyable and I miss them both very much. I would also like to thank Matthew and Ed for their help with the NMR experiments, especially Matthew for taking apart the NMR spectrometer for me.

I would like to thank Dr. Alex Cowan and Dr. James Walsh from the SIRE for their help with the conductivity measurements and photochemistry experiments, Dr. Tom McDonald for all the SEM imaging and Dr. Oleksandr Mykhaylyk from the University of Sheffield for the RheoOptics.

My final and biggest thanks go to my supervisor Prof. Dave Adams for giving me the opportunity to do this PhD. Thank you for seeing something in me that I could never see myself. With your help and guidance I have not only developed as a scientist but have become a more confident and happier person and for that I am forever grateful. I will never forget the all the amazing places I have got to visit for conferences and collaborations. The success I have had during my PhD has been down to you and I hope I have made you proud.

LIST OF PUBLICATIONS ARISING FROM THIS THESIS

"Air-stable Photoconductive Films formed from Perylene Bisimide Gelators", E. R. Draper, J. J. Walsh, T. O. McDonald, M. A. Zwijnenburg, P. J. Cameron, A. J. Cowan and D. J. Adams, *J. Mater. Chem. C*, 2014, **2**, 5570-5575.

"The Effect of Self-Sorting and Co-Assembly on the Mechanical Properties of Low Molecular Weight Hydrogels", C. Colquhoun, E. R. Draper, E. G. B. Eden, B. N. Cattoz, K. L. Morris, L. Chen, T. O. McDonald, A. E. Terry, P. C. Griffiths, L. C. Serpell and D. J. Adams, *Nanoscale*, 2014, **6**, 13719-13725.

"A Low Molecular Weight Hydrogel with Unusual Gel Aging", E. R. Draper, T. O. McDonald and D. J. Adams, *Chem. Commun*., 2015, **51**, 6595-6597.

"Probing Gelation Ability for a Library of Dipeptide Gelators", S. Awhida, E. R. Draper, T. O. McDonald and D. J. Adams, *J. Coll. Int. Sci*., 2015, **455**, 24-31.

"Hydrogels formed from Fmoc Amino Acids", E. R. Draper, K. L. Morris, M. A. Little, J. Raeburn, C. Colquhoun, E. R. Cross, T. O. McDonald, L. C. Serpell and D. J. Adams, *Cryst. Eng. Comm.*, 2015, **22**, 13719-13725.

"Photodimerisation of a Coumarin-Dipeptide Gelator", E. R. Draper, T. O. McDonald and D. J. Adams, *Chem. Comm*., 2015, **51**, 12827-12830.

"Spatially Resolved Multicomponent Gels", E. R. Draper, E. G. B. Eden, T. O. McDonald and D. J. Adams*, Nature Chem*., 2015, **7**, 848-852.

"Responsive Materials by the Self-assembly of Low Molecular Weight Gelators", E. R. Draper and D. J. Adams, Chapter 12, Chemoresponsive Materials: Stimulation by Chemical and Biological Signals, ed. H. -J. Schneider, RSC, 2015. Pp 332-363.

"Using the hydrolysis of anhydrides to control gel properties and homogeneity in pH-triggered gelation", E. R. Draper, L. L. E. Mears, A. M. Castilla, S. M. King, T. O. McDonald, R. Akhtar, D. J. Adams, *RSC Adv*., 2015, **5**, 95369-95378.

"Complex Shear Modulus of Hydrogels Using a Dynamic Nanoindentation Method", R. Akhtar, E. R. Draper, D. J. Adams, H. Pfaff, Mechanics of Biological Systems and Materials, Volume 6, 2016, Pp 141-145.

LIST OF ABBREVIATIONS

AFM	Atomic force microscopy
BHJ	Bulk heterojunction
CD	Circular dichroism
CV	Cyclic voltammetry
DCM	Dichloromethane
DMF	Dimethylformamide
DMSO	Dimethylsulphoxide
E_{ebe}	Energy of binding electron
FTIR	Fourier transform infrared
FTO	Fluorine doped tin oxide
G′	Storage modulus
G″	Loss modulus
GdL	Glucono-δ-lactone
HCl	Hydrochloric acid
HOMO	Highest occupied molecular orbital
ITO	Indium doped tin oxide
LED	Light emitting diode
LiOH	Lithium hydroxide
LMWG	Low molecular weight gelator
LUMO	Lowest unoccupied molecular orbital
NaOH	Sodium hydroxide
NDI	Naphthalene diimide
NIR	Neat infrared
NMR	Nuclear magnetic resonance
OFET	Organic field effect transistor
OLED	Organic light emitting diode
OPV	Organic photovoltaic
PBI	Perylene bisimide
PDI	Perylene diimide
PTCDA	Perylenetetracarboxylic dianhydride
pXRD	Powder X-ray diffraction
SANS	Small angle neutron scattering
SEM	Scanning electron microscopy
TAS	Transient absorption spectroscopy
TEM	Transmission electron microscopy
TFA	Trifluoroacetic acid
TGA	Thermogravmetric analysis
THF	Tetrahydrofuran
UV	Ultra violet

TABLE OF CONTENTS

Abstract i

Acknowledgements ii

List of Publications Arising from this Thesis iii

List of Abbreviations iv

Chapter 1 - Introduction 1

1. 1. Low Molecular Weight Gels 2

1. 2. Gelation Triggers 4

1. 2. 1. Change in pH 4

1. 2. 2. Solvent Switch 5

1. 2. 3. Temperature Switch 5

1. 2. 4. Use of an Enzyme 6

1. 2. 5. Addition of a Salt 6

1. 3. Photoresponsive Gelators 7

1. 3. 1. Photoisomerisable Gels 8

1. 3.1. 1. Azobenzenes 9

1. 3. 1. 2. Stilbenes 11

1. 3. 2. Photocleavable Gelators 12

1. 3. 2. 1. Dithienylethenes 12

1. 3. 2. 2. Spiropyrans and Spironaphthoxazines 15

1. 3. 2. 3. 2H-Chromene 17

1. 3. 3. Photodimerisation 18

1. 3. 3. 1. Coumarins 19

1. 3. 3. 2. Anthracenes 22

1. 3. 4. Photoconductivity 23

1. 3. 4. 1. PeryleneBisimides 24

1. 3. 4. 2. Napthalene Diimides 25

1. 4. Applications 26

1. 5. Rheology 29

1. 6. Introduction to Work in this Thesis 30

1. 7. References 31

Chapter 2 – Photodimerisation of a Coumarin-Based Dipeptide Gelator 37

2. 1. Introduction 38

2. 2. Results and Discussion 40

2. 3. Conclusions 57
2.4. Experimental 58
2. 4. 1. Synthetic Procedures 58
2. 4. 2. Instruments and Procedures 60
2. 5. References 64

Chapter 3 - Spatially Resolved Multi-Component Gels 65
3. 1. Introduction 67
3. 2. Results and Discussion 71
3. 3. Conclusions 88
3. 4. Experimental 89
3. 4. 1. Synthetic Procedures 89
3. 4. 2 Instruments and Procedures 94
3. 5. References 98

Chapter 4 – Photoconductive Perylene Bisimide Gelator 99
4. 1. Introduction 101
4. 2. Results and Discussion 103
4. 2. 1. Gel Properties 103
4. 2. 2. Photoconductivity Measurements 113
4. 2. 3. Aligned Thin Films 130
4. 3. Conclusions 150
4. 4. Experimental 151
4. 4. 1 Synthetic Procedures 151
4. 4. 2 Instruments and Procedures 153
4. 5. References 162

Chapter 5 – Self-Sorted Hydrogels Towards Bulk p-n Heterojunctions 165
5. 1. Introduction 167
5. 2. Results and Discussion 171
5. 2. 1. Using hole scavengers 171
5. 2. 2. Self-sorted p and n-type gelator systems 175
5. 2. 3. Photoresponse of multi-component system 182
5. 3. Conclusions 186
5. 4. Experimental 186
5. 5. References 190

Chapter 6 – Summary, Conclusions and Future Work 192

CHAPTER 1

Introduction

1. 1. Low Molecular Weight Gels

Hydrogels are a class of soft materials that have a wide range of applications.[1, 2] These include use in cosmetics,[3] medicine,[4] food[5] and electronics.[6] Gels consist of a dilute cross-linked network that consists mainly of liquid. Some examples are made up of up to 99.9 % water, however they still exhibit many properties of a solid. This composition gives the gels interesting physical properties. Most gels are formed from long fibres that are in a solution. These then entangle and cross-link, trapping the solution and forming a self-supporting gel matrix. When the solvent is an organic solvent these are called organogels. When the solvent is water, these gels are called hydrogels, which are the focus of this Thesis. The high water content of these materials leads to increased biocompatibility and, as a result, hydrogels can be used in biological applications such as drug delivery, therapeutics and cell culture.[7-11] Hydrogels can be made from high molecular weight polymers that occur naturally, such as pectin and collagen, and also from synthetic polymers.[12, 13] In the latter case, the polymer fibres are cross-linked irreversibly *via* covalent bonds. This makes gelation irreversible and results in stiff gels as bonds are less easily broken by force or other stimuli (Fig. 1.1a).[12, 14-16] Another class of non-polymeric hydrogels is formed by low molecular weight gelators (LMWG), which are molecules that are typically less than 1000 Daltons.[1, 2] These LMWG self-assemble through non-covalent interactions such as hydrogen bonding, π-π stacking and ion pairing to form fibres, which entangle (Fig. 1.1b).[17]

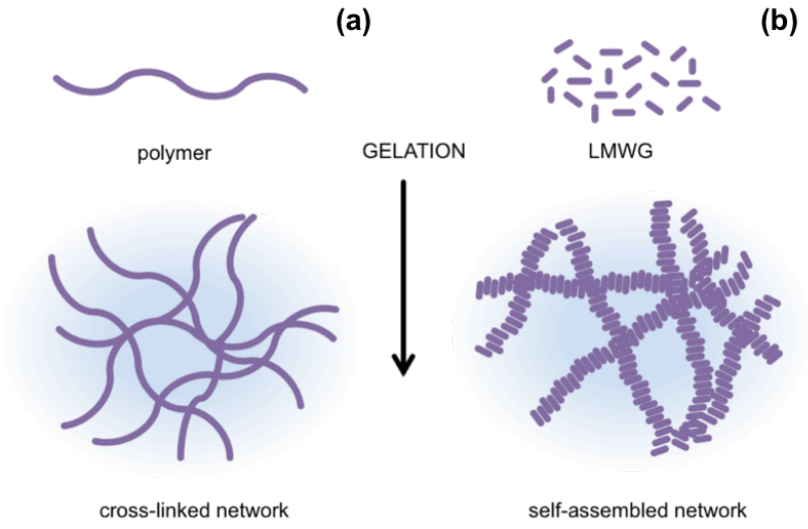

Figure 1.1 Gelation using (a) polymers and (b) low molecular weight gelators.

LMWGs can be peptides, quaternary ammonium salts, functionalized sugars, metallic soaps and aliphatic hydrocarbons.[1, 10, 18, 19] These gelators can have a wide variety of structures, and so can have many functions. To form hydrogels, typically the LMWG are initially dissolved or suspended in water (Fig. 1.2a). These molecules then self-assemble in water when a suitable trigger is applied, which results in the LMWG becoming significantly less soluble. As the molecules become less soluble, they assemble into long fibres in order to minimize their interactions with the surrounding water (Fig. 1.2b). These fibres then interact further with each other by cross-linking and entanglement resulting in the gel network (Fig. 1.2c). This self-assembly of fibres is still poorly understood, but the use of circular dichroism and X-ray scattering gives us some insight into the fibre structure,[20, 21] while rheology can be used to gain some information about the entanglement of the network.[22, 23]

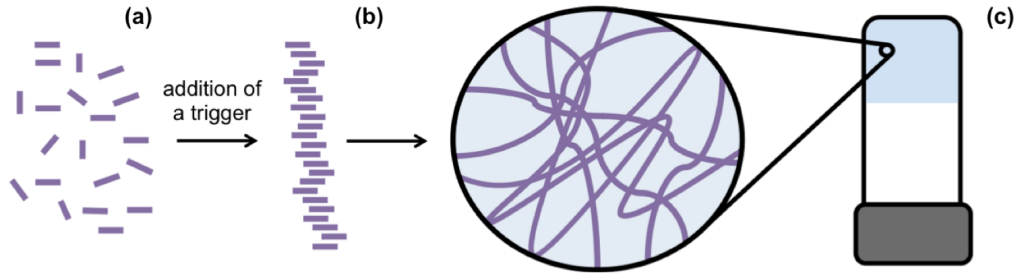

Figure 1.2 Scheme showing self-assembly of LMWG into a self-supporting hydrogel. (a) Molecules are freely dissolved in solution until a gelation trigger is applied. (b) Molecules start to assemble into 1D structures to minimise their interaction with the solution and (c) further assembly occurs forming long fibres that entangle and trap water forming a self-supporting 3D matrix of fibres.

An advantage of gels formed from LMWG compared to cross-linked polymeric hydrogelators is that gelation can be reversible. This is owing to the gel structure being held together by non-covalent interactions. This reversibility is important when thinking about applications of the gels such as the controlled release of guest molecules or as use in sensors in logic gates.[24, 25] The weak covalent forces holding fibres together can also allow the gels to quickly recover back to their original strength upon breaking. This so-called thixotropic behaviour means that the gels are

often suitable for injection or other processing allowing them to be processed for the use in devices.[26]

1. 2. Gelation Triggers

As mentioned previously, the LMWGs discussed in this Thesis require a trigger in order to self-assemble. There are several potential triggers that have been described such as a solvent switch,[27] pH change,[28] temperature change,[29] shear force,[30] addition of a salt[31] and addition of enzymes.[32] All of these methods work by making the LMWG less soluble and so inducing self-assembly. The method used is critically important as it controls the bulk properties of the gel. Even within one type of trigger there are different methods and rates at which they occur, gain leading to different bulk properties of the gel.[33-35] Due to rate of gelation being an important factor in the gel properties, it is important to find a reproducible method of gelation to insure that each gel made has the same properties and therefore will function the same. This is especially important when using the gels in applications. The way in which gelation is triggered often leads to the gels being unsuitable for an application. For example, organogels cannot be used for cell culturing.[36]

1. 2. 1. Change in pH

A pH trigger can be used when the gelator molecule has a functional group that can be deprotonated and protonated, for example carboxylic acids or amines. In the case of carboxylic acids, the LMWG can be freely dissolved in water above the pK_a. However, when acid is added and the pH is adjusted to below the pK_a, the carboxylate is re-protonated, decreasing the solubility of the LMWG and inducing self-assembly leading to gelation.[37-39] In the case of an amine, when the pH is raised above the pK_a of the LMWG, deprotonation of the amine reduces the solubility, again resulting in self-assembly of the molecules. There are different ways that the pH can be lowered giving different rheological properties.[35, 40] A mineral acid such as hydrochloric acid (HCl) can be directly added to a high pH solution of gelator to quickly lower pH. This often leads to irreproducible gels due to the solution gelling very quickly at the top of the solution and the acid having to then diffuse through the gel to lower the pH of the rest of the solution.[41] Other ways of lowering pH exploit

the hydrolysis of sugars or anhydrides, which results in an acid being formed (this is discussed in more detail in Chapter 3). This often happens more slowly and allows the acid to be dispersed uniformly throughout the solution and a more uniform drop in pH occurs.[41, 42] This slow hydrolysis gives more reproducible and homogeneous gels, but of course depends on the solubility and rate of hydrolysis of the anhydride or sugar.

The drop in pH can be spatially controlled by using electrochemical methods or by using a photoacid. Hydroquinone can be easily oxidised to quinone[43] which releases a proton by applying a current.[44-46] This results in a drop in pH at the surface of an electrode and so gelation will occur on a surface rather than in the bulk (this is described in more detail in Chapter 2). This method of gelation also gives reproducible gels when formed using the same conditions. The use of a photoacid allows a drop in pH only where the sample has been irradiated with a light source.[43] By using a mask this gives spatial control over gelation. This method does not give reproducible gels due to diffusion of the light through the samples and other variables.

1. 2. 2. Solvent Switch

A common assembly method is a solvent switch approach. This is where molecules are first dissolved in an organic solvent, followed by the rapid addition of a miscible anti-solvent, again reducing solubility and inducing self-assembly.[34, 47-49] Gelation usually occurs in a few minutes and so is quicker than using the slower pH switch method. This method of gelation if a useful method of forming hydrogel from molecules that are not soluble in water, as they can be first added to an organic solvent and water can be added as the anti-solvent. The final gel properties are determined by the ratio of the two solvents used as well as the concentration of the gelator.[47]

1. 2. 3. Temperature Switch

Change in temperature is also a common method of gelation. This method relies on the gelator being soluble in a solvent (or solvent mixture) at higher temperatures but

not when the temperature is lowered. This change in solubility at the colder temperature drives the self-assembly.[29] Rheological properties of gels formed using this gelation trigger depend on how quickly the temperature is lowered and again on the solvents used and concentration of the gelator.[50]

1. 2. 4. Use of an Enzyme

Enzymes work in two ways, by making or breaking bonds. Enzymatic triggers for LMWG work by synthesizing the gelator *in situ*, either by cleaving a solubilizing group from a precursor molecule or by forming the LMWG *via* reaction between two soluble precursors (Fig. 1.3).[51-53] Enzymatic triggers are useful as they are highly specific and can be used in biological systems.[54] They can be used in both intracellular and extracellular environments and in complex fluids such as blood.[55] Other conditions need to be considered when using enzymes as triggers, such as pH and temperature. The enzyme's normal function can be slowed or the enzyme even denatured if not in a suitable environment.

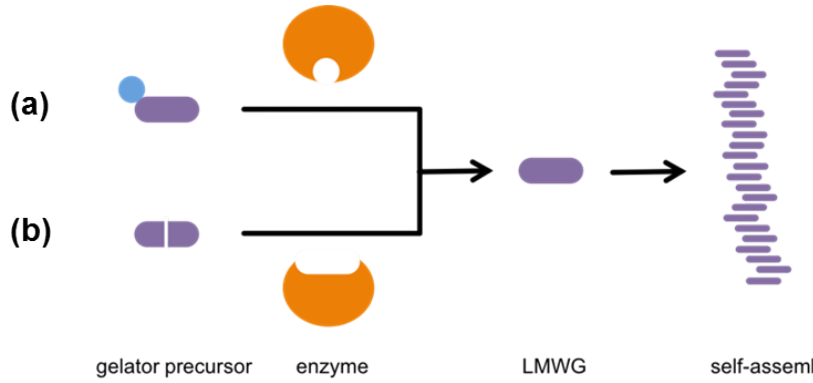

Figure 1.3 Schematic showing enzymatic self-assembly by (a) bond breaking and (b) bond making.

1. 2. 5. Addition of a Salt

Metal-ion triggers for gelation such as calcium and zinc ions work by enhancing ionic strength of interactions between fibres. Metal-ions can bind to specific groups on gelator molecules and encourage self-assembly.[56-58] This type of gelation can only occur when there are worm-like micelles present in solution. For example, Ca^{2+} gelation works by bridging fibres together through acid groups *via* positively charged metal-ions. Ca^{2+} binds together the negatively charged carboxylic acid groups on

neighbouring worm like micelles (Fig. 1.4).[31, 50, 59] This cross-linking assembles the fibrous network and traps the solvent forming the gel. Metal ion triggered gels are advantageous as they are able to form in biological pH and can be tuned using temperature and strengthened by use of salts.

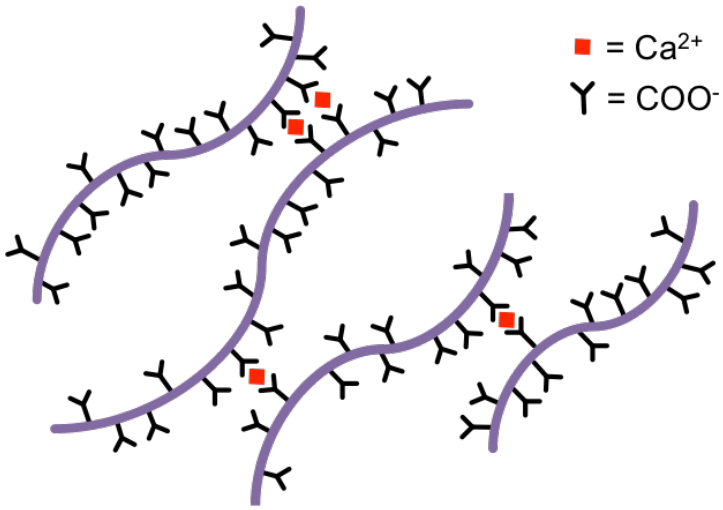

Figure 1.4 Gelation by the use of Ca^{2+} ions.

For this Thesis, a pH switch will be used throughout as the gelation trigger. This is due to the pH triggers being more reproducible and versatile than the other methods.[41] This means that the gels will have to be hydrogels. Hydrogels are more biocompatible, less likely to dry out as the solvent is not volatile and can be used for many applications.[12] There are fewer examples of low molecular weight hydrogels than organogels and so more research needs to be done on these types of materials

1. 3. Photoresponsive Gelators

Gels can be responsive to external stimuli.[36, 60, 61] This can be used to alter the material after gelation has happened.[16] Gels can respond to temperature,[62] mechanical stress,[30] light,[63] chemical stimulus,[64] enzymes,[65] pH[61] *etc*. Responses include a change in colour, gel-sol transitions, gel-to-gel transitions, isomerisation, dimer formation, morphology, change in electronic properties to name a few.[66] This makes gels ideal for the use in applications such as sensors, logic gates, organic electronics and organic photovoltaic devices.[1] Post-modification of gels allows tuning of gel properties. The use of light to modify gels is of particular interest due to

the possibility to target a specific area of the gel leading to patterned gel surfaces.[67, 68] This is useful for such applications as microfluidics, cell culture and differentiation and electronic materials such as p-n heterojunctions.[69] The use of light to alter the gel is clean and controllable way of modifying the gel as when the light source is switched off the reaction causing the change stops. This means the change can be spatially located, unlike for most other stimuli such as chemical or temperature.

Photoresponsive gelators usually contain a chromophore, which is the photoresponsive group, attached to other groups that aid with gelation.[70] Chromophores are conjugated system that absorbs light. The conjugated systems can also aid self-assembly by π-π stacking and forming 1D fibres. The chromophores collect light of a specific wavelength and covert it leading to a photoreaction.[71] These photoreactions include isomerisation, dimerization, bond formation, bond cleavage and exciton formation depending on the chromophore present.[36, 72] The diversity in reactions allows for different applications.

1. 3. 1. Photoisomerisable Gels

Photoisomerisation is the changing of a *cis* isomer to a *trans* isomer or *vice versa* (Fig. 1.5).[73, 74] The *trans* isomers of the molecule often is the gelator and whereas the *cis* isomer is the non-gelator. The *cis* isomer does not form gels due to change in polarisation and the lack of preferential stacking of the molecules in solution. This isomerisation leads to a gel-sol transition.[75] This type of response is useful for removing part of the gel to create a patterned surface.[76] This could be especially useful when using a multicomponent system so that the integrity of the gel remains but one gelator is removed from a specific area leading to different properties on specific part of the gel. Gel-sol transitions or sol-gel transitions can also be used in sensors such as logic gates.[77, 78]

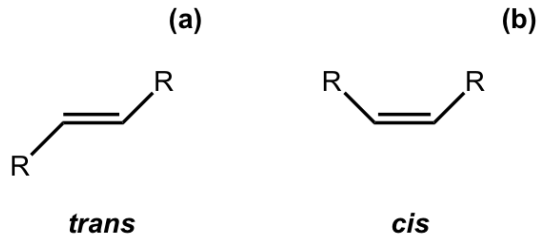

Figure 1.5 Two isomers of the same molecule (a) the *trans* isomer and (b) the *cis* isomer.

1. 3. 1. 1. Azobenzenes

Azobenzene-based gelator molecules have been extensively studied.[63, 73, 75, 79-81] Azobenzene consists of two benzene rings connected by a diazo group (Fig. 1.6). The benzene rings can then functionalised to make a range of different gelators with different properties. The diazo group allows the *cis* to *trans* transitions and the benzene rings aid with self-assembly.

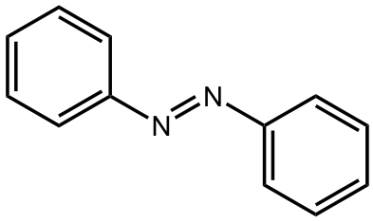

Figure 1.6 Molecular structure of *trans*-azobenzene

Zhang and co-workers developed short peptide functionalised azobenzene gelator molecules. [81] They investigated varying the peptide sequence and the length of the peptide chain. They concluded that if the molecule contained a phenylalanine or tyrosine moiety it would more likely gel, whereas arginine and other cationic functionalities did not promote gelation. The gelator molecules were dissolved in water and the pH was adjusted a heat cool method was then used as the gelation trigger. The use of buffers was used to see if salts affected gelation, which a few did. Different salt concentrations and peptide sequences gave gels with different gel strengths. A UV light was used to irradiate the gels and changed the yellow gels to a yellow liquid due to the *cis* isomer being a non-gelator. This was found to be reversible with the use of visible light. The different strength gels had different sensitivities to the UV light. They used this gel-sol transition to look at a method of controlled release of vitamin B12. This method allowed all the vitamin B12 to be

released within 5 hours, as opposed to only 30 % of the vitamin being released by the non-irradiated gel.

Moriyama *et al.* mixed a discotic liquid crystal (Fig. 1.7a **1**) with a hydrogen-bonded photoresponsive gelator based on two azobenzenes (Fig. 1.7a **2**) to give a liquid crystalline gel.[82] The mixed gel system was heated to 160 °C and then cooled to a different temperature. Two things happened as a result of this change in temperature: gelation of molecule **2** occurred and the liquid crystal phase of **1** also formed. When the system was cooled under UV light the *cis*-**2** was formed along with liquid crystals. The *trans*-**2** was then formed when the system was heated allowing gelation to occur after liquid crystal formation. This could be used to give two different processes, where gelation either happens first then liquid crystal formation or where the liquid crystals are formed first and gelation happens second. The use of the the photoresponisve gelator allows two different templated materials to be made from the same molecules. The also managed to photopattern this system using a mask and irradiating the sample. They found where the sample was irradiated there were aligned liquid domains whereas were the mask covered there was no alignment (Fig. 1.7b). The alignment was fixed by the aggregates of **2**. This alignment of liquid crystals could be of use in organic electronic materials as aligned liquid cystals have been shown to have enhanced hole mobility.[83]

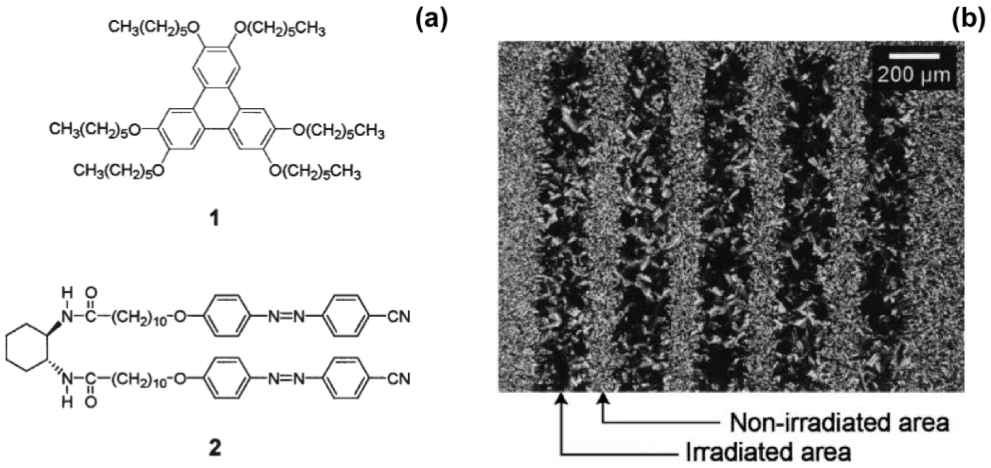

Figure 1.7 (a) Molecular structures of **1** and **2** (b) Optical polarized light microscope image of a patterned sample of **1**,**2** at 65 °C prepared by cooling under UV light using a photomask. Adapted from ref [82] Huang *et al.*

A problem when using azobenzene gelators is the reversibility of the *trans* to *cis* isomerisation. The samples do not go completely *trans* or *cis* and so normally there is a mixture of the two isomers in the gel or in the solution, leading to irreproducible results.[66, 84] The research into these materials often claim they will undergo a *cis* to *trans* transition with the use a visible light, although many groups also heat and sonicate the solutions before doing this, meaning that they are actually just reformed the gel through heat. This implies that it is not a truly reversible photoresponse.[85]

1. 3. 1. 2. Stilbenes

Stilbenes are similar in structure to azobenzenes as seen above; they differ by having a C=C instead of a N=N bond (Fig. 1.8). They act similarly to the azobenzene, with the *trans* to *cis* isomerisation occurring upon irradiation with UV light. Again, these have been extensively studied in the literature.[71, 86, 87] The *cis*-stilbene is less thermally stable than the *trans*-stilbene and so in the dark the *cis*-isomer will convert to the *trans*-isomer. The wavelength needed for the *trans* to *cis* isomeriation is shorter than for azobenzene, and the *cis*-stilbene is more stable than *cis*-azobenzene.[74] This reversibility and stability makes them ideal for sensing applications.

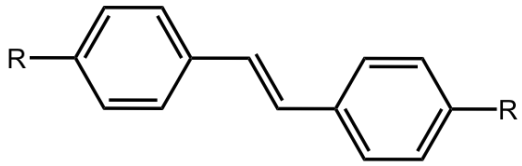

Figure 1.8 Molecular structure of *trans*-stilbene.

Heenan and co-workers made organogels based on a stilbene with a gemini photo-surfactant (Fig. 1.9a).[84] They refluxed the gelator in toluene and 0.4 % *N,N'*-dimethylaminedodecylamine. The solution was then cooled to room temperature to form the organogel. This method of gelation gave reproducible gels, even when changing the amount of gelator in solution and the amount of *N,N'*-dimethylaminedodecylamine. These gels were opaque when formed (Fig. 1.9b). Upon irradiation with a mercury lamp, the gels changed to a clear solution (Fig. 1.9c). ^{1}H NMR showed that the isomerisation went 100 % to the non-gelling *cis*-isomer. They then used mask and selectively de-gelled parts of the gel (Fig. 1.9d). This selective removal could be used to create patterned surfaces.

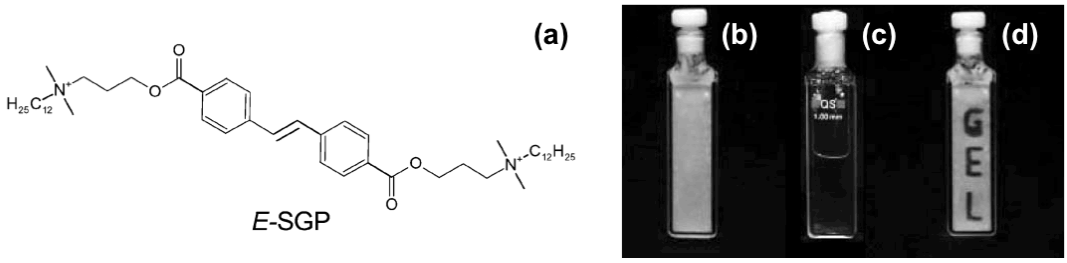

Figure 1.9 (a) Molecular structure of stilbene gemini surfactant gelator. Photographs of (a) the organogel (b) after irradiation (c) selective removal of part of the gel. Adapted from ref [84] Eastoe *et al*.

Miljanić *et al.* looked at the gelation ability of an oxamide-based gelator bearing a stilbene functional group. They varied the substituents on the stilbene and investigated the gelation abilities. They made a series of symmetric and asymmetric gelators, with some bearing two oxamide groups and some bearing one oxamide and one long alkyl chain. They tried all the molecules in a variety of solvents and reported whether they were soluble, formed gels or precipitates. The molecule containing the long alkyl chains were more likely to gel, but not all the molecules with the alkyl chains formed gels. This shows that the substituents is important, but there does not seem to be any design rules for what makes a gelator, which is has been seen by many research groups.[88] They then investigated whether the corresponding *cis*-molecules still gelled. Most of the *cis*-iomers did not gel, but one of the *cis*-molecules that was functionalized with an oxalamide and an alkyl chain gelled in toluene and tetralin. This is very unusual, as normally the *cis*-isomer does not gel, but for this particular molecule both isomers gel when using the same solvent. Stilbenes can be functionalized with many different groups to give gels that can be used in different applications.[66] Although there is a lot of literature on these systems, there are very few examples of these molecules forming hydrogels. This is most likely due to them being less soluble than azobenzenes in water.

1. 3. 2. Photocleavable Gelators

Instead of isomerisation, another photoreaction can be the making or breaking of bonds. In photoresponsive gelators, this is most likely a ring opening or ring closing reaction.[89, 90] This ring opening or ring closing can have several responses; these include a change in colour,[91] change in electronic properties[92] and gel-sol

transitions.[93] This response to light makes them ideal for applications such as sensors, optical switches and displays.[66] Molecules that can undergo ring opening reactions under UV light are often referred to as the 'open' molecule and 'closed' molecule depending on whether the ring is open or not.

1. 3. 2. 1. Dithienylethenes

Dithienylethenes are a type of molecule which have two thienyl group attached *via* cyclopentene. The cyclopentene and thienyl groups can be functionalised to give a range of different molecules with different functions.[94, 95] The open form of the molecule can be converted to the closed form with the use of UV light. This is reversible, with the open molecule being formed on irradiation with visible light (Fig. 1.10). When the molecule is closed, this restricts rotation around the cyclopentene and the thienyl groups are conjugated, giving very different electronic properties and flexibility to the open form.[96] This change in conjugation and electronic properties gives interesting responses from the molecules, often leading to a change in colour.[97] Furthermore, this reversible photoresponse can be carried out hundreds of times without loss of efficiency.[94] Photochromic response to light and efficiency of this reaction makes these molecules useful for devices such as photo switches.[97]

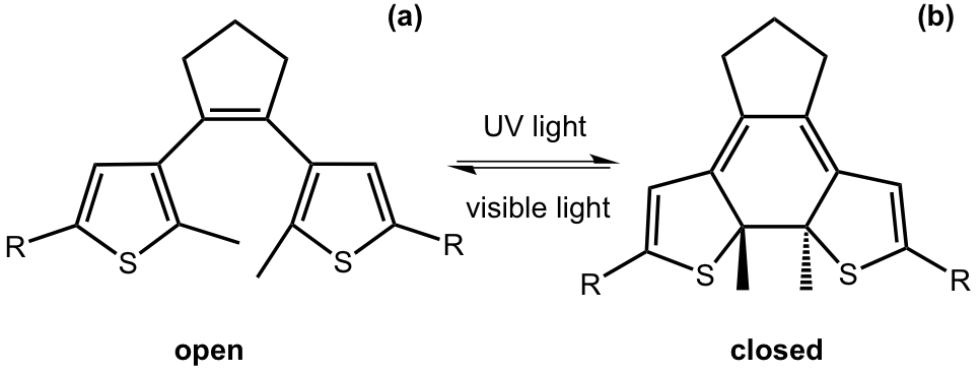

Figure 1.10 Molecular structure of dithienylethene in (a) the open form and (b) the closed form.

Feringa and co-workers functionalised a ring open dithienylethene with various dipeptides on the 3-position of the cyclopentene.[76] This changed the polarity of the molecule and allowed it to be soluble in water. Therefore, it was able to be used in a hydrogel. By changing the amino acids in the dipeptide, the polarity of the molecules could be tuned. They found if the dipeptide contained a phenylalanine group, it

would not be soluble due its hydrophobicity. The gelator molecules were dissolved at different concentrations in a phosphate buffer, or in water with the pH adjusted. The solution were heated and sonicated to give a clear solution and, when cooled, formed weak gels which were frequency dependent. They also tried a solvent switch by dissolving the molecules in DMSO and then adding water. Only some of the molecules could gel this way, but gave inhomogeneous hydrogels that were not suitable for analysis. The lysine-glycine functionalised ring-open dithienylethene was then irradiated with 312 nm to form the ring-closed dithienylethene. This resulted in a change in colour of the gel from yellow to red, without a change in the rheological properties of the gel. This ring closing was reversible when using visible light >500 nm and the gel returned to the original yellow colour. This change in colour arises due to the molecule being more conjugated and so has a change in the highest occupied molecular orbital (HOMO)/lowest unoccupied molecular orbital (LUMO) gap. They were also able to selectively change the colour by using a photo mask. These molecules are promising for the use as a photo switch, owing to it maintaining its gel structure.

A naphthalimide and cholesterol-appended dithienylethene was synthesised by functionalising both the thienyl groups by Wang *et al*.[98] This gave extra fluorescent properties to the molecule due to the naphthalimde group and the cholesterol group aiding with gelation. Again, when gelled, there was a photochromic response with the gel changing from a yellow to a red colour when irradiated with UV light (Fig. 1.11a and b). Unlike the example above, the authors showed that this molecule also responded to heat, fluoride ions and protons in both the open and closed form of the molecule. Both the open and closed form of the gel went through a gel-sol transition when heated. They showed that there was also a photochromic response when the molecule was in solution, again showing a yellow to red transition when irradiated with UV light (Fig. 1.11c and d). In the presence of fluoride ions, the open yellow solution changes to an orange colour due to the fluoride ion deprotonating the amide group giving a negative charge on the nitrogen and promoting a internal charge transfer and the change in colour, this was reversible upon the addition of protons (Fig. 1.11c and e). This orange solution also responds to the UV light and then orange colour deepens to a dark orange colour (Fig. 1.11e and f). This multi-responsive system would be ideal for the use in sensors and logic gates.

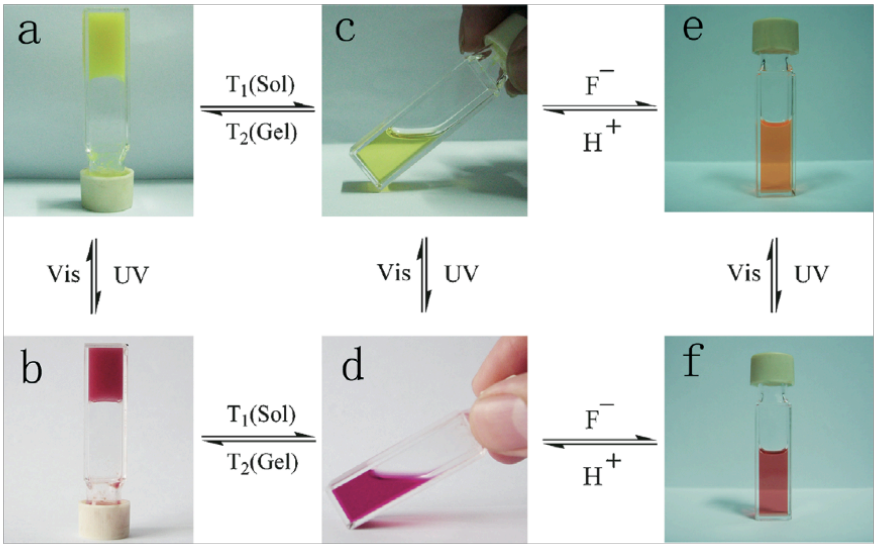

Figure 11.1 Colour change and state change upon different stimuli for a naphthalimide and cholesterol appended dithienylethene gelator. Figure taken from ref [98] Tian and co-workers.

Dithienylethene gels are very interesting materials due to them being able to maintain their rheological properties but still responding to visible and UV light. They show little fatigue after multiple cycles of ring opening/closing. The ability to be responsive to multiple stimuli also makes it possible for these materials to be used for many different applications.

1. 3. 2. 2. Spiropyrans and Spironaphthoxazines

Another photoresponsive gelator molecule that undergoes cleavage is spiropyrans. These molecules have a reversible photochemical cleavage of their C-O bond in the spiro unit.[99] These are very closely related to spironaphthoxazines, which also have the same photochemical cleavage of the C-O bond.[100, 101] Under visible light or heat, there is a cyclisation and the C-O bond is formed, this is referred to as the closed form (Fig. 1.12b) and is the most stable form. This can then be ring opened using UV light and is referred to as the open form (Fig, 1.12a). The open form is normally more soluble and the ring is closed. The consequence of the ring closure is a sol-gel transition as the closed form is planar, less flexible and has unfavourable π-stacking. This differs from the photoisomerisable gelators where there is gel-sol transition under UV light rather than a sol-gel transition as for this group of gelators. There are

many examples of spiropyran incorporated into polymers systems, but few for low molecular weight gelators.

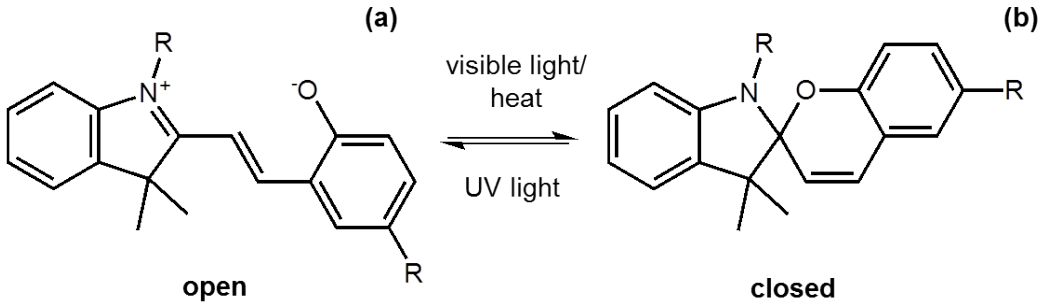

Figure 1.12 Molecular structure of a spiropyran molecule (a) in the open form and (b) the closed form.

Zhang and co-workers functionalised a spiropyran with dipeptide containing to alanine amino acids.[93] The dipeptide promotes self-assembly with H-bonding and Van der Waals interactions. The open form of the molecule was dissolved at neutral pH and formed a dark red gel when the pH was lowered to 3 using HCl (Fig. 1.13a). The closed form was unable to form a gel this way and remained as a yellow liquid. The gels formed from the open form needed to be kept away from visible light, as they became unstable. This sensitivity to visible light is not ideal for the use in applications. The gel could be irradiated with wavelengths of light >400 nm to form a yellow gelatinous precipitate (Fig. 1.13b), and the pH had to be altered to get a solution, meaning this is not truly photoreversible. The yellow solution could then be irradiated with UV light to get a red gelatinous precipitate; again, the pH had to adjusted to form a gel. They also added vancomycin to the gel, which resulted in a gel-sol transition. This change in state is due to the ligand specific vancomycin binding to the dipeptide and increasing the solubility. Hence, this spiropyran molecule shows a multiple responses to pH, light and vancomycin.

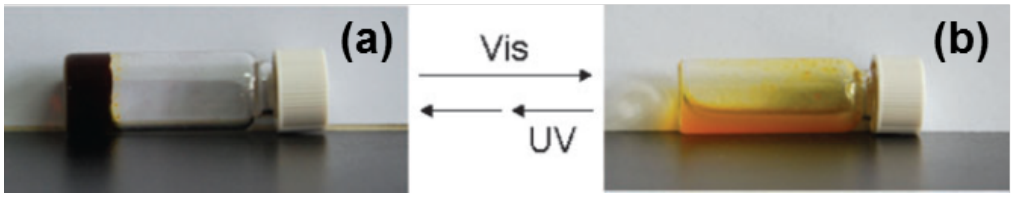

Figure 1. 13 Photographs of (a) open spiropyran gel and (b) closed spiropyran solution open irradiated with different light sources. Adapted from ref [93] Qui *et al*.

A gelator molecule based on spironaphthoxazines was prepared by Li *et al*.[102] It was functionalised with gallic acid, aiding with gelation by providing more intermolecular forces between π-π stacked molecules. This also allowed the molecule to be sensitive to pH. Gelation was carried out is different organic solvents and a heat-cool method was used initiate gelation. Samples were heated to 50 °C until all the gelator was dissolved and the samples were cooled to room temperature. Closed forms of the spironaphthoxazines gave a colourless gel. When irradiated with UV light they became blue in colour, which could be monitored by UV-Vis absorption spectroscopy. This was due to an increased conjugation through the molecule due to the ring opening. The change in colour did not last long, due to the open form being thermally unstable. When dissolved in ethanol, these molecules were responsive to the addition of *p*-toluenesulfonic acid, which changed the sample from colourless to purple. These samples could be gelled using the heat-cool method to form purple gels. Spiropyrans and spironaphthoxazines are excellent candidates for the use in sensing applications due to their multi-responsive behaviour.[100] They would also be used in optical devices due to the ability to tune the colour by changing the molecule. The biggest problem is the thermal and visible light instability.

1. 3. 2. 3. *2H*-Chromene

2H-Chromenes go through a photocleavage of a C-O bond upon the irradiation with UV light and ring opening the molecule (Fig. 1.14). This ring-opening is reversible upon heating due to the ring-closed molecule being more thermally stable than ring-opened molecule.[89, 91, 103]

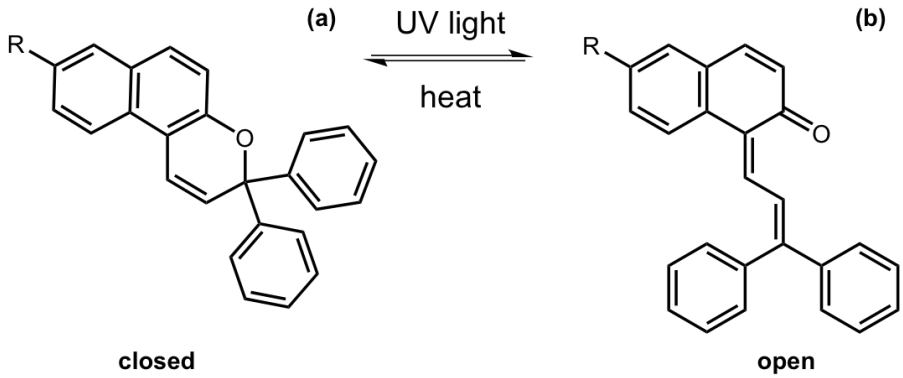

Figure 1.14 Molecular structure change of *2H*-chromene from (a) closed to (b) open.

This ring-closure occurs through an electrocyclisation. These two forms of the molecule are again referred to as the open and the closed form. The closed form is usually colourless and the ring-closed form is coloured. This change in colour makes these molecules of interest due the resistance to fatigue over multiple cycles.[66] Despite this photochromic behaviour, there are only a few examples of these molecules being used as gelators.

A series of 2*H*-chromene *N*-acylamino acid conjugates were reported by both Shanab and Pozzo.[89, 91] Both dissolved the ring open molecules in an organic solvent and heated whilst stirring until the solution was clear; they then cooled the solution to 25 °C using ice to give a colourless gel. The different molecules showed different gelation abilities and solubility in different solvents. Molecules with a longer chain length of the acylamino group were more likely to gel. They also found that if the molecule contained a dipeptide rather than a single amino acid group then it was able to gel in some solvents at low temperature and at room temperature gave a gelatinous precipitate. The molecules that did gel were irradiated with 366 nm light. This caused a colour change of the gel to yellow, due to the formation of the ring open *2H*-chromene. When irradiation was stopped, then the gel quickly converted back to the colourless state due to the instability of the closed form. The gel was disrupted by this irradiation; this was probably due to the closed form of the molecule not being a gelator and so breaking the gel structure and therefore did not fully go into solution due to insufficient penetration depth of the UV light into the bulk sample. The authors did note that they were able to reform the gel upon heating and cooling again. This group of molecules also showed sensitivity to the presence of sodium ions as the protonated amino acid of the open form of the molecule did not gel, but the sodium salts did. This shows that the there is a delicate balance of molecular interactions needed for gelation to occur.

1. 3. 3. Photodimerisation

Photodimerisations is when two of the same molecules that are close enough or in the right position with respect to each other form covalent bonds between them when irradiated with light to form a dimer.[104, 105] This normally happens in conjugated molecules.[106] In solution, this can be very difficult due to the molecules being able to

freely move around and so are less likely to be in the right position for this photodimerisation to occur. However, in the gelled state the molecules are very close to each other due to π-π stacking of the molecules, making it more likely that the molecules are close enough to each other for dimerisation to occur. Dimerisation of the gelator molecule often leads to the molecules being less soluble due to the molecule doubling in size and so becoming more hydrophobic. This decrease in solubility can lead to destruction of the gel or a decrease in the rheological properties due to the gel network being disruption of the gel network.[107] This gel – sol transition or change in gel properties makes them good candidates for use in sensing applications.[66]

1. 3. 3. 1. Coumarins

Coumarins are class of molecules based on a dye molecule that is often found in plants. They have been studied for their photoresponsive behaviour in materials and for biological applications.[36] Dimerisation of the coumarin molecule occurs upon irradiation with light >300 nm (Fig. 1.15).

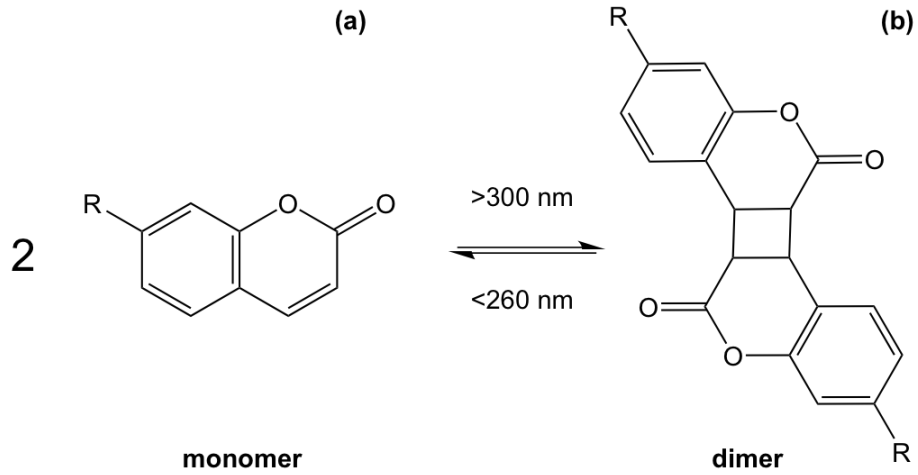

Figure 1.15 The reversible photodimerisation of a coumarin from (a) the monomer to (b) the dimer.

Dimersisation is where two coumarin molecules (or monomers) form covalent bonds between them to form a new molecule called the dimer.[104] This dimerisation of coumarins is reversible when light with a wavelength of <260 nm is used. The [2+2] photodimerisation of coumarins is known to occur both in solution and in the solid

state,[108-110] often to give a mixture of *syn-syn*, *syn-anti*, *anti-syn* and *anti-anti* cyclobutanes depending on how the molecules are orientated to each other.[111] Coumarin can then be functionalised to give different gelation properties.[112, 113 110]

Parquette and co-workers designed a coumarin dipeptide hydrogelator containing two coumarin groups connected by a dipeptide.[113] The two coumarin groups allowed each gelator to react with two other gelator molecules to increase the amount of cross-linking upon irradiation. Gels were prepared in water, saline or buffer and left for 24 hours before any rheology tests were done on the system. They saw that the buffer increased the amount of bundling of the fibres due to salt-induced electrostatic screening due to lysine side chains on the gelator. Photoisomerisation with 365 nm light was explored. The hydrogel not exposed to UV light was stable for up to 3 weeks. However, upon irradiation with 365 nm light, a dark yellow precipitate was formed. After 7 days under the UV light, this precipitate became insoluble in water due to the gelators becoming cross-linked. The precipitate could be then collected by centrifugation. This cross-linked precipitate was soluble in trifluoroethanol and could be analysed. Analysis revealed the presence of uniform nanofibres (Fig. 1.16) around 15 nm in diameter. Rheology and microscopy revealed that two different dimerisations were occurring within the system, there were intra-fibre dimerisation within the fibres and inter-fibre dimerisation of coumarin molecules. This cross-linking stiffened the fibres and so could be used for post-modification of the hydrogel surfaces for applications such as surface patterning.

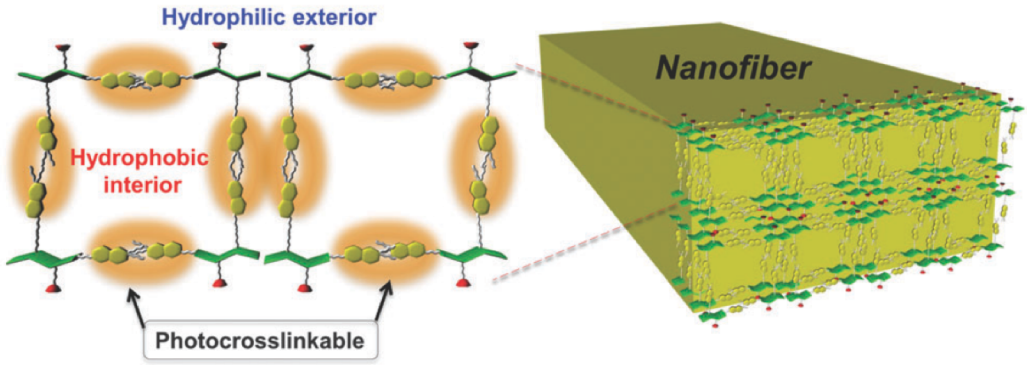

Figure 1.16 Diagram showing the possible cross-linking within a fibre due to coumarin dimerisation of the dipepetide functionalised hydrogelator. Figure taken from ref [113] Parquette *et al*.

Organogels based on coumarin molecules were made by Yu *et al*.[114] They investigated the gelation properties of the coumarin molecules with different length alkyl chains in a variety of solvents. A heat-cool method was used to test whether gelation could occur. They then looked at how the different solvents, and different length alkyl chain affected the morphology of the fibres formed. They observed different morphologies such as helical ribbons and spheres depending on which solvents were used, showing that the solvent used is critical to gel properties. A gel formed in cyclohexane was chosen to be studied under irradiation with >300 nm and >280 nm light. Upon irradiation with 300 nm light, the gel structure was maintained and the dimerisation was monitored by UV-Vis absorption spectroscopy, as was the reverse reaction with 280 nm. Scanning electron microscopy (SEM) revealed that morphology of the fibres changed from helical fibres to lumps upon irradiation with >300 nm and then changed to a sponge like morphology when irradiated with <280 nm. Throughout irradiation, the gel maintained its structure whilst the morphologies drastically changed.

1. 3. 3. 2. Anthracenes

Anthracene is a molecule made of three fused benzene rings. Anthracenes undergo a reversible photodimerisation under UV light.[115, 116] They undergo a [4 + 4] cycloaddition reaction when irradiated with >300 nm light and the reverse reaction when irradiated with light of <300 nm or with heat (Fig. 1.17a).

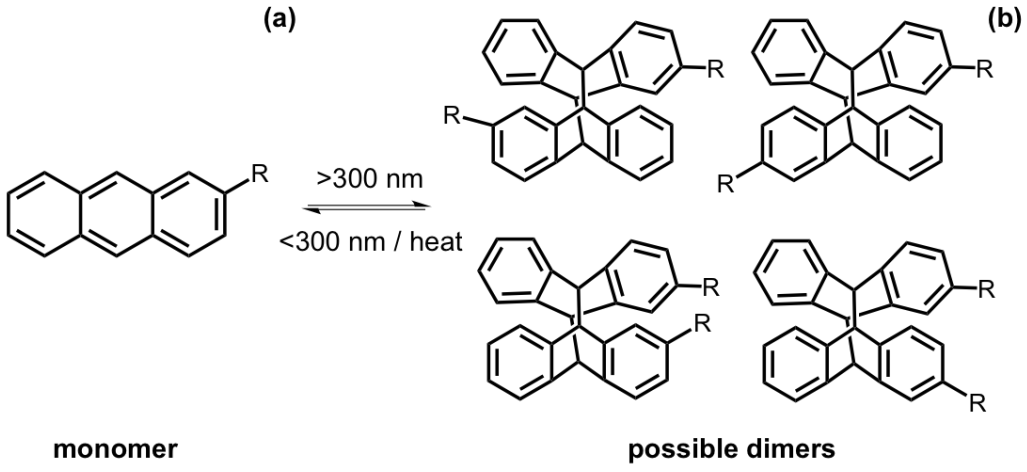

Figure 1.17 Dimerisation using >300 nm of anthracene from the (a) monomer to (b) the dimer.

[117, 118] It has been found that this reaction is affected by the presence of oxygen.[119] Like coumarin, there are different isomers of dianthracene that can be formed due to the position of the anthracenes with respect to each other when the cylcoaddition occurs. These are the *anti* head to tail, *syn* head to tail, *anti* head to head and *syn* head to head stereodimers (Fig. 1.17b). The photodimerisation of anthracene gels often leads to a gel-sol transition due to the dimer disrupting the gel network.[120, 121] There are many examples of these used for organogels, but very few for hydrogel systems.

An anthracene modified with urea was investigated as a gelator in organic solvents.[122] Several solvents were tested but the molecule was only able to gel using dichloroethane. A heat-cool method was used to form an opaque gel. This method was reversible with several heat-cool cycles (Fig, 1.18). Upon gelation, there was a ten times increase in fluorescence as compared to the solution and so this could have potential use as a thermal sensor. When irradiated with >300 nm light, the gel remained stable and, by NMR spectroscopy, it was seen that little dimer was formed. This could be due to the molecules not being the right orientation to each other. Photodimerisation of the urea-modified anthracene molecule in solution was monitored by ^{1}H NMR spectroscopy and UV-Vis absorption spectroscopy. From ^{1}H NMR spectroscopy, the change from a monomer to dimer resulted in a head to tail dimerisation. The dimer was able to form a transparent gel in cyclohexane, *n*-hexane, and *n*-heptane and shows greater gelation ability than the monomer. In addition, these dimers we stable to heat and <300 nm light and only a small portion of the gel changed to solution.

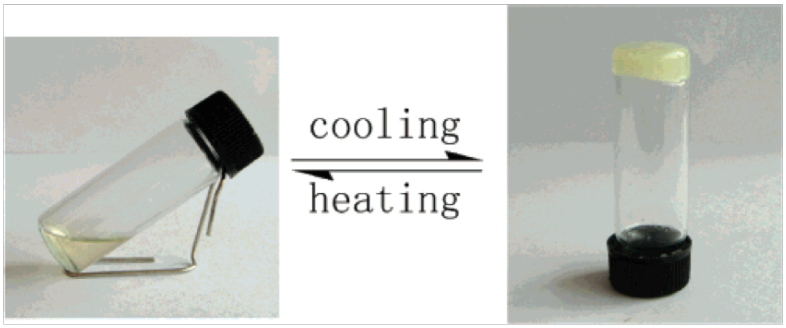

Figure 1.18 Gelation of urea functionalised anthracene molecule in dichloroethane using a heat-cool method. Adapted from ref [122] Wang *et al.*

Dawn *et al.* also investigated anthracene as organogelators.[123] They used 2-anthracenecarboxylic acid to control the stereochemical formation of exclusively the head to head dimer. Gelation was achieved by the noncovalent attachment with a gelator component containing the gallic acid backbone coupled with $_D$-alanine. This was chosen as it should enhance gelation through H-bonding and π-π stacking; it would also allow the anthracene to be close enough to allow dimerisation to occur. The incorporation of the chiral $_D$-alanine could also induce enantioselectivity in the anthracene photoproducts *via* perturbation of the pre- orientation in the ground state. Cyclohexane was chosen as it had a low critical gelation concentration and was thermally reversible. The lower concentration of gelator allowed more efficient photodimerisation. When irradiated with 366 nm light, there was a gel-sol transition and from high-pressure liquid chromatography, it was shown only the head to head isomer was present. They also investigated this process at a higher temperature were they found the head to head in excess. In the solid state no isomerisation occurred and in tetrahydrofuran the head to tail isomer was formed. This system shows stereochemical control in a supramolecular assembly created by organogel systems.

1. 3. 4. Photoconductivity

Semi-conductor molecules can exhibit photoconductive behaviour upon the irradiation with UV, visible or infrared light.[124] This increase in free electrons and holes increases the electrical conductivity of the semi-conductor.[125] The light must have the right energy to promote an electron from the HOMO to the LUMO. This HOMO-LUMO gap is also referred to as the band gap and the electron is promoted from a valance band to the conductance band. This promotion of an electron creates free holes and electrons. The increase of free electrons and holes increases the electrical conductivity of the semi-conductor. This change electrical conductivity due to the absorption of light is called photoconductivity. Photoconductivity is dependent on the concentration of holes and electrons and their mobility. Materials that have photoconductive properties can be used in application such as organic solar cells (OPVs), organic light emitting diodes (OLEDs), photoresistors and organic field-effect transistors (OFETs) as n-type materials.[66, 126]

1. 3. 4. 1. Perylene Bisimides

Perylene bisimides (PBIs), also referred to as perylene diimides (PDI), are based on perylenetetracarboxylic dianhydrides which are polycyclic aromatic hydrocarbons (Fig. 1.19).[126] They come from the rylene family of dyes. These molecules are commonly used a dyes and pigments and can be functionalised to give a range of coloured materials.[127] They are useful as they have a high stability, high quantum yields and intense light absorption.[128] They also exhibit photoconductive behaviour due to the formation of a radical anion upon irradiation, and with further irradiation can even form the dianion.[129] The anion and dianion are stabilised by the aromatic core of the molecule. The HOMO-LUMO gap can be tuned by substituting in the bay area and so can tune the light energy needed for photoconductivity but also the amount of light it emits.[130] PBIs exhibit π-π stacking that allows electrons to pass through the stacked molecules easily. This stacking also allows them to be used as gelators.[131] Gelation of these molecules has been used to drive the self-assembly of these molecules and so enhance the photoconductive properties of the materials.[132] A problem with these molecules is low solubility, making them more difficult to work with. These molecules often show different absorption spectra in different solvents and at different concentration.[133]

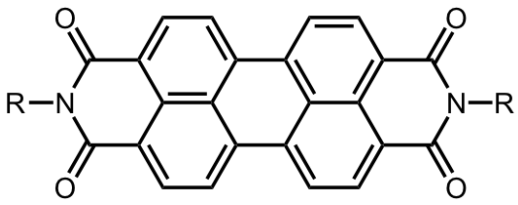

Figure 1.19 Molecular structure of perylene bisimides.

An amino acid functionalised PBI was prepared by Banerjee and co-workers.[132] As the PBI molecule was functionalised with $_{L}$-tyrosine, this allowed the molecule to be water soluble at pH 9 due to the carboxylic acid of the amino acid. The PBI gelator was then dissolved in different buffers from pH 9 to pH 5, and then heated to 80 °C and cooled to room temperature to form a gel (Fig. 1.20a). It was found that the minimum gelation concentration was higher at pH 9 than for pH 5, showing it was pH dependent. They reported the gels were frequency independent with a storage modulus (G′) of 6 x10^2 Pa and loss storage (G″) of 24 Pa. They then took the gel and dried it in between two gold electrodes to allow them to measure the conductivity

properties of the xerogels. The tyrosine-functionalised PBI showed photoconductivity under white and visible light (Fig. 1.20b). The sample also showed good photo-switching behaviour, as the current increased as soon as the light source was switched on and then decreased when the light was switched off again. Although there are many examples of self-assembled PBIs in the literature, there are fewer examples of these as hydrogelators[134] and even fewer looking at the photoconductivity of these materials.

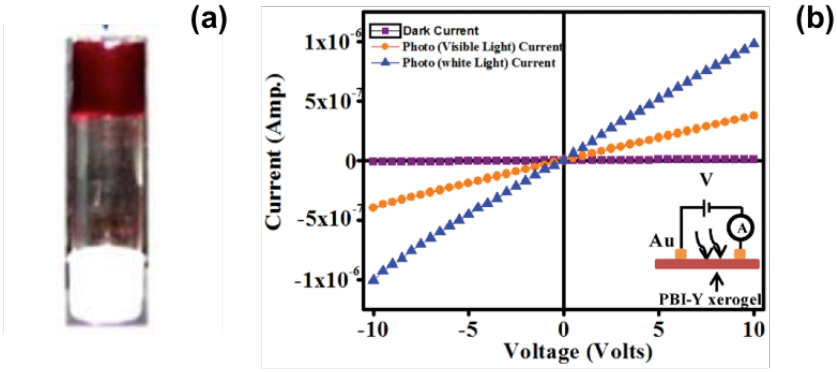

Figure 1.20 (a) Photograph of tyrosine-functionalised PBI gel (b) Photoresponse under visible light (yellow data), white light (blue data) and in the dark (purple data) of the xerogels. Adapted from ref [132] Banerjee and co-workers.

1. 3. 4. 2. Naphthalene Diimides

Naphthalene diimides (NDIs) are based on naphthalenes and are prepared by the oxidation of pyrene (Fig. 1.21).[135] They also belong to the rylene dyes. These materials are similar to PBIs but less conjugated, smaller quantum yields and are more soluble.[136] They show a photoresponse with light and are able to form a radical anion upon irradiation due to an electron being accepted into the conjugated core. NDIs are also able to gel to π-π stacking of their conjugated core.[137-139]

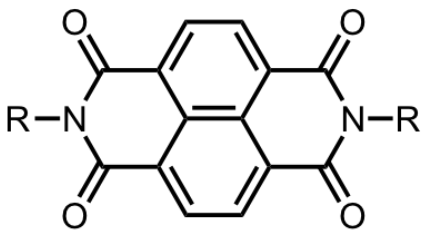

Figure 1.21 Molecular structure of naphthalene diimide.

They are fluorescent and the fluorescence can be tuned by the substituents on the naphthalene rings.[140] These materials have also shown photochromic responses upon the irradiation with light as well as being photoconductive.[141] NDIs have been used in charge transfer complexes with crown ethers due to its electron accepting properties.[142] Zheng *et al.* used NDIs to make near-infrared electrochromic and chiroptical switching materials.[141] They used an NDI that was functionalised with two sugar groups. It was able to form gels *via* the heat-cool method in *n*-butanol with J-aggregates of the fibres determined by circular dichroism (CD) and UV-Vis absorption spectroscopy. Cyclic voltammetry (CV) was performed on the system to show that the gel could undergo a two-electron reduction, when light was used to create the anion. The gel was dried to form a thin film, which was also able to undergo a two-electron reduction. Upon radical anion formation, the film appeared light brown and showed new peaks in the infrared region unlike in solutions. The dianion film appeared purple and showed peaks at 406 nm and others at 537 and 579 nm. This electrochromic behaviour makes them useful for optical switches. Again, there are few examples of naphthalene diimides used in hydrogels and not much literature on the photoresponse of the NDI hydrogels.

1. 4. Applications

Photoresponsive gelators can have a variety of applications. In biomedical applications, they are a particularly interesting option to advance drug delivery systems and tissue engineering.[1, 36, 66, 143] Gels have been made that can be used for drug release upon irradiation by using gelators that undergo a gel-sol transition.[15, 74] For example, when using an isomerisible group like azobenzene, Kros and co-worker showed controllable release of proteins from the gel.[144] Another way photoresponsive gels have been used is to 3D photopattern gels using a coumarin moiety.[145] The photoresponsive unit was used to spatially resolve the gel network to be used as a cell culture medium.[143, 146] Different strength gels can be used to support the cells growth and be used for cell differentiation, which is essential for regenerative medicine.[147] For biomedical application, only hydrogels can be used for biocompatibility reasons.

Multi-responsive gelators have use in sensors such as logic gates.[25, 77, 78, 148] Song's group has constructed LMWGs that can be used to make supramolecular logic gates that respond to multiple stimuli.[149] Logic gates are devices that use one or more inputs (in this case stimuli) to produce a single response.[150] These can be used for intelligent soft materials to perform functions in response to various stimuli, and so could be used in sensors, drug delivery and organic electronics.[151, 152] The LMWG were based on sorbitol and naphthalene-based salicylideneanilines. These gels were found to respond to copper by a reversible sol-to-gel transition with a colour change from yellow to colourless. The gels also showed a response to UV light, anions and temperature, again resulting in a gel-sol transition. The photoresponse resulted from an isomerisation upon irradiation that destroyed the gel state. When returned to visible light, a gel re-formed. The response from anions comes from the deprotonation of the phenolic group leading to dissolution of the gel. Again, this is reversible upon re-protonation. From these responses, an OR logical gate was constructed where only one of the stimuli is needed to cause a response. The presence of the stimulus was represented as 1 and if not present 0. This showed that one or more of these stimuli caused a response in which the gel dissolved which is represented by 1.

Organic materials for the use in electronic applications are a popular area of research owing to them being cheaper alternatives to crystalline silicon currently used. They also can be more versatile due to the variety in structures and functionalities.[152] Gels are a promising material for this due to the self-assembly of the molecules as well as their electronic and photonic properties.[126] Gels also offer the opportunity to process the materials into thin films. Applications include OPVs and OFETs.[153] Most organic electronic devices use p-n heterojunctions, which contain two materials (a p-type and n-type); where these materials meet is the heterojunction. n- and p-type materials are defined by the nature of their primary charge carriers. The p-type material can donate an electron to the n-type material and become positively charged and so contain the holes. The n-type material then becomes negatively charged and carries the electrons. The use of photoresponsive gelators have been used in these materials, as they have a good absorption spectra and so can absorb light and convert it into an electrical response in the p-n heterojunction.[66] The molecules can be tailored so they can absorb different wavelengths of light. The gelators are π-π stacked so electrons

and holes can travel these gel fibres like a wire where they can be collected at the electrodes.[154] Gels can also be used to give a well-defined heterojunctions that has been a problem in some bulk heterojunctions. This problem could be avoided by using a self-sorted multi-component gelator system.[155,156] By using a photoresponsive multi-component systems where one gelator can go through gel-sol transition, one gelator could be selectively removed again giving a well-defined p-n heterojunction. There are many examples of polymers systems being used in for these applications but not as many examples of LMWGs being used.[157]

OPVs are a type of solar cell and so use light to produce electricity.[126] Unlike traditional solar cells these use organic based materials rather than crystalline silicon, which is expensive. Using organic materials also allows better processing therefore cells can be thinner and can be used over a large area.[158, 159] Perylene bisimides have been used in OPV devices as a n-type material as they can accept an electron, have good spatial HOMO/LUMO overlap and a high quantum yield.[153, 160, 161] Many groups have used self-assembled perylene bisimide in OPVs combined with a p-type material such as oligophenylvinylenes, oligothiophenes and stilbenes.[156, 162-164] There are not many examples of these being used in multi-component gelator systems. OFETs are transistors that use an electric field to control the electrical conductivity of a channel of one type of charge carrier in a semiconductor material.[165] They are used as components in flexible circuits, sensors electric papers and active matrix displays. Self-assembling molecules have been used in these materials to reduce cost due them being to be processed at room temperature rather than expensive vacuum sublimation and vapor deposition techniques.[166] Photoresponsive LMWGs such as NDIs, PBIs and dithienylethenes could be used in OFETs for sensors as they become more conductive when a certain wavelength of light is used.[167] There are already several examples of organogels being used in OFETs.[167, 168]

Gels that show photochromism can be used in applications such as optical switches due to their change in colour when a light stimulus is used.[169] Optical switches are made form a photoemitter (e.g. LED) and a photodetector (e.g. photodiode) mounted in a component so that the photoemitter illuminates the photodetector, but an opaque object can be inserted in a slot between them so as to break the beam. A change in the beam would give an electrical response.[170, 171] These systems are used in printers

and computer mice. Gelators such as *2H*-chromene, dithienylethenes, NDIs and PBIs can all be functionalised to give different colours.[1, 172] The reversible photoresponsive behaviour means that they could be used in used for these applications. Overall, photoresponsive gels show great potential for the use in a wide range of applications. This is due to their absorption properties, possibility of post-modification and HOMO/LUMO overlap. The use of LMWGs allows a variety of responses due to the many different molecules that can be used to make them. These gelator molecules can be further tuned by functionalising them making them very versatile molecules. The use of light to get a response from a system is preferable due to the speed of response, the different wavelengths giving different responses and the ability to spatially resolve this response in the material.

1. 5. Rheology

Rheology is used as the main characterisation tool in this Thesis. Gels are initially characterised by a vial inversion test, known as table top rheology. If the material does not flow upon inversion, then it can be then be further analysed using a rheometer.[1] Two different tests are then performed on the gel, a strain sweep and a frequency sweep. Both tests measure the storage modulus, how solid like the material is (G′) and the loss storage, how liquid like the material is (G″). When G′ is approximately and order of magnitude larger than G″, and the G′/G″ value (defined as tanδ) is less than 0.1 the material is a true gel.[2, 88] The strain tests then measures how much strain is needed to break the gel, and so can be used to determine how strong the gel is. The strain percentage at which the gel breaks is defined as where G′ deviates from linearality. Complete breakdown of the gel is where G″ has become larger than G′, and the sample is now more liquid-like than solid-like. Frequency tests can then be used see how the gels react under increasing frequency and so can be used to determine how stiff the gel is. The larger G′ and G″ are the stiffer the gel, as it has a more solid like properties. It should be noted that rheological properties of different gels can only be compared if the gels have been measured using the same measuring system, and prepared in the same ways. This makes interpreting the literature difficult. It can be seen that polymer gels generally have a larger G′ and G″

than LMWG, but each have a wide overlapping reported values for G′ and G″ and types of gels cannot be defined by their G′ and G″.[33]

1. 6. Introduction to Work in this Thesis

The overall aim of this Thesis was to synthesis new LMWGs which respond to light in different ways. The new gelators are each based on different chromophores functionalised with amino acids or dipeptides. The different chromosphores leads to the materials responding in different ways. The gels are then formed by a change in pH by using GdL of electrochemistry. The change in the gels upon irradiation with light was then analysed by rheology and UV-Vis absorption spectroscopy. This irradiation was done to either strengthen, pattern or change the electronic properties of the gels with the use of UV light. Further work was carried out looking at mixed gelator systems containing one or more photoresponsive units. The use of GdL leads to self-sorting of the gel fibres giving a well-defined system. These self-sorted materials are then measured for their photoconductive properties under different wavelength of light. The ultimate aim for these self-sorted gelator systems are for the use in p-n heterojunctions.

1. 7. References

1. M. de Loos, B. L. Feringa and J. H. van Esch, *Eur. J. Org. Chem.*, 2005, **2005**, 3615-3631.
2. P. Terech and R. G. Weiss, *Chem. Rev.*, 1997, **97**, 3133-3160.
3. V. Jenning, A. Gysler, M. Schäfer-Korting and S. H. Gohla, *Eur. J. Pharm. Biopharm.*, 2000, **49**, 211-218.
4. B. Xu, *Langmuir*, 2009, **25**, 8375-8377.
5. W. Pilnik and F. M. Rombouts, *Carbohyd. Res.*, 1985, **142**, 93-105.
6. D. Wall Brian and D. Tovar John, *Pure Appl. Chem.*, 2012, **84**, 1039.
7. K. J. Skilling, F. Citossi, T. D. Bradshaw, M. Ashford, B. Kellam and M. Marlow, *Soft Matter*, 2014, **10**, 237-256.
8. S. Maude, E. Ingham and A. Aggeli, *Nanomedicine*, 2013, **8**, 823-847.
9. N. Stephanopoulos, J. H. Ortony and S. I. Stupp, *Acta Mater.*, 2013, **61**, 912-930.
10. G. Fichman and E. Gazit, *Acta Biomater.*, 2014, **10**, 1671-1682.
11. R. Tian, J. Chen and R. Niu, *Nanoscale*, 2014, **6**, 3474-3482.

12. S. J. Buwalda, K. W. M. Boere, P. J. Dijkstra, J. Feijen, T. Vermonden and W. E. Hennink, *J. Control. Release*, 2014, **190**, 254-273.
13. V. Javvaji, A. G. Baradwaj, G. F. Payne and S. R. Raghavan, *Langmuir*, 2011, **27**, 12591-12596.
14. J. Jagur-Grodzinski, *Polymer Adv. Tech.*, 2010, **21**, 27-47.
15. V. B. R. Prashant P. Kalshetti, Deepashree N. Dixit, Pranav P. Parekh, *Int. J. Pharm. Pharm. Sci.*, 2012, **4**, 1-7.
16. B. Guo and P. Ma, *Sci. China Chem.*, 2014, **57**, 490-500.
17. S. Zhang, *Nat. Biotech.*, 2003, **21**, 1171-1178.
18. H. Cui, A. G. Cheetham, E. T. Pashuck and S. I. Stupp, *J. Am. Chem. Soc.*, 2014, **136**, 12461-12468.
19. L. A. Estroff and A. D. Hamilton, *Chem. Rev.*, 2004, **104**, 1201-1218.
20. Y.-H. Chen, J. T. Yang and K. H. Chau, *Biochemistry*, 1974, **13**, 3350-3359.
21. L. A. Estroff, L. Leiserowitz, L. Addadi, S. Weiner and A. D. Hamilton, *Adv. Mater.*, 2003, **15**, 38-42.
22. C. Yan and D. J. Pochan, *Chem. Soc. Rev.*, 2010, **39**, 3528-3540.
23. C. Chassenieux and L. Bouteiller, *Supramolecular Chemistry*, John Wiley & Sons, Ltd, 2012.
24. J. A. Foster and J. W. Steed, *Angew. Chem. Int. Ed.*, 2010, **49**, 6718-6724.
25. K. Fan, J. Yang, X. Wang and J. Song, *Soft Matter*, 2014, **10**, 8370-8375.
26. H. Wang and Z. Yang, *Nanoscale*, 2012, **4**, 5259-5267.
27. A. Mahler, M. Reches, M. Rechter, S. Cohen and E. Gazit, *Adv. Mater.*, 2006, **18**, 1365-1370.
28. C. Tang, R. Ulijn and A. Saiani, *Eur. Phys. J. E*, 2013, **36**, 1-11.
29. R. Vegners, I. Shestakova, I. Kalvinsh, R. M. Ezzell and P. A. Janmey, *J. Pept. Sci.*, 1995, **1**, 371-378.
30. Z. Xie, A. Zhang, L. Ye, X. Wang and Z.-g. Feng, *J. Mater. Chem.*, 2009, **19**, 6100-6102.
31. L. Chen, G. Pont, K. Morris, G. Lotze, A. Squires, L. C. Serpell and D. J. Adams, *Chem. Commun.*, 2011, **47**, 12071-12073.
32. Y. Gao, Z. Yang, Y. Kuang, M.-L. Ma, J. Li, F. Zhao and B. Xu, *Pept. Sci.*, 2010, **94**, 19-31.
33. J. Raeburn, A. Zamith Cardoso and D. J. Adams, *Chem. Soc. Rev.*, 2013, **42**, 5143-5156.
34. J. Raeburn, G. Pont, L. Chen, Y. Cesbron, R. Levy and D. J. Adams, *Soft Matter*, 2012, **8**, 1168-1174.
35. E. R. Draper, L. L. E. Mears, A. M. Castilla, S. M. King, T. O. McDonald, R. Akhtar and D. J. Adams, *RSC Adv.*, 2015, **5**, 95369-95378.
36. I. Tomatsu, K. Peng and A. Kros, *Adv. Drug Deliv. Rev.*, 2011, **63**, 1257-1266.
37. D. J. Adams, L. M. Mullen, M. Berta, L. Chen and W. J. Frith, *Soft Matter*, 2010, **6**, 1971-1980.
38. L. Chen, K. Morris, A. Laybourn, D. Elias, M. R. Hicks, A. Rodger, L. Serpell and D. J. Adams, *Langmuir*, 2009, **26**, 5232-5242.
39. Z. Yang, G. Liang, M. Ma, Y. Gao and B. Xu, *J. Mater. Chem.*, 2007, **17**, 850-854.

40. J. Nanda, A. Biswas and A. Banerjee, *Soft Matter*, 2013, **9**, 4198-4208.
41. D. J. Adams, M. F. Butler, W. J. Frith, M. Kirkland, L. Mullen and P. Sanderson, *Soft Matter*, 2009, **5**, 1856-1862.
42. E. Draper, l. Mears, A. M. Castilla, S. M. King, T. O. McDonald, R. Akhtar and D. J. Adams, *RSC Adv.*, 2015, 2015, **5**, 95369-95378.
43. J. Raeburn, T. O. McDonald and D. J. Adams, *Chem. Commun.*, 2012, **48**, 9355-9357.
44. J. Raeburn, B. Alston, J. Kroeger, T. O. McDonald, J. R. Howse, P. J. Cameron and D. J. Adams, *Mater. Horiz.*, 2014, **1**, 241-246.
45. E. K. Johnson, L. Chen, P. S. Kubiak, S. F. McDonald, D. J. Adams and P. J. Cameron, *Chem. Commun.*, 2013, **49**, 8698-8700.
46. K. L. Morris, L. Chen, J. Raeburn, O. R. Sellick, P. Cotanda, A. Paul, P. C. Griffiths, S. M. King, R. K. O'Reilly, L. C. Serpell and D. J. Adams, *Nat. Commun.*, 2013, **4**, 1480.
47. L. Chen, J. Raeburn, S. Sutton, D. G. Spiller, J. Williams, J. S. Sharp, P. C. Griffiths, R. K. Heenan, S. M. King, A. Paul, S. Furzeland, D. Atkins and D. J. Adams, *Soft Matter*, 2011, **7**, 9721-9727.
48. X. Wang and M. Liu, *Chem. Eur. J.,* 2014, **20**, 10110-10116.
49. P. A. Korevaar, C. J. Newcomb, E. W. Meijer and S. I. Stupp, *J. Am. Chem. Soc.* 2014, **136**, 8540-8543.
50. Q. F. Dang, J. Q. Yan, J. J. Li, X. J. Cheng, C. S. Liu and X. G. Chen, *Carbohydr. Polym.*, 2011, **83**, 171-178.
51. M. J. Webber, C. J. Newcomb, R. Bitton and S. I. Stupp, *Soft Matter*, 2011, **7**, 9665-9672.
52. Z. Yang, H. Gu, D. Fu, P. Gao, J. K. Lam and B. Xu, *Adv. Mater.*, 2004, **16**, 1440-1444.
53. H. Liu, Z. Lv, K. Ding, X. Liu, L. Yuan, H. Chen and X. Li, *J. Mater. Chem. B*, 2013, **1**, 5550-5556.
54. Z. Yang, G. Liang and B. Xu, *Acc. Chem. Res.*, 2008, **41**, 315-326.
55. S. C. Bremmer, J. Chen, A. J. McNeil and M. B. Soellner, *Chem. Commun.*, 2012, **48**, 5482-5484.
56. J. Dong, J. M. Canfield, A. K. Mehta, J. E. Shokes, B. Tian, W. S. Childers, J. A. Simmons, Z. Mao, R. A. Scott, K. Warncke and D. G. Lynn, *Proc. Natl. Acad. Sci.*, 2007, **104**, 13313-13318.
57. J. P. Schneider, D. J. Pochan, B. Ozbas, K. Rajagopal, L. Pakstis and J. Kretsinger, *J. Am. Chem. Soc.*, 2002, **124**, 15030-15037.
58. P. J. Knerr, M. C. Branco, R. Nagarkar, D. J. Pochan and J. P. Schneider, *J. Mater. Chem.*, 2012, **22**, 1352-1357.
59. L. Chen, T. O. McDonald and D. J. Adams, *RSC Adv.*, 2013, **3**, 8714-8720.
60. T. Watanabe, M. Akiyama, K. Totani, S. M. Kuebler, F. Stellacci, W. Wenseleers, K. Braun, S. R. Marder and J. W. Perry, *Adv. Func. Mater.*, 2002, **12**, 611-614.
61. X.-Q. Dou, X.-M. Yang, P. Li, Z.-G. Zhang, H. Schonherr, D. Zhang and C.-L. Feng, *Soft Matter*, 2012, **8**, 9539-9544.
62. A. C. Carmen Alvarez-Lorenzo, *Smart Materials for Drug Delivery: Volume 1*, Royal Society of Chemistry, Cambridge, UK, 2013.
63. S. Peng, Q. Guo, P. G. Hartley and T. C. Hughes, *J. Mater. Chem. C*, 2014, **2**, 8303-8312.

64. A. C. Carmen Alvarez-Lorenzo, *Smart Materials for Drug Delivery: Volume 2*, Royal Society of Chemistry, Cambridge, UK, 2013.
65. R. V. Ulijn, N. Bibi, V. Jayawarna, P. D. Thornton, S. J. Todd, R. J. Mart, A. M. Smith and J. E. Gough, *Mater. Today*, 2007, **10**, 40-48.
66. S. S. Babu, V. K. Praveen and A. Ajayaghosh, *Chem. Rev.*, 2014, **114**, 1973-2129.
67. S. Khetan and J. A. Burdick, *Soft Matter*, 2011, **7**, 830-838.
68. C. Maity, W. E. Hendriksen, J. H. van Esch and R. Eelkema, *Angew. Chem. Int. Ed.*, 2015, **54**, 998-1001.
69. Z. Sun, Q. Huang, T. He, Z. Li, Y. Zhang and L. Yi, *Chem. Phys. Chem.*, 2014, **15**, 2421-2430.
70. G. S. Vadehra, B. D. Wall, S. R. Diegelmann and J. D. Tovar, *Chem. Commun.,* 2010, **46**, 3947-3949.
71. N. R. King, E. A. Whale, F. J. Davis, A. Gilbert and G. R. Mitchell, *J. Mater. Chem.*, 1997, **7**, 625-630.
72. T. Nagamura, *Coll. Surf. A*, 1997, **123–124**, 457-471.
73. H. M. D. Bandara and S. C. Burdette, *Chem. Soc. Rev.*, 2012, **41**, 1809-1825.
74. C. Dugave and L. Demange, *Chem. Rev.*, 2003, **103**, 2475-2532.
75. S. Tamesue, Y. Takashima, H. Yamaguchi, S. Shinkai and A. Harada, *Angew. Chem. Int. Ed.*, 2010, **49**, 7461-7464.
76. J. T. van Herpt, M. C. A. Stuart, W. R. Browne and B. L. Feringa, *Chem. Eur. J.*, 2014, **20**, 3077-3083.
77. P. A. d. Silva, *Chem. Asian J.*, 2011, **6**, 750.
78. A. Richter, G. Paschew, S. Klatt, J. Lienig, K.-F. Arndt and H.-J. Adler, *Sensors*, 2008, **8**, 561-581.
79. H. Kobayashi, A. Friggeri, K. Koumoto, M. Amaike, S. Shinkai and D. N. Reinhoudt, *Org. Lett.*, 2002, **4**, 1423-1426.
80. A. Srivastava, S. Ghorai, A. Bhattacharjya and S. Bhattacharya, *J. Org. Chem.,* 2005, **70**, 6574-6582.
81. R. Yang, S. Peng, W. Wan and T. C. Hughes, *J. Mater. Chem. C*, 2014, **2**, 9122-9131.
82. M. Moriyama, N. Mizoshita and T. Kato, *Polym. J.*, 2004, **36**, 661-664.
83. N. Mizoshita, H. Monobe, M. Inoue, M. Ukon, T. Watanabe, Y. Shimizu, K. Hanabusa and T. Kato, *Chem. Commun.*, 2002, 428-429.
84. J. Eastoe, M. Sanchez-Dominguez, P. Wyatt and R. K. Heenan, *Chem. Commun.*, 2004, 2608-2609.
85. Y. Huang, Z. Qiu, Y. Xu, J. Shi, H. Lin and Y. Zhang, *Org. Biomol. Chem.*, 2011, **9**, 2149-2155.
86. S. Miljanić, L. Frkanec, Z. Meić and M. Žinić, *Eur. J. Org. Chem.*, 2006, **2006**, 1323-1334.
87. S. Miljanić, L. Frkanec, Z. Meić and M. Žinić, *Langmuir*, 2005, **21**, 2754-2760.
88. R. G. Weiss, *J. Am. Chem. Soc.*, 2014, **136**, 7519-7530.
89. S. A. Ahmed, X. Sallenave, F. Fages, G. Mieden-Gundert, W. M. Müller, U. Müller, F. Vögtle and J.-L. Pozzo, *Langmuir*, 2002, **18**, 7096-7101.
90. Y. Li, K. M.-C. Wong, A. Y.-Y. Tam, L. Wu and V. W.-W. Yam, *Chem. Eur. J.*, 2010, **16**, 8690-8698.

91. A. R. Katritzky, R. Sakhuja, L. Khelashvili and K. Shanab, *J. Org. Chem.*, 2009, **74**, 3062-3065.
92. S. Xiao, T. Yi, F. Li and C. Huang, *Tet. Lett.*, 2005, **46**, 9009-9012.
93. Z. Qiu, H. Yu, J. Li, Y. Wang and Y. Zhang, *Chem. Commun.*, 2009, 3342-3344.
94. A. Fihey, A. Perrier and F. Maurel, *J. Photochem. Photobio. A.*, 2012, **247**, 30-41.
95. W. Zhu, X. Meng, Y. Yang, Q. Zhang, Y. Xie and H. Tian, *Chem. Eur. J.*, 2010, **16**, 899-906.
96. O. Tosic, K. Altenhoner and J. Mattay, *Photochem. Photobio. Sci.*, 2010, **9**, 128-130.
97. M. Irie, K. Sakemura, M. Okinaka and K. Uchida, *J. Org. Chem.*, 1995, **60**, 8305-8309.
98. S. Wang, W. Shen, Y. Feng and H. Tian, *Chem. Commun.*, 2006, 1497-1499.
99. R. Klajn, *Chem. Soc. Rev.*, 2014, **43**, 148-184.
100. G. Berkovic, V. Krongauz and V. Weiss, *Chem. Rev.*, 2000, **100**, 1741-1754.
101. B. S. Lukyanov and M. B. Lukyanova, *Chem. Heterocycl. Compd.*, 2005, **41**, 281-311.
102. L. Chen, S. Revel, K. Morris, L. C. Serpell and D. J. Adams, *Langmuir*, 2010, **26**, 13466-13471.
103. M.-J. R. P. Queiroz, A. S. Abreu, P. M. T. Ferreira, M. M. Oliveira, R. Dubest, J. Aubard and A. Samat, *Org. Lett.*, 2005, **7**, 4811-4814.
104. M. D'Auria and R. Racioppi, *J. Photochem. Photobio. A,* 2004, **163**, 557-559.
105. W. Davies and F. C. James, *J. Chem. Soc.*, 1955, 314-317.
106. R. F. C. Brown and R. K. Solly, *Tet. Lett.*, 1966, **7**, 169-174.
107. G. Ahmed, I. Petkov and S. Gutzov, *J. Incl. Phenom. Macrocycl. Chem.*, 2009, **64**, 143-148.
108. K. Gnanaguru, N. Ramasubbu, K. Venkatesan and V. Ramamurthy, *J. Org. Chem.*, 1985, **50**, 2337-2346.
109. K. Muthuramu and V. R. Murthy, *J. Org. Chem.*, 1982, **47**, 3976-3979.
110. W. Ji, G. Liu, M. Xu, X. Dou and C. Feng, *Chem. Commun.*, 2014, **50**, 15545-15548.
111. K. Tanaka, *Molecules*, 2012, **17**, 1408-1418.
112. M. A. Azagarsamy, D. D. McKinnon, D. L. Alge and K. S. Anseth, *ACS Macro Lett.*, 2014, **3**, 515-519.
113. S. H. Kim, Y. Sun, J. A. Kaplan, M. W. Grinstaff and J. R. Parquette, *New J. Chem.*, 2015, **39**, 3225-3228.
114. H. Yu, H. Mizufune, K. Uenaka, T. Moritoki and H. Koshima, *Tetrahedron*, 2005, **61**, 8932-8938.
115. I. Zouev, D.-K. Cao, T. V. Sreevidya, M. Telzhensky, M. Botoshansky and M. Kaftory, *Cryst. Eng. Comm.*, 2011, **13**, 4376-4381.
116. M. O'Donnell, *Nature*, 1968, **218**, 460-461.
117. M. George and R. G. Weiss, *Acc. Chem. Res.*, 2006, **39**, 489-497.
118. H. D. Becker, *Chemical Reviews*, 1993, **93**, 145-172.
119. H. Bouas-Laurent, A. Castellan, J.-P. Desvergne and R. Lapouyade, *Chem. Soc. Rev.*, 2000, **29**, 43-55.
120. I. Furman and R. G. Weiss, *Langmuir*, 1993, **9**, 2084-2088.

121. P. Terech, I. Furman and R. G. Weiss, *J. Phys. Chem.*, 1995, **99**, 9558-9566.
122. C. Wang, D. Zhang, J. Xiang and D. Zhu, *Langmuir*, 2007, **23**, 9195-9200.
123. A. Dawn, N. Fujita, S. Haraguchi, K. Sada and S. Shinkai, *Chem. Commun.*, 2009, 2100-2102.
124. R. L. Petritz, *Phys. Rev.*, 1956, **104**, 1508-1516.
125. J. T. Calow, P. J. Deasley, S. J. T. Owen and P. W. Webb, *J. Mater. Sci.*, 1967, **2**, 88-96.
126. C. Li and H. Wonneberger, *Adv. Mater.* 2012, **24**, 613-636.
127. F. Wurthner, *Chem. Commun.*, 2004, 1564-1579.
128. P. Osswald and F. Würthner, *Chem. Eur. J.*, 2007, **13**, 7395-7409.
129. S. S. Babu, S. Prasanthkumar and A. Ajayaghosh, *Angew. Chem. Int. Ed.*, 2012, **51**, 1766-1776.
130. F. Würthner, V. Stepanenko, Z. Chen, C. R. Saha-Möller, N. Kocher and D. Stalke, *J. Org. Chem.*, 2004, **69**, 7933-7939.
131. Y. Chen, Y. Feng, J. Gao and M. Bouvet, *J. Colliod Interface Sci.*, 2012, **368**, 387-394.
132. S. Roy, D. Kumar Maiti, S. Panigrahi, D. Basak and A. Banerjee, *RSC Adv.*, 2012, **2**, 11053-11060.
133. D. Görl, X. Zhang and F. Würthner, *Angew. Chem. Int. Ed.*, 2012, **51**, 6328-6348.
134. A. Datar, K. Balakrishnan and L. Zang, *Chem. Commun.*, 2013, **49**, 6894-6896.
135. S. V. Bhosale, C. H. Jani and S. J. Langford, *Chem. Soc. Rev.*, 2008, **37**, 331-342.
136. Ş. Erten, Y. Posokhov, S. Alp and S. İçli, *Dyes Pigments*, 2005, **64**, 171-178.
137. F. Allix, P. Curcio, Q. N. Pham, G. Pickaert and B. Jamart-Grégoire, *Langmuir*, 2010, **26**, 16818-16827.
138. Q. Wang, J. Wu, Z. Gong, Y. Zou, T. Yi and C. Huang, *Soft Matter*, 2010, **6**, 2679-2684.
139. L.-H. Hsu, S.-M. Hsu, F.-Y. Wu, Y.-H. Liu, S. R. Nelli, M.-Y. Yeh and H.-C. Lin, *RSC Adv.*, 2015, **5**, 20410-20413.
140. S. Basak, N. Nandi, A. Baral and A. Banerjee, *Chem. Commun.*, 2015, **51**, 780-783.
141. J. Zheng, W. Qiao, X. Wan, J. P. Gao and Z. Y. Wang, *Chem. Mater.*, 2008, **20**, 6163-6168.
142. T. Shu, J. Wu, M. Lu, L. Chen, T. Yi, F. Li and C. Huang, *J. Mater. Chem.*, 2008, **18**, 886-893.
143. X. Yang, G. Zhang and D. Zhang, *J. Mater. Chem.*, 2012, **22**, 38-50.
144. K. Peng, I. Tomatsu and A. Kros, *Chem. Commun.*, 2010, **46**, 4094-4096.
145. Z. Liu, Q. Lin, Y. Sun, T. Liu, C. Bao, F. Li and L. Zhu, *Adv. Mater.*, 2014, **26**, 3912-3917.
146. V. Jayawarna, M. Ali, T. A. Jowitt, A. F. Miller, A. Saiani, J. E. Gough and R. V. Ulijn, *Adv. Mater.*, 2006, **18**, 611-614.
147. T. D. Sargeant, C. Aparicio, J. E. Goldberger, H. Cui and S. I. Stupp, *Acta Biomater.*, 2012, **8**, 2456-2465.

148. D. Buenger, F. Topuz and J. Groll, *Prog. Polym. Sci.*, 2012, **37**, 1678-1719.
149. K. Fan, J. Yang, X. Wang and J. Song, *Soft Matter*, 2014, **10**, 8370-8375.
150. A. Pichon, *Nat. Chem.*, 2009, **1**.
151. T. Konry and D. R. Walt, *J. Am. Chem. Soc.*, 2009, **131**, 13232-13233.
152. D. J. Gundlach, *Nat Mater*, 2007, **6**, 173-174.
153. J. H. Oh, S. Liu, Z. Bao, R. Schmidt and F. Würthner, *Appl. Phys. Lett.*, 2007, **91**, 212107.
154. Y. Che, A. Datar, X. Yang, T. Naddo, J. Zhao and L. Zang, *J. Am. Chem. Soc.*, 2007, **129**, 6354-6355.
155. J. Raeburn and D. J. Adams, *Chem. Commun.*, 2015, **51**, 5170-5180.
156. S. Prasanthkumar, S. Ghosh, V. C. Nair, A. Saeki, S. Seki and A. Ajayaghosh, *Angew. Chem. Int. Ed.*, 2015, **54**, 946-950.
157. A. Facchetti, *Mater. Today*, 2013, **16**, 123-132.
158. M. Scholz, R. Schmidt, S. Krause, A. Schöll, F. Reinert and F. Würthner, *Appl. Phys. A*, 2009, **95**, 285-290.
159. R. d. Schmidt, J. H. Oh, Y.-S. Sun, M. Deppisch, A.-M. Krause, K. Radacki, H. Braunschweig, M. Könemann, P. Erk, Z. Bao and F. Würthner, *J. Am. Chem. Soc.*, 2009, **131**, 6215-6228.
160. B. A. Jones, M. J. Ahrens, M.-H. Yoon, A. Facchetti, T. J. Marks and M. R. Wasielewski, *Angew. Chem. Int. Ed.*, 2004, **43**, 6363-6366.
161. B. A. Gregg, J. Sprague and M. W. Peterson, *J. Phys. Chem. B*, 1997, **101**, 5362-5369.
162. P. Xue, P. Wang, B. Yao, J. Sun, P. Gong, Z. Zhang, C. Qian and R. Lu, *ACS Appl. Mater. Inter.*, 2014, **6**, 21426-21434.
163. B. Maennig, J. Drechsel, D. Gebeyehu, P. Simon, F. Kozlowski, A. Werner, F. Li, S. Grundmann, S. Sonntag, M. Koch, K. Leo, M. Pfeiffer, H. Hoppe, D. Meissner, N. S. Sariciftci, I. Riedel, V. Dyakonov and J. Parisi, *Appl. Phys. A*, 2004, **79**, 1-14.
164. V. Kamm, G. Battagliarin, I. A. Howard, W. Pisula, A. Mavrinskiy, C. Li, K. Müllen and F. Laquai, *Adv. Ener. Mater.*, 2011, **1**, 297-302.
165. L. Torsi, M. Magliulo, K. Manoli and G. Palazzo, *Chem. Soc. Rev.*, 2013, **42**, 8612-8628.
166. J. Smith, R. Hamilton, I. McCulloch, N. Stingelin-Stutzmann, M. Heeney, D. D. C. Bradley and T. D. Anthopoulos, *J. Mater. Chem.*, 2010, **20**, 2562-2574.
167. J.-P. Hong, M.-C. Um, S.-R. Nam, J.-I. Hong and S. Lee, *Chem. Commun.*, 2009, 310-312.
168. A. Bonfiglio and P. Cosseddu, in *Functional Supramolecular Architectures*, WILEY-VCH Verlag & Co. KGaA, 2011, Ch23, pp. 719-740.
169. M. Heilemann, E. Margeat, R. Kasper, M. Sauer and P. Tinnefeld, *J. Am. Chem. Soc.*, 2005, **127**, 3801-3806.
170. L. L. Beecroft and C. K. Ober, *Chem. Mater.*, 1997, **9**, 1302-1317.
171. W. Russ Algar, M. Massey and U. J. Krull, *Trends Anal. Chem.*, 2009, **28**, 292-306.
172. E. Krieg, E. Shirman, H. Weissman, E. Shimoni, S. G. Wolf, I. Pinkas and B. Rybtchinski, *J. Am. Chem. Soc.* 2009, **131**, 14365-14373.

CHAPTER 2

Photodimerisation of a Coumarin-Based Dipeptide Gelator

2. 1. Introduction

Low molecular weight gelators (LMWGs) self-assemble in a solvent to form fibres. At a sufficiently high concentration, the fibres entangle and cross-link to form a network, immobilising the solvent.[1-3] The mechanical properties of the gel arise from the average thickness and mechanical properties of the fibres, the degree of branching (i.e. the distance between the cross-linking points), the type of cross-link (i.e. branching or entanglements) and how the fibres are distributed across the whole gel.[4] These properties are difficult to control and there is limited information available for these systems.[3, 5]

The self-assembly is driven by non-covalent interactions. This means that the gels are often reversible as (for example) heating is often sufficient to break these non-covalent bonds and so the LMWG re-dissolves.[6] The cross-links between fibres are also such that the gels often break at relatively low strains as compared to polymeric gels.[7, 8] As a result, stretching for example is often impossible. For some applications, these properties can be desirable, but for others they can be a drawback. Hence, it is of interest to be able to covalently cross-link or post-modify a gel once formed to lock in the structure.

A number of methods have been used to post – modify LMWGs after gel formation. For example, tyrosine-containing gelators can be cross-linked by the formation of dityrosine, which has been shown to enhance the mechanical properties of the gels.[9] An increase in the rheological properties of gels has also been reported by the reaction of an amine-containing LMWG with glutaraldehyde post-gel formation.[10] Click chemistry has also been used to cross-link LMWG fibres post gelation, and this cross-linking was shown to affect the rate of release of a drug entrapped in the network.[11]

There are a number of photo reactive moieties, (as discussed in detail in Chapter 1) including conjugated diyne units,[12, 13] alkynes, and diazides,[14] which have been used to strengthen materials post-gelation. There are also many examples of photoisomerising groups such as stilbene[15] and

azobenzene.[16-18] These often lead to a conformational change of the molecules from the gelling *trans*-isomer to the non-gelling *cis*-isomer or vice versa. This post-gelation modification is useful for surface photopatterning applications.[19] Anthracene and coumarins are known to photodimerise when irradiated with light > 280 nm.[20, 21] The dimerisation of coumarins is reversible when light with a wavelength of less than 260 nm is used. The [2+2] photodimerisation of coumarins is known to occur both in solution and in the solid state, often to give a mixture of *syn-syn*, *syn-anti*, *anti-syn* and *anti-anti* cyclobutanes shown respectively in Fig. 2.1.[21, 22]

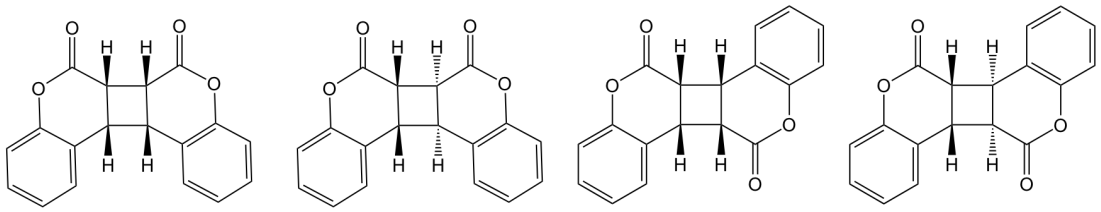

Figure 2.1 Possible isomers resulting from the dimerisation of coumarin.

It was hypothesised that incorporating coumarin into a LMWG would allow dimerization within a self-assembled fibre to stiffen the fibre rather than reaction between different fibres, as the coumarin molecules would not be close enough to each other to allow the dimerization to happen (Fig. 2.2). This dimerisation within the fibres should lead to a change in the rheological properties of the fibres and hence a controllable change in the mechanical bulk properties of the gel, without destruction of the fibrous network.

It is noted that Kim *et al.* have recently shown that by incorporating two coumarin groups into a β-sheet forming LMWG that the gel properties can be modified post-gelation with the use of UV light.[23] This change in properties of the gel arises from the cross-linking of both coumarin units, which ultimately results in destruction of the gel due to disruption of fibres and formation of an insoluble network. Feng and coworkers have also recently incorporated a coumarin group into a LMWG to be used in cell imaging due to the fluorescence of the coumarin moeity.[24]

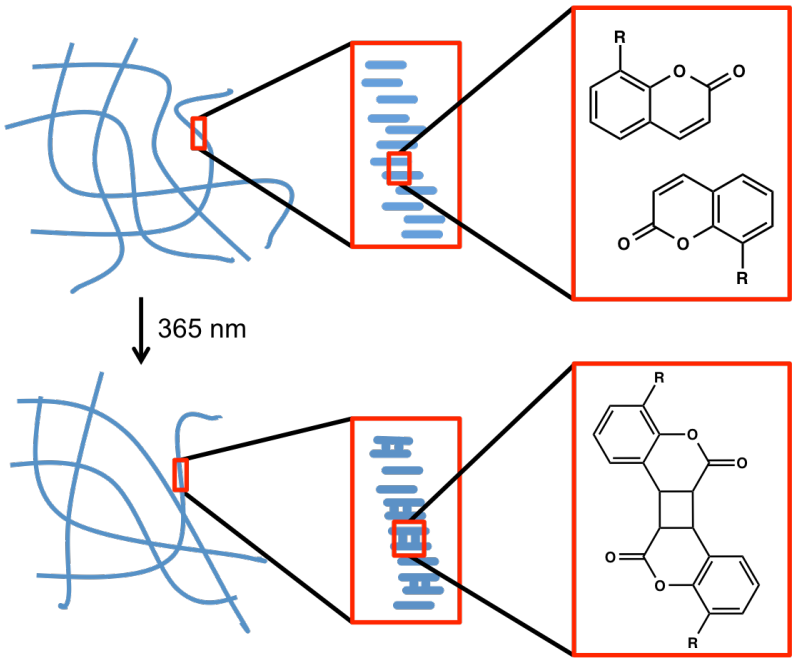

Figure 2.2 Schematic showing possible stacking of gelator molecules in the gel before and after irradiation with UV light. Only one isomer of the coumarin dimer has been shown for clarity.

2. 2. Results and Discussion

The LMWG is related to the many other dipeptide-based hydrogelators, where a large aromatic group is attached to the *N*-terminus (Fig. 2.3).[25] The full synthetic procedure is described in section 2. 4. 1. The large aromatic group allows π-π stacking for fibre formation[26] and allows the coumarin moieties to be close enough for the [2+2] photodimerisation to occur. The diphenyalanine make the molecule sufficiently hydrophobic as well as providing other intermolecular interactions such as H-bonding to aid gelation.

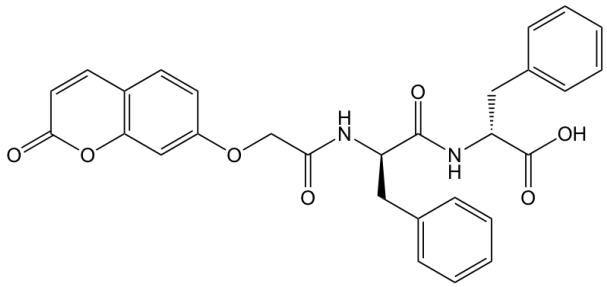

Figure 2.3 Molecular structure of coumarin-diphenylalanine gelator.

Gels were prepared by dissolving the gelator at high pH (typically > 10), followed by reducing the pH by the addition of glucono-δ-lactone (GdL). GdL hydrolyses slowly over time to gluconic acid (Fig. 2.4), resulting in a homogeneous drop in pH as shown previously for related gelators.[27, 28] This approach leads to homogeneous and reproducible gelation. This homogeneity is due to the fast dissolution of the GdL in the solution, followed by slow hydrolysis and acidification, resulting in a uniform pH drop.

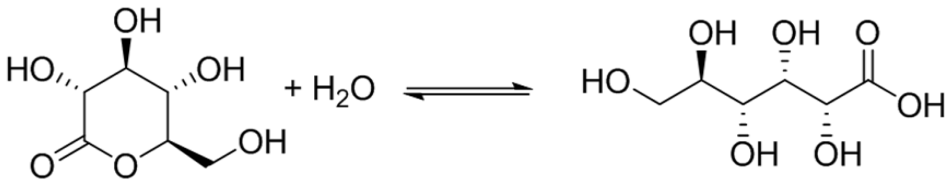

Figure 2.4. Scheme showing the hydrolysis of glucono-d-lactone to gluconic acid in water.

Using this approach, transparent, self-supporting gels are formed at a gelator concentration of 5 mg/mL when 8 mg/mL of GdL is used. The properties of this gel are entirely consistent with gels of this type with breakage of the gel occurring at low strain (1 %, Fig. 2.5a) and G´ and G˝ being independent of frequency (Fig. 2.5b). The storage modulus (G′, 82,000 Pa) is approximately an order of magnitude higher than the loss modulus (G″, 10,000 Pa).

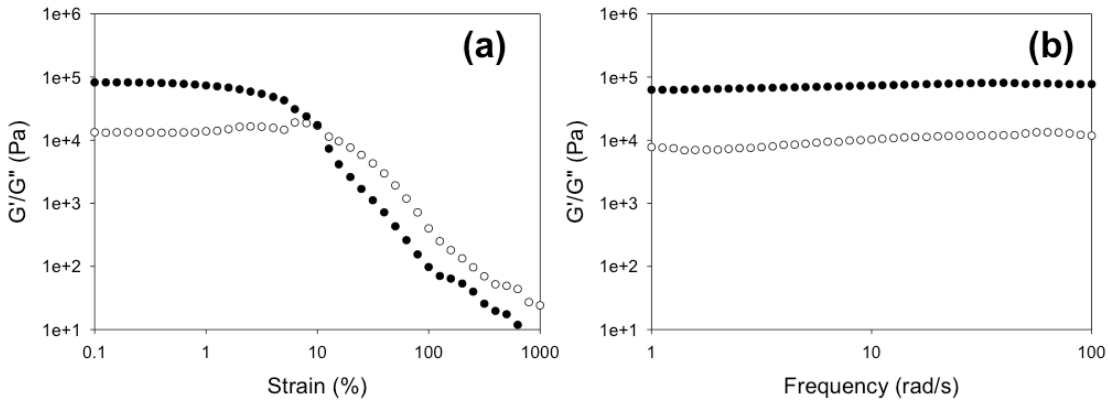

Figure 2.5 Rheology data for GdL triggered gels (a) strain sweep performed at 10 rad/s and (b) frequency sweeps performed at 0.5 % strain. Full symbols are G' and open shapes are G".

Scanning electron microscopy (SEM, carried out by Dr. T. McDonald, University of Liverpool) shows that the gel arises from a network of fibres (Fig. 2.6a) with an average diameter of 42 nm ± 20 nm as seen by the distributions in Fig. 2.6b. The diameter of the fibres was calculated from over 90 fibres using the SEM images using ImageJ analysis software. Analysis of SEM images of gels, such as morphology of fibres, may not accurately represent the gel network and so should be done with caution.[29, 30] SEM images are of dried gels, whereas tests such as rheology are carried out on wet gels. Therefore, the structures observed by SEM could be due to drying effects.[31]

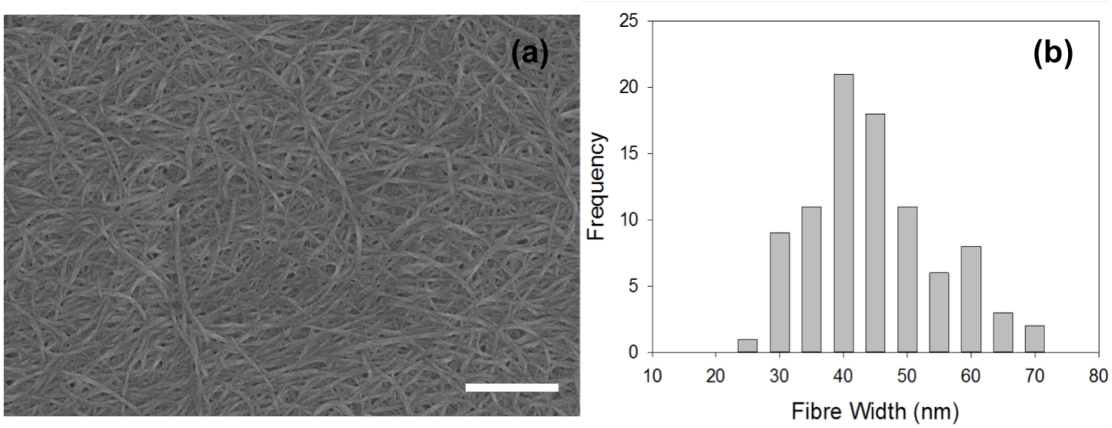

Figure 2.6 (a) SEM image of GdL-triggered gel, scale bar represents 500 nm. (b) Graph showing distribution fibres widths from SEM images of gels formed using GdL

Fluorescence measurements show that the coumarin molecules in solution at a concentration of 1.25 mg/mL have a maximum emission of 390 nm when excited at 340 nm. A different concentration is used for fluorescence as at 5 mg/mL the solution was too concentrated and upon gelation the fluoresence was quenched. When gelled, the same molecules now have a maximum emission at 380 nm (Fig. 2.7). This blue shift in the spectrum upon gelation shows H-aggreagtion of the coumarin gelator molecules.

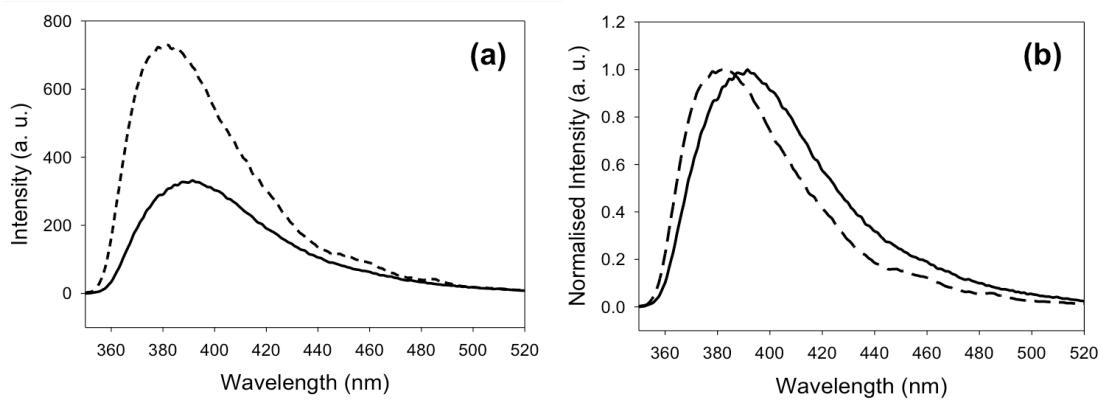

Figure 2.7 Fluorescence spectra of gelator in solution (solid line) and gelled using GdL (dashed line). Both at a concentration of 1.25 mg/mL and excited at 340 nm. (a) has not been normalised and (b) has been normalised

UV-Vis absorption measurements show a maximum absorption at 320 nm with a shoulder at 290 nm. Irradiating the solution at high pH using a 365 nm LED placed 1 cm away from he sample shows that the absorbance at 320 nm readily reduces in intensity, consistent with photodimerisation (Fig. 2.8a).[32] After 260 minutes of irradiation, the intensity of this peak has halved (Fig. 2.8b).

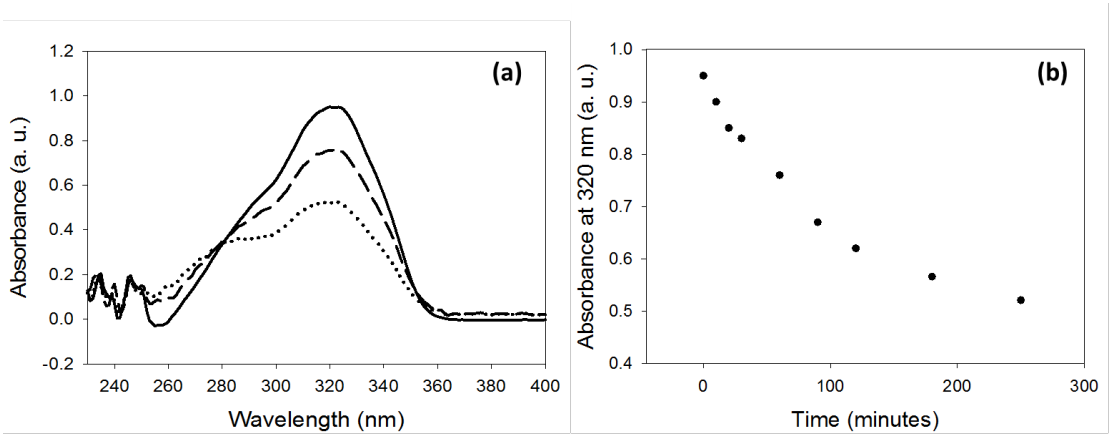

Figure 2.8 (a) UV-vis absorption spectra of solution (solid line) and after 15 minutes (dashed line) and 120 minutes (dotted line) of irradiation with 365 nm LED. (b) Graph showing decrease of absorption of solution at 320 nm with time on irradiation with 365 nm LED.

UV-vis measurement of the gel formed at low pH from the coumarin shows a broad peak with a maxiumum intensity at 320 nm (Fig. 2.9a). After irradiation with UV light for 30 minutes, the intensity of the peak at 320 nm had decreased by 70 % (Fig. 2.9.b).

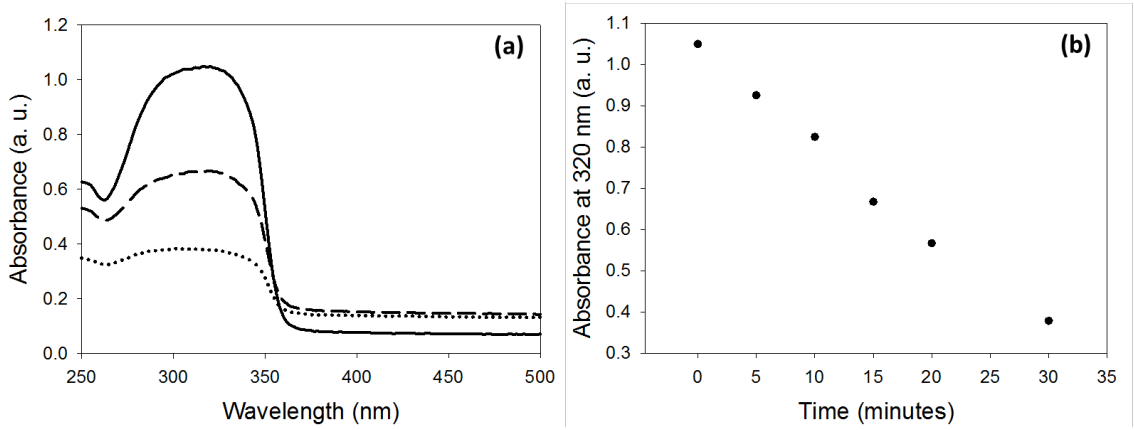

Figure 2.9 (a) UV-vis absorption spectra of gel (solid line) and after 15 minutes (dashed line) and 30 minutes (dotted line) of irradiation with 365 nm LED. (b) Graph showing decrease of absorption at 320 nm with time after irradiation with 365 nm LED.

In the gel state, the photodimerisation is significantly faster. It was hypothesised that this is due to the coumarin molecules being closer to each other when self-assembled into and so dimerisation can more easily occur in the fibres as compared to when dispersed at high pH (Fig. 2.10).

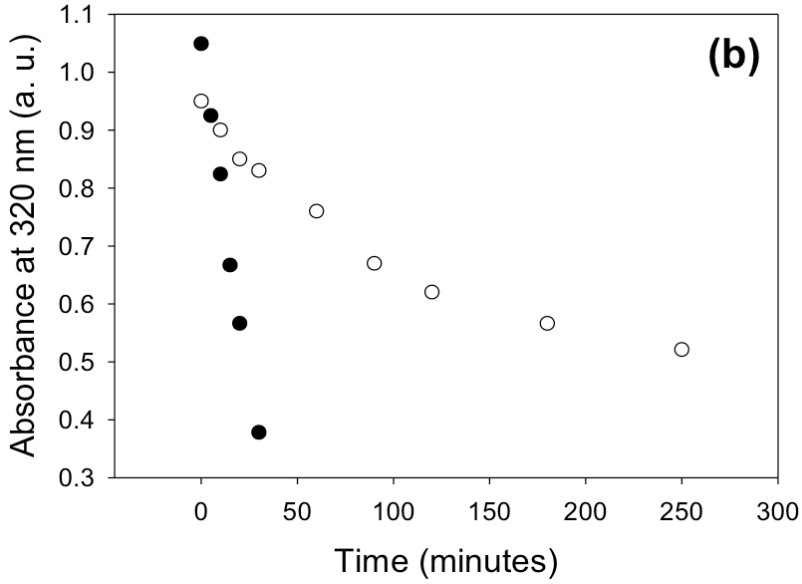

Figure 2.10 Decrease in UV-vis absorption at 320 nm with time on irradiation with a 365 nm LED showing dimerisation of gelator in a high pH solution (open circles) and in a gel at low pH (full circles).

Photodimersation of the coumarin gelators was further confirmed by mass spectrometry of the irradiated samples (Fig. 2.11). The data show the $[M^{-}H]^{-}$ peak for

both the monomer at 513.2 m/z and the dimer at 1027.2 m/z. Mass spectrometry showed the dimer to be in excess of the monomer indicating that the majority of the sample was dimerised after 4 hours of irradiation with the 365 nm LED.

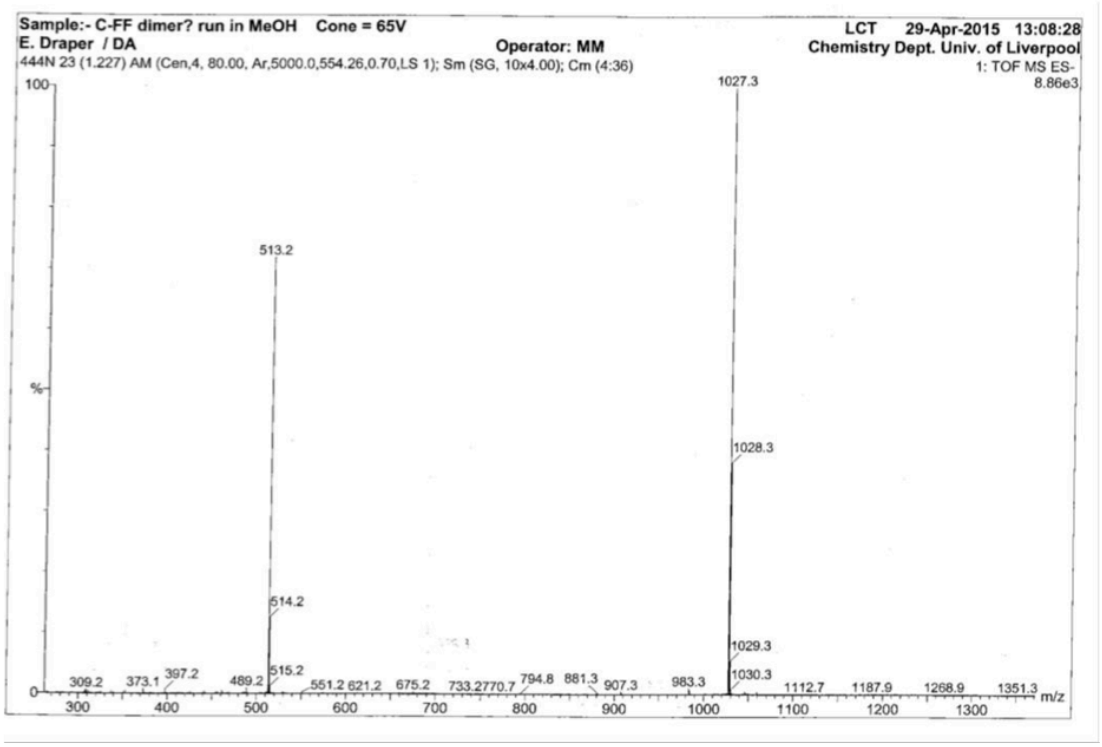

Figure 2.11 Mass spectrum of an air dried gel formed by GdL after 4 hours of irradiation with a 365 nm LED showing $[M-H]^-$ peaks for coumarin gelator and the coumarin dimer.

The degree of photodimerisation relates to the time over which the gel is exposed to UV light, as seen in the UV-vis absorption measurements above. The gel becomes slightly turbid on being exposed to UV light, with the turbidity being most pronounced at the front of the gel that is directly exposed to the LED (Fig. 2.12). This is due to photodimerisation only being able to occur where the light can penetrate. The light intensity at the far side of the gel is significantly less than at the front where the light is, and so the whole sample cannot be uniformly irradiated in this way.

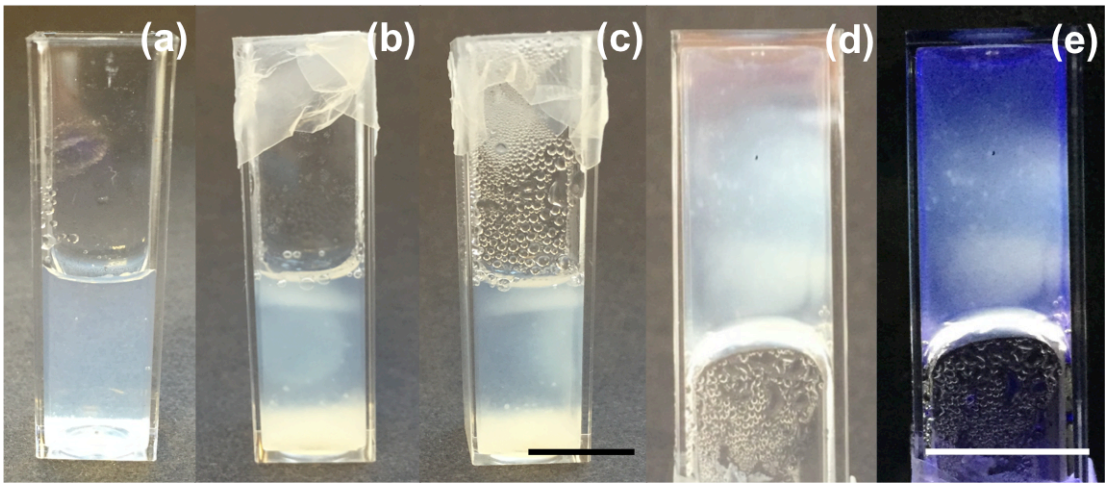

Figure 2.12 Photograph showing gel (a) before irradiation (b) after 2 hours of irradiation viewed from the front (c) and viewed from the side showing irradiation of gel is not homogeneous and is more pronounced at the front of the gel. (d) Photograph showing the inhomogeneity of the irradiated sample in natural light and (e) under UV light. Scale bar represents 1 cm.

This lack of homogeneity presents difficulties for analysing the effect of the irradiation on the rheological properties of the gels. This inhomogeneous change in gel network is also shown in the SEM images (collected by Dr. T. McDonald, University of Liverpool) of the irradiated sample shown in Fig. 2.13a, with an average fibre diameter of 39 nm ± 22 nm with the distribution of the fibres becoming broader as seen in Fig. 2.13b. The shift in distribution shows that there are smaller fibres present than before irradiation. There are still larger fibres present, showing change in fibres is not uniform throughout the sample.

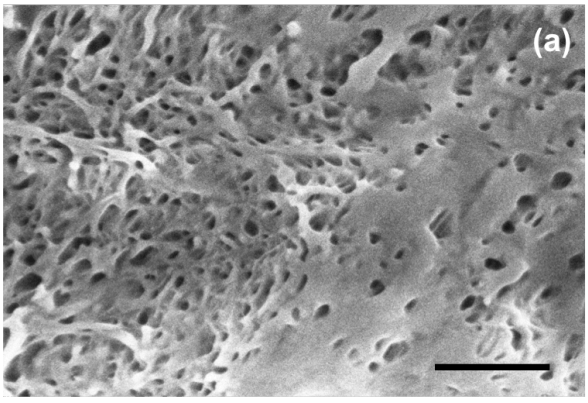

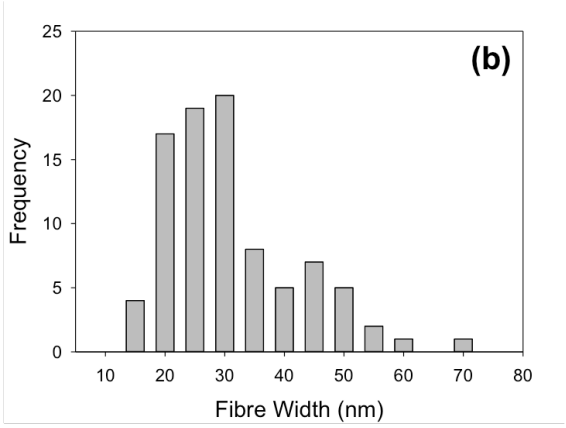

Figure 2.13 (a) An SEM image of the air-dried coumarin gel after irradiation for 2 hours. Scale bar represents 500 nm. (b) Graph showing distribution fibres widths from SEM.

Fourier Transformed Infra-Red (FTIR) spectroscopy for GdL formed gels show peaks in the amide I region at 1620 and 1650 cm^{-1} which can be characteristic for anti-parallel β-sheets and random coil secondary structures respectively (Fig. 2.14).[33] When irradiated with UV light the spectra does not show a change in the amide I region and shows the secondary structure has not changed upon dimerisation. However, interpreting this data for short dipeptide molecules is often difficult as has been seen with other LMWGs.[34]

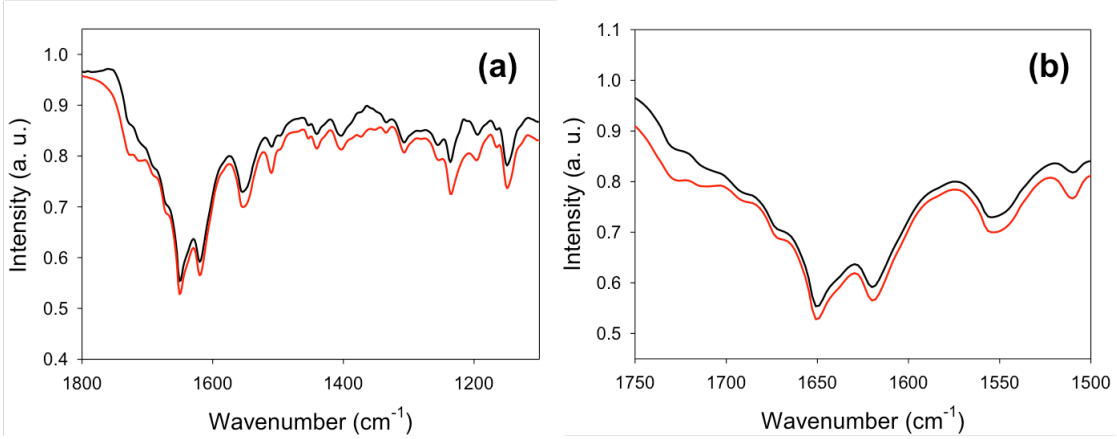

Figure 2.14 FTIR spectra of gel formed with GdL before irradiation (black line) and after irradiation (red line) (a) shows the whole spectra and (b) shows the peaks in the amide I region between 1500-1750 cm^{-1}.

Hence, thin hydrogel films were prepared (of the order of 2 mm thick) utilising an electrochemical approach, which have been previously reported.[35-37] Hydroquinone (HQ) is electrochemically oxidised to 1,4-benzoquinone by applying a current to an electrode. The oxidation of HQ releases protons close surface of the electrode, as only hydroquinone close enough to the electrode surface can be oxidised. This creates a pH gradient at the surface of the cathode (Fig. 2.15a)

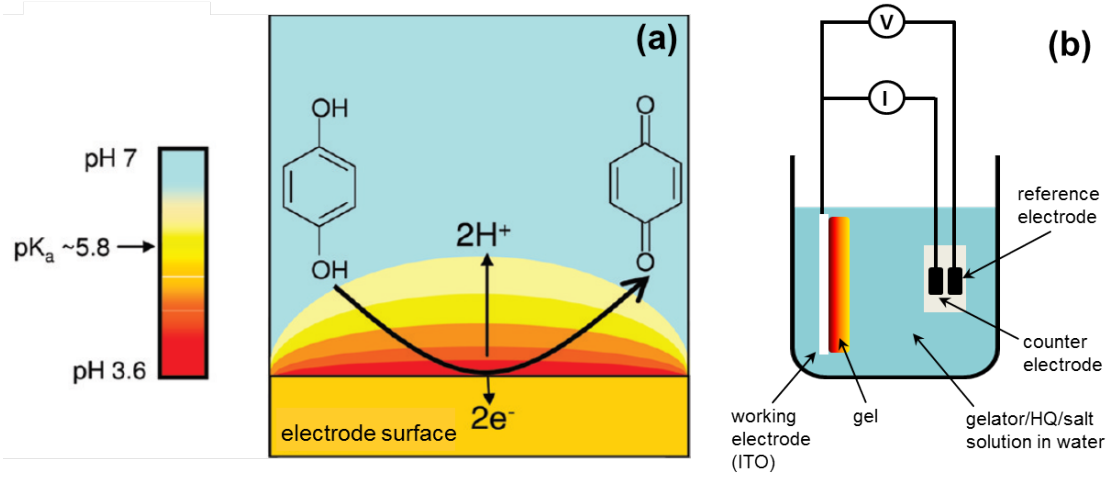

Figure 2.15 (a) Scheme showing the pH gradient at the electrode surface from the oxidation of hydroquinone. Adapted from ref. 35, Johnson *et al.* (b) Diagram showing the setup of the electrochemical gelation apparatus.

When a gelator is placed in the hydroquinone solution, this results in a gel being formed only at the electrode as opposed to in the bulk (Fig. 2.15b), with the thickness of the gel being controlled by both the current used and the time for which the current is applied.[37] The electrochemical gelation is essentially a pH switch the same as GdL, but allowing spatial control over gelation. Using this approach, films could be formed on ITO-coated glass slides (Fig. 2.17a). The gels were carefully removed off the slide and the rheological properties measured. The absolute gel properties were weaker than those formed in the bulk (G´, 6,100 Pa and G˝, 510 Pa), but were consistent in behaviour, with the gels breaking at relatively low strain (5 %) and G′ being independent of frequency (Fig. 2.16).

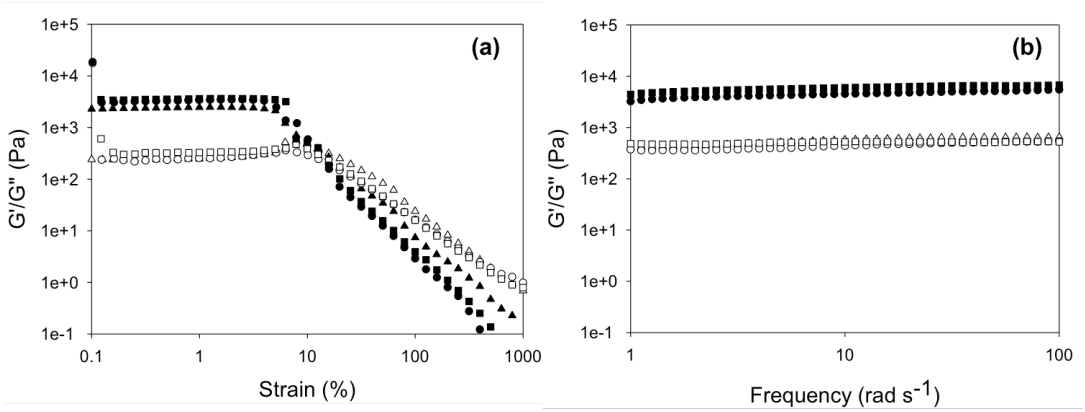

Figure 2.16 Three sets of rheology data for electrochemically grown gels (a) strain sweep performed at 10 rad/s and (b) frequency sweeps performed at 0.5 % strain. Full symbols are G' and open symbols are G". Different shapes represent data for different gels.

This method of gelation was also found to give gels with very reproducible rheological properties as shown by the multiple repeats shown in Fig. 2.16.To probe the effect of irradiation on the rheological properties, the gels were removed from the bulk liquid and sealed in a hydrated chamber. The gel was then irradiated by a 365 nm LED through a small hole in the top of the chamber. The gel was moved periodically to ensure uniform exposure of the entirety of the sample to the LED. As the sample was irradiated, it became slightly more turbid (Fig. 2.17b). After one hour of irradiation the gel was more opaque (Fig. 2.17c). Using this thin film method, irradiation appeared more uniform over the entire gel. This can be seen clearly when the gels are viewed under UV light (Fig. 2.17d, e and f).

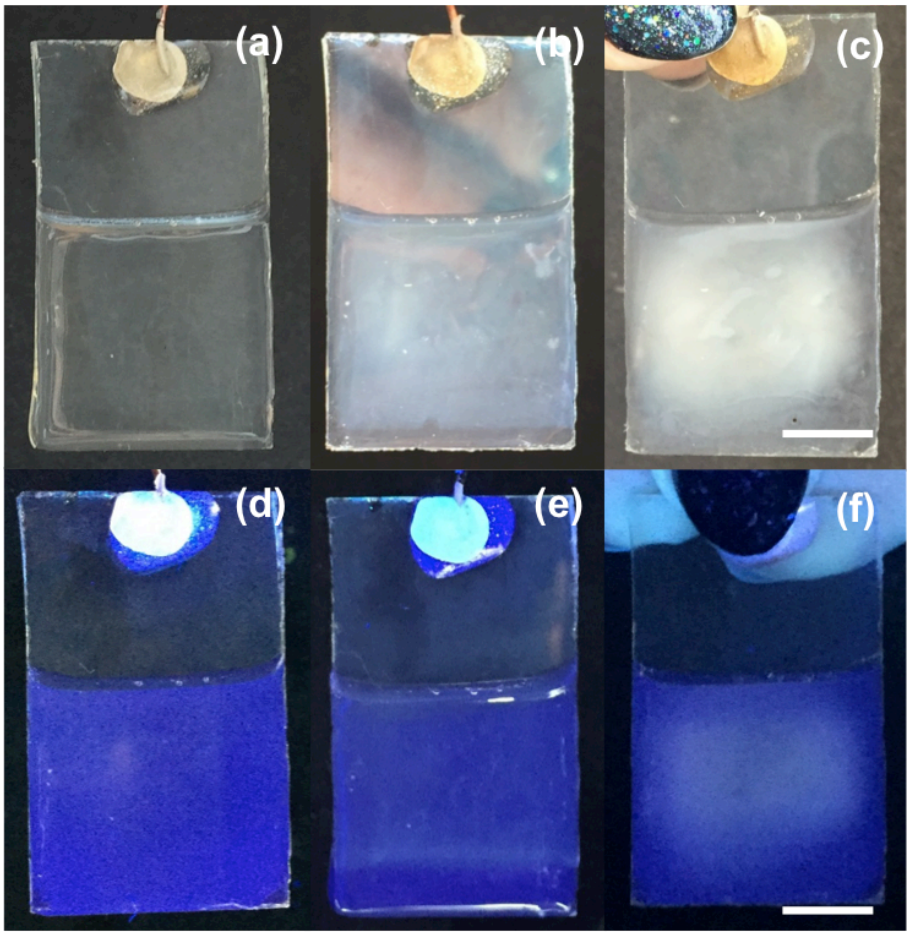

Figure 2.17 Photographs of electrochemically grown gels taken under natural light (a) before irradiation, (b) after 15 minutes irradiation with 365 nm LED and (c) after 1 hour of irradiation. Photographs of gels taken under UV light (d) before irradiation, (e) after 15 minutes irradiation and (f) after 2 hours irradiation with 365 nm LED. Scale bars represent 1 cm.

This more homogenous dimerisation method was also demonstrated using UV-Vis absorption spectroscopy. An electrochemically grown gel was irradiated under UV light for 1 hour then divided into four equal parts (Fig. 2.18b). The four different parts were then removed from the glass slide and re-dissolved in DSMO. These solutions were diluted equally and the UV-Vis absorption spectra recorded showing similar amounts of dimer present (Fig. 2.18a).

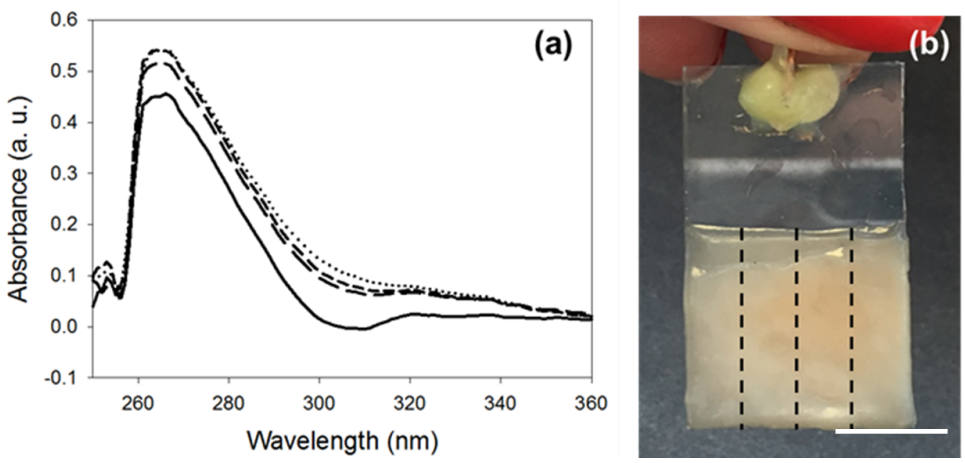

Figure 2.18 UV-vis spectra of different parts of the gel dissolved in DMSO. (b) Photograph of electrochemically formed gel after irradiation for 1 hour. The dotted lines show how the gel was divided for the UV-vis measurements. The brown colour of the gel is due to the oxidation of hydroquinone. The scale bar represents 1 cm.

FTIR of formed gels electrochemically also show peaks in the amide I region at 1620 and 1650 cm^{-1} which again can be characteristic for anti-parallel β-sheets and random coil secondary structures respectively (Fig. 2.19).[33] This suggests the secondary structure for both gels formed by the GdL method and the electrochemical method have the same secondary structure. As with gels formed with GdL, the electrochemically formed gel after being irradiated with UV light the spectra do not show a change in the amide I region.[33] This lack of change again shows the secondary structure has not changed upon dimerisation, but as previously mentioned FTIR of gels is often difficult to interpret.[34, 38]

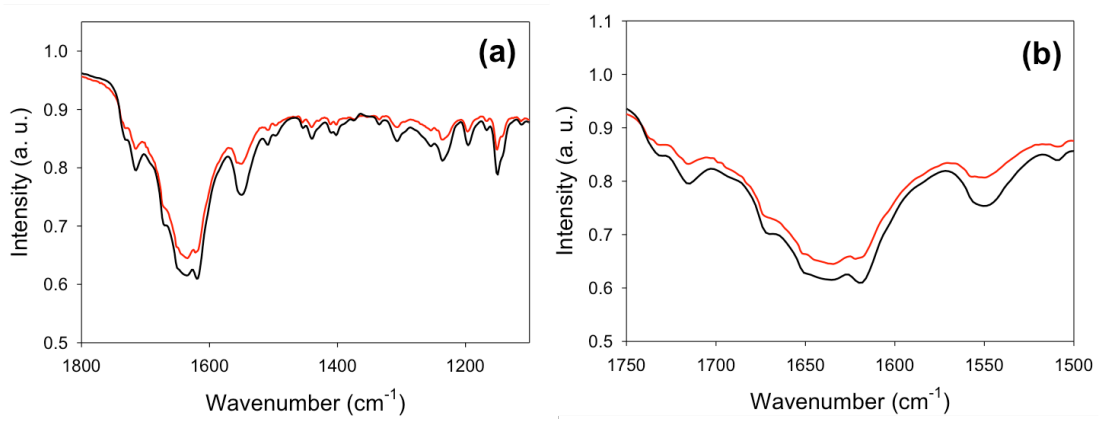

Figure 2.19 FTIR spectra of gel formed electrochemically before irradiation (black line) and after irradiation (red line) (a) shows the whole spectra and (b) shows the peaks in the amide I region between 1500-1750 cm^{-1}.

Measuring the rheological properties of the gels shows that after 15 minutes of irradiation with a 365 nm LED, G′ increased to 9000 Pa and G″ to 1000 Pa (Triangle data Fig. 2.20). This is significantly stronger than before irradiation with UV light (circle data Fig. 2.20). The point at which the gel network breaks remains similar for both irradiated and non-irradiated gels, showing that the way the fibres entangle and interact with each has not changed. This rules out dimerisation happening between the coumarin moieties in different fibres.[39]

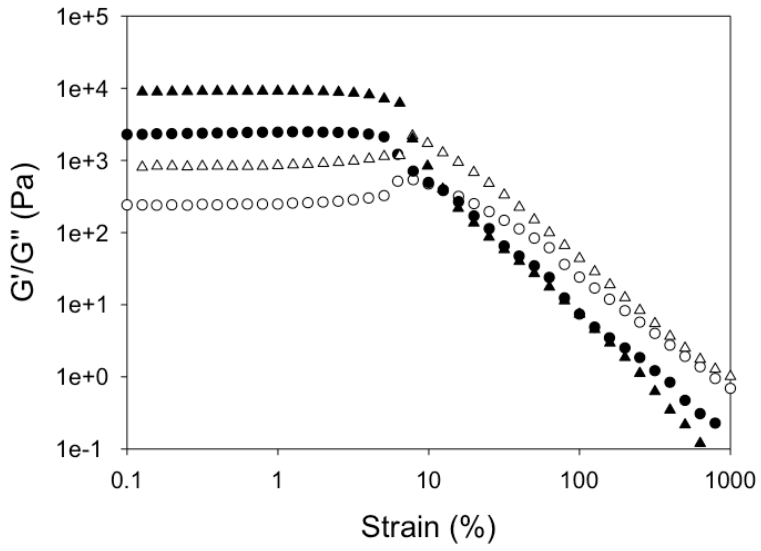

Figure 2.20 Rheological strain sweep data for electrochemically grown gels before irradiation (circles) and after 15 minutes of irradiation with a 365 nm LED (triangles). G′ (open symbols) and G″ (full symbols). Measurements recorded at 10 rad/s.

Further irradiation time resulted in a decrease in the gel strength compared to that after 15 minutes, but the gels were still stiffer than before irradiation (Fig. 2.21). Similar effects have recently been reported by Kim *et al*.[23] After 60 minutes irradiation, there was no further decrease in G′, but the turbidity of the gel noticeably increased (Fig. 2.17c). Samples were not irradiated for longer than 2 hours as samples will start drying out after this time, so any change in rheology would be due to that rather than a real change in the system. The increase in the rheological properties after 15 minutes was attributed to the photodimerisation of the coumarin on the gelator molecules. This dimerisation strengthens the fibres in the network due to the formation of covalent bonds between molecules rather than just non-covalent. Since we have only one coumarin group per gelator, complete polymerisation of the fibres is not possible. It was rather envisaged that this photodimerisation leads to an increase in stiffness of the individual fibres rather than a change in the network. Upon further irradiation of the gels resulted in a decrease G′ is an interesting observation. The fibres are though to stiffen to a sufficient degree that the network is disrupted or strained, and so leading to a weaker network. The irradiation of the gels was reproducible as shown by the small error bars in Fig. 2.21 from four repeat measurements.

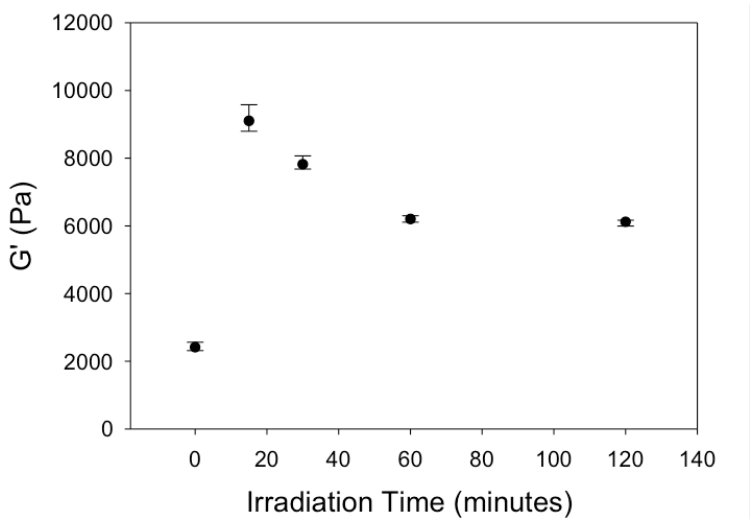

Figure 2.21 Graph showing the change in G′ of electrochemically grown gels after increasing time under 365 nm. Error bars are calculated from an average of four repeat measurements.

Before irradiation, SEM images (collected by Dr. T. McDonald, University of Liverpool) of electrochemically formed gels show a random fibrous network (Fig. 2.22a), similar to that seen for gels formed by the GdL method. After an hour of irradiation, SEM images show that the network has changed, instead showing less defined structure, again as for gels formed with GdL (Fig. 2.22b). Electrochemically grown gels show a more uniform change in the structure as also seen in the change in transparency of the gels. Both gels show significant change in the morphology of the gel with smooth featureless areas that could be due to surface effects.

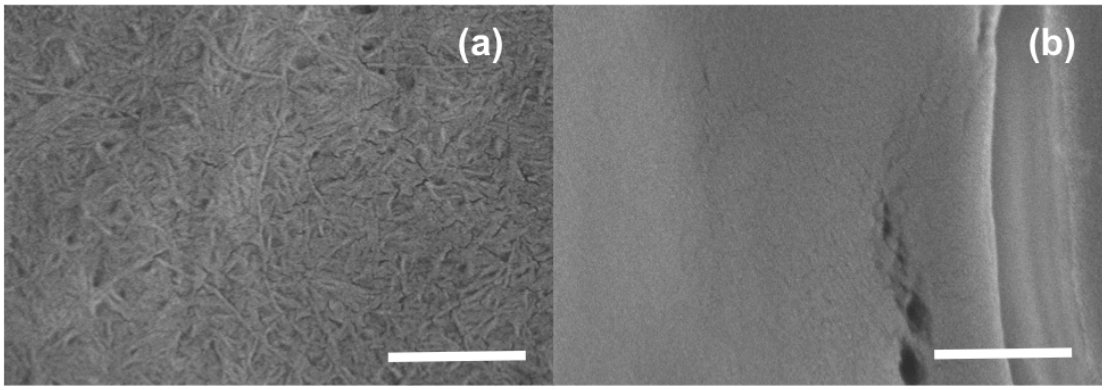

Figure 2.22 SEM of gels formed electrochemically before (a) and after irradiation with a 365 nm LED for an hour (b). Scale bar represents 1 μm.

As the dimerisation of the coumarin molecule is reversible with wavelengths < 260 nm, the irradiated samples were then irradiated with 254 nm light in a quartz cuvette for 5 hours. There was no change in the samples visibly or by NMR (Fig. 2.23), but this could be due to the power output of the light source used, and the light being unable to penetrate through the gel.

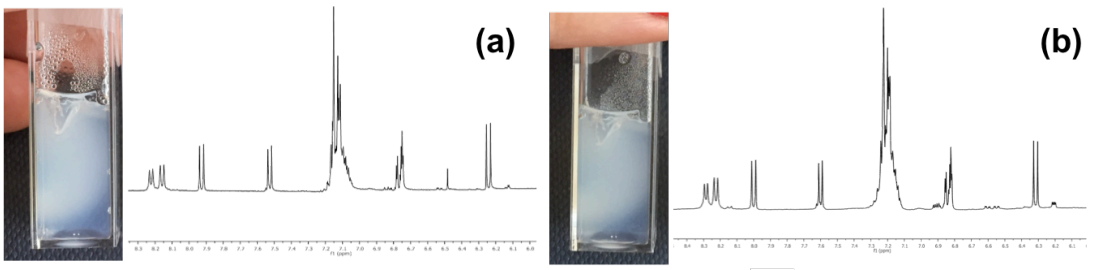

Figure 2.23(a) Photograph showing a gel formed using GdL irradiated with 365 nm for 2 hours and its NMR spectra when dried down and re-dissolved in deuterated DMSO. (b) Photograph of (a) after being irradiated with 254 nm for 5 hours and again its NMR spectra.

The effect of light intensity of the 365 nm LED was also investigated. This was done by moving the lamp to various distances away from the sample and irradiating for 15 minutes. The further away the lamp from the sample, the less intense the light. Results showed that the more intense the light, the greater the increase in G′ after 15 minutes of irradiation (Fig. 2.24). This is due to the dimerisation being slower due to the lower light intensity.

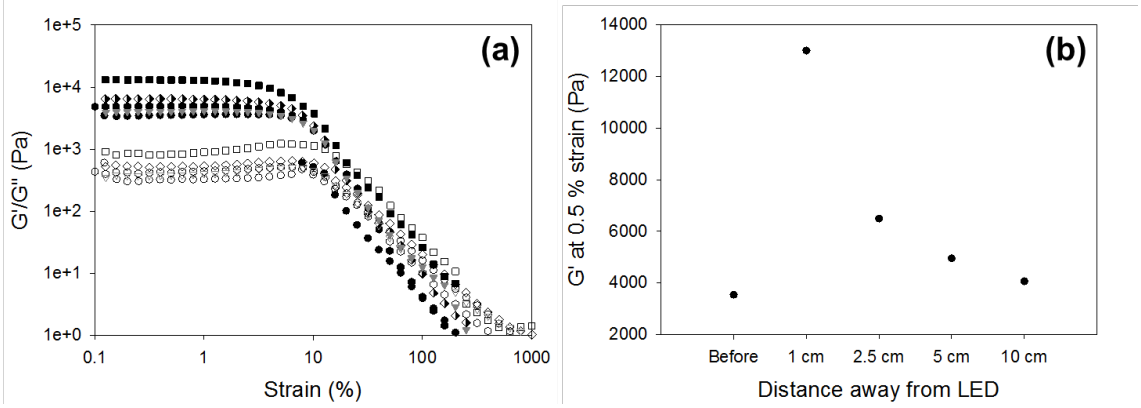

Figure 2.24 (a) Rheology data collected when placing the 365 nm LED at different distances away from the gel and irradiating for 15 minutes. Full symbols are G′ and open symbols are G″. Black data is before irradiation; square data is 1 cm away from the sample, diamond data is 2.5 cm away, hexagon data is 5 cm away and triangle data is 10 cm away. Strain sweeps were performed at 10 rad/s. (b) Graph showing G′ at 5 % strain against distance away from the sample.

As a control, drying effects were ruled out by placing a gel in the same chamber used for the irradiation; after 2 hours, the appearance (Fig. 2.25b and c) and rheological properties (Fig. 2.25a) of the gel were not changed compared to a fresh gel. The temperature of the gel during irradiation was also monitored. A 2 °C rise was measured, and hence it is unlikely that the changes in the rheological properties are due to an increase in temperature.

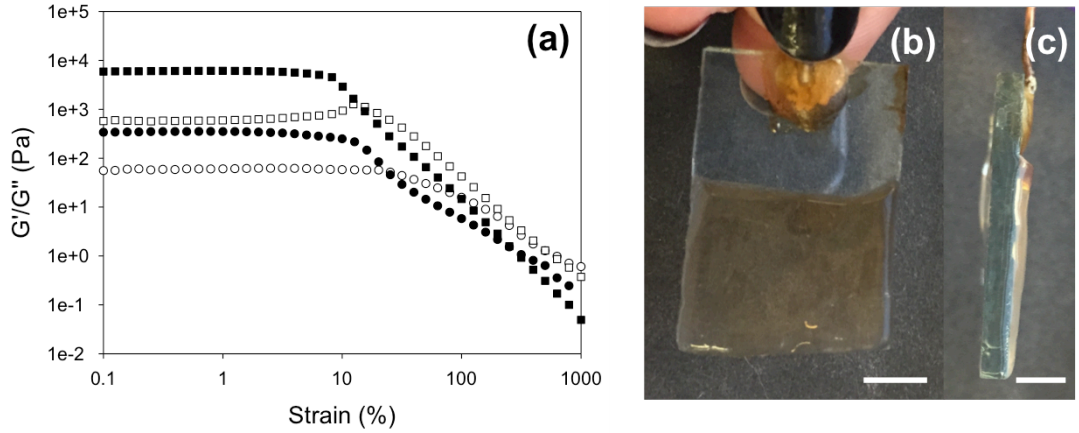

Figure 2.25 (a) Rheology strain sweeps of sample in hydrated chamber after two hours (circles) and sample irradiated with 365 nm LED for two hours (squares). Tests performed at 10 rad/s. Full symbols are G' and open symbols are G". (b) Photograph from the front of gel after two hours in chamber showing no increase in turbidity. (c) Photograph of same gel as viewed from the side showing the gel has not dried out. Scale bar represents 1 cm.

The dimer was ruled out being able to self-assemble and increase the G′ of the gel by forming the dimer in solution by irradiation for two hours (Fig. 2.26a). The pH was then lowered using GdL. Instead of gelation occurring, a precipitate was formed (Fig. 2.26b). The dimer does not form a gel and so is unlikely to be self-assembling and strengthening the gel (for example, as a second independent, self-sorted network).[40]

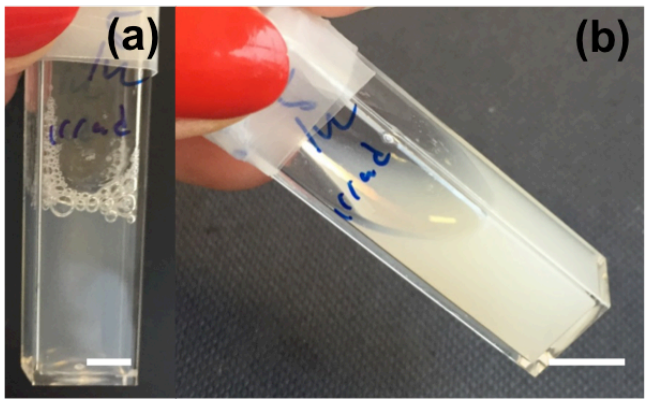

Figure 2.26 Photograph of a solution after irradiation (a) at high pH and (b) at low pH, showing no gel is formed due to the presence of the dimer. Scale bars represent 0.5 cm.

An irradiated gel formed by GdL was also re-dissolved using a small amount of sodium hydroxide solution (Fig. 2.27a), and the same was done for a gel that had not been irradiated. The UV-Vis spectrum was recorded for both solutions (Fig 2.27c

and e). The pH of both these solutions was then lowered again using GdL to a pH where a gel ought to form from the data above. The irradiated gel did not gel (Fig. 2.27b) but the non-irradiated gel did (Fig. 2.27d). This again demonstrates that the dimer is not a low molecular weight gelator and so does not form a gel.

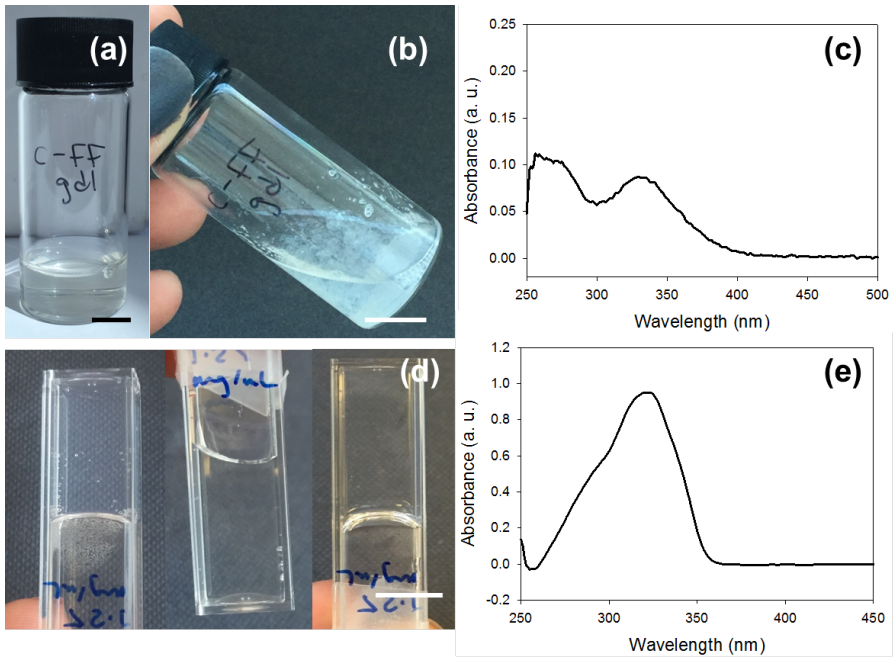

Figure 2.27 (a) Photograph showing an irradiated gel of gelator formed by GdL re-dissolved at high pH to form a transparent solution. (b) Photograph of when the pH is lowered again using GdL and no gel is formed. (c) UV-vis of solution in (a) showing that the dimer is present. (d) Control showing when a gel is not irradiated and the dimer is present that gelation is reversible with change in pH giving a transparent gel. (e) UV-Vis spectrum of gel that was not irradiated and then re-dissolved at high pH showing no dimerisation had occurred. Scale bars in all photographs represent 1 cm.

2. 3. Conclusions

In summary, a coumarin-based dipeptide gelator was synthesised that is able to form hydrogels using a pH switch, using both GdL and electrochemistry. Both gels can be photodimerised after irradiation with a 365 nm LED. Irradiation of gels formed electrochemically is more homogeneous due to the gel being thinner and the light being able to penetrate through the sample better than the bulk GdL formed gels. This irradiation leads to an increase in the rheological properties, this is believed to be caused by the dimerisation within fibres stiffening them, rather than cross-links

being formed between fibres. Irradiation for 15 minutes gave the greatest increase in rheological properties. When irradiated for more than 15 minutes with 365 nm LED the rheological strength did increase but not as much as for shorter irradiation times. This decrease in gel strength was attributed to fibres stiffening and disrupting the gel network. This opens up the possibilities to enhance gels post-gelation, or the locking in a structure by the covalent dimerization. The use of UV light could also be used to photopattern surfaces for applications such as cell culture and differentiation.[41-43]

2.4. Experimental

2. 4. 1. Synthetic Procedures

All chemicals were obtained from Sigma Aldrich and were used as received. Deionized water was used throughout.

The LMWG was prepared using the following synthetic route:

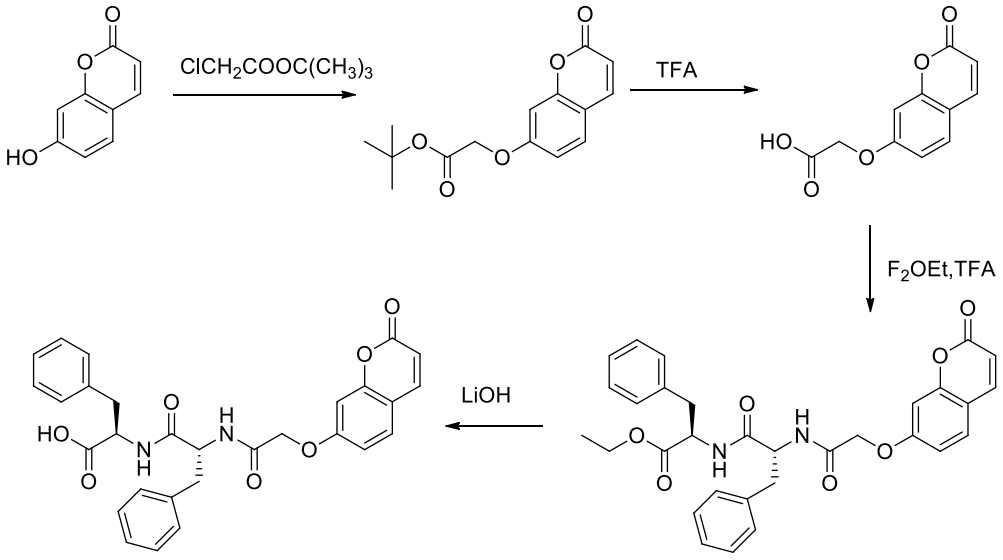

To a solution of 7-hydroxycoumarin (5.36 g, 0.033 mol) in acetone (100 mL) was added chloro-tert-butylacetate (5.21 mL, 0.036 mol) and potassium carbonate (13.8 g, 0.099 mol). The mixture was heated to 70 °C for 9 hours. After cooling, chloroform (200 mL) was added and the organic layer washed four times with water (200 mL). The organic layer was dried with magnesium sulphate and the solvent removed *in vacuo* to give a clear oil.

^{1}H NMR ($CDCl_3$) 7.63 (d, C=CH, 1H, J_{HH} = 9.5 Hz), 7.39 (d, ArH, 1H, J_{HH} = 8.6 Hz), 6.87 (dd, ArH, 1H, J_{HH} = 8.6 Hz, J_{HH} = 2.5 Hz), 6.76 (d, ArH, 1H, J_{HH} = 2.5 Hz), 6.27 (d, C=CH, 1H, J_{HH} = 9.5 Hz), 4.58 (s, OCH_2, 2H), 1.49 (s, $(CH_3)_3$, 9H) ppm. ^{13}C NMR ($CDCl_3$) 167.0, 161.1, 155.7, 143.3, 128.9, 113.7, 113.2, 112.9, 101.6, 83.1, 65.7, 41.9, 28.1 ppm. MS (ES) 299 ($[M+Na]^+$). Accurate mass calculated for $C_{15}H_{16}O_5Na$: 299.0895. Found: 299.0891.

The corresponding acid was formed by deprotecting the above product. The product was dissolved in chloroform (20 mL) and trifluoroacetic acid was added (10 mL). The solution was stirred overnight. Diethyl ether (200 mL) was added to precipitate a white solid, which was collected by filtration, washed well with ether. The solid was suspended in chloroform (100 mL), stirred for 1 hour to remove traces of the starting material and collected by filtration. The final product was isolated as a white solid in an overall 47 % yield for both steps.

^{1}H NMR (DMSO) 7.99 (d, ArH, 1H, J_{HH} = 9.5 Hz), 7.64 (d, ArH, 1H, J_{HH} = 9.1 Hz), 6.96 (m, ArH, 2H), 6.31 (d, ArH, 1H, J_{HH} = 9.5 Hz), 4.83 (s, OCH_2, 2H) ppm. ^{13}C NMR (DMSO) 169.6, 160.8, 160.2, 155.2, 129.5, 112.8, 112.7, 112.6, 101.4, 64.8 ppm. MS (CI) 221 ($[M+H]^+$). Accurate mass calculated for $C_{11}H_8O_5$: 221.0444. Found: 221.0453.

To a solution of the coumarin (1.07 g, 0.0049 mol) in chloroform (50 mL) was added N-methylmorpholine (0.60 mL, 0.0054 mol). The solution was cooled using an ice bath. To this solution was added isobutylchloroformate (0.64 mL, 0.0049 mol), followed by a mixture of the trifluoroacetate salt of diphenylalanine ethyl ester (2.24 g, 0.0049 mol) and N-methylmorpholine (0.60 mL, 0.0054 mol).[44] The solution was stirred overnight, before being washed with water (100 mL), dilute hydrochloric acid (0.1 M, 100 mL) and water (100 mL). The organic layer was dried using magnesium sulphate. The solvent was removed *in vacuo* to give a white solid, which was washed with methanol and dried. The final product was collected in an 87 % yield.

^{1}H NMR ($CDCl_3$) 7.64 (d, ArH, 1H, J_{HH} = 9.4 Hz), 7.40 (d, ArH, 1H, J_{HH} = 8.6 Hz), 7.16 (m, ArH and NH, 10H), 6.98 (m, ArH, 3H), 6.81 (dd, ArH, 1H, J_{HH} = 8.6 Hz, J_{HH} = 2.5 Hz), 6.76 (d, ArH, 1H, J_{HH} = 2.5 Hz), 6.31(m, ArH and NH, 3H), 4.73 (m,

CHNH, 2H), 4.46 (d, OCH, 1H, J_{HH} = 14.8 Hz), 4.41 (d, OCH, 1H, J_{HH} = 14.8 Hz), 4.12 (m, CH_2, 2H), 3.08 (m, CH_2Ph, 4H), 1.24 (t, CH_3, 3H, J_{HH} = 7.1 Hz) ppm. ^{13}C NMR ($CDCl_3$) 170.8, 169.8, 167.0 160.7, 159.8, 155.7, 140.1, 135.9, 135.6, 129.3, 129.2, 129.2, 128.8,128.7, 128.6, 128.5, 127.1, 128.1, 114.2, 113.8, 112.3, 102.2, 67.3, 61.6, 53.8, 53.4, 37.9, 37.8, 14.1 ppm. MS (ES) 565 $(M+Na]^+$). Accurate mass calculated for $C_{31}H_{30}N_2O_7Na$: 565.1951. Found: 565.1939.

The above product was dissolved in THF (20 mL). After dissolution, water was added (10 mL), followed by lithium hydroxide (0.25 g). Periodically, small samples were removed and added to excess water. When no precipitate was observed (typically after around 20 minutes), water was added (200 mL). The solution was filtered and then hydrochloric acid (1 M) was added until the pH of the solution was around 4. The solid product was collected by filtration, washed well with water and dried under vacuum to give the pure product in a 75 % yield.

^{1}H NMR (DMSO) 8.41 (d, NH, 1H, J_{HH} = 7.8 Hz), 8.18 (d, NH, 1H, J_{HH} = 8.6 Hz), 7.98 (d, ArH, 1H, J_{HH} = 9.5 Hz),7.60 (d, ArH, 1H, J_{HH} = 8.4 Hz), 7.16 (m, ArH, 11H), 6.83 (m, ArH, 2H), 6.31 (d, ArH, 1H, J_{HH} = 9.5 Hz), 4.63 (m, CHNH, 1H), 4.55 (s, OCH_2, 2H), 4.46 (m, CHNH, 1H), 3.09 (dd, CHPh, 1H, J_{HH} = 13.9 Hz, J_{HH} = 5.1 Hz), 3.02 (dd, CHPh, 1H, J_{HH} = 13.9 Hz, J_{HH} = 5.1 Hz), 2.93 (dd, CHPh, 1H, J_{HH} = 8.7 Hz, J_{HH} = 8.7 Hz), 2.81 (dd, CHPh, 1H, J_{HH} = 9.9 Hz, J_{HH} = 9.8 Hz) ppm. ^{13}C NMR (DMSO) 172.8, 170.7, 166.6, 160.7, 160.2, 155.1, 144.2, 137.5, 137.4, 129.4, 129.2, 129.1, 128.1, 127.9, 126.4, 126.2, 112.8, 112.6, 101.5, 66.8, 53.6, 53.3, 37.4, 36.7 ppm. MS (ES) 537 ($[M+Na]^+$). Accurate mass calculated for $C_{29}H_{26}N_2O_7$-Na: 537.1638. Found: 537.1635.

2. 4. 2. Instruments and Procedures

Mass Spectroscopy

Measurements were carried out using a Micromass LCT Mass Spectrometer in positive mode at 40 V in methanol. Samples were run by the University of Liverpool mass spectrometry service.

Nuclear Magnetic Resonance (NMR) Spectroscopy

NMR spectra were recorded using a Bruker DPX-400 spectrometer operating at 400 MHz for ^{1}H NMR and 100 MHz for ^{13}C, in deuterated DMSO.

Hydrogel Formation

Gels formed using a pH switch were prepared at a concentration of 5 mg/mL of gelator unless otherwise stated. Glucono-δ-lactone (GdL) was used to lower the pH. The gelator was added to 2 mL of water with an equimolar amount of sodium hydroxide (NaOH) (0.1 M, aqueous). The solution was stirred until all the gelator was dissolved. This solution was then transferred to a vial containing 8 mg/mL of GdL and shaken gently. This was then left to stand to allow gelation to occur within a few hours. Rheological properties of these gels were measured around 16 hours after the GdL was added.

For gels formed electrochemically, the gelator was added to 20 mL of water at a concentration of 5 mg/mL. After the gelator was fully dissolved using an equimolar amount of 0.1 M sodium hydroxide solution the pH was adjusted to pH 9 using 0.1 M aqueous hydrochloric acid. A background electrolyte of 0.1 M sodium chloride (100 μL per 10 mL solution) was then added to the gelator solution and then 7.2 mg/mL of hydroquinone. The solution was stirred until the hydroquinone was fully dissolved. Gels were formed on an indium doped tin oxide (ITO) covered glass slide working electrode cut to 2.5 cm by 5 cm. The counter and reference electrode used were Dropsens printed electrodes. The working, counter and reference electrodes were placed in the gelator solution and a current of 1 μA was applied for 800 seconds using a Dropsens potentiostat. This current reduced the pH at the glass slide by oxidising the hydroquinone to quinone. The glass slide with the now formed gel could be removed from solution. The same solution was then used to form the gels.

Rheological Measurements

Dynamic rheological measurements were performed using an Anton Paar Physica MCR101 rheometer and MCR301. For electrochemically formed gels, measurements were carried out using a parallel plate system with a gap of 1 mm. A 25 mm plate was used for both strain and frequency sweeps. Gels were formed electrochemically on ITO as described above. These gels were carefully removed from the glass and

onto the plate so that measurements could be performed. For gels formed by GdL a vane and cup measuring system was used with a gap of 1 mm. All experiments were performed at 25 °C.

Strain sweep: Strain scans were performed from 0.1 – 1000% strain at a frequency of 10 rad/s. Gel breakdown was quoted as the strain at which the storage modulus (G′) deviates from linearity.

Frequency sweep: Frequency scans were performed at 1 rad/s to 100 rad/s under a strain of 0.5 %. The shear modulus (storage modulus (G′) and loss modulus (G″)) are read at 10 rad/s. These measurements were done within the viscoelastic region were G′ and G″ are independent of strain amplitude.

UV-Vis Absorption Measurements

Solution UV-Vis absorption data were measured using a Thermo Scientific Nanodrop 2000/2000c spectrophotometer. The spectrophotometer was used in cuvette mode where samples were prepared in plastic cuvettes with a pathlength of 1.0 cm. Aqueous samples were prepared at high pH using equimolar amounts of 0.1 M aqueous NaOH solution to gelator and made up to 2 mL with distilled water. The solution was then diluted with basic water until the absorbance was visible in the spectrum. The cuvette top was then sealed with parafilm before being irradiated with 365 nm LED and the absorption measured again.

UV-Vis absorption spectra of electrochemically formed gels were recorded by removing the gel from glass slides and dissolved in DMSO and diluted until a spectrum could be recorded. For pieces of the same gel, samples were diluted by the same amount each time.

UV-Vis absorption measurements of gelled samples were prepared at a concentration of 1.25 mg/mL in a 1 mm pathlength quartz cuvette. Measurements were recorded using a Shimadzu UV-2550 UV−Vis spectrophotometer running the UV Probe software, version 2.34 with a slit width of 5 nm. Again, the cuvette top was sealed before being irradiated.

Fluorescence Measurements

Fluorescence was carried out on the gels formed by GdL and solutions at a concentration of 1.25 mg/mL using 1 mm pathlength plastic cuvettes with a pathlength of 1 cm. Measurements were recorded using a Perkin Elmer LS 55 Fluorescence Spectrometer with 5 nm slit widths and at an excitation of 340 nm.

Fourier Transformed Infra-Red (FTIR) Spectroscopy

IR spectra were collected on a Bruker Tensor 27 FTIR spectrometer at a resolution of 2 cm^{-1} with spectral averaging over 64 scans. Measurements were collected using the ATR accessory. Both GdL and electrochemically formed samples were measured wet and measured before and after irradiation with UV light.

Irradiating Samples

Gels were kept on the ITO glass electrode and placed inside a plastic petri dish with a wet paper towel in to keep the air saturated with water and to prevent the gel drying out. The lid of the petri dish had a hole around 3 cm x 3 cm cut out to allow the LED to be able to irradiate the sample. A 365 nm LED (LedEngin Inc, LZ1-10U600) light source powered by a TTi QL564P power supply operating at 1.0 W was used to irradiate gel samples. The sample was moved around to ensure whole sample was exposed to the UV light. Samples were exposed for different set time times before their rheological properties were measured. Samples for UV-vis were prepared in cuvettes and again left for set times before measurements were recorded.

Scanning Electron Microscopy (SEM) Imaging

SEM images were obtained using a Hitachi S-4800 FE-SEM at 3 keV. Gel was deposited onto glass cover slips that were fixed onto aluminium SEM stubs with carbon tabs and left to dry for 24 hours. The samples were gold coated for 3 minutes at 15 mA prior to imaging using a sputter coater (EMITECH K550X). Fibre widths were measured from the SEM images. The diameter of at least 90 fibres were measured using the ImageJ line tool (version 1.49) and a frequency distribution obtained. SEM images and image analysis were done by Dr. Tom McDonald.

Temperature Measurements

The temperature of the gels was recorded before and after irradiation with 365 nm LED using a Precision Gold N85FR infrared thermometer with dual laser targeting. The temperature of the gels before irradiation was typically around 18 °C and after irradiation for 2 hours the temperature of the gels rose to 20 °C.

2. 5. References

1. P. Terech and R. G. Weiss, *Chemical Reviews*, 1997, **97**, 3133-3160.
2. S. Datta and S. Bhattacharya, *Chem. Soc. Rev.*, 2015, DOI: 10.1039/C5CS00093A.
3. J. Raeburn, A. Zamith Cardoso and D. J. Adams, *Chem. Soc. Rev.*, 2013, **42**, 5143-5156.
4. R. G. Weiss, *J. Am. Chem. Soc.*, 2014, **136**, 7519-7530.
5. J. Raeburn, C. Mendoza-Cuenca, B. N. Cattoz, M. A. Little, A. E. Terry, A. Zamith Cardoso, P. C. Griffiths and D. J. Adams, *Soft Matter*, 2015, **11**, 927-935.
6. K. J. C. van Bommel, C. van der Pol, I. Muizebelt, A. Friggeri, A. Heeres, A. Meetsma, B. L. Feringa and J. van Esch, *Angew. Chem. Int. Ed.*, 2004, **43**, 1663-1667.
7. G. M. Kavanagh and S. B. Ross-Murphy, *Prog. Polym. Sci.*, 1998, **23**, 533-562.
8. C. Chassenieux and L. Bouteiller, *Supramolecular Chemistry*, John Wiley & Sons, Ltd, 2012..
9. Y. Ding, Y. Li, M. Qin, Y. Cao and W. Wang, *Langmuir*, 2013, **29**, 13299-13306.
10. M. A. Khalily, M. Goktas and M. O. Guler, *Org. Biomol. Chem.*, 2015, **13**, 1983-1987.
11. D. D. Diaz, E. Morin, E. M. Schon, G. Budin, A. Wagner and J.-S. Remy, *J. Mater. Chem.*, 2011, **21**, 641-644.
12. M. George and R. G. Weiss, *Chem. Mater.*, 2003, **15**, 2879-2888.
13. C. Kim, S. J. Lee, I. H. Lee, K. T. Kim, H. H. Song and H.-J. Jeon, *Chem. Mater.*, 2003, **15**, 3638-3642.
14. D. D. Díaz, J. J. Cid, P. Vázquez and T. Torres, *Chem. Eur. J.*, 2008, **14**, 9261-9273.
15. S. Miljanić, L. Frkanec, Z. Meić and M. Žinić, *Eur. J. Org. Chem.*, 2006, 1323-1334.
16. Y. Huang, Z. Qiu, Y. Xu, J. Shi, H. Lin and Y. Zhang, *Org. Biomol. Chem.*, 2011, **9**, 2149-2155.
17. C.-S. Chen, X.-D. Xu, S.-Y. Li, R.-X. Zhuo and X.-Z. Zhang, *Nanoscale*, 2013, **5**, 6270-6274.
18. T. M. Doran, D. M. Ryan and B. L. Nilsson, *Polym. Chem.*, 2014, **5**, 241-248.
19. S. Khetan and J. A. Burdick, *Soft Matter*, 2011, **7**, 830-838.
20. Y. Sako and Y. Takaguchi, *Org. Biomol. Chem.*, 2008, **6**, 3843-3847.
21. K. Tanaka, *Molecules*, 2012, **17**, 1408-1418.
22. K. Gnanaguru, N. Ramasubbu, K. Venkatesan and V. Ramamurthy, *J. Org. Chem.*, 1985, **50**, 2337-2346.

23. S. H. Kim, Y. Sun, J. A. Kaplan, M. W. Grinstaff and J. R. Parquette, *New J. Chem.*, 2015, DOI: 10.1039/C5NJ00038F.
24. W. Ji, G. Liu, M. Xu, X. Dou and C. Feng, *Chem. Commun.*, 2014, **50**, 15545-15548.
25. S. Fleming and R. V. Ulijn, *Chem. Soc. Rev.*, 2014, **43**, 8150-8177.
26. F. Allix, P. Curcio, Q. N. Pham, G. Pickaert and B. Jamart-Grégoire, *Langmuir*, 2010, **26**, 16818-16827.
27. D. J. Adams, M. F. Butler, W. J. Frith, M. Kirkland, L. Mullen and P. Sanderson, *Soft Matter*, 2009, **5**, 1856-1862.
28. Y. P. a. E. Green, *J. Am. Chem. Soc.*, 1973, **95**, 113-119.
29. M. Kolbel and F. M. Menger, *Chem. Commun.*, 2001, 275-276.
30. L. A. Estroff and A. D. Hamilton, *Chem. Rev.*, 2004, **104**, 1201-1218.
31. J. Perdigao, P. Lambrechts, B. Van Meerbeek, G. Vanherle and A. L. B. Lopes, *J. Biomed. Mater. Res.*, 1995, **29**, 1111-1120.
32. K. Muthuramu and V. R. Murthy, *J. Org. Chem.,* 1982, **47**, 3976-3979.
33. J. T. Pelton and L. R. McLean, *Anal. Biochem.*, 2000, **277**, 167-176.
34. K. L. Morris, L. Chen, A. Rodger, D. J. Adams and L. C. Serpell, *Soft Matter*, 2015, **11**, 1174-1181.
35. E. K. Johnson, D. J. Adams and P. J. Cameron, *J. Am. Chem. Soc.*, 2010, **132**, 5130-5136.
36. E. K. Johnson, L. Chen, P. S. Kubiak, S. F. McDonald, D. J. Adams and P. J. Cameron, *Chem. Commun.*, 2013, **49**, 8698-8700.
37. J. Raeburn, B. Alston, J. Kroeger, T. O. McDonald, J. R. Howse, P. J. Cameron and D. J. Adams, *Mater. Horiz.,* 2014, **1**, 241-246.
38. X. Mu, K. M. Eckes, M. M. Nguyen, L. J. Suggs and P. Ren, *Biomacromolecules*, 2012, **13**, 3562-3571.
39. K. Hyun, M. Wilhelm, C. O. Klein, K. S. Cho, J. G. Nam, K. H. Ahn, S. J. Lee, R. H. Ewoldt and G. H. McKinley, *Prog. Polym. Sci.*, 2011, **36**, 1697-1753.
40. J. Raeburn and D. J. Adams, *Chem. Commun.*, 2015, **51**, 5170-5180.
41. A. M. Kloxin, M. W. Tibbitt and K. S. Anseth, *Nat. Protocols*, 2010, **5**, 1867-1887.
42. J. Jagur-Grodzinski, *Polym. Adv. Tech.*, 2010, **21**, 27-47.
43. S. Maude, E. Ingham and A. Aggeli, *Nanomedicine*, 2013, **8**, 823-847.
44. D. J. Adams and I. Young, *J. Polym. Sci. A*, 2008, **46**, 6082-6090.

CHAPTER 3

Spatially Resolved Multi-Component Gels

3. 1. Introduction

Low molecular weight hydrogels are responsive materials, where the self-assembled small molecule gelators are held together by non-covalent forces such as π-π stacking, H-bonding and hydrophobic forces.[1-3] These gels can be responsive to changes in their environment such as temperature or pH, going back and forth between a gel and a liquid.[4] This gel-sol transition is due to a disruption in the non-covalent forces that are holding the gel network together making the gelator molecules more soluble. These forces can be restored and then gelation occurs again.[5] For example, with pH responsive gelators at high pH the molecules are soluble and so are in solution. When the pH is lowered, a gel is formed. The pH can be raised again to form a solution (Fig 3.1). This can go through many cycles, often with the strength of the gel unchanged.[6] This reversibility of gelation makes these materials useful for responsive materials such as sensors[7] and logic gates.[8-10]

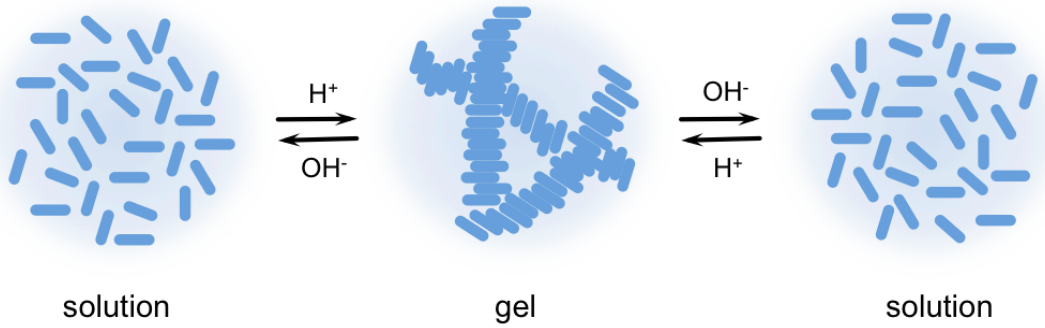

Figure 3.1 Scheme showing pH cycling sol-gel-sol process

Typically, single molecules self-assemble into one-dimensional fibres, which form the gel matrix. However, using two different molecules, each of which can individually form a gel, presents the opportunity to tune the properties of the gels further.[11, 12] When there are two gelators present in the system three types of co-assembly can occur (Fig. 3.2). The first is called narcissistic self-sorting where the molecules only form fibres with like molecules, so there are fibres consisting only of one type of molecule. Another way gelator molecules can assemble is called social self-sorting (or specific co-assembly) where there are different molecules in the same fibre but have sorted themselves into a pattern, for example ABAB. The third is

random co-assembly where there is no order in which the molecules sort themselves within the fibres.[13]

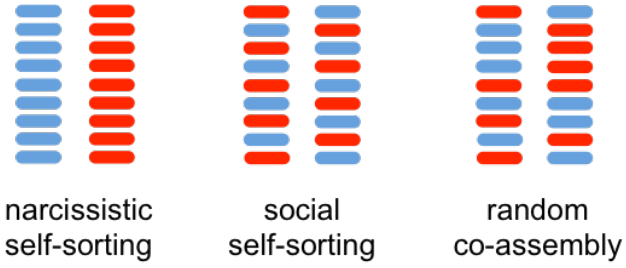

Figure 3.2 The three possible types of co-assembled fibres from a two component system.

Specific functionality could be placed within the gelators and controlled fibrous architectures suitable for bulk heterojunctions[14, 15] and cell culture[16] could be formed. Such systems could be extremely useful if the internal spatial structure of the gel could be controlled such that both networks existed in some regions, but only one network existed elsewhere. For this type of system we would need narcissistic self-sorting to occur, as social and random co-assembly would not allow one fibre to have one specific property. In the case of bulk heterojunctions, this would allow recombination of charges to happen, this is not preferential when designing a bulk heterojunction system. Narcissistic self-sorting could allow gels to be formed with specific functional groups presented only within certain areas of the gel.

To build such multi-component networks requires that we are able to control both the primary fibres and their assembled structures in space. This is difficult enough for a single component system, where there are few reliable design rules[17,18] and it is becoming more and more clear that the process of self-assembly is critical to the final gel properties.[19] For a two-component self-assembled system, the fibres could interact in different ways. Fibres of different molecules could interact with each other like for example in Fig 3.3a where they have coiled around each other. Alternatively, fibres could have little interaction with other, only in the entangling like in Fig. 3.3b. For both of these systems, it is difficult to analyse and determine what structures are present.[12]

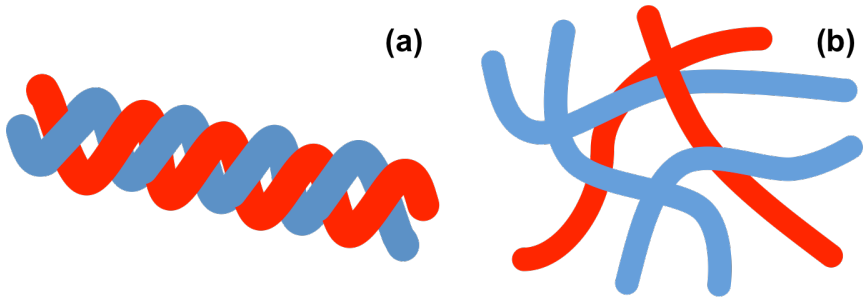

Figure 3.3 Diagrams of two self-sorted fibres systems in a gel (a) fibres interacting with each other (b) fibres with little interaction with each other.

Analysis of all these systems is difficult in the bulk and on smaller length scales. Often rheology of the mixed systems is dominated by the strongest network, but even when self-assembly or co-assembly has been proven the rheology can be stronger than expected.[20] Scattering techniques such as small angle neutron scattering (SANS) can be used to probe the primary fibre width and the structure of this fibre, but is unable to show what molecules make up the fibre.[21] In a multicomponent system, if the fibres have a significant difference in width or structure then two different signals can be seen. However, if fibres have the similar structures or width then an average of the two fibres would be seen. Microscopy techniques such as scanning electron microscopy (SEM), transmission electron microscopy (TEM), atomic force microscopy (AFM) and confocal microscopy all show fibre widths and structures. These numbers often differ than that found by scattering techniques. This is thought to be due to these microscopy techniques showing the hierarchally aggregated assembly of the primary fibres, rather than the primary fibres themselves.[12] Again this technique cannot show how the molecules are assembled, but like in the scattering analysis might show differences in structure and fibre width if they are significantly different to each other.[20] As previous mentioned in Chapter 2, it is important to consider how these samples are processed to do the image analysis, for example, in SEM samples are dried down and so my not represent the system accurately anymore.[22, 23] Other techniques such as Fourier transformed infrared (FTIR) spectroscopy show very little different for co-assembled and self-assembled gels and often look the same.[24, 25] ^{1}H nuclear magnetic resonance (NMR) spectroscopy also is not useful for determining whether the fibres are co-assembled or self-assembled, or what structures are present. When the molecules are assembled they become NMR invisible due to them being unable to diffuse.[26] Now the signal

from the protons becomes so broad due to anisotropy of all the molecules it cannot be distinguished from the baseline. Samples would need to be re-dissolved, but this would not provide any information about the systems.

A more informative way is instead looking at the assembly process as it happens by using a combination of these techniques. We have previously looked at the assembly process over time using rheology, ^{1}H NMR, change in pH, SEM and SANS.[20, 21, 26] Using these techniques we were able to distinguish between a self-assembled and co-assembled network, but were unable to understand how the fibres were arranged. To understand more about how the fibres interact, we hypothesised we could design one of the gelators to be responsive. The responsive gelator could be switched from gel-to-sol (degelation) and removed from the network to leave one gelator in the network. What happens to the remaining network would give us information about how the two different fibres were interacting with each other. This also gives the opportunity to create spatially resolved gels where both the fibres would be present in one area of the gel and only one in another.

Conceptually, these spatially resolved multi-component networks could be generated if we could form two independent self-assembled networks, and then selectively remove one of these networks only at specific points using a trigger such as, pH, light and heat. Selective melting of one network in a two-component system has been shown previously,[27] but is difficult to get accurate removal of one of the gelator in a specific area. Similarly, it is difficult to selectively remove one network using a change in pH without changing the other network or removing an area which were not targeted. To optimize spatial resolution, light-responsive gelators are a clear choice as one of the component of the system, as a mask can be used to cover parts of gel. The light will then be able to only remove the fibres exposed to the light. A number of such gelators exist such as stilbene and azobenzenes as discussed in Chapter 1. However, in all cases these have been investigated as single component systems, where the light-triggered degelation results in a spatially resolved system where one region is a gel and the other a liquid.[28-36] One example exists where the spectral properties of the gel can be altered using a light-sensitive gelator, with a gel being maintained throughout.[37] Light-responsive polymeric gel networks have also been reported.[37, 38] In order to incorporate a light-sensitive gelator as one component

of two-gelator system, we need to be able to assemble and then disassemble such a network in the presence of a second gelator network.

3. 2. Results and Discussion

We have recently shown that self-sorted networks can be formed by the slow acidification of a solution containing two different pH-triggered gelators.[20, 21, 26] To ensure that the system is self-assembled, the gelators need to have different pK_as. As the pH decreases slowly, the gelator with the highest pK_a assembles first, buffering the system before the pH reaches the pK_a of the second gelator. The slow acidification is achieved by using glucono-δ-lactone (GdL) as discussed in Chapter 2. 2. This method most often leads to the assembly of self-sorted fibres, where each fibre only contains one of the two gelators. This has already been shown that this was the case using a combination of SANS and fibre X-ray diffraction.[21] We hypothesized therefore that if one of the gelators was not only pH-triggered, but also light-triggered, this method could be used to form our required network (Fig. 3.4).

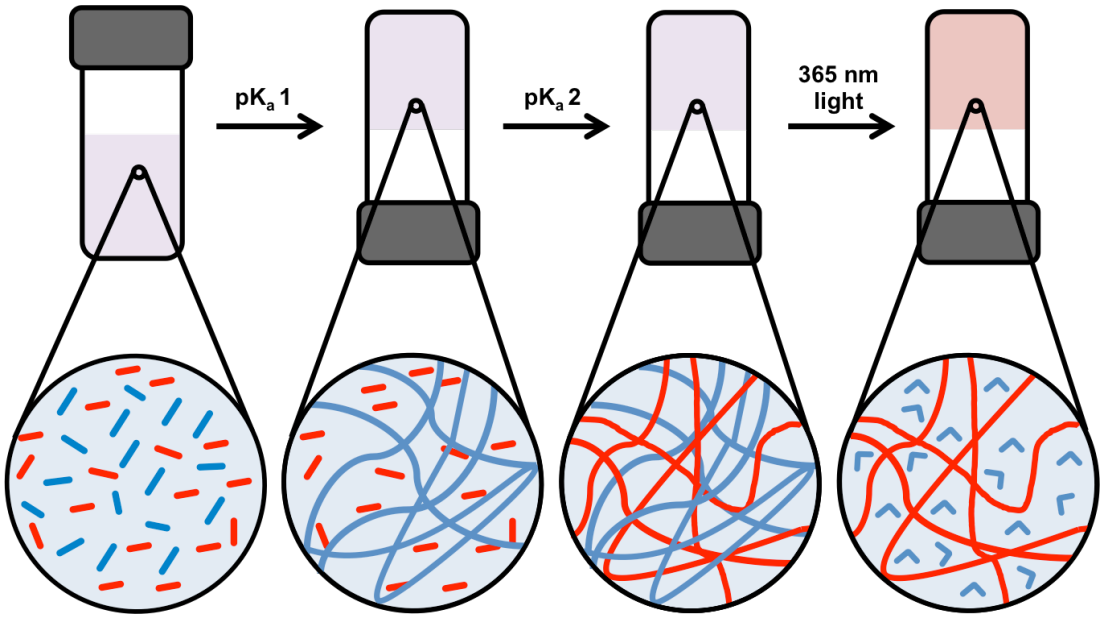

Figure 3.4 Schematic showing self-assembly of a two-component system. From left to right, both gelators at high pH, the pH then decreases to the pK_a of the first gelator and self-assembly occurs. The pH then decreases to that of the second gelator pK_a and then assembles. The first network can then be selectively removed using UV light, leaving the second network undisturbed.

A stilbene gelator, (**1**), was chosen to be part of the two-component system as it is light responsive.[39] Under 365 nm light, the *trans*-isomer (Fig. 3.5a) is changed to the *cis*-isomer (Fig. 3.5b).[40] Gelator-**1** was synthesized by the reaction of the acid chloride of 4,4'-stilbene dicarboxylic acid with phenylalanine ethyl ester, followed by deprotection with lithium hydroxide (for the full synthetic procedure see Section 3. 3). The gelator was functionalised with L-phenylalanine as it enabled the gelator to be pH responsive as the carboxylic acid is able to be deprotonated at high pH and reprotonated at low pH. The L-phenylalanine also allows extra stabilisation of self-assembled structures through π-π stacking and hydrophobic interactions. Other amino acid functionalised stilbene molecules were synthesised (L-alanine, L-tyrosine, L-leucine and L-valine functionalised stilbenes) but did not form gels. This is most likely be due to them being less hydrophobic moieties and may not provide favourable interactions. The reason for molecules being able to gel is still a poorly understood subject.

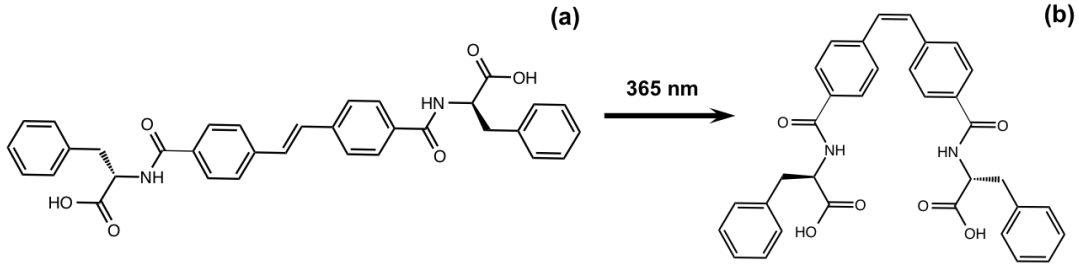

Figure 3.5 Isomerisation of (**1**) from the (a) *trans*-stilbene to the (b) *cis*-stilbene using a 365 nm LED.

The *trans*-isomer formed hydrogels when the pH of a solution at a concentration of 5 mg/mL of **1** is decreased from 10 to 4. To controllably lower the pH in a uniform manner throughout the sample, the slow hydrolysis of GdL to gluconic acid[41] was used as described in Chapter 2. 2. 5 mg/mL of GdL was used to give a translucent hydrogel (Fig. 3.6, referred to as gel-**1** throughout).[42] Gels were prepared in two ways, in a Sterilin vial (Fig. 3.6b) and using a 20 mL syringe mould (Fig. 3.6a). As discussed in Chapter 2, gels prepared in a vial could not be irradiated fully. Gel-**1** could not be formed electrochemically and so gels were prepared in a mould to give gels around 2 mm thick and 2 cm in diameter (method shown in detail in Section 3. 4. 2). Gels were prepared in this way throughout this Chapter.

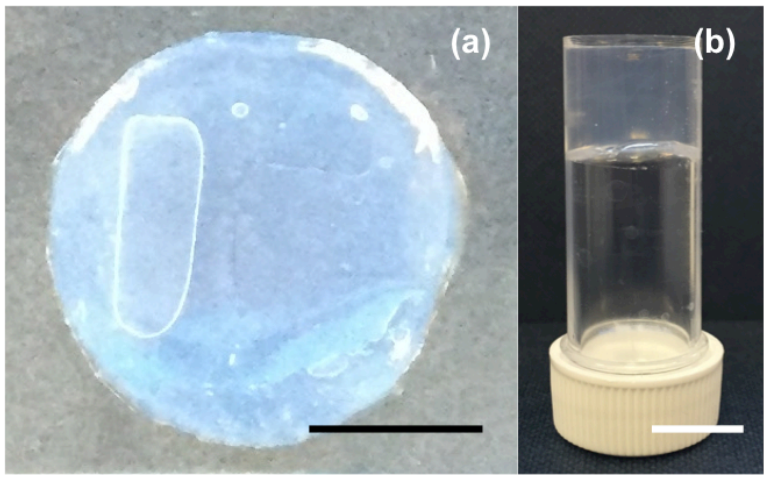

Figure 3.6 Photographs of gel-**1** prepared (a) in a mould and (b) in a vial. Scale bar represents 1 cm in both photographs.

Gel-**1** has rheological properties that are typical of this type of low molecular weight hydrogel. The storage modulus (G′) and loss modulus (G″) are relatively independent of frequency, with G′ being approximately an order of magnitude higher than G″ (9500 Pa and 700 Pa respectively) (Fig. 3.7b). Gels break at relatively low strain (~6 %) shown in Fig. 3.7a).

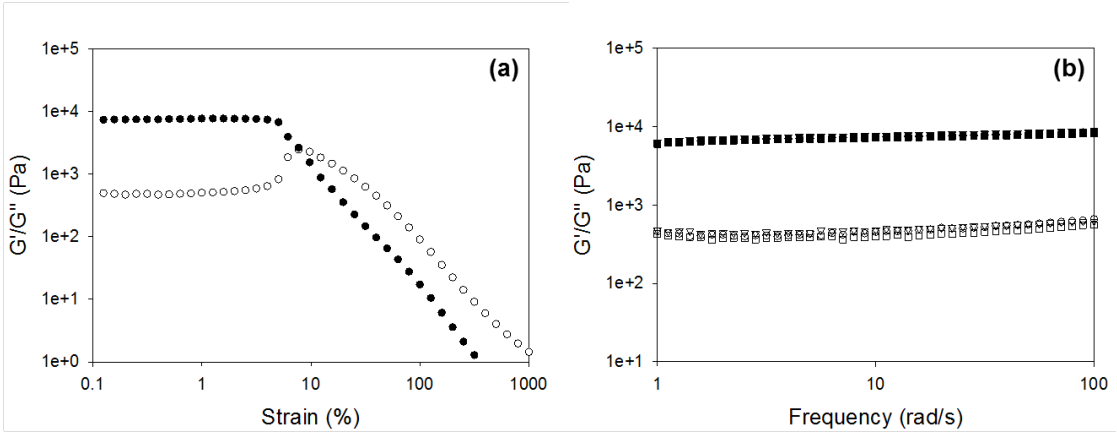

Figure 3.7 Graphs showing the rheology of gel-**1** (a) strain sweep performed at 10 rad/s and (b) frequency sweep performed at 0.5 % strain Different symbols (just seen) are for repeat experiments. All tests were carried out at 25 °C. Full symbols represent G´ and open symbols represent G″.

The apparent pK_a of **1** is 5.8 and, in agreement with our previous work, **1** forms gels when the pH is below this pK_a.[43] The apparent pK_a was determined monitoring the pH overtime when acid was added. This was done using GdL and recording the pH every minute until a gel was formed. The pK_a was then quoted as where the pH plateaued (Fig. 3.8a). This plateau is due to the carboxylic acid on the molecule

becoming protonated, and it buffers the system. This pK_a was further confirmed by adding 5 µL of 0.1 M aqueous hydrochloric acid (HCl) and then recording the pH, again this was continued until a gel was formed. (Fig 3.8b)

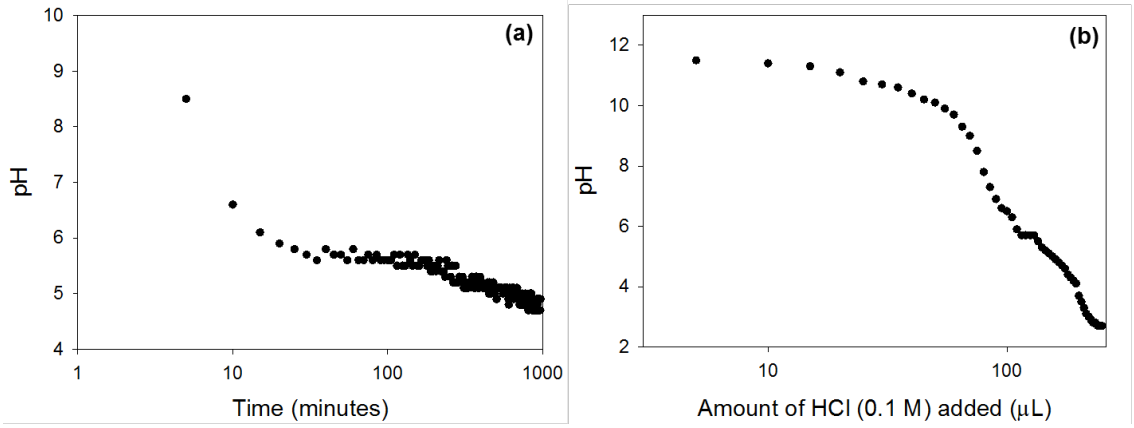

Figure 3.8 Apparent pK_a measurements of **1** using (a) GdL and (b) HCl

The corresponding *cis*-isomer of gelator **1** was formed by irradiation of a solution of **1** with a 365 nm LED at pH 10 which could be seen by UV-Vis of the solution (Fig. 3.9a).[40] The *trans*-**1** shows a peak with a maximum absorption at 340 nm (solid line) and the *cis*-**1** shows a maximum absorption at 310 nm (dashed line).[39] The attempts to carry out its gelation in a similar manner to that of *trans*-isomer **1** – by slowly decreasing the pH of the *cis*-isomer containing solutions – resulted in a precipitate rather than a gel (Fig. 2.9b), showing that the *cis*-isomer is not an effective gelator. Instead of showing a fibrous network, the SEM (Fig. 2.9c, Collected by Dr. T. McDonald, University of Liverpool.) shows spherical, undefined aggregates, again showing that *cis*-**1** is not an effective gelator.

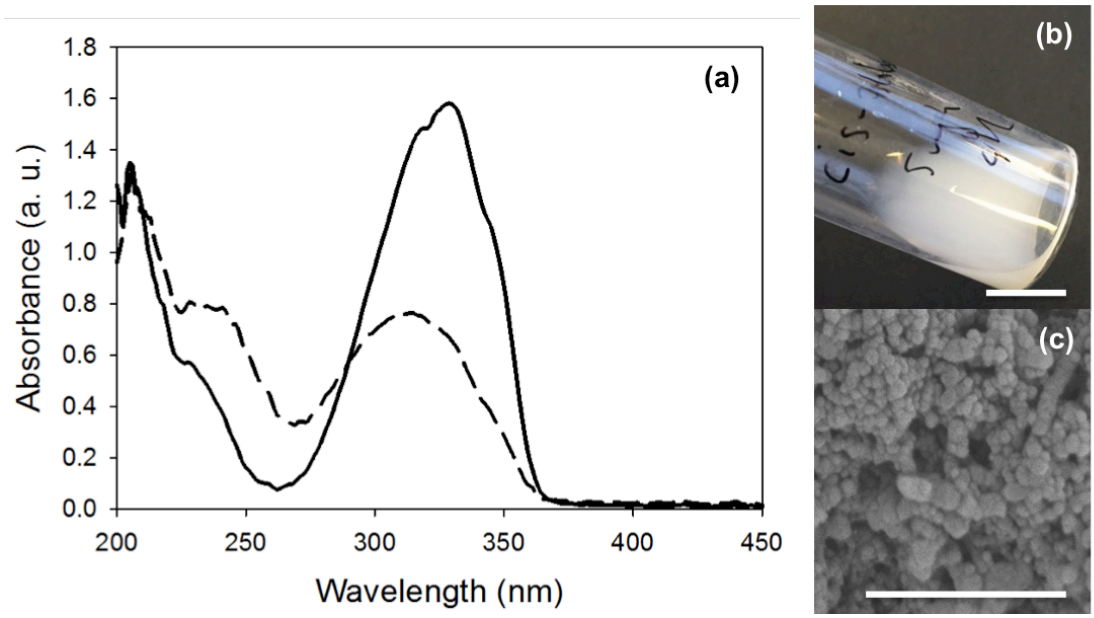

Figure 3.9 Formation of the *cis*-**1** isomer (a) UV/vis of *trans*-**1** in solution (solid line) and after 30 minutes irradiation with a 365 nm LED to form the *cis*-**1** isomer (dashed line), both at a concentration of 1.25 mg/mL in pH 10 water. (b) Photograph of 5 mg/mL solution of *cis*-**1** at pH 3. Scale bar represents 1 cm. (c) SEM image of dried down solution of solution in (b). Scale bar represents 500 nm. SEM collected by Dr. T. McDonald, University of Liverpool.

When the gel prepared using *trans*-isomer **1** was irradiated with the 365 nm LED, it converted to a liquid (Figure 3.10a). The rheology also shows that **1** is no longer a gel (Fig. 3.10b). A gel-sol transition has occurred due to *cis*-**1** being formed in the gel, as it is no longer an effective gelator, the gel falls apart.

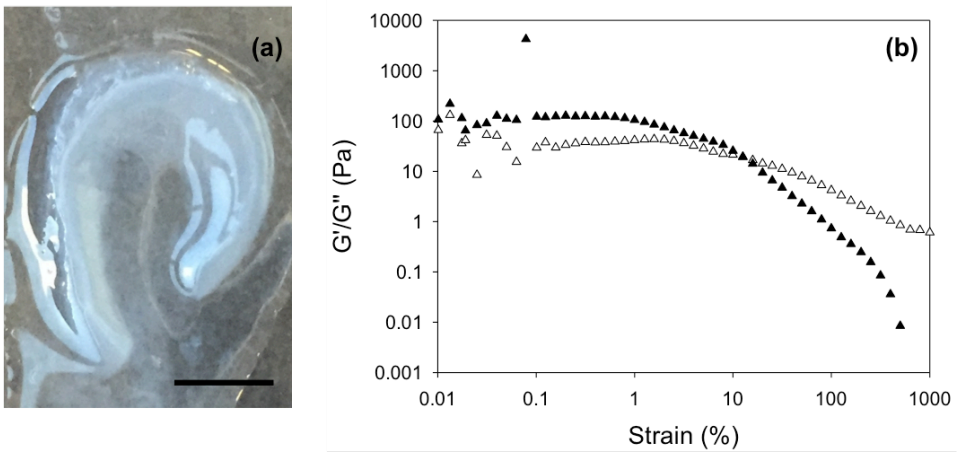

Figure 3.10 (a) Photograph of gel-**1** after irradiation with a 365 nm LED for 30 mins. (b) Strain sweep, full symbols represent G´ and open symbols represent G˝.

When a mask was used, selective spatial conversion of the gel to a liquid could be achieved, similar to other light-triggered gelators (Fig. 3.11). Where the mask was not covering the gel, the *trans*-**1** molecule is isomerised to *cis*-**1** and no longer forms a gel. This looks slightly turbid in Fig. 3.11a. The area of gel where *cis*-**1** is present then becomes a liquid and is removed from the gel without affecting the rest of the gel (Fig. 3.11b).

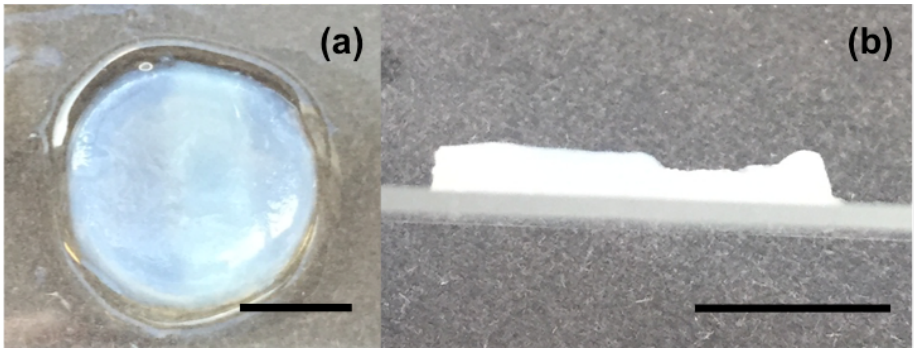

Figure 3. 11 Photographs of gel-**1** after irradiation with a 365 nm LED using a mask as viewed from (a) the top and from (b) the side. A line of removal of the gelator where the mask was not covering the gel can be seen from on top but more clearly from the side.

Xerogels of gel-**1** were imaged using SEM (collected by Dr. T. McDonald, University of Liverpool). The images showed that the gels are a result of the self-assembly of the gelator into a network of fibres (Fig. 3.12a). After irradiation, the fibres are transformed into ill-defined spherical aggregates (Fig. 3.12b). These aggregates are similar to those formed on lowering a pH of solutions containing *cis*-**1** using GdL (Fig. 3.9a).

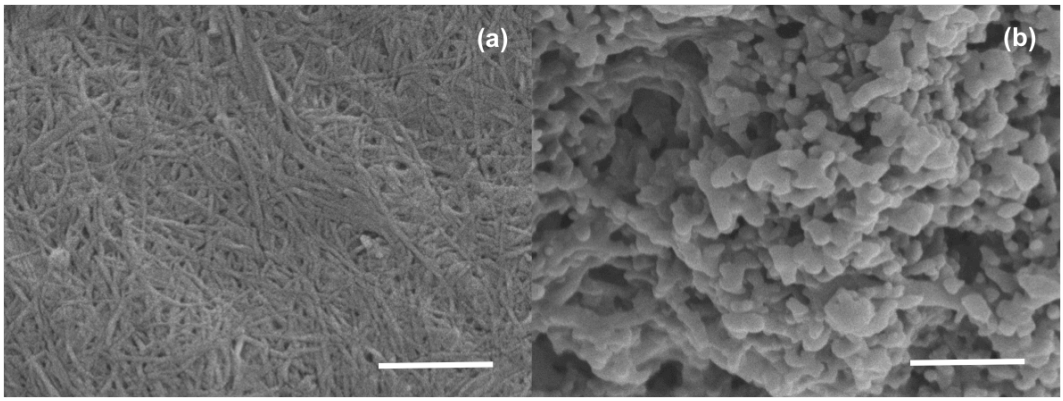

Figure 3.12 SEM images of xerogels-**1** (a) before irradiation and (b) after irradiation with a 365 nm LED. Scale bar in both pictures represents 1 μm. Collected by Dr. T. McDonald, University of Liverpool.

1 was then combined with a second gelator, **2** (Fig. 3.13). Gelator **2** was chosen on the basis of a significantly different molecular structure and the apparent pK_a of the terminal carboxylic acid (5.0);[44] our previous data suggested that both of these factors should encourage self-sorting. [20, 21]

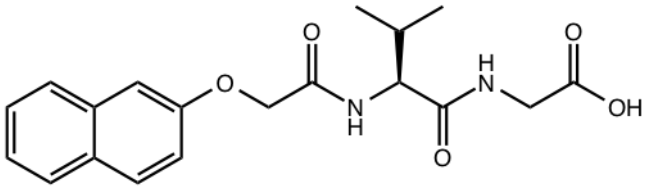

Figure 3.13 Molecular structure of gelator **2.**

Gelator **2** formed translucent gels at a gelator concentration of 5 mg/mL prepared the same was as for **1**-gel but using 8 mg/mL of GdL. Gel-**2** forms stable gels with G′ = 21,000 Pa and G″ = 6100 Pa, which break at low strain (~ 1 % strain) and are frequency independent. These gels have been reported previously (Fig. 3.14).[44]

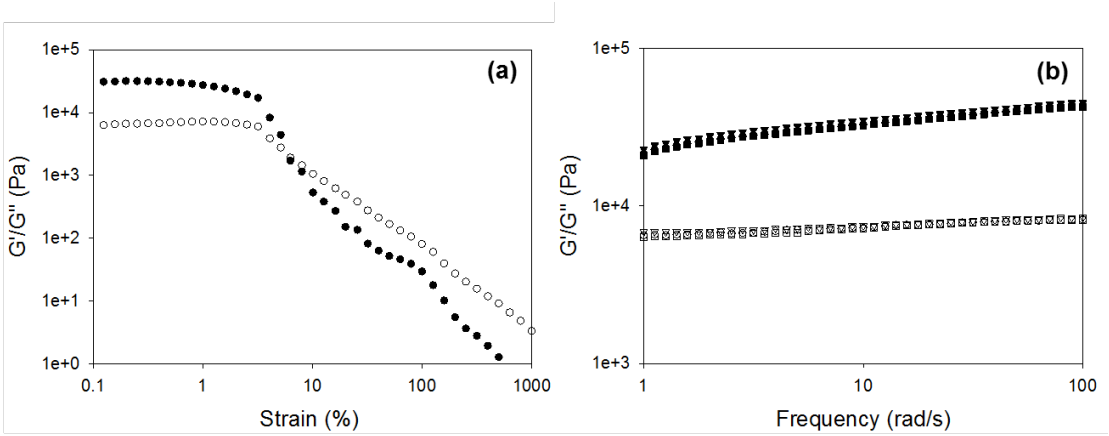

Figure 3.14 Graphs showing the rheology of gel-**2** (a) strain sweep performed at 10 rad/s and (b) frequency sweep performed at 0.5 % strain Different symbols are for repeat experiments. All tests were carried out at 25 °C. Full symbols represent G′ and open symbols represent G″.

Control experiments showed that gels formed from **2** alone (gel-**2**) were not affected by irradiation by the 365 nm LED for two hours, either visually (Fig. 3.15b) or rheologically (Fig. 3.15). Hence, it was expected that any changes in the two-component network would be due to gelator-**1** rather than gelator-**2**.

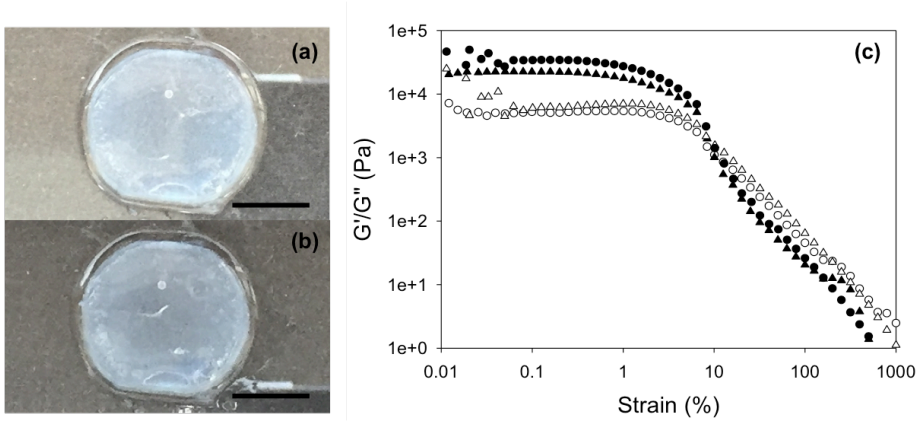

Figure 3.15 Photographs of gel-**2** (a) before irradiation and (b) after irradiation with a 365 nm LED for two hours. Scale bars represent 1 cm. (c) Rheology strain sweeps of gel-**2** before irradiation (triangle data) and after irradiation with a 365 nm LED for 2 hours (circle data). Full symbols are G´ and open symbols are G˝. Strain sweep were performed at a frequency of 10 rad/s and at 25 °C.

A mixed solution of gelator **1** and **2** was prepared at pH 10. Each gelator was prepared at 10 mg/mL at pH 10 as previously described, these solutions were then added in equal ratio to give each gelator a final concentration of 5 mg/mL and hence a total concentration of 10 mg/mL. Gels were formed from the mixed solution again by the addition of GdL, and are referred to as gel-**1,2** throughout. Gel-**1**,**2** formed translucent gels with 13 mg/mL GdL. The gels were again reproducible and stable that broke at low strain and were frequency independent with a G´ of 36,000 Pa and G˝ of 3500 Pa (Fig. 3.15a and b). Gel-**1,2** has a higher G´ and G˝ than either gel-**1** or gel-**2**. This is due to there being more material present in gel-**1,2** which has a total concentration of 10 mg/mL compared to 5 mg/mL of gel-**1** and gel-**2**.

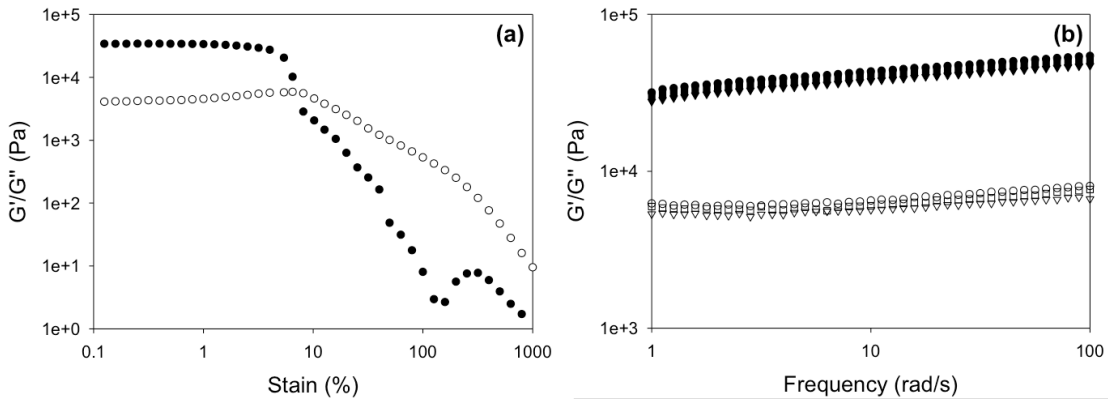

Figure 3.16 Rheology of gel-**1,2** (a) strain sweep performed at 10 rad/s and (b) frequency sweep performed at 0.5 % strain Different symbols are for repeat experiments. All tests were carried out at 25 °C. Full symbols represent G´ and open symbols represent G˝.

The use of GdL and the therefore slow pH change allows us to monitor the gelation process with time.[21, 42] The pH change over time can be used to see the stages of the gelation process. If the molecules are self-assembling, then two different plateaus should be seen for **1** and **2**. If co-assembly occurs then there would be a broader blurred plateau between the two different pK_as,[20] or no plateau at all. Fig. 3.16 show the change in pH during the gelation of **1**,**2** system. Two small plateaus can be seen at pH 5.8 and pH 5.0, with the final pH of the gel being pH 3.6. This would suggest the gelator assembling at different pH and could suggest they are self-assembled. This in formation alone does not allow us to determine how they are assembling, but gives us a clue. It also allows us to see what stage in the gelation process is at when using other techniques due to GdL high reproducibility.[19]

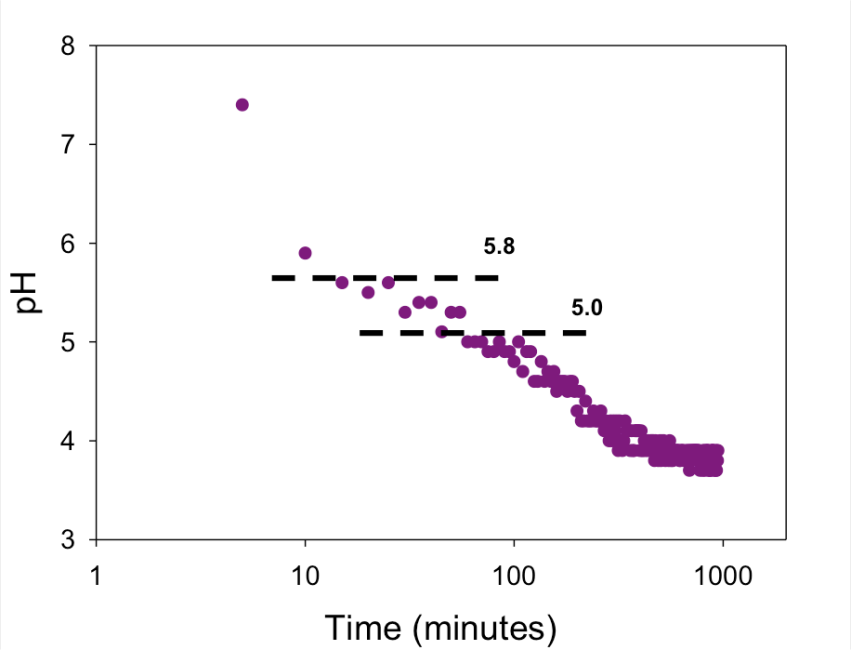

Figure 3.17 Graph showing the change in pH overtime during the gelation of **1**,**2**.

Characterization by ^{1}H NMR spectroscopy can be used to monitor gelation; as the molecules self-assemble and form fibres, the structures become NMR-invisible due to the structures becoming immobile and the signal disappearing into the baseline. A ^{1}H NMR spectrum of the solution at pH 10 was recorded and the integrals from each gelator recorded. The pH was then lowered using GdL and the spectra were recorded overtime until gelation of both molecules had occurred. An ethanol standard was added to the solution to integrate the peaks from the gelators against. This NMR data was collected by Edward Eden, University of Liverpool. The change in integral of

the peaks from each gelator was recorded overtime. In Fig. 3.17 the disappearance of CH_2 from the phenylalanine was plotted for gelator **1** (blue data), and the CH_3 peak from the valine for gelator **2** (red data). The evolution of ^{1}H NMR spectra throughout the reaction clearly demonstrates that a sequential assembly process occurs, with **1** becoming NMR-invisible before **2**. This was expected due to the differences in pK_a. Again, this data alone cannot be used to confirm absolutely whether the system is self-assembled or co-assembled.

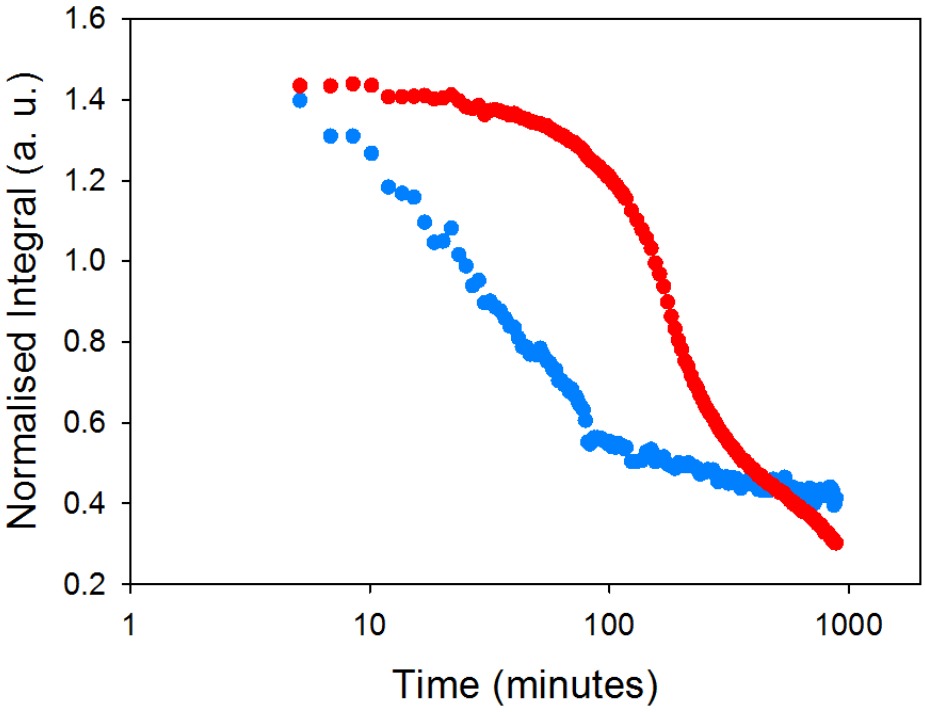

Figure 3.18 Graph showing the disappearance of ^{1}H NMR signal during gelation overtime. Blue data corresponds to the CH_2 from the phenylalanine on molecule-**1**. Red data corresponds to the CH_3 groups on the valine from molecule-**2**. Data is normalised to an ethanol standard in the sample. (Data collected by Edward Eden, University of Liverpool).

In a parallel experiment, the evolution of the rheological properties can be measured (Fig. 3.18). Rheology shows the evolution of structures in the solution. Between 0 and 8 minutes, G″ is greater than G′ (which is so low it is not recorded) showing that sample is liquid and self-assembly of the molecules has not yet occurred. After around 8 minutes, there is an increase in both G′ and G″, with a second increase occurring at around 20 minutes. Such a two-stage development in the moduli is common for this kind of gelator when using GdL to trigger the gelation.[42, 45] There is

a third increase in G′ and G″ and then a plateau after 3 hours when the sample has finished assembling.

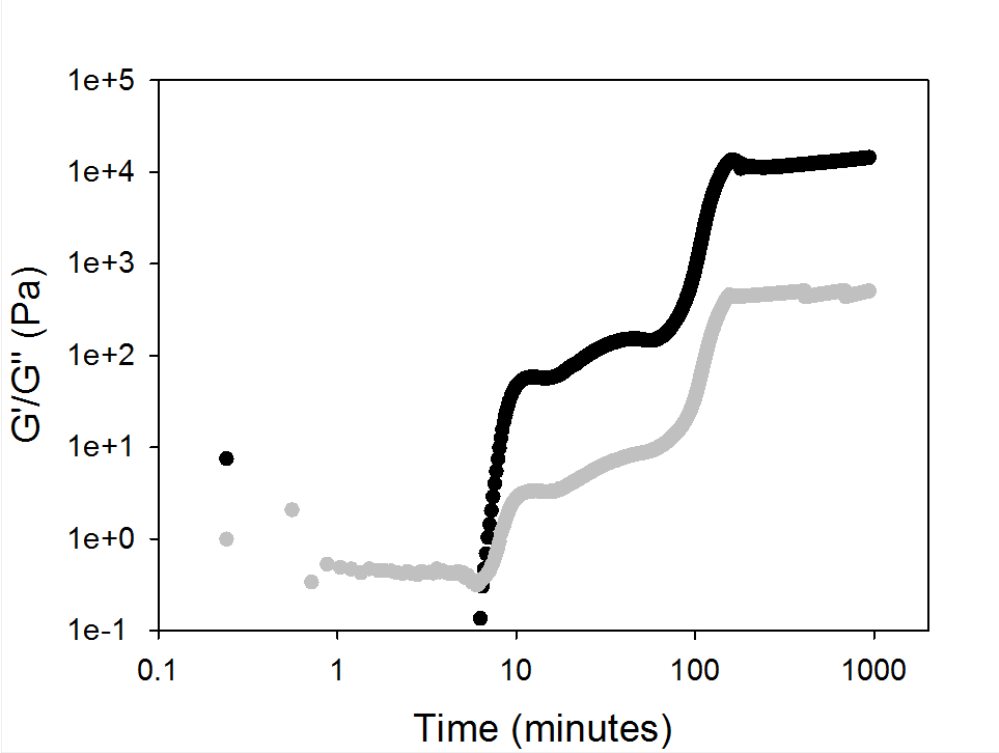

Figure 3.19 Rheological data for the evolution of gel-**1,2** network overtime. G´ is the black data and G˝ is the grey data. Measurements were performed under a strain of 0.5 %, a frequency of 10 rad/s and at 25 °C.

As previously mentioned, the hydrolysis of GdL is highly reproducible. The pH of a separate solution can be correlated with the NMR data and rheology data. It is not until this data is looked at as a whole that it can be determined what it happening (Fig. 3.19) during assembly of the molecules. It shows at 8 minutes when the pH is 5.8 (pK_a of gelator-**1**) G′ and G″ increase and intensity of ^{1}H NMR peak for gelator-**1** starts to decrease. This shows that **1** is starting assemble before **2** which remains in solution. As the pH drops further **1** continues to disappear in NMR and G′ and G″ increase further. Then the pH drops to around 5 at around 90 minutes, **2** also starts to become NMR-invisible, as expected from the pK_a of this gelator. Concurrently, there is a significant further increase in both G′ and G″. This correlates with gel-**2** formed in a single component system being significantly stronger than gel-**1**. It is noticeable that G′ at the point where only **1** has self-assembled is lower than might be expected from the data for **1** alone (Fig. 3.7). This may be due to the network forming in the presence of **2**, which may be acting as a surfactant above its apparent pK_a. Indeed,

Ulijn and co-workers have shown that similar gels can be affected by the presence of surfactant-like gelators.[46]

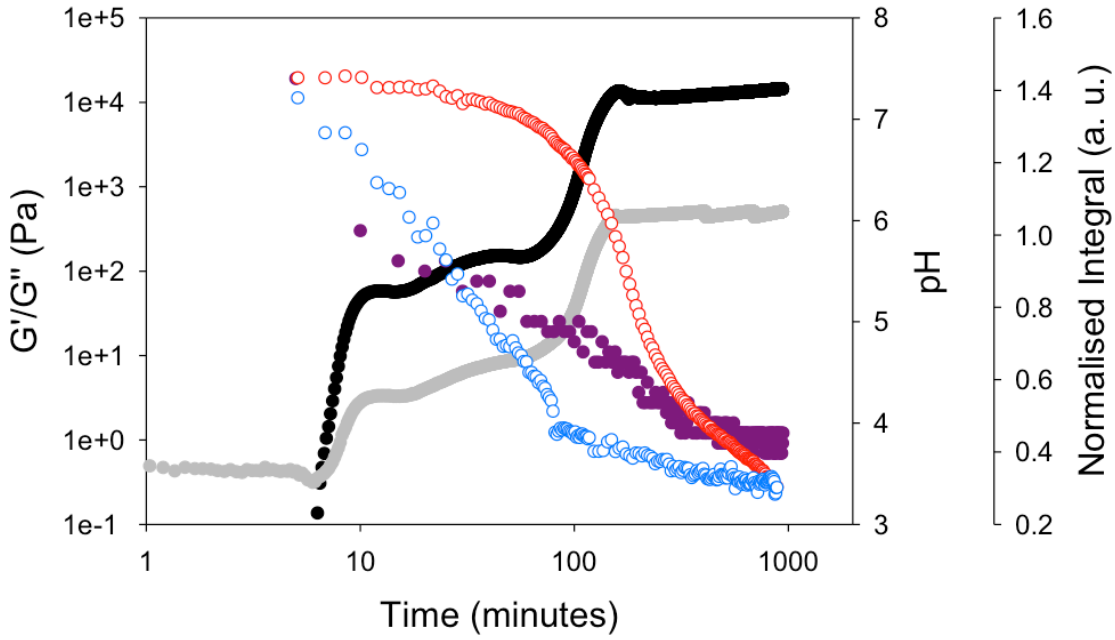

Figure 3.20 Evolution of pH (purple), G′ (black) and G″ (grey), and ^{1}H NMR integrals with time for a mixture of **1** and **2** (data for **1** in blue and for **2** in red). The sequential assembly of **1** and **2** can be seen from the changes in the NMR integrals, with the concurrent changes in the gel rheology, as each gelator assembles into fibres. The sequential assembly is controlled by the pH of the system.

It is clear that the self-assembly of **1** and **2** is a sequential process across multiple length scales. The final gel-**1,2** formed from the self-sorting mixture is both translucent and homogeneous (Fig. 3.20a). Under a hand-held UV lamp, the fluorescence from the gel is uniform in colour and intensity (Fig. 3.20b), indicating that there is no bulk phase separation or segregation of the gelators over these longer length scales. Based on our previous work, it is proposed that the sequential assembly leads to a self-sorted two-component network.[20, 21]

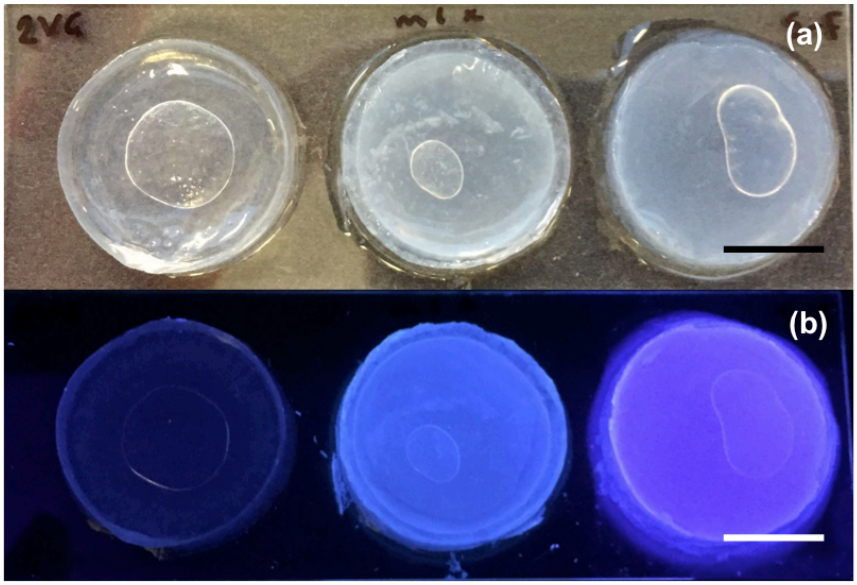

Figure 3.21 From left to right, photographs of gel-**2**, gel-**1**,**2** and gel-**1** (a) under natural light and (b) under UV light showing homogeneous two-component self-sorted networks.

Proving that the two networks are independent from each other is difficult, as the fibres from both networks look very similar, making differentiation by microscopy impossible (Fig. 3.21).

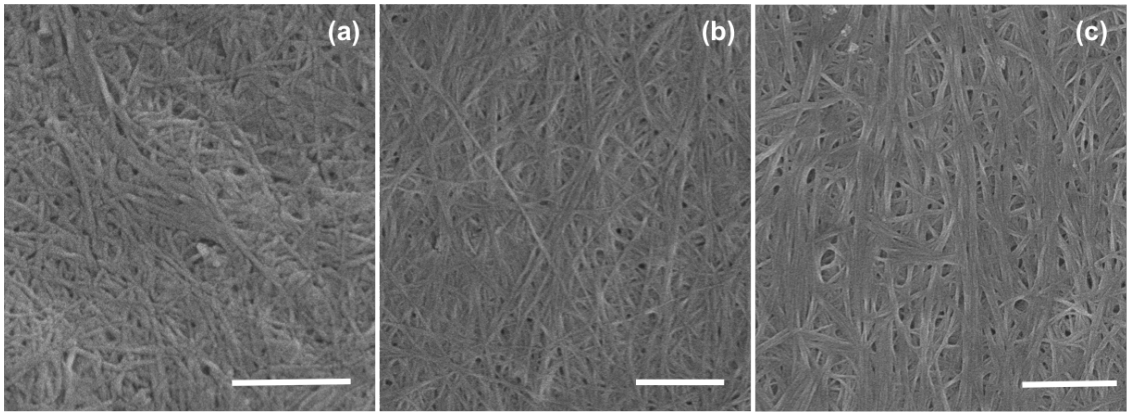

Figure 3.22 SEM images of (a) xerogel-**1,2** (b) xerogel-**1** and (c) xerogel-**2**. Scale bar on all images is 1 μm. Collected by Dr. T. McDonald, University of Liverpool.

However, if the networks are truly self-sorted then selective removal of one network should leave the other intact (Fig. 3.18). Unlike the gel-**1**, when a self-sorted gel-**1,2** is irradiated using the 365 nm LED, the gel retains its structural integrity, (Fig. 3.23) even after 2 hours irradiation with the 365 nm LED. There is change in turbidity in the gel. This is due to the now *cis*-**1** being unable to leave the gel and is now

scattering the light more due to large spherical aggregates as seen in the SEM of *cis*-**1** (Fig. 3.12b).

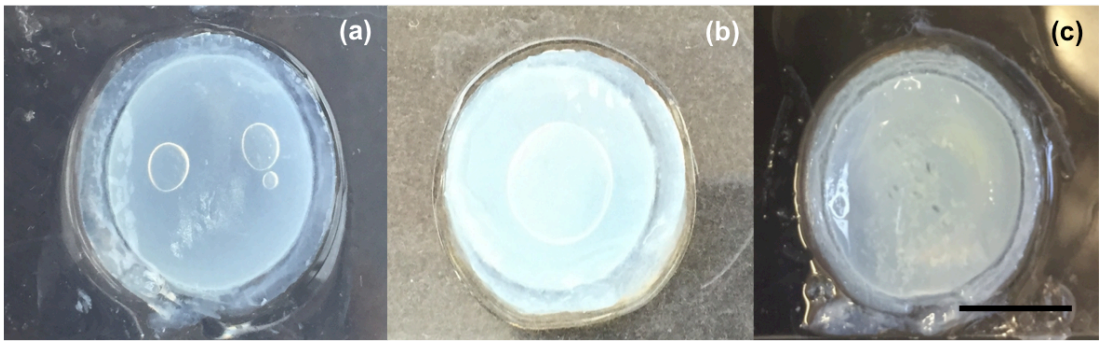

Figure 3.23 Photographs of gel-**1,2** (a) as initially formed (b) after irradiated for 30 minutes and (c) after irradiation for 2 hours under 365 nm LED.

The mechanical properties of the irradiated gels were then measured. There was a slow decrease in the rheological data for the irradiated gel compared to the as-prepared gel when the irradiation was carried out over time, with G′ decreasing from approximately 3.8 x 10^4 Pa to 1.9 x 10^4 Pa (Fig. 3.24a). After 2 hours irradiation, the rheological data then stabilised, with G′ and G″ being significantly lower than for the initially as-prepared gel (Fig. 3.24b). The data was in close agreement with that for the gel-**2**.

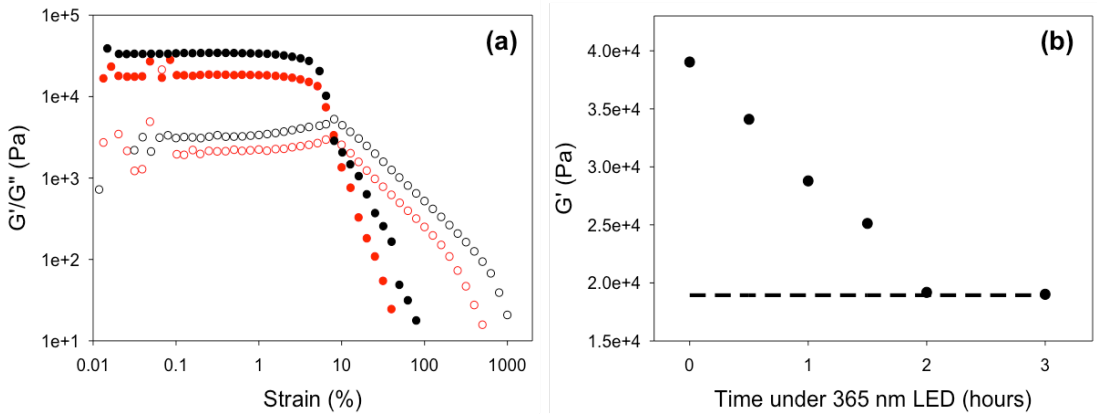

Figure 3.24 Irradiation of gel-**1,2** with 365 nm LED (a) rheology strain sweeps of gel-1,2 as formed (black data) and after 2 hours irradiation (red data). G´ is full symbols and G˝ is open symbols. Strain sweeps were performed at a frequency of 10 rad/s at 25 °C. (b) Graph showing the change of G´ at 1 %, after irradiation for up to 3 hours. Black circles represents gel-**1**,**2** and dashed data is gel-**2**.

As can be seen from the control experiments (Fig. 3.15a and b), the rheological properties of gel-**2** are essentially unaffected by light irradiation, whilst those from gel-**1** are strongly affected. The implication of this data is that under irradiation the fibres formed from **1** have been selectively removed as **1** is isomerised and that the remaining network is essentially that which would have formed in the absence of **1**. This shows a high degree of control over the fibre networks in a supramolecular gel. It should be noted that the temperature of the gels only rose by 2 °C after being irradiated for one hour, so drying out or increased temperature of the gels is unlikely to be a factor in the changes in the rheology of the system. This data suggests that the two interpenetrating networks have little interaction with each other, like in Fig. 3. 3b, as when gelator-**1** leaves the gel it does not affect gel-**2.** If the two different fibres were interacting with each other, as in Fig. 3.3a, it would be expected that when gel-**1** was removed from the network it would destroy the other gel network as it did.

Further spatial patterning was achieved by combining the irradiation step with a mask. Photographs are shown in Fig. 3.25a and b, where a star-shaped mask (shown in Fig. 3.25c) has been used to pattern the gel. Here, only the star shape was exposed to UV light for 2 hours. As can be seen, the bulk gel structure is maintained, but (most clearly under UV light), it is clear that the network formed by **1** has only been disrupted where the mask was not covering the gel.

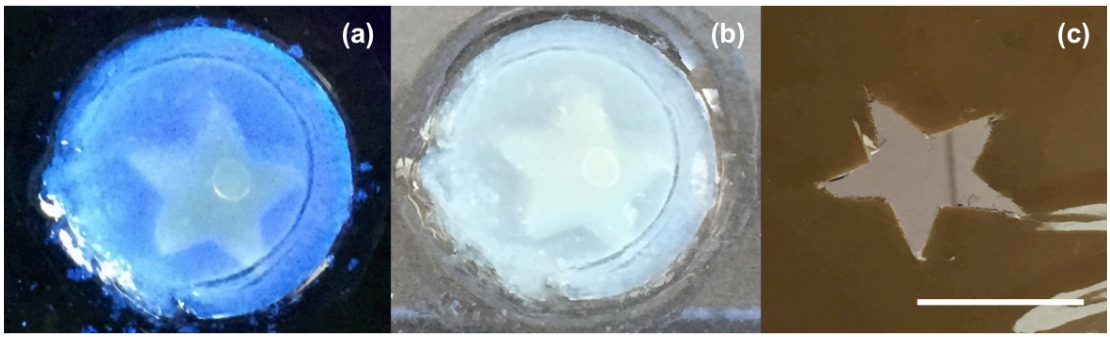

Figure 3.25 Photographs of gel-**1,2** after irradiation with a 365 nm LED for 2 hours using a mask as viewed under (a) UV light and (b) natural light. (c) Photograph of the mask used in (a) and (b). Scale bar represents 1 cm.

SEM of the dried sample shows that the areas not irradiated by the LED are still composed of fibres (Fig. 3.26a), which are similar to the networks formed by **1** and **2**. However, in the centre of the star where the self-sorted gel has been irradiated, a

dense network was found, where fibres covered in spheres can be seen in Fig. 3.26b. This is consistent with the spherical structures formed by *cis*-**1** being deposited on the fibres formed by the self-assembly of **2**.

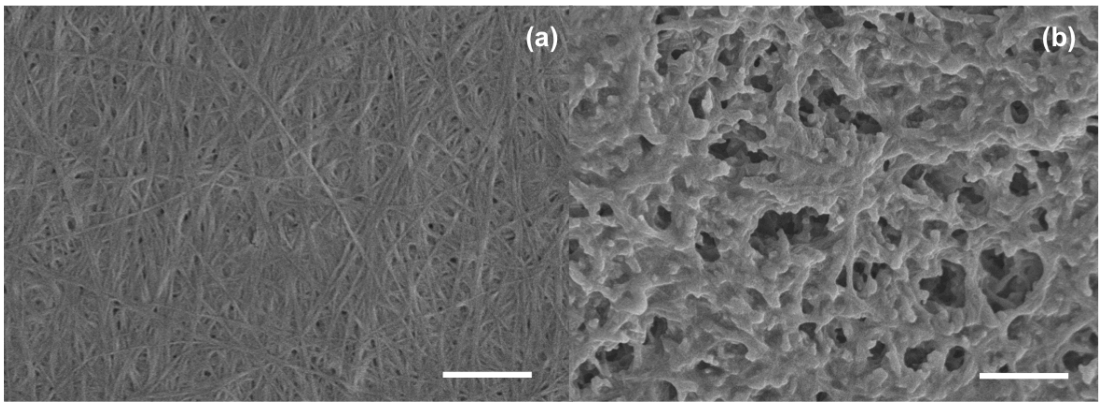

Figure 3.26 SEM images of gel-**1,2** from Fig. 3. 25. (a) is the part of the gel under the mask and so not exposed to the 365 nm LED. (b) is the centre of the star which was exposed to the 365 nm LED. Scale bars represent 1 μm. Collected by Dr. T. McDonald, University of Liverpool.

To further prove spatial resolution, a gel was freeze-dried where one half had been irradiated and the other not, again using a mask. The data (Fig. 3.27) clearly shows that where the gel was exposed to UV light, both *cis*-1 and *trans*-1 are present. The region of the gel not exposed to irradiation only contains *trans*-1. In all cases, the gels were freeze-dried before being dissolved in d_6-DMSO. Hence, all of the gelators are NMR-visible. From this data in Fig. 3.27a, it is clear that the *cis*-**1** has a doublet at approximately 8.34 ppm, whilst the *trans*-**1** has a doublet at 8.43 ppm. Before irradiation, the mixture only shows the presence of the *trans*-**1**. After irradiation, there is clearly a mixture of the *cis*-**1** and *trans*-**1**. This shows that 2 hours irradiation is not sufficient for complete isomerization, although it is sufficient for the destruction of the gel. For the gel where only one half was irradiated using a mask (Fig. 3.27b), it can clearly be seen that the side that has not been irradiated only contains the *trans*-**1**, whereas the irradiated side again contains a mixture of *cis*-**1** and *trans*-**1**. Hence, this shows that our hypothesis is correct: the mask allows spatial resolution.

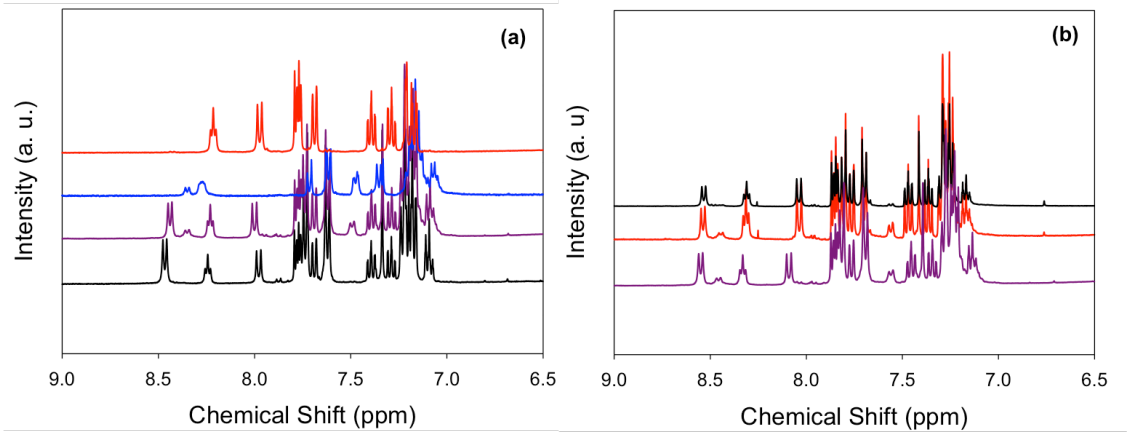

Figure 3.27 NMR data for irradiated and non-irradiated gels. (a) Data for a gelled mixture of **1** and **2** before irradiation (black data), a gelled mixture of **1** and **2** after irradiation for 2 hours (purple data), a gel of **1** alone after irradiation for 2 hours (blue data), and a gel of **2** alone after irradiation for 2 hours (red data). (b) shows the data for the non-irradiated side in black, compared to the irradiated side in red. Also shown again the irradiated mixed gel (as in (a)) in purple.

3. 3. Conclusions

It has been shown how the concept of self-sorted low molecular weight gels can be combined with photo-responsive gelators to allow a high degree of control over the rheological properties of bulk gels. Spatially resolved gels can also be prepared; one network can be selectively removed, which is a huge step forward from the state of the art. This demonstrates that the two networks initially formed must be truly independent, in close analogy with interpenetrating polymer hydrogels.[47] To the best of our knowledge, this is the first example of this type of control over multiple-component low molecular weight gels. This methodology opens up the possibility of spatially controlling the rheological properties of a gel, and allows a significant advance over the simple gel / no-gel switch that is normally observed with photoswitchable gelators. It is envisaged that this methodology could be used to prepare complex structured gels, such as p-n heterojunctions, microfluidic devices and logic gates.

3. 4. Experimental

3. 4. 1. Synthetic Procedures

All chemicals were purchased from Sigma Aldrich and were used as received unless otherwise stated. Deionized water was used throughout.

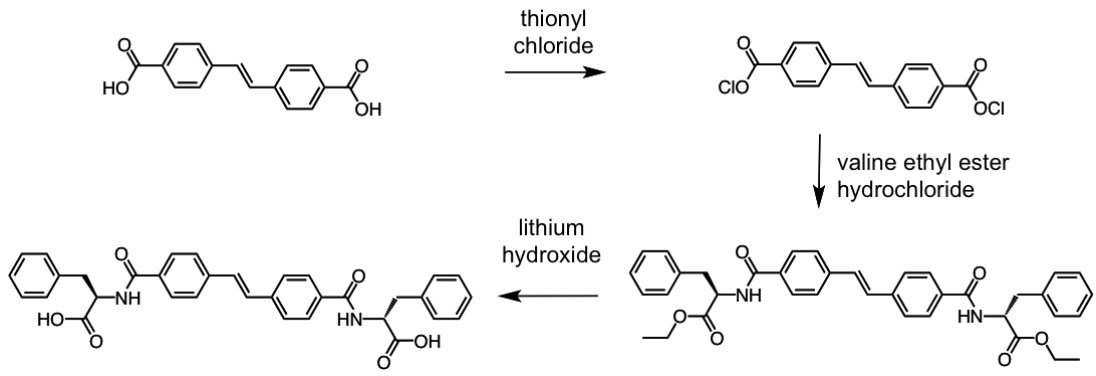

4,4'-Stilbene diphenylalanine ethyl ester

0.8 g (0.003 mol) of 4,4'-stilbene dicarboxylic acid was added to an excess of thionyl chloride (5 mL). This was refluxed at 70 °C for 90 minutes to form 4,4'-stilbene diacylchloride. Excess thionyl chloride was removed *in vacuo*. A sodium hydroxide pellet trap was used to neutralise any hydrochloric acid produced. The 4,4'-stilbene diacylchloride was suspended in 20 mL of dichloromethane (DCM) at 0 °C. A solution of 1.4 g (0.006 mol) $_{L}$-phenylalanine ethyl ester hydrochloride and 3.3 mL (0.03 mol) N-methylmorpholine in 30 mL DCM was then added dropwise to the 4,4'-stilbene diacylchloride. This was then left to react for 16 hours. The solution was then filtered to remove any unreacted 4, 4'-stilbene dicarboxylic acid. The filtered solution was then washed in 3 x 100 mL water and 1 x 10 mL acidic water. The DCM was then removed *in vacuo* to give 4,4'-stilbene diphenylalanine ethyl ester. A typical yield was around 60 – 73 %. ^{1}H NMR (400 MHz, d_6-DMSO): 8.82 (d, 2H, NH, J = 9 Hz), 7.82 (d, 4H, ArH, J = 9 Hz), 8.75 (d, 4H, ArH, J = 9 Hz), 7.42 (s, 2H, CH), 7.22 – 7.35 (m, 10H, ArH), 4.64 (m, 2H, CH), 4.17 (q, 4H, CH_2, J = 5 Hz), 3.21 (m, 4H, CH_2) and 1.21 (t, 6H, CH_3, J = 5 Hz) ppm. ^{13}C (101 MHz, d_6-DMSO): 174.9 (O-C=O), 166.0 (C=O), 137.9 (ArC), 135.6 (ArC), 133.8 (ArC),

130.0 (ArC), 129.4 (ArC), 128.6 (ArC), 128.1 (ArC), 126.5 (ArC), 54.1 (CH), 36.2 (O-CH_2), 32.2 (CH_2) and 25.2 ppm (CH_3). MS: ES^-: $[M-H]^-$. Accurate mass calculated: 617.2780. Found 617.2781.

4, 4'-Stilbene diphenylalanine (1)

Deprotection of the $_L$-phenylalanine was carried out by dissolving 4,4'-stilbene diphenylalanine ethyl ester in a THF: water mixture of 30 mL: 10 mL. Lithium hydroxide (LiOH) (0.35 g) was then added and the solution allowed to react for two hours until no precipitate was formed when a small portion was added into water. Then, 100 mL of water was added and the solution was then filtered to remove any starting material. The pH of the filtered solution was then lowered to between 3 and 4 until a white precipitate was formed. This solid was removed by filtration and dried under vacuum to give a white solid. This was then washed chloroform to remove any impurities. A typical yield was around 80 %.^{1}H NMR (400 MHz, d_6-DMSO): 12.80 (bs, 2H, OH), 7.85 (d, 4H, ArH, J = 9 Hz), 7.75 (d, 4H, ArH, J = 9 Hz), 7.44 (s, 2H, CH), 7.20-7.47 (m, 10H, ArH), 4.63 (m, 2H, CH) and 3.10-3.25 (m, 4H, CH_2) ppm. ^{13}C (101 MHz, d_6-DMSO): 174.5 (O-C=O), 162.3 (C=O), 138.2 (ArC), 135.1 (ArC), 132.9 (ArC), 129.4 (ArC), 129.0 (ArC), 128.2 (ArC), 127.8 (ArC), 136.4 (ArC), 54.0 (CH) and 32.1 ppm (CH_2). MS: ES^-: $[M-H]^-$. Accurate mass calculated: 561.2104. Found 561.2028.

Stepwise synthesis procedure for **2** is shown below:

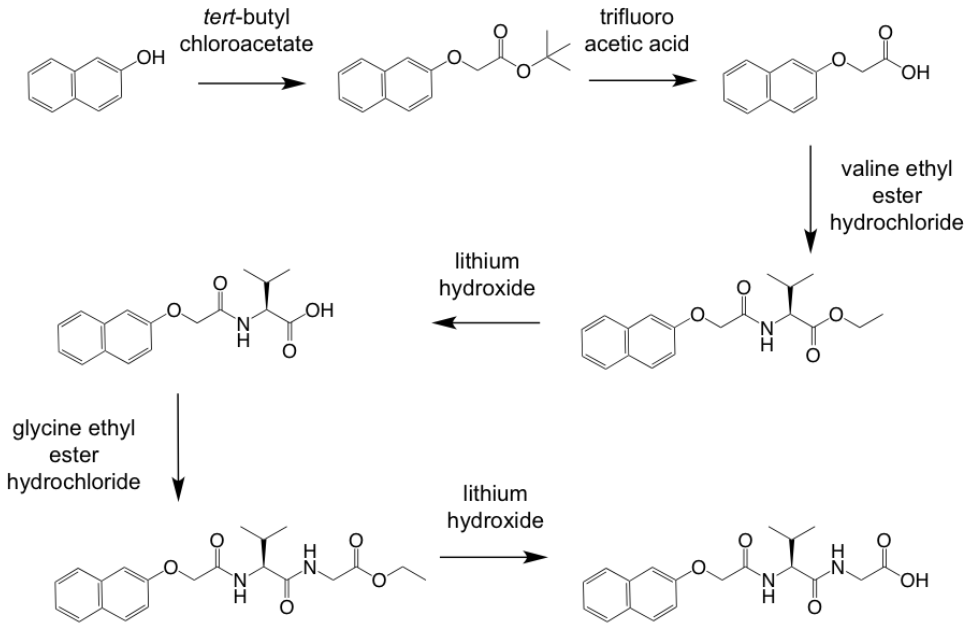

Tert-butyl 2-(naphthalen-2-yloxy)acetate

10.0 g (45.2 mmol) of 2-napthol was dissolved in 150 mL acetone before adding 30 g (226 mmol) potassium carbonate and then followed by 7.1 mL (49.7 mmol) of *tert*-butyl chloroacetate, The solution was heated to reflux for 24 hours. When cooled to room temperature, 100 mL of chloroform was added and the solution was washed with 4 x 100 mL water, dried with magnesium sulphate and the solvent removed *in vacuo* to afford a white powder. The crude product was directly used in the next step of the reaction. $_1$H NMR ($CDCl_3$): 7.77 (d, ArH, 1H, J = 8.0 Hz), 7.76 (d, ArH, 1H, J = 9.0 Hz), 7.70 (d, ArH, 1H, J = 8.2 Hz), 7.43 (t, ArH, 1H, J = 6.9 Hz), 7.34 (t, ArH, 1H, J = 7.0 Hz), 7.23 (dd, ArH, 1H, J = 9.0 Hz, J = 2.6 Hz) , 7.06 (d, ArH, 1H, J = 2.4 Hz), 4.63 (s, OCH_2, 2H), 1.49 (s, $C(CH_3)_3$, 9H) ppm.

2-(Naphthalen-2-yloxy)acetic acid

The *tert*-butyl protecting group was then removed by dissolving tert-butyl 2-(naphthalen-2-yloxy)acetate from previous step in 30 mL chloroform. Around 10 mL trifluoroacetic (TFA) acid was added and the solution was left to stir overnight. Next 200 mL of hexane was added to precipitate out the solid product. The white solid material was washed with hexane to give the product with a yield of ~87%. ^{1}H NMR (d_6-DMSO): 7.85 (d, ArH, 1H, J = 9.1 Hz), 7.79 (d, ArH, 1H, J = 8.1 Hz), 7.46 (t, ArH, 1H, J = 6.7 Hz), 7.36 (t, ArH, 1H, J = 6.9 Hz), 7.27 (d, ArH, 1H, J = 2.5 Hz), 7.22 (dd, ArH, 1H, J = 8.9 Hz, J = 2.6 Hz), 4.81 (s, OCH2, 2H) ppm.

2-(Naphthalen-2-yloxy)valine ethyl ester

N-methylmorpholine (1.7 ml, 15.5 mmol) and isobutylchloroformate (2.2 mL, 17.0 mmol) were added to a solution of 2-(naphthalen-2-yloxy)acetic acid (5.21 g, 15.5 mmol) in 100 mL chloroform and stirred for 5 min at 0 ºC. A solution of $_L$-valine methyl ester (2.5 g, 16.3 mmol) and N-methylmorpholine (1.7 mL, 15.5 mmol) in chloroform (25 mL) was added. The solution was allowed to warm to room temperature with stirring overnight. The solution was washed with 4 x 100 mL water 1 x 30 mL 0.1 M HCl and dried with magnesium sulphate before removing the solvent in vacuo to give a white powder. ^{1}H NMR (d_6-DMSO): 8.23 (m, NH, 1H), 8.20 (d, ArH, 1H, J = 8.6 Hz), 7.88 (d, ArH, 1H, J = 6.6 Hz), 7.54 (m, ArH, 3H), 7.40 (t, ArH, 1H, J = 8.0 Hz), 6.90 (d, ArH, 1H, J = 7.7 Hz), 4.82 (d, OCH_2, J = 3.9 Hz), 4.26 (dd, CHNH, 1H, J = 5.6 Hz, J = 8.6 Hz), 2.50 (m, $CH(CH_3)_2$, 1H), 0.92 (d,

CH_3, 3H, J = 4.0 Hz), 0.89 (d, CH_3, 3H, J = 4.0 Hz) ppm. ^{13}C NMR (DMSO) 173.1, 168.0, 153.6, 134.4, 127.9, 126.9, 126.4, 125.8, 125.2, 121.9, 120.9, 106.0, 67.3, 57.2, 30.3, 19.5, 18.3 ppm. MS (CI) 319 ($[M+NH_4]^+$). Analysis calculated for $C_{17}H_{19}NO_4$: C, 67.76 %; H, 6.36 %; N, 4.65 %. Found: C, 67.69 %; H, 6.37 %; N, 4.63 %.

2-(Naphthalen-2-yloxy)valine

Deprotection of 2-(naphthalen-2-yloxy)valine methyl ester was dome by dissolving in in a THF: water mixture of 30 mL: 10 mL. LiOH (0.35 g) was then added and the solution allowed to react for two hours until no precipitate was formed when a small portion was added into water. Then, 100 mL of water was added and the solution was then filtered to remove any starting material. The pH of the filtered solution was then lowered to between 3 and 4 until a white precipitate was formed. This solid was removed by filtration and dried under vacuum to give a white solid. This was then washed chloroform to remove any impurities. A typical yield was around 85 %. ^1H NMR (DMSO) 8.23 (m, NH, 1H), 8.20 (d, ArH, 1H, J = 8.6 Hz), 7.88 (d, ArH, 1H, J = 6.6 Hz), 7.54 (m, ArH, 3H), 7.40 (t, ArH, 1H, J = 8.0 Hz), 6.90 (d, ArH, 1H, J = 7.7 Hz), 4.82 (d, OCH_2, J = 3.9 Hz), 4.26 (dd, CHNH, 1H, J = 5.6 Hz, J = 8.6 Hz), 2.50 (m, $CH(CH_3)_2$, 1H), 0.92 (d, CH_3, 3H, J = 4.0 Hz), 0.89 (d, CH_3, 3H, J = 4.0 Hz) ppm. ^{13}C NMR (DMSO) 173.1, 168.0, 153.6, 134.4, 127.9, 126.9, 126.4, 125.8, 125.2, 121.9, 120.9, 106.0, 67.3, 57.2, 30.3, 19.5, 18.3 ppm. MS (CI) 319 ($[M+NH4]^+$). Analysis calculated for $C_{17}H_{19}NO_4$: C, 67.76 %; H, 6.36 %; N, 4.65 %. Found: C, 67.69 %; H, 6.37 %; N, 4.63 %.

2-(Naphthalen-2-yloxy)valine glycine methyl ester

N-methylmorpholine (1.7 ml, 15.5 mmol) and isobutylchloroformate (2.2 mL, 17.0 mmol) were added to a solution of 2-(naphthalen-2-yloxy)valine (5.21 g, 15.5 mmol) in 100 mL chloroform and stirred for 5 min at 0 ºC. A solution of $_L$-glycine methyl ester (2.5 g, 16.3 mmol) and N-methylmorpholine (1.7 mL, 15.5 mmol) in chloroform (25 mL) was added. The solution was allowed to warm to room temperature with stirring overnight. The solution was washed with 4 x 100 mL water 1 x 30 mL 0.1 M HCl and dried with magnesium sulphate before removing the solvent in vacuo to give a white powder. ^1H NMR ($CDCl_3$) 7.78 (m, ArH and NH,

2H), 7.73 (d, ArH, 1H, J = 8.2 Hz), 7.46 (dt, ArH, 1H, J = 6.9 Hz, J = 1.2 Hz), 7.38 (dt, ArH, 1H, J = 6.9 Hz, J = 1.2 Hz), 7.22 (dd, ArH, 1H, J = 9.0 Hz, J = 2.6 Hz), 7.17 (m, ArH, 2H), 6.49 (d, NH, 1H, J = 5.0 Hz), 4.68 (d, OCH, 1H, J = 14.9 Hz), 4.64 (d, OCH, 1H, J = 14.9 Hz), 4.41 (dd, CHNH, 1H, J = 6.9 Hz, J = 6.7 Hz), 4.19 (q, CH2CH3, 2H, J = 7.2 Hz), 3.99 (dq, CH2NH, 2H, J = 11.0 Hz, J = 5.6Hz), 2.18 (m, CH(CH3)2, 1H), 1.27 (t, CH2CH3, 3H, J = 7.2 Hz), 0.97 (d, CH3, 3H, 3J = 6.8 Hz), 0.93 (d, CH3, 3H, J = 6.8 Hz) ppm. ^{13}C NMR ($CDCl_3$) 170.8, 169.4, 168.4, 154.9, 134.2, 129.9, 129.5, 127.7, 126.9, 126.7, 124.4, 118.2, 107.6, 67.3, 61.6, 58.0, 41.3, 30.9, 19.2, 18.0, 14.1 ppm. MS (ES) 409 ($[M+Na]^+$). Accurate mass calculated for $C_{21}H_{26}N_2O_5Na$: 409.1739. Found: 409.1719.

2-(Naphthalen-2-yloxy)valine glycine(2)

Deprotection of 2-(naphthalen-2-yloxy)valine, glycine ethyl ester was dome by dissolving in in a THF: water mixture of 30 mL: 10 mL. LiOH (0.35 g) was then added and the solution allowed to react for two hours until no precipitate was formed when a small portion was added into water. Then, 100 mL of water was added and the solution was then filtered to remove any starting material. The pH of the filtered solution was then lowered to between 3 and 4 until a white precipitate was formed. This solid was removed by filtration and dried under vacuum to give a white solid. This was then washed chloroform to remove any impurities. A typical yield was around 85 %. ^{1}H NMR (d_6-DMSO) 12.60 (s, COOH, 1H), 8.46 (t, NH, 1H, J = 5.7 Hz), 8.03 (d, ArH, 1H, J = 9.0 Hz), 7.86 (d, ArH, 1H, J = 4.8Hz), 7.84 (d, ArH, 1H, J = 3.9 Hz), 7.75 (d, ArH, 1H, J = 8.2 Hz), 7.47 (dt, ArH, 1H, J = 7.0 Hz, J = 1.2 Hz), 7.36 (dt, ArH, 1H, J = 8.0 Hz, J = 1.0 Hz), 7.28 (m, NH, 1H), 7.24 (dd, ArH, 1H, J = 8.8 Hz, J = 2.4 Hz), 4.76 (d, OCH, 1H, J = 14.7 Hz), 4.70 (d, OCH, 1H, J = 14.7 Hz), 4.31 (dd, CHNH, 1H, J = 8.6 Hz, J = 6.5 Hz), 3.75 (dq, CH_2NH, 2H, J = 14.7 Hz, J = 5.9 Hz), 2.04 (m, CH(CH_3)2, 1H), 0.88 (d, CH_3, 3H, J = 6.7 Hz), 0.84 (d, CH_3, 3H, J = 6.8 Hz) ppm. ^{13}C NMR (DMSO) 171.1, 171.0, 167.3, 155.5, 133.9, 129.4, 128.6, 127.5, 126.6, 126.5, 123.8, 118.5, 107.1, 66.6, 57.0, 30.8, 19.1, 17.8 ppm. MS (ES) 381 ($[M+Na]^+$). Analysis calculated for $C_{19}H_{22}N_2O_5$: C, 63.68 %; H, 6.19 %; N, 7.82 %. Found: C, 63.63 %; H, 6.19 %; N, 7.78 %.

3. 4. 2 Instruments and Procedures

Nuclear Magnetic Resonance Spectroscopy (NMR)

NMR spectra were recorded using a Bruker DPX-400 spectrometer operating at 400 MHz for ^{1}H NMR and 101 MHz for ^{13}C NMR, in d_6-DMSO or D_2O.

For monitoring gelation with time NMR spectra were recorded on a Bruker DPX-400 spectrometer, operating at 400 MHz for ^{1}H NMR. The gelator solution was mixed with glucono-δ-lactone (GdL) and then directly loaded into an NMR tube to gel. During this time, NMR spectra were collected every 90 seconds for the first 70 acquisitions, and then typically every 5 minutes for the remaining experiment time (typically 14 hours total). The experiments were carried out at 25 °C. For the samples for NMR spectroscopy studies, ethanol (1 μL/mL) was added as an internal standard. A ^{1}H NMR spectrum of the solution was recorded prior to adding GdL to ensure that the ethanol present was accurately known relative to the dipeptides. This ensured any slight variations in weighing were taken into account for each sample.

Hydrogel Formation

A pH switch method was used to form the hydrogels. Single component gels were prepared at a concentration of 5 mg/mL. The gelator was dissolved at high pH in 2 mL of water. In the case of gelator 1 2 molar equivalents of 0.1 M sodium hydroxide was used and for gelator 2 one molar equivalent of 0.1 M sodium hydroxide was used. The solution was stirred until all the gelator was dissolved. This solution was then transferred to a vial containing a 10 mg of GdL and shaken gently. 1 mL was then transferred to a 20 mL plastic syringe with the top removed (Fig. 3. 28 a and b). The open syringe was covered with Parafilm and the solution was left to gel overnight (Fig. 3. 28c). The gel was removed from the syringe by pushing the plunger (Fig. 3. 28d).

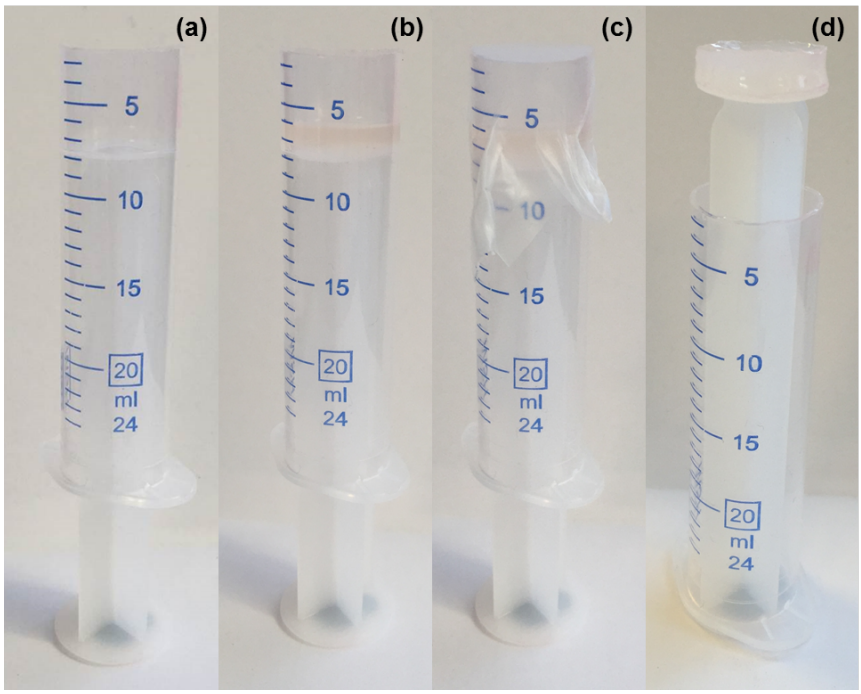

Figure 3. 28 Photographs showing gelation in a syringe mould. (a) Empty syringe with top removed. (b) 1 mL of gelator solution with GdL added to the mould. (c) Top of syringe is covered with Parafilm and left overnight. (d) When gel is formed gel can be removed by gently pushing on the plunger to reveal gel which then can be used.

For mixed component gels, separate solutions of each gelator were prepared at 10 mg/mL. 1 mL of each solution was then added together to get 2 mL with each gelator at 5 mg/mL. This was then added to 20 mg of GdL and again allowed to gel the same as previously described.

For NMR experiments, solutions are prepared as reported above except using D_2O and NaOD. An ethanol standard of 1 µL/mL was also added before transferring the gelator/GdL solutions into an NMR tube and allowed to gel inside the NMR spectrometer.

Rheological Measurements

Dynamic rheological measurements were performed using an Anton Paar Physica MCR101 rheometer. A parallel measuring system was used to perform all tests. For strain tests the gels were prepared as described above and transferred onto the bottom plate for measurement. For time sweeps, 1 mL of gel was prepared on the plate and, once the top plate was lowered, mineral oil was placed around the plate to prevent solution from drying out. All experiments were performed at 25 °C.

Time sweeps: Time sweeps were performed with a 25 mm sandblasted plate with a plate gap of 0.8 mm. Tests were performed at an angular frequency of 10 rad/s and with a strain of 0.1 %.

Strain sweeps: Strain scans were performed with a 25 mm plate from 0.1 % to 100 % with a frequency of 10 rad/s. The critical strain was quoted as the point that G' starts to deviate for linearity and ultimately crosses over the G″, resulting in gel breakdown.

pH Measurements

A FC200 pH probe (HANNA instruments) with a 6 mm × 10 mm conical tip was used for pH measurements. The stated accuracy of the pH measurements is ±0.1. The pK_a values of the gelators were determined *via* the addition of GdL as reported previously.[20] Measurements were recorded every 5 minutes. The temperature was maintained at 25 °C during the titration by using a circulating water bath.

SEM Imaging

SEM images were obtained using a Hitachi S-4800 FE-SEM at 3 keV. Gel was deposited onto glass cover slips which were fixed onto aluminium SEM stubs with carbon tabs and left to dry for 24 hours. The samples were gold coated for 3 minutes at 15 mA prior to imaging using a sputter coater (EMITECH K550X).

Mass Spectroscopy

Measurements were carried out using a Micromass LCT Mass Spectrometer in negative mode at 40 V in methanol. Samples were run by the University of Liverpool mass spectrometry service.

UV-Vis Absorption Measurements

Solution UV-Vis absorption data was measured using a Thermo Scientific Nanodrop 2000/2000c spectrophotometer. The spectrophotometer was used in cuvette mode were samples were prepared in PMMA plastic cuvettes with a pathlength of 1.0 cm. Aqueous samples were prepared at high pH using equimolar amounts of 0.1 M aqueous NaOH solution to gelator and made up to 2 mL with distilled water. The solution was then diluted until the absorbance was visible in the spectrum.

Irradiating Samples

Gels were placed onto a glass microscope slide and placed inside a plastic petri dish with a wet paper towel in to keep the air saturated with water and to prevent the gel drying out. The lid of the petri dish had a hole cut out to allow the LED to be able to irradiate the sample (Fig 3.29a and b). A 365 nm LED (LedEngin Inc, LZ1-10U600) with a light source powered by a TTi QL564P power supply operating at 1.0 W was used to irradiate gel samples (set up shown in Fig. 3.29d). When using a mask, a shape was cut out of a sheet of opaque plastic and placed over the sample prior to irradiation (Fig. 3.29c).

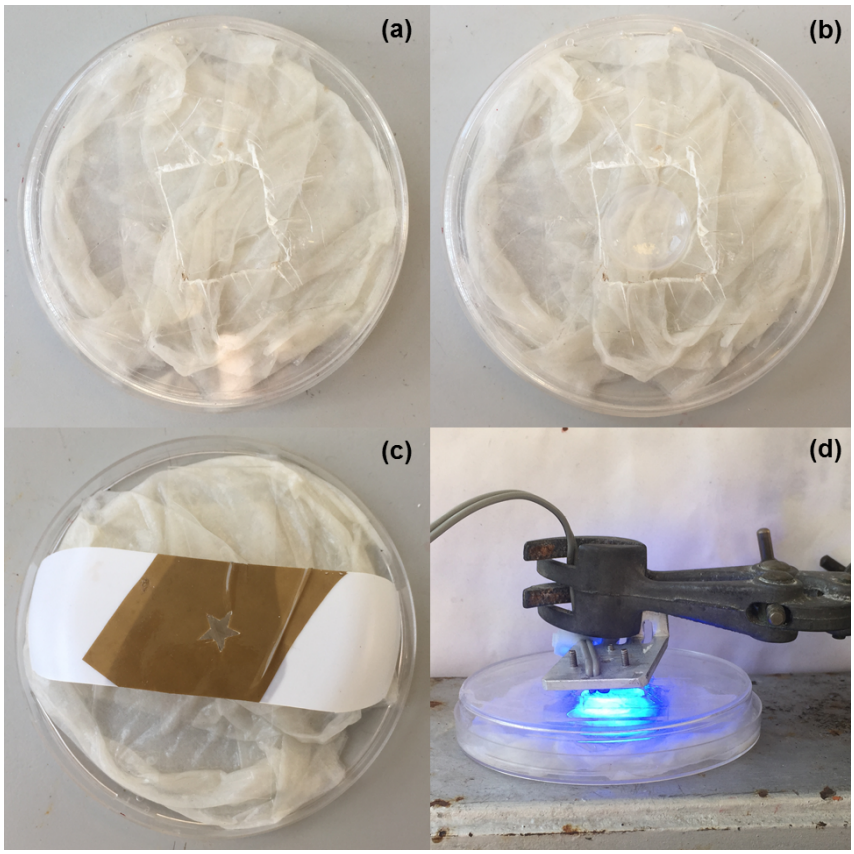

Figure 3.29 Photographs showing the irradiation set up and hydration chamber. (a) Empty hydration chamber (b) hydration chamber with a gel visible through the cut out window (c) hydration chamber with a mask used for spatially resolved removal of **1** (d) gel sample in the hydration chamber being irradiated with a 365 nm LED.

Temperature Measurements

The temperature of the gels was recorded before and after irradiation with 365 nm LED using a Precision Gold N85FR infrared thermometer with dual laser targeting. The temperature of the gels before irradiation was typically around 18 °C and after

irradiation for an hour, the temperature of the gels rose to 20 °C. This was recorded using the infrared thermometer measuring at the centre of the sample every 20 minutes during irradiation. The sample was removed from under the LED whilst this measurement was done.

3. 5. References

1. M. de Loos, B. L. Feringa and J. H. van Esch, *Eur. J. Org. Chem.*, 2005, **2005**, 3615-3631.
2. R. G. Weiss, *J. Am. Chem. Soc.*, 2014, **136**, 7519-7530.
3. S. Zhang, *Nat. Biotech.*, 2003, **21**, 1171-1178.
4. E. R. Draper and D. J. Adams, in *Chemoresponsive Materials: Stimulation by Chemical and Biological Signals*, The Royal Society of Chemistry, Editon edn., 2015, pp. 332-363.
5. P. Terech and R. G. Weiss, *Chem. Rev.*, 1997, **97**, 3133-3160.
6. K. J. C. van Bommel, M. C. A. Stuart, B. L. Feringa and J. van Esch, *Org. & Biomol. Chem.*, 2005, **3**, 2917-2920.
7. D. Buenger, F. Topuz and J. Groll, *Prog. Polym. Sci*, 2012, **37**, 1678-1719.
8. M. Ikeda, T. Tanida, T. Yoshii, K. Kurotani, S. Onogi, K. Urayama and I. Hamachi, *Nat. Chem.*, 2014, **6**, 511-518.
9. P. A. d. Silva, *Chem. Asian J.*, 2011, **6**, 750.
10. K. Fan, J. Yang, X. Wang and J. Song, *Soft Matter*, 2014.
11. L. E. Buerkle and S. J. Rowan, *Chem. Soc. Rev.*, 2012, **41**, 6089-6102.
12. J. Raeburn and D. J. Adams, *Chem. Commun.*, 2015, **51**, 5170-5180.
13. M. M. Safont-Sempere, G. Fernández and F. Würthner, *Chem. Rev.*, 2011, **111**, 5784-5814.
14. S. Prasanthkumar, S. Ghosh, V. C. Nair, A. Saeki, S. Seki and A. Ajayaghosh, *Angew. Chem. Int. Ed.*, 2015, **54**, 946-950.
15. K. Sugiyasu, S.-i. Kawano, N. Fujita and S. Shinkai, *Chem. Mater.*, 2008, **20**, 2863-2865.
16. J. B. Matson and S. I. Stupp, *Chem. Commun.*, 2012, **48**, 26-33.
17. D. J. Adams, L. M. Mullen, M. Berta, L. Chen and W. J. Frith, *Soft Matter*, 2010, **6**, 1971-1980.
18. S. Awhida, E. R. Draper, T. O. McDonald and D. J. Adams, *J. Coll. Inter. Sci.*, 2015, **455**, 24-31.
19. J. Raeburn, A. Zamith Cardoso and D. J. Adams, *Chem. Soc. Rev.*, 2013, **42**, 5143-5156.
20. C. Colquhoun, E. R. Draper, E. G. B. Eden, B. N. Cattoz, K. L. Morris, L. Chen, T. O. McDonald, A. E. Terry, P. C. Griffiths, L. C. Serpell and D. J. Adams, *Nanoscale*, 2014, **6**, 13719-13725.
21. K. L. Morris, L. Chen, J. Raeburn, O. R. Sellick, P. Cotanda, A. Paul, P. C. Griffiths, S. M. King, R. K. O'Reilly, L. C. Serpell and D. J. Adams, *Nat. Commun.*, 2013, **4**, 1480.
22. L. A. Estroff, L. Leiserowitz, L. Addadi, S. Weiner and A. D. Hamilton, *Adv. Mater.*, 2003, **15**, 38-42.
23. M. Kolbel and F. M. Menger, *Chem. Commun.*, 2001, 275-276.

24. J. T. Pelton and L. R. McLean, *Anal. Biochem.*, 2000, **277**, 167-176.
25. K. L. Morris, L. Chen, A. Rodger, D. J. Adams and L. C. Serpell, *Soft Matter*, 2015, **11**, 1174-1181.
26. J. Raeburn, B. Alston, J. Kroeger, T. O. McDonald, J. R. Howse, P. J. Cameron and D. J. Adams, *Mater. Horiz.*, 2014, **1**, 241-246.
27. M. R. Molla, A. Das and S. Ghosh, *Chem. Commun.*, 2011, **47**, 8934-8936.
28. Y. Huang, Z. Qiu, Y. Xu, J. Shi, H. Lin and Y. Zhang, *Org. Biomol. Chem.*, 2011, **9**, 2149-2155.
29. X. Li, Y. Gao, Y. Kuang and B. Xu, *Chem. Commun.*, 2010, **46**, 5364-5366.
30. Z. Qiu, H. Yu, J. Li, Y. Wang and Y. Zhang, *Chem. Commun.*, 2009, 3342-3344.
31. Y. Sako and Y. Takaguchi, *Org. Biomol. Chem.*, 2008, **6**, 3843-3847.
32. L. A. Haines, K. Rajagopal, B. Ozbas, D. A. Salick, D. J. Pochan and J. P. Schneider, *J. Am. Chem. Soc.*, 2005, **127**, 17025-17029.
33. T. Muraoka, C.-Y. Koh, H. Cui and S. I. Stupp, *Angew. Chem. Int. Ed.*, 2009, **48**, 5946-5949.
34. T. M. Doran, D. M. Ryan and B. L. Nilsson, *Polym. Chem.*, 2014, **5**, 241-248.
35. M. He, J. Li, S. Tan, R. Wang and Y. Zhang, *J. Am. Chem. Soc.*, 2013, **135**, 18718-18721.
36. R. Yang, S. Peng, W. Wan and T. C. Hughes, *J. Mater. Chem. C*, 2014, **2**, 9122-9131.
37. J. T. van Herpt, M. C. A. Stuart, W. R. Browne and B. L. Feringa, *Chem. Eur. J.*, 2014, **20**, 3077-3083.
38. B. Yan, J.-C. Boyer, D. Habault, N. R. Branda and Y. Zhao, *J. Am. Chem. Soc.*, 2012, **134**, 16558-16561.
39. S. Miljanić, L. Frkanec, Z. Meić and M. Žinić, *Eur. J. Org. Chem.*, 2006, **2006**, 1323-1334.
40. R. H. Dyck and D. S. McClure, *J. Chem. Phys.,* 1962, **36**, 2326-2345.
41. Y. Pocker and E. Green, *J. Am. Chem. Soc.*, 1973, **95**, 113-119.
42. D. J. Adams, M. F. Butler, W. J. Frith, M. Kirkland, L. Mullen and P. Sanderson, *Soft Matter*, 2009, **5**, 1856-1862.
43. L. Chen, K. Morris, A. Laybourn, D. Elias, M. R. Hicks, A. Rodger, L. Serpell and D. J. Adams, *Langmuir*, 2010, **26**, 5232-5242.
44. K. A. Houton, K. L. Morris, L. Chen, M. Schmidtmann, J. T. A. Jones, L. C. Serpell, G. O. Lloyd and D. J. Adams, *Langmuir*, 2012, **28**, 9797-9806.
45. L. Chen, S. Revel, K. Morris, L. C. Serpell and D. J. Adams, *Langmuir*, 2010, **26**, 13466-13471.
46. S. Fleming, S. Debnath, P. W. J. M. Frederix, N. T. Hunt and R. V. Ulijn, *Biomacromolecules*, 2014, **15**, 1171-1184.
47. M. A. Haque, T. Kurokawa and J. P. Gong, *Polymer*, 2012, **53**, 1805-1822.

CHAPTER 4

Photoconductive Perylene Bisimide Gelators

4. 1. Introduction

Chapter 3 discussed the use of a stilbene-based gelator in a spatially resolved multicomponent self-assembled system. This molecule was ideal for use in such a system due to its ability to isomerise and become a non-gelator. Stilbenes have also been used in p-n heterojunctions as p-type materials.[1] p-n heterojunctions are used in electronic devices, including solar cells and light emitting diodes.[2] P-type materials are able to donate electrons and become positively charged and n-type materials are able to accept an electron and so become negatively charged (hence the terms p and n). p-n heterojunctions are discussed in more detail in Chapter 5. This Chapter discusses the synthesis and use of a π-conjugated n-type material for the use in electronic devices. Self-assembly is a simple method of organizing optoelectronically active π-conjugated molecules in a defined manner with precise control at both the nano- and micro-scale.[3] Efforts have been made in aligning these materials to create more defined and reproducible coating of the materials.[4] One self-assembly route is to exploit low molecular weight gelators (LMWG).[3] Gelation using suitably designed LMWG results from self-assembly of the gelator into well-defined one-dimensional structures, which then can entangle or cross-link. When the LMWG contain π-conjugated groups, the result of this assembly is the stacking of these groups, which can be exploited to form conductive pathways for electronic devices.[5] Electrons are able to pass along the electron accepting conjugated self-assembled structures.[6]

The assembly of LMWG based around perylene bisimides (PBIs) is of great interest from the perspective of electronic materials, since PBIs are n-type materials.[5, 7, 8] PBIs have strong absorption, long fluorescence lifetimes, high quantum yields and are very stable to heat. They are considered to be the best alternative to fullerenes in organic solar cells[9, 10] or in field-effect transistors.[5] There are a growing number of reports showing the formation of self-assembled wires and fibres from PBI-based gelators.[6, 7, 11, 12] This is because PBIs have a large conjugated centre that enables π-stacking into one-dimensional fibres.[13] These large aromatic PBIs are often quite insoluble in many solvents, which also promotes self-assembly.[11, 14] PBIs can also be (photo)conductive and have been suggested as candidates for many organic electronic devices.[15, 16] PBIs are readily sequentially reduced to the radical anion and

dianion by light, electrochemically[17] or by the use of a reducing agent.[18, 19] This radical anion has been shown to be the cause of the conductivity, with the anion being more conductive than the dianion.[20] Electron diffusion has been shown to occur in one-dimension in PBI-aggregates, again showing their use for electronic devices.[21] A significant amount of work has been done on the formation of one-dimensional structures based on PBIs, for example showing supramolecular chirality[22] and the formation of liquid crystallinity[23]. A key point is that the optoelectronic performance of such materials can depend not only on the chemical structure, but also on the morphology and uniformity of the aggregates formed.[24-26] PBI aggregates formed are critically controlled by functional group, solvent, or concentration.[26-28] The majority of the reported PBI-based LMWG gel organic solvents, due to the high hydrophobicity of the perylene group.[29-31] Examples have been used in light harvesting and also in bulk heterojunctions, formed from self-sorted gel fibres.[30]

Recently, PBI-based hydrogelators have been reported. For example, an amino acid-based PBI was shown to form photoconductive xerogels.[13, 32] The LUMO level of an aspartic acid-based PBI has been suggested to be suitable for use as an electron acceptor in a solar cell; however the reduced PBI solution formed was highly sensitive to the presence of O_2, which is not promising for organic photovoltaics (OPV) applications.[20] It is therefore highly desirable to have reduced PBI species in thin films that are resistant to anion oxidation by O_2.[33] Such devices are normally formed using deposition or coating routes that can lead to the formation of aggregates with different size and shape distributions, which can influence the electronic properties. Conductivity of the thin films is a balance between crystallinity and flexibility of the molecules[34], so alignment of one-dimensional aggregates might be the best way to produce highly conductive reproducible thin films.[35] Alignment of materials in general can be achieved through spin-coating,[35] shear,[36] electrical currents,[37] gravity[38] and magnetic fields[39] to name a few techniques.

4. 2. Results and Discussion

4. 2. 1. Gel Properties

Four amino acid functionalised PBIs were prepared by the reaction of 3,4:9,10-perylenetetracarboxyldianhydride as described in Section 4. 4. PBIs were functionalised with L-alanine (**1**), L-histidine (**2**), L-phenylalanine (**3**) and L-valine (**4**) (Fig. 4.1). **1** and **2** have been previously reported, but not used as LMWGs.[40, 41]

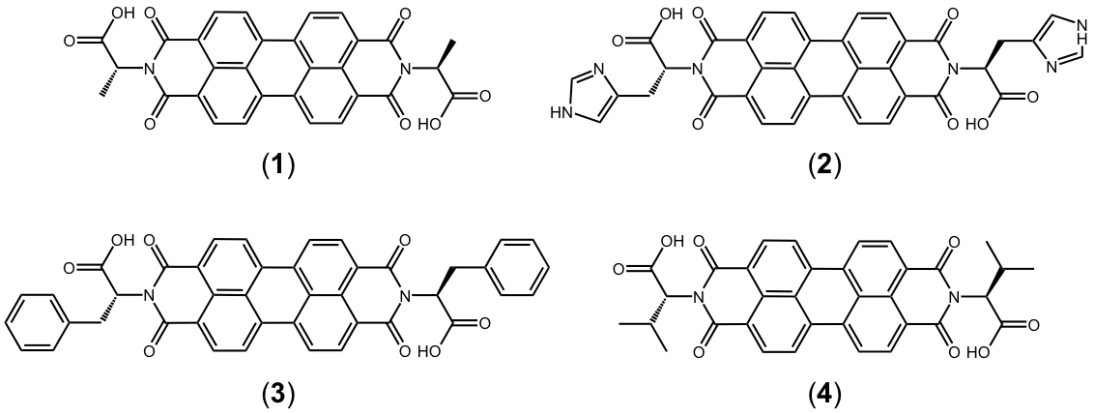

Figure 4.1 Molecular structure of PBIs functionalised with L-alanine (**1**), L-histidine (**2**), L-phenylalanine (**3**) and L-valine.(**4**).

1-**4** all form deep red solutions at high pH (above pH 9) at a concentration of 5 mg/mL (photographs are shown in Fig. 4.2) using 0.1 M aqueous sodium hydroxide as described in Section 4. 4.

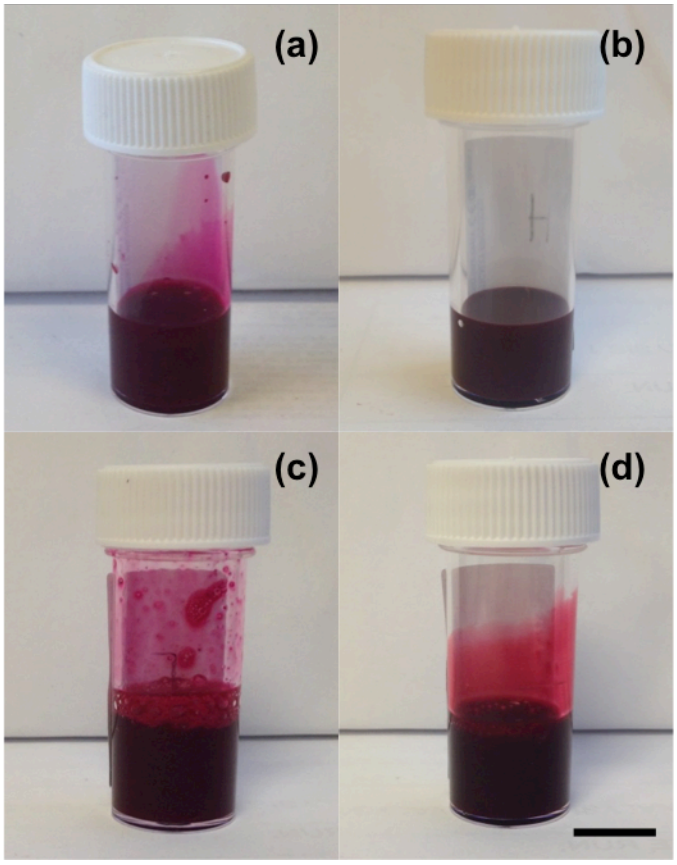

Figure 4.2 Photographs of PBI solutions at a gelator concentration of 5 mg/mL at high pH (a) **1**, (b) **2**, (c) **3** and (d) **4**. Scale bar represents 1 cm.

Viscosity measurements of solutions of **1**-**4** at high pH show them to be shear thinning (Fig. 4.3). The decrease in viscosity with increasing shear rate suggests that there are structures present in solution, rather than single molecules. The decrease in viscosity is due to the structures aligning at high shear causing the lower viscosity.[42] Solutions of **3** have much higher viscosity than the other LMWG. It has been previously noted that certain hydrophobic LMWG with similar molecular structures form worm-like micelles at high pH, leading to viscous solutions.[43, 44] Since all of the solutions are shear thinning and so it is likely that worm-like micelles are formed at high pH from **1**-**4**. Phenylalanine is the most hydrophobic of the amino acids used here and so **3** would most likely form the most viscous solutions due to worm-like micelles having different persistence lengths and properties.[38, 42]

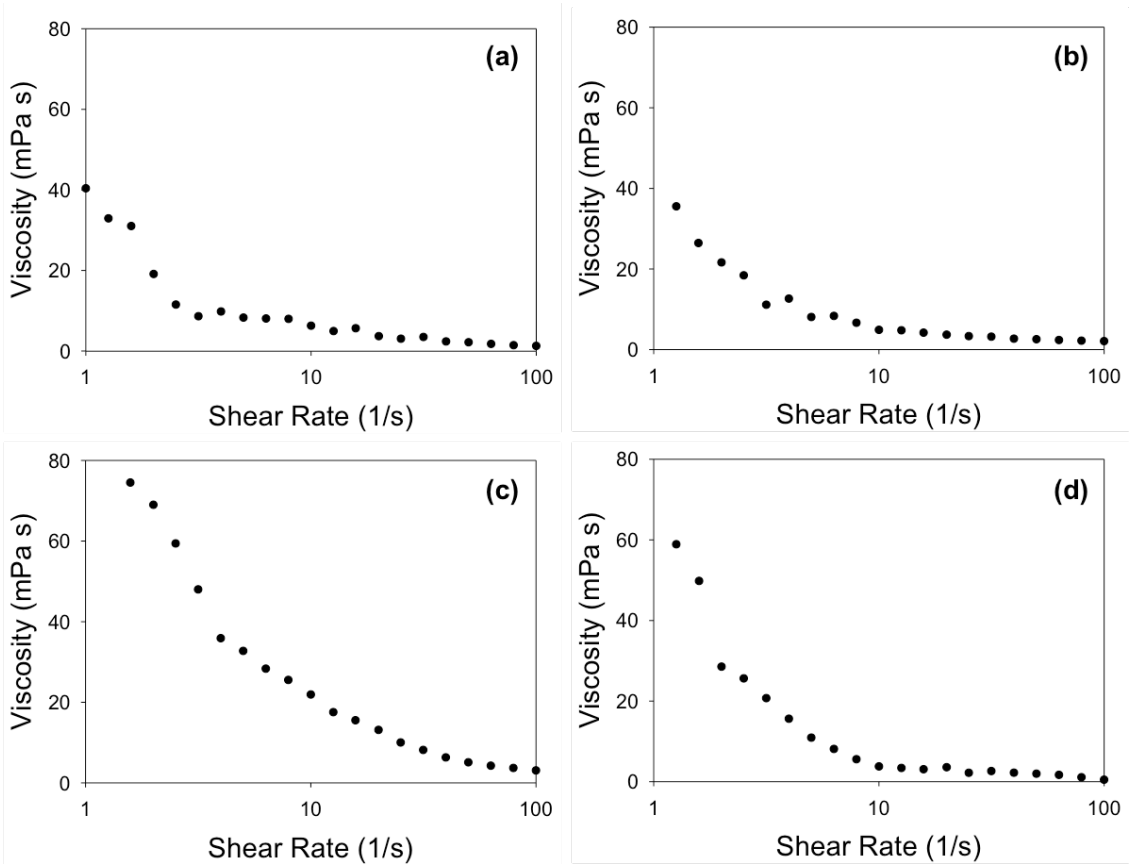

Figure 4.3 Graphs showing change in viscosity with increasing shear rate for solutions of (a) **1**, (b) **2**, (c) **3** and (d) **4**.

The dried solutions generally showed the presence of long one-dimensional structures by scanning electron microscopy (SEM, performed by Dr. T. McDonald, University of Liverpool) as shown in Fig. 4.4. To the best of our knowledge, this is the first observation of such structures formed from a pre-hydrogel solution state for PBIs. Dried solutions of **1**, **2** and **4** show similar fibre-like structures with fibres widths of around 10 nm. Dried solutions of **3** however only showed disordered structures, but as previously mentioned in Chapters 3 and 4 this could be due to drying effects.[45]

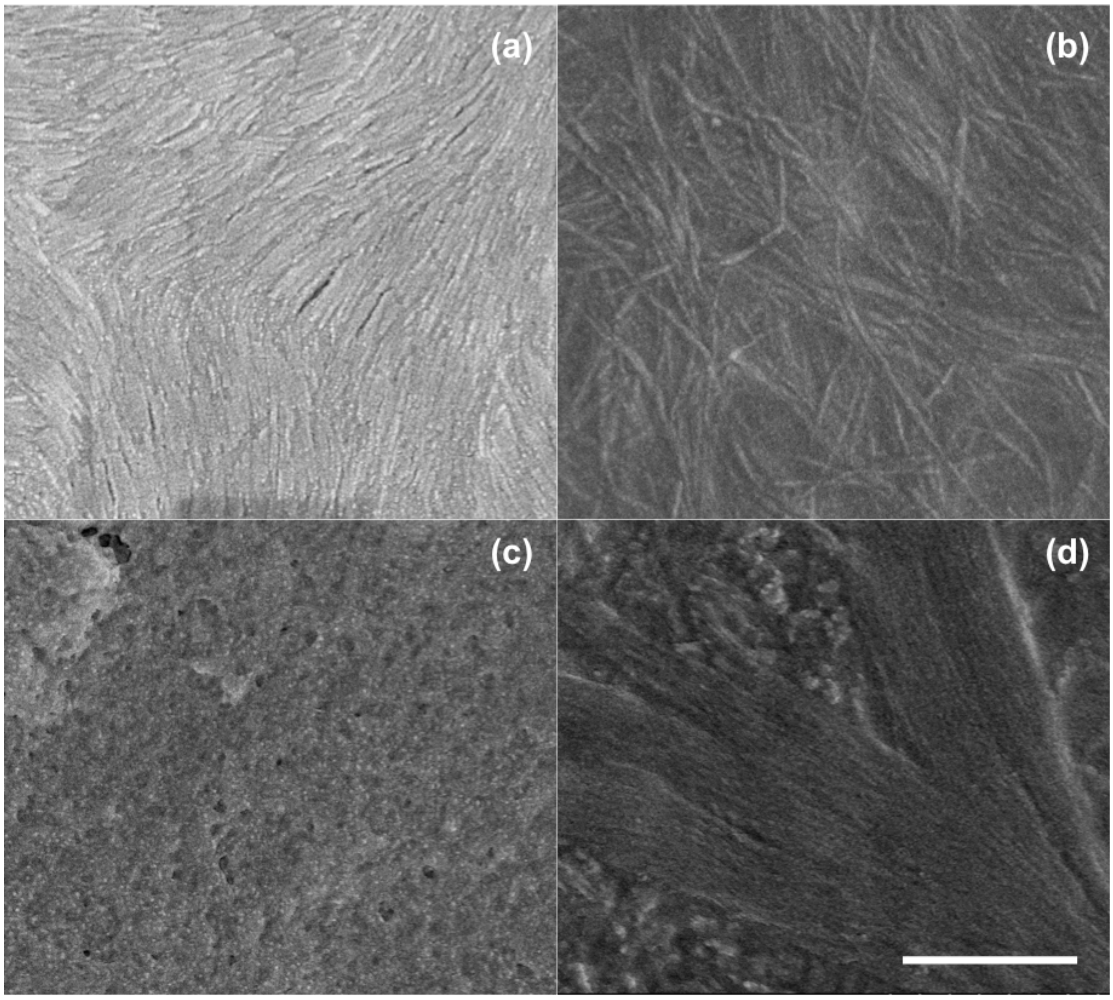

Figure 4.4 SEM images of a dried solution of (a) **1**, (b) **2**, (c) **3** and (d) **4**. Scale bar represents 500 nm.

The solutions formed self-supporting dark red gels on lowering the pH (shown in Fig. 4.5). The pH was lowered by adding glucono-δ-lactone (GdL), which hydrolyses slowly to gluconic acid discussed in Chapter 3. 2.[46] Solutions of **2**, **3** and **4** formed gels using 3 mg/mL of GdL. Solutions of **1** formed gels with 5 mg/mL and took a longer time to form a self-supporting gel as compared to the other PBIs. On gelation, **1**, **2**, and **4** formed red, optically transparent gels while **3** forms gels that are turbid. Turbid gels suggest larger aggregates which scatter light more making them opaque.

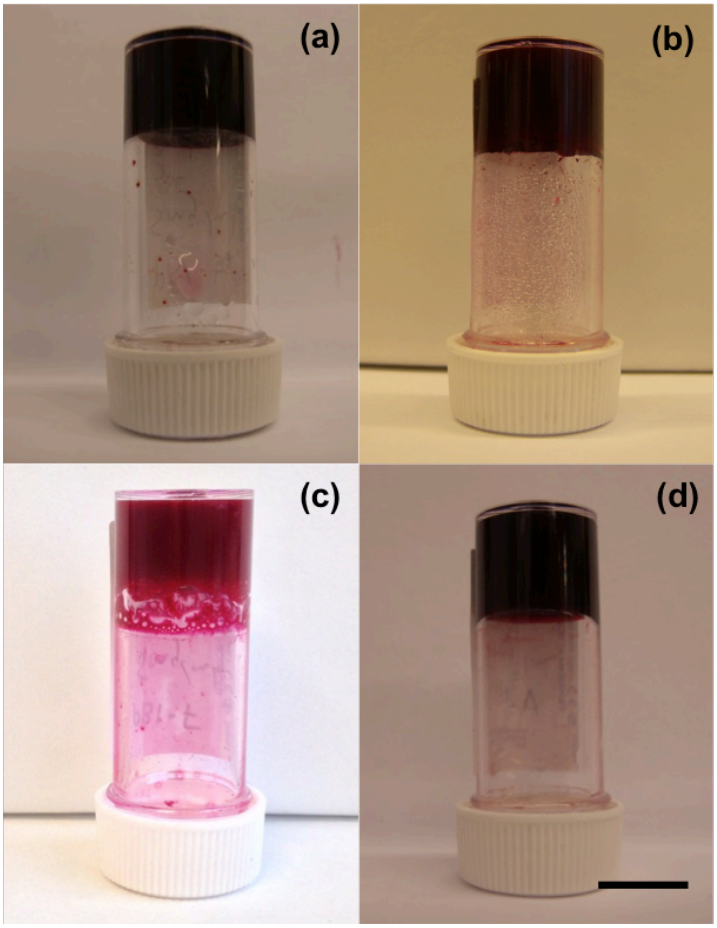

Figure 4.5 Photographs of gels formed from (a) **1**, (b) **2**, (c) **3** and (d) **4**. Scale bar represent 1 cm. (b), (c) and (d) are formed with 3 mg/mL GdL and (a) with 5 mg/mL.

The rheological properties of these gels are similar for those formed from related LMWG. All gels break at low strain (Fig. 4.6 and Table 4.1). Gel-**3** shows a different strain sweep compared to the other gels. Gels-**1**, **2** and **4** all show a single break point (where the storage modulus (G′) and loss modulus (G″) deviate from linearity as the gel network starts to break) at around 4-5 % strain. This is followed by a sharp decrease in G′ and G″ until they cross over and the gel is completely broken and so is now acting as a liquid rather than a gel. Gel-**3** still has a break point at around 5 % strain, but then does not have a sharp decrease in G′ and G″. Instead, G′ and G″ slowly decrease in steps until 500 % strain and then rapidly decrease until the gel is completely broken. This suggests that gel-**3** has a different gel network than **1**, **3** and **4** as it has two break points. Multiple break points either suggests that either there are two different types of network with the weakest breaking first, or a more complex structured network.[47, 48] This agrees with gel-**3** being turbid whilst the others are transparent.

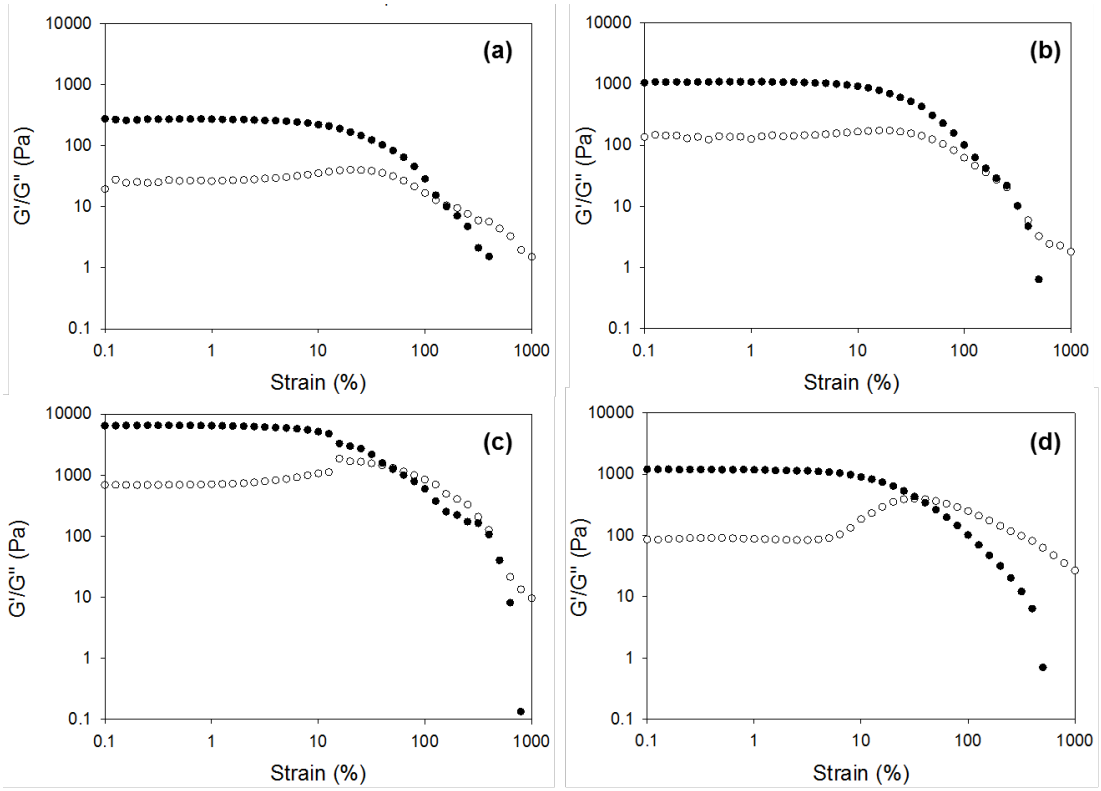

Figure 4.6 Strain sweeps performed at a frequency of 10 rad/s at 25 °C. Full symbols represent G´ and open symbols G˝ (a) gel-**1**, (b) gel-**2**, (c) gel-**3** and (d) gel-**4**.

Again, frequency sweeps show the rheological properties of these gels are similar for those formed from related LMWG, with G' and G" being only weakly dependent on frequency (Fig. 4.7). Gel-**3** has the highest G' and G". Gel-**1** is the weakest gel, and gel-**2** and gel-**4** have similar gel strength. This shows that the functional group on the perylene has a significant effect on rheological properties of the gels formed. This is most likely due to the amino acid functionalities having different hydrophobicity and molecular interactions with each other.

	Gel-1	**Gel-2**	**Gel-3**	**Gel-4**
Break (%)	4	5	5	4
G´ (Pa)	400	1500	7300	1900
G˝ (Pa)	30	149	680	85

Table 4.1 Table showing rheological properties G´, G˝ and the strain at which Gels-**1**, **2**, **3** and **4** break. Break defined as when G' deviates from linearality in the strain sweeps. G' and G" are quoted at 10 rad/s in the frequency sweeps.

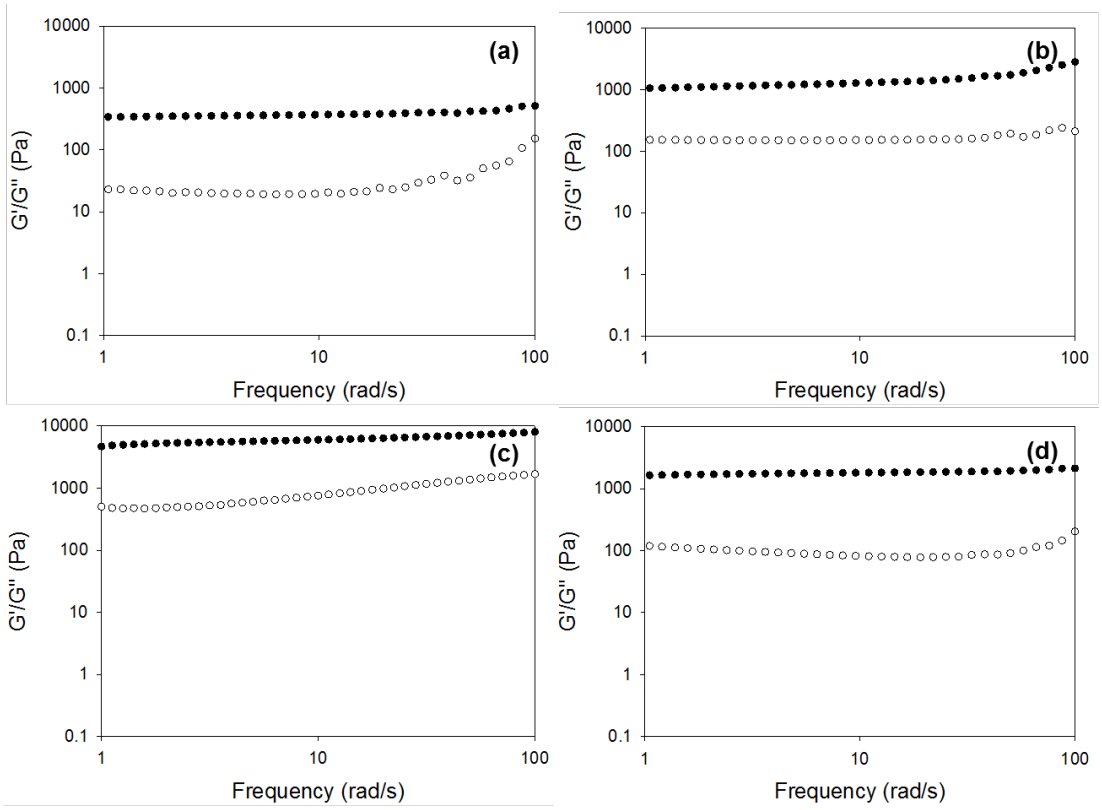

Figure 4.7 Frequency sweeps performed at 0.5 % strain and at 25 °C. Full symbols represent G´ and open shapes G˝ (a) gel-**1**, (b) gel-**2**, (c) gel-**3** and (d) gel-**4**.

The gels were then dried down in air at room temperature until the water was removed; this method maintains the fibrous network, but removing the solvent and collapsing the structure upon itself. These are referred to as xerogels. SEM of the xerogels of **1**, **2** and **4** showed the presence of thin entangled fibres (Fig. 4.8a, b and d) with widths of around 30 nm (SEM images were collected by Dr. T. McDonald, University of Liverpool). These fibres are thicker than that seen in the corresponding dried films showing further assembly has taken place upon gelation (or possibly drying). Xerogel-**3** shows large undefined shapes, this my be due to drying effects or due to there being larger aggregates in gel-**3** that dry down to form these large shapes seen in the SEM images (Fig. 4.8c). Within the large aggregates, more structure can be seen. These could be the primary fibres, which have then further assembled into these larger aggregates. This difference in xerogel-**3** could account for the difference in appearance and rheological properties of gel-**3**.

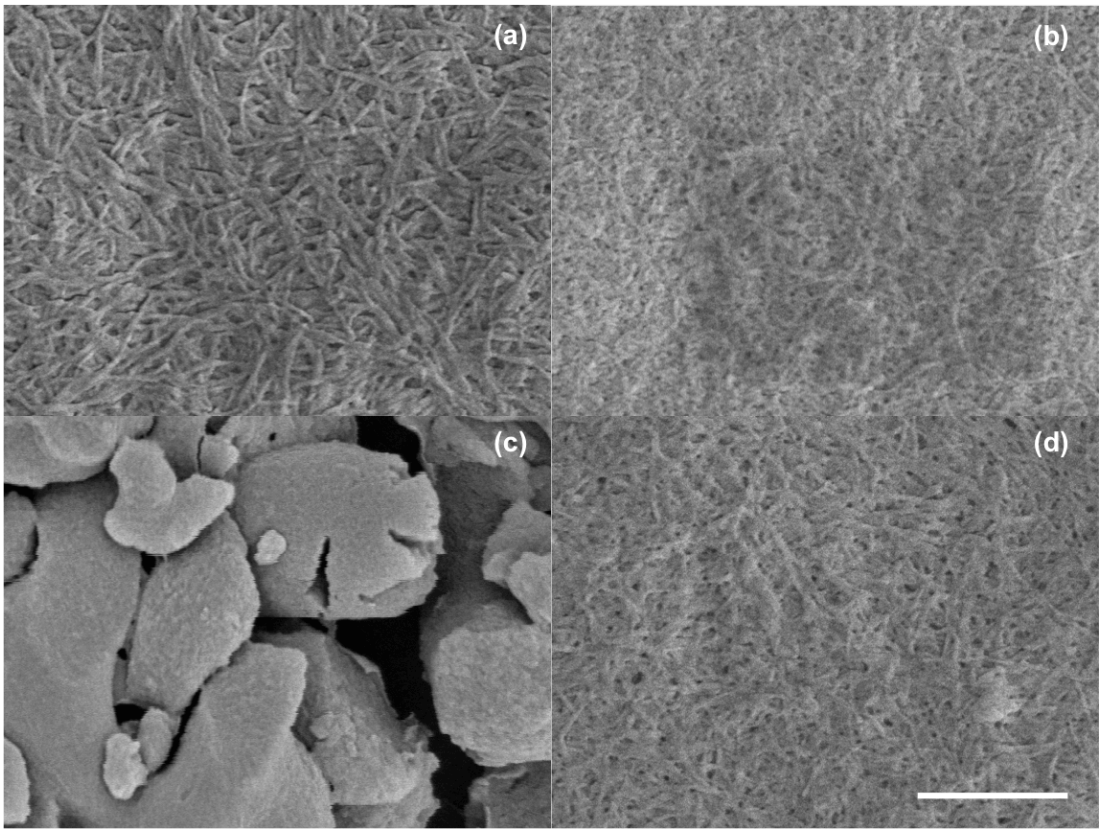

Figure 4.8 SEM images of xerogels (a) **1**, (b) **2**, (c) **3** and (d) **4**. The scale bar represents 500 nm.

In all cases, powder X-ray diffraction (pXRD) data shows both the dried solutions (Fig 4.9) and xerogels (Fig. 4.10) contain a low degree of crystallinity. The most intense peak in all samples is at $2\theta = \sim 25.5°$, corresponding to approximately 3.5 Å, arising from π-π stacking. The dried solution powder patterns look very similar to each other apart from dried solution **3**, which has two sharp peaks at around 20° and 23°. However, upon gelation the powder pattern looks the same as those for the other gels. It has been shown that pXRD gives little information about the gel structures or fibres, as does the crystal structures of the gelators.[49] It does however give us information about the thin film formed when drying the solution and the gels.

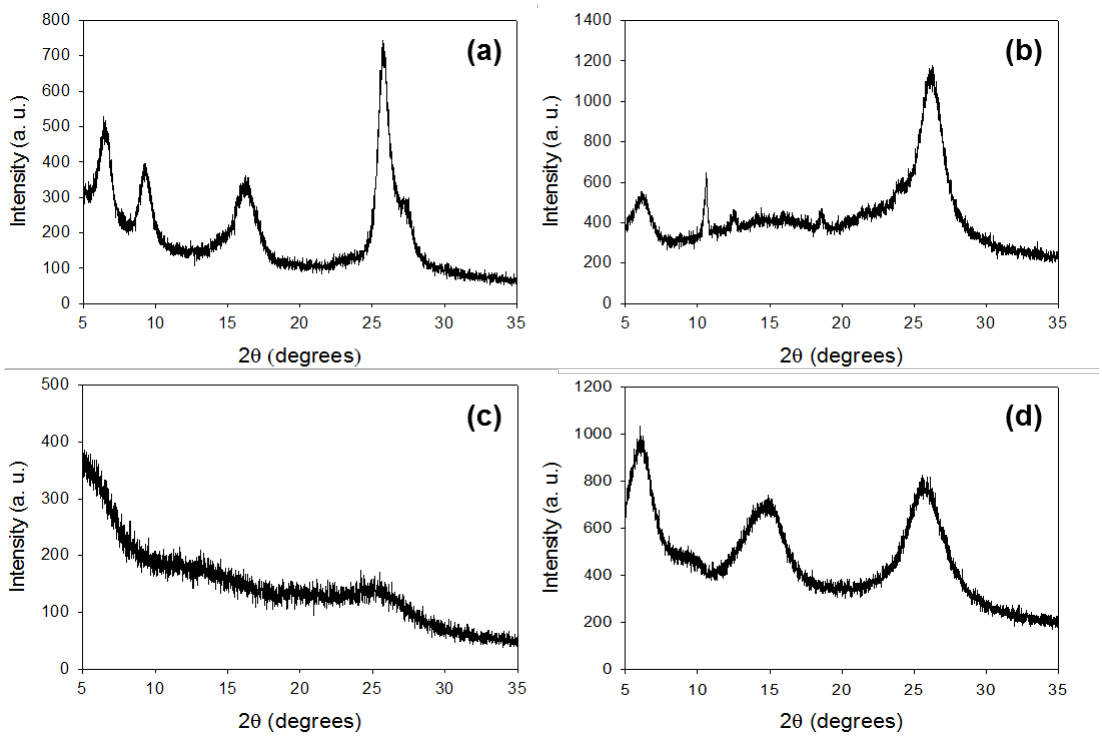

Figure 4.9 Powder X-ray diffraction patterns of the dried solution of (a) **1**, (b) **2**, (c) **3** and (d) **4**.

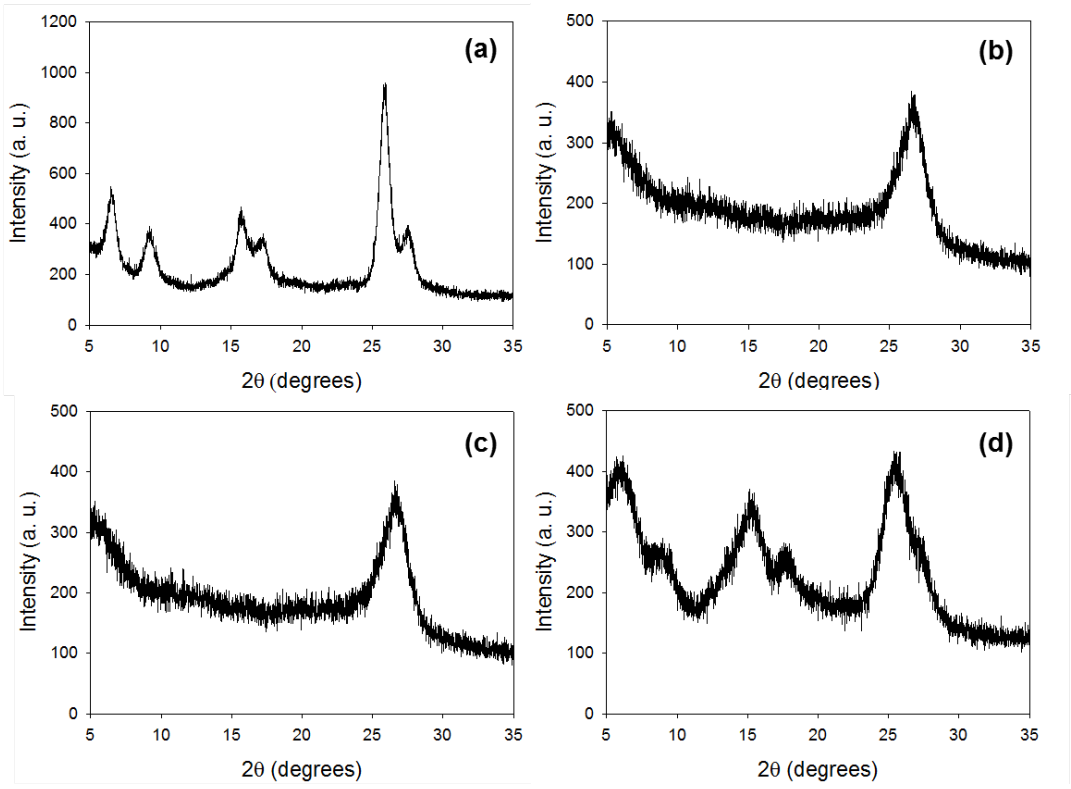

Figure 4.10 Powder X-ray diffraction patterns of the xerogels of (a) **1**, (b) **2**, (c) **3** and (d) **4**.

The absorption spectra of these materials in solution (5 mg/mL) are typical of PBI-LMWG. UV-Vis data at high pH (Fig. 4.11 solid line) showed a shoulder at 470 nm, and peaks at 490 nm and 540 nm, attributed to the 0-0 and 0-1 vibronic bands of the $S_0 \rightarrow S_1$ transitions.[50] The ratio of the peak intensities at 490 nm and 540 nm indicates a significant degree of aggregation.[13, 51] In the gel state, the UV-Vis data showed strong absorption at 470 nm and 590 nm, with the peak at 470 nm now being dominant (Fig. 4.11 dashed line). This change in relative intensity suggests a change in the aggregation of the perylenes.[13] The spectra for both the solution and gel showed peaks at 325 nm and 380 nm, corresponding to the electronic $S_0 \rightarrow S_2$ transition.[50] The spectra for the different gelators all have varying peak intensities showing slightly different packing and structures, but the overall peak positions from the perylenes are the same. This shows that changing the functionality of the amino acid does not change the electronic properties of the perylene core.

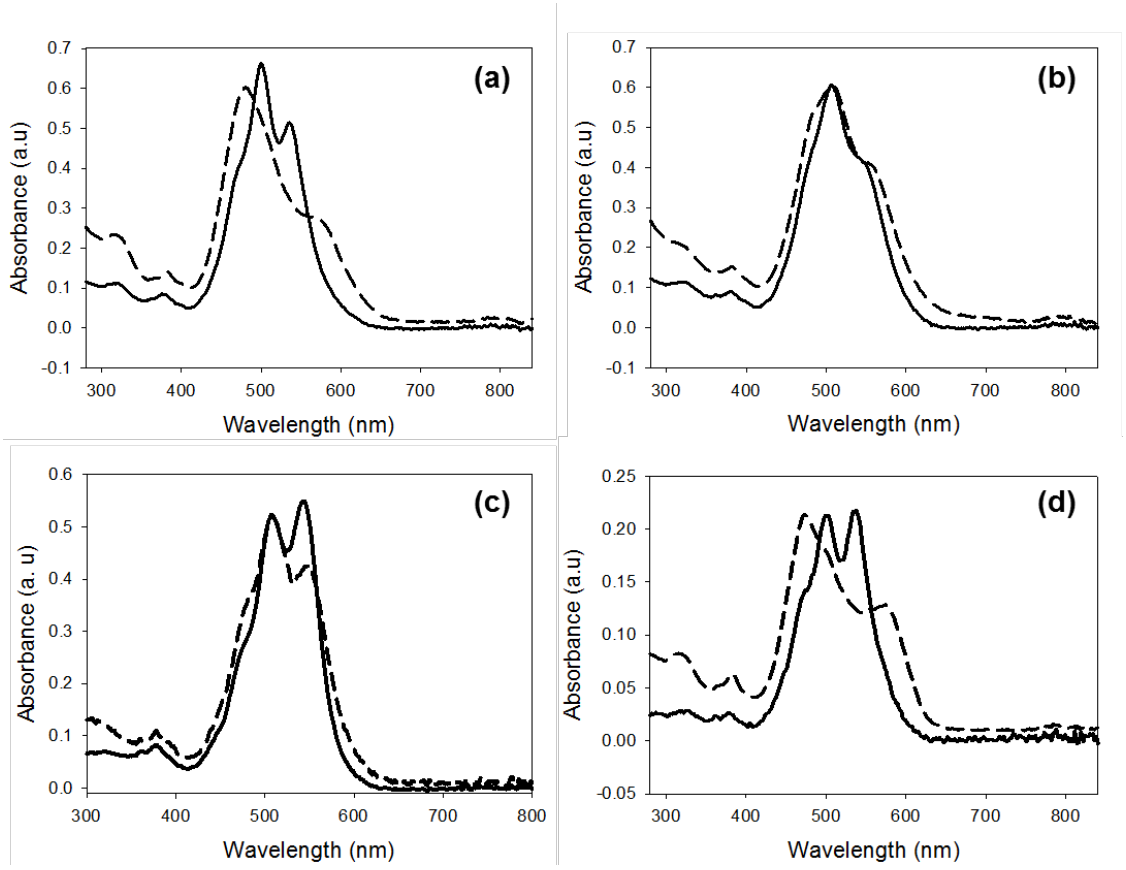

Figure 4.11 UV-vis absorption spectra for (a) **1**, (b) **2**, (c) **3** and (d) **4.** Solid lines show data for the solutions at high pH and the dashed line data for the gels.

Fluorescence data showed fine structure emission with maxima at 540 nm and 595 nm for the solution on excitation at 365 nm or 490 nm (Fig. 4.12). The fluorescence

intensity of the gel is significantly lower due to self-quenching, with the peak maxima slightly shifted to shorter wavelength. Again, this is due to a change in aggregation. This bathochromic shift in the spectra also suggests the formation of H-aggregates. The decrease in the intensity of the peaks upon gelation is due to fluorescence quenching as the perylenes are now closer together in solution.

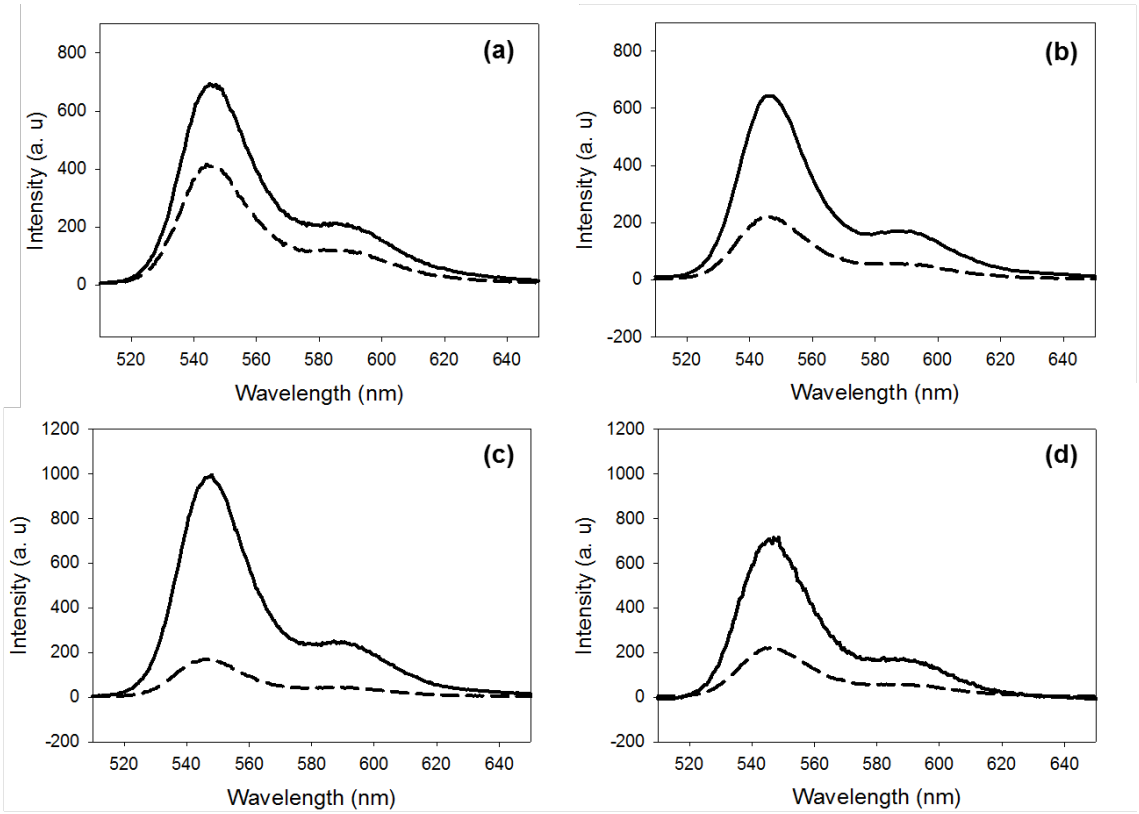

Figure 4.12 Fluorescence spectra of (a) **1**, (b) **2,** (c) **3** and (d) **4.** The solid line shows data for the solutions and the dashed line data for the gels. Fluorescence spectra were collected at an excitation of 365 nm and at a gelator concentration of 0.05 mg/mL.

4. 2. 2. Photoconductivity Measurements

To investigate the photoconductivity of these materials, we dried both the solution and gel phases. Films were readily obtained from both the solutions and gels of **1**, **2** and **4** simply by drying in air (final water content ~6 wt% as determined by thermogravimetric analysis (TGA) in all samples, Fig. 4.13). Samples of the same volume were cast between two silver electrodes which were attached to a potentiostat, which used to perform the two electrode experiment. This set up is discussed and shown in more detail in Section 4. 4.

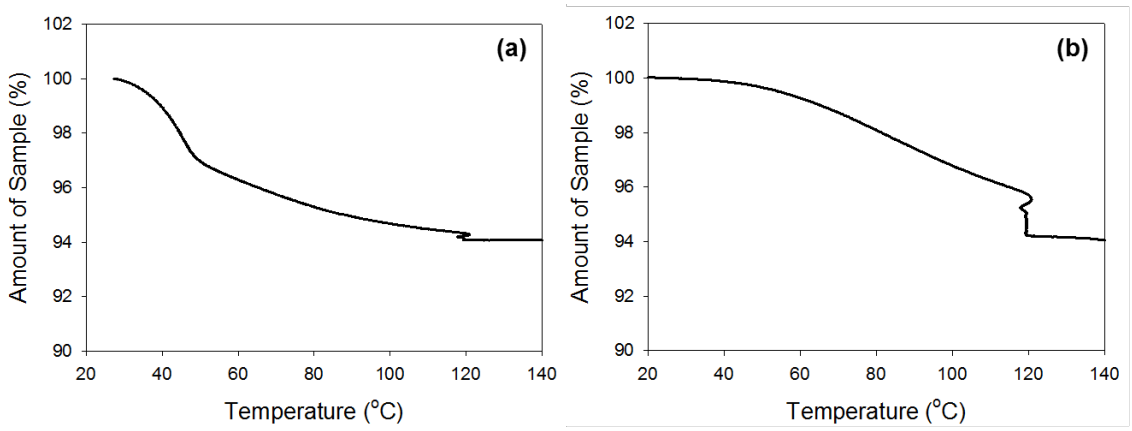

Figure 4.13 Thermogravimetric analysis of (a) a dried solution **1** and (b) a xerogel-**1** to determine the percentage of water in the films.

Photographs in Fig. 4.14 show the xerogel when dried on a glass substrate. For xerogel-**3**, drying led to an inhomogenous film that did not adhere well to the substrate (Fig. 4.14c). This correlates with the SEM data which also showed large aggregates (Fig. 4.8).

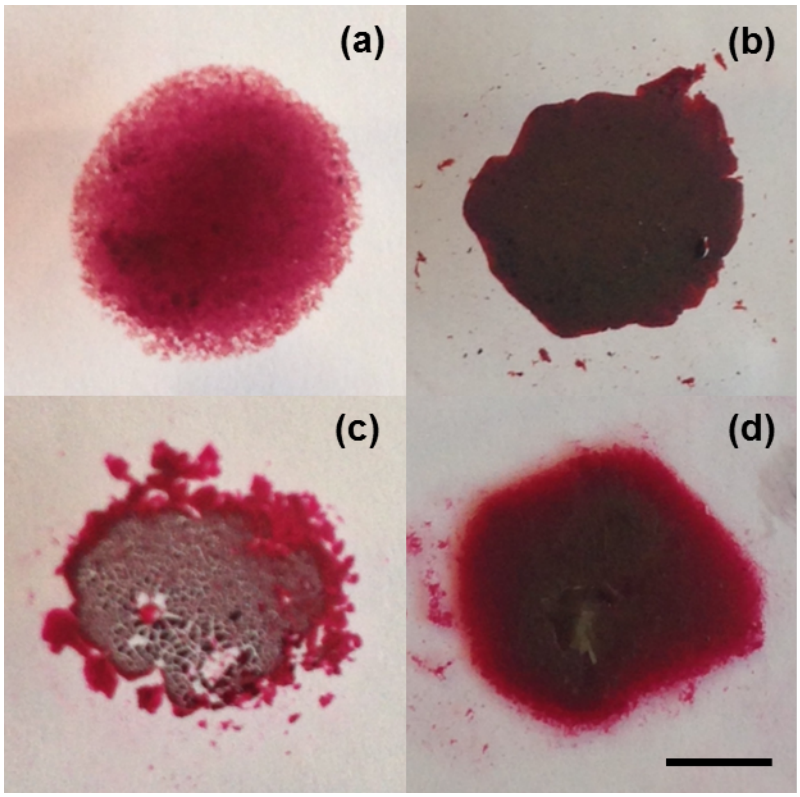

Figure 4.14 Photographs of thin films of a xerogel on glass for (a) **1**, (b) **2**, (c) **3** and (d) **4**. Scale bar represents 1 cm.

There are fundamental changes in the UV-Vis absorption spectra on drying. For both dried solutions and xerogels, the UV-Vis data showed an increase of absorbance in the UV region where there is a change in the intensity ratio of the peaks at 375 nm and those in the region of 470-590 nm (Fig. 4.15). This suggests a difference in the arrangement of the perylene aggregates upon drying. The xerogels were considerably darker in colour than the dried solution and so spectra were difficult to collect. Hence, the samples were moved several times in the detector to collect an average spectrum. For the case of xerogel-**3**, this was especially difficult as the film did not form an even film and flaked off. The spectrum was therefore quite noisy. The most intense peak at around 420-450 nm in the dried solution red shifts in the xerogel compared to the gel to around 460 nm in all samples, with xerogel-**2** shifting the least. The other peaks in the spectra do not appear to shift. This shift of the most intense peak is different than comparing the solution to the dried solution, where the most intense peak blue shifts upon gelation.

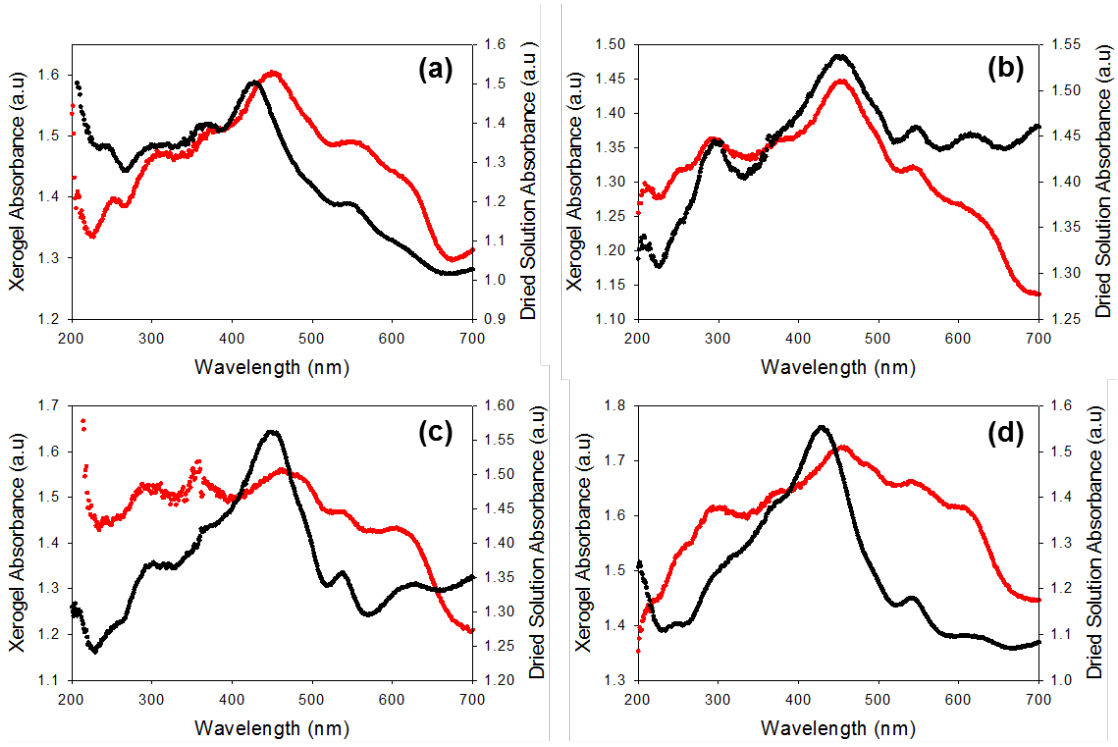

Figure 4.15 UV-Vis spectra of dried samples on glass of (a) **1**, (b) **2**, (c) **3** and (d) **4**. Black data is for the dried solutions and the red data is for the xerogels.

The macroscopic conductivity of the dried solutions and gels was measured both in the dark and under illumination with a xenon lamp. Both showed Ohmic response and a significantly increased current under illumination. This is assigned to the

samples becoming photoconductive (see Fig. 4.16), with symmetric data during the voltage sweep.

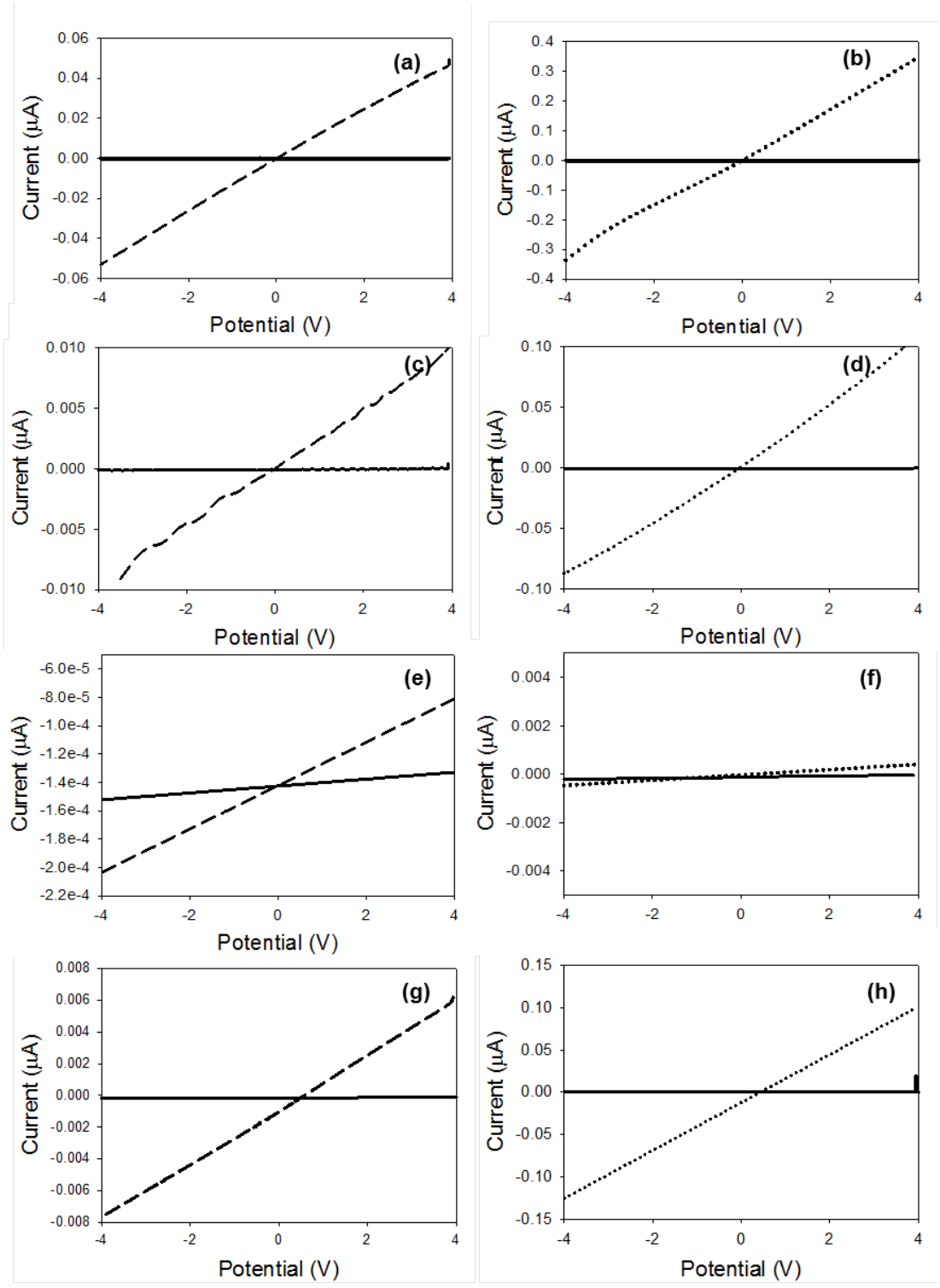

Figure 4.16 I-V curves showing the conductivity of thin film samples in the dark (solid lines) and under a 150 W xenon lamp (dashed line is for the xerogels and dotted line for the dried solutions). (a) and (b) are **1,** (c) and (d) are **2**, (e) and (f) are **3,** and (g) and (h) are **4**.

In general, the dried solutions were more conductive than the xerogels. **1** showed the highest current under illumination of the LMWG, and the photo-response was significantly greater for the dried solution than for the dried gel. **3** showed a very weak response, which we attribute primarily to the poor film quality.

The photoconductivity of these films was further investigated by varying the wavelength of light used to irradiate the samples. As the xenon lamp used above includes UV, visible and near IR wavelengths, it was unclear which energy of light was giving the response. This information could give us an insight to what is causing the conductivity. The wavelength of light used to irradiate the samples was varied by using a stabilized 75 W Xenon lamp coupled to a monochromator. The change in current resulting from irradiation of the sample by each selected wavelength was recorded. Samples were allowed to recover back to the dark current before the next wavelength was used. The intensity of the light was also recorded and the response was then scaled to the amount of photons present and then normalised. In all cases, despite the expected correlation between absorption spectrum of the perylene group and the proposed photoconductivity, both the dried gel and solution remain highly resistive when irradiated with light above 400 nm. Instead, a significant photocurrent was only induced when irradiated with wavelengths shorter than 400 nm (Fig. 4.17). The onset wavelength of the photoresponse of the dried solution and xerogel varied. For **1, 2** and **4**, the xerogel resistance decreased significantly with irradiation of wavelengths shorter than 400 nm, whereas the dried solutions only became active when irradiated at wavelengths of 375 nm or shorter. Due to the poor film quality it was not possible to collect this data for **3**.

This response to UV light is different to other perylene bisimides discussed in the literature, where it is common to use visible light for photoconductivity measurements, or a xenon lamp.[5, 32, 52] The lowest energy required for light to be absorbed in a material is referred to as the optical gap. Absorption of light of this energy results in the formation of excitons; excited electron-hole pairs bound through electrostatic interaction. Photoconductivity, however, requires free charge carriers (free electrons, free holes or both) and not bound excitons. The minimum energy needed to generate such free charge carriers is the transport (or quasiparticle) gap. [53] This transport gap is always larger or equal to the optical gap, with the difference

between the two equal to the exciton binding energy E_{ebe}; the amount of energy by which excitons are stabilized with respect to free electrons and holes.[53] E_{ebe} can be very small but for organic materials is typically in the order of tenths of an eV. Hence, the difference between absorption and photoconductivity onset to the E_{ebe} represents the extra energy required to form free electrons and holes from excitons and keep them separated long enough so recombination does not occur. This wavelength dependence is also rarely discussed, as is the difference between a gelled and pre-gelled sample.

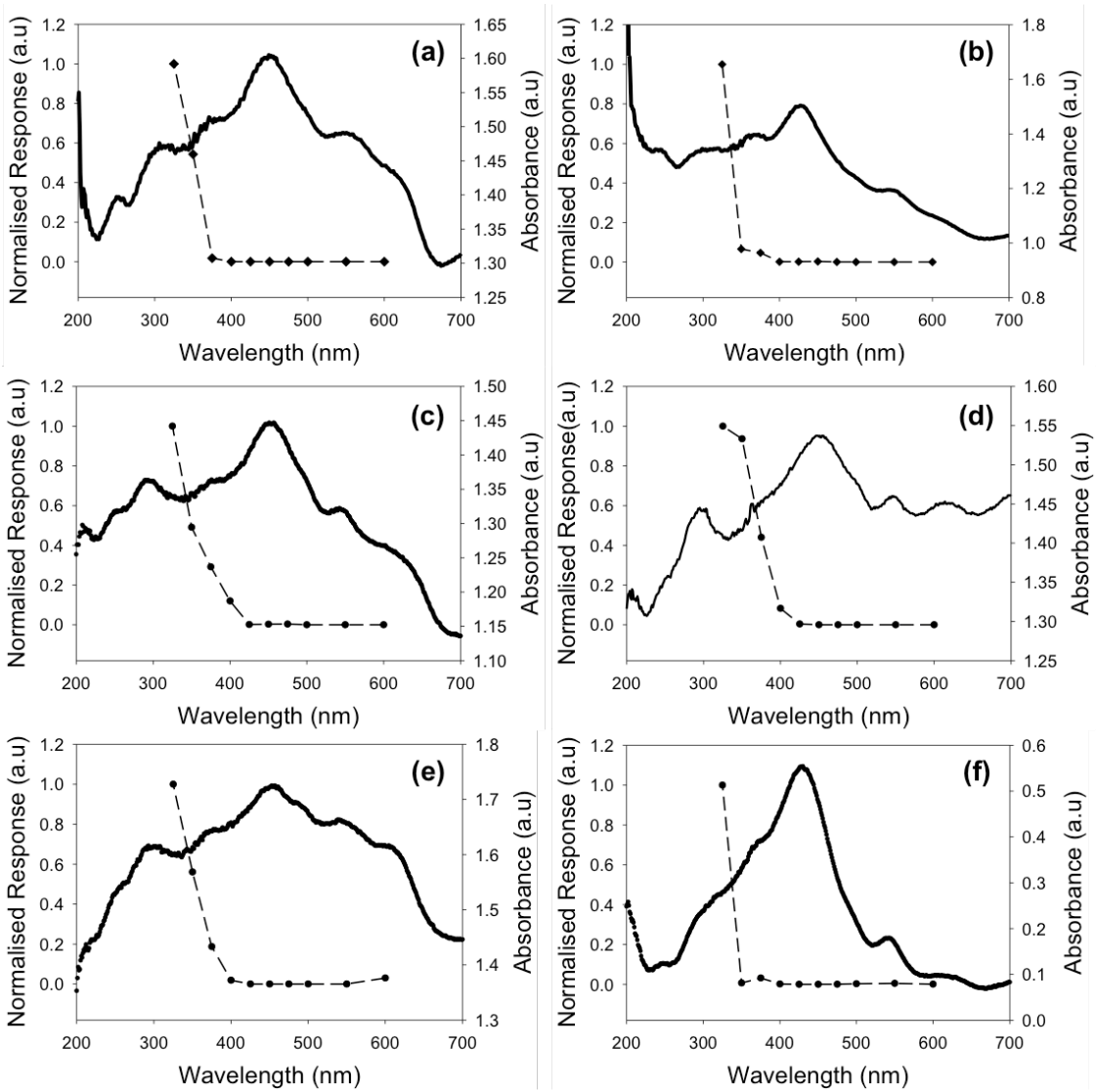

Figure 4.17 Graphs showing wavelength dependence of the conductivity of samples compared to their UV-vis spectrum. (a) xerogel-**1**, (b) dried solution **1**, (c) xerogel-**2**, (d) dried solution **2**, (e) xerogel-**4** and (f) dried solution **4**. The solid line is the UV-Vis spectrum and the circles are the wavelength response. The dashed lines connecting the circles have been added for clarity.

Irradiation of samples of **1**, **2** and **4** with 365 nm LED irradiation again showed a significant decrease in resistance, indicating photoconductivity (Fig. 4.18). For **1** and **4**, the dried solution was found to be approximately one order of magnitude less resistive under irradiation than the xerogels.

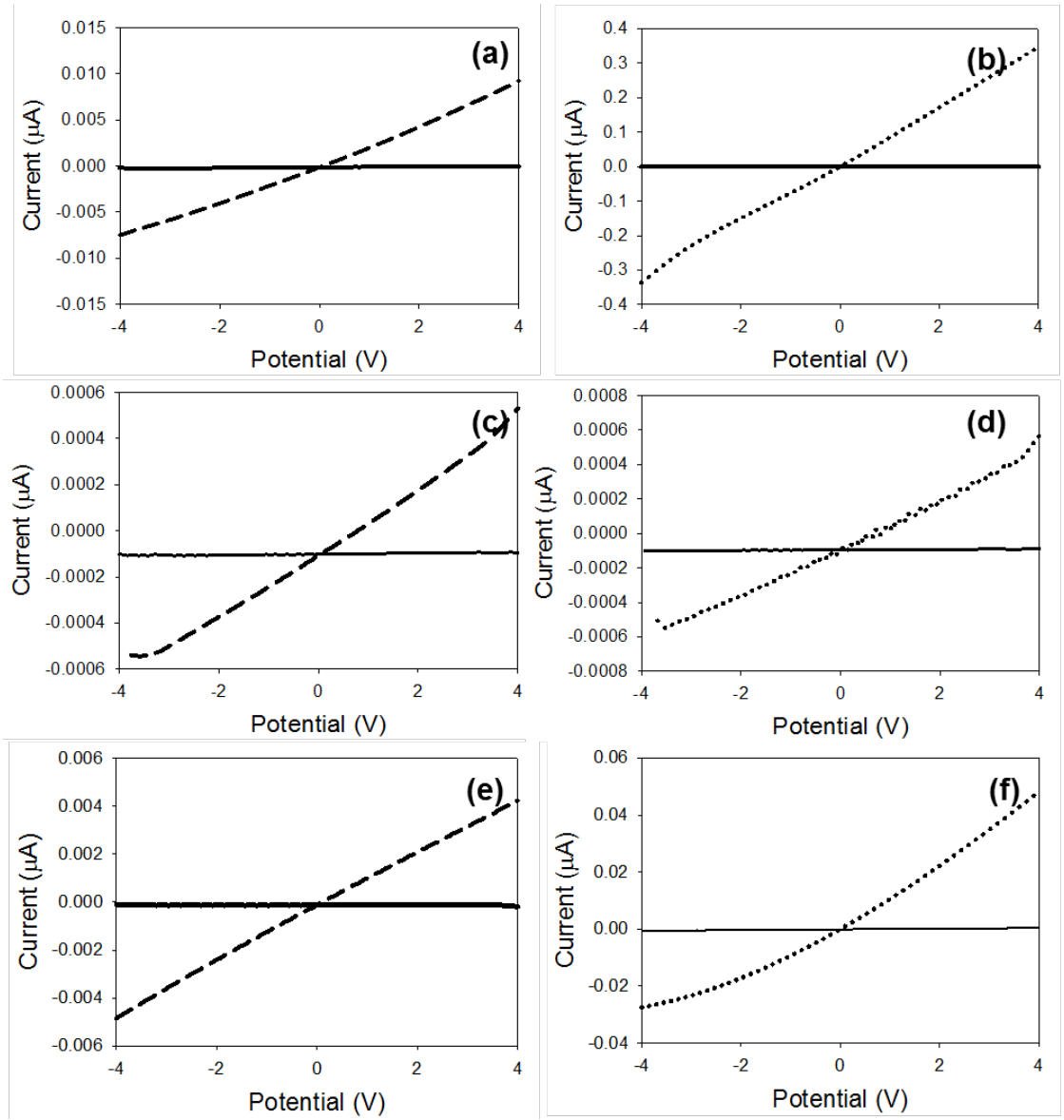

Figure 4.18 I-V curves showing the conductivity of thin film samples in the dark (solid lines) and under a 365 nm LED (dashed line is for the xerogels and dotted line for the dried solutions). (a) xerogel-**1**, (b) dried solution **1**, (c) xerogel-**2**, (d) dried solution **2**, (e) xerogel-**4** and (f) dried solution **4**.

This may be due to the packing in the solution versus gel state, but could also be due to differences in fibre thicknesses, density, and orientation. However, the photocurrents measured in the two electrode experiment were consistently greater with both the dried solutions and xerogels of **1** than for **2** and **4**, indicating a greater

degree of photoconductivity. The conductivity for PBIs has been related to well-ordered π-stacking and the morphology has also been shown to be key.[26] The UV-Vis and pXRD data for **1**, **2** and **4** are similar; hence, we ascribe the higher conductivity of **1** to differences in fibre morphology over molecular packing.

As mentioned earlier, the response varied slightly from sample to sample. As experimental set up was kept the same as far as possible (light intensity, measurement distance, copper wire thickness and amount of material deposited), the sample thickness was measured. This was done using a profilometer, which works like atomic force microscopy by dragging a cantilever across the sample and measuring the difference in height. Measurements were performed with help from Dr. L. Phillips, University of Liverpool. As a mask was used to cast the films of both the xerogel and dried solution, the films had a sharp edge that could be measured. Film thicknesses of xerogels and dried solutions of **1** were measured and compared to the photoresponse. Three xerogel films were compared (Fig. 4.20a and b). Two had a thickness of around 1.5 μm and the third was thicker at around 4.5 μm. All the films seem to be uniform in height across the sample. The thickest film shows a much lower conductivity than the other two samples. This could be due to light not being able to penetrate the sample. The two other samples with similar thickness show different conductivities to each other. This data suggests that film thickness does not have any major effects until the film becomes too thick.

For the dried solutions (Fig. 4.19c and d), the height of the samples is not uniform with the sample being thicker on the edge. This could be due to the sample edge drying quicker than the centre and so drawing material to the edge of the samples. Focusing on the centre of the samples, two of the samples were similar in height at around 1.8 μm and another sample had a height of 3 μm. There is no significant difference in conductivity of these samples, and it does not seem to vary according to sample thickness. The xerogel and the dried solution sample thickness are both around the same height, but the photoresponse is very different. This again illustrates that differences in conductivity would appear to be due to fibre morphology rather than sample thickness.

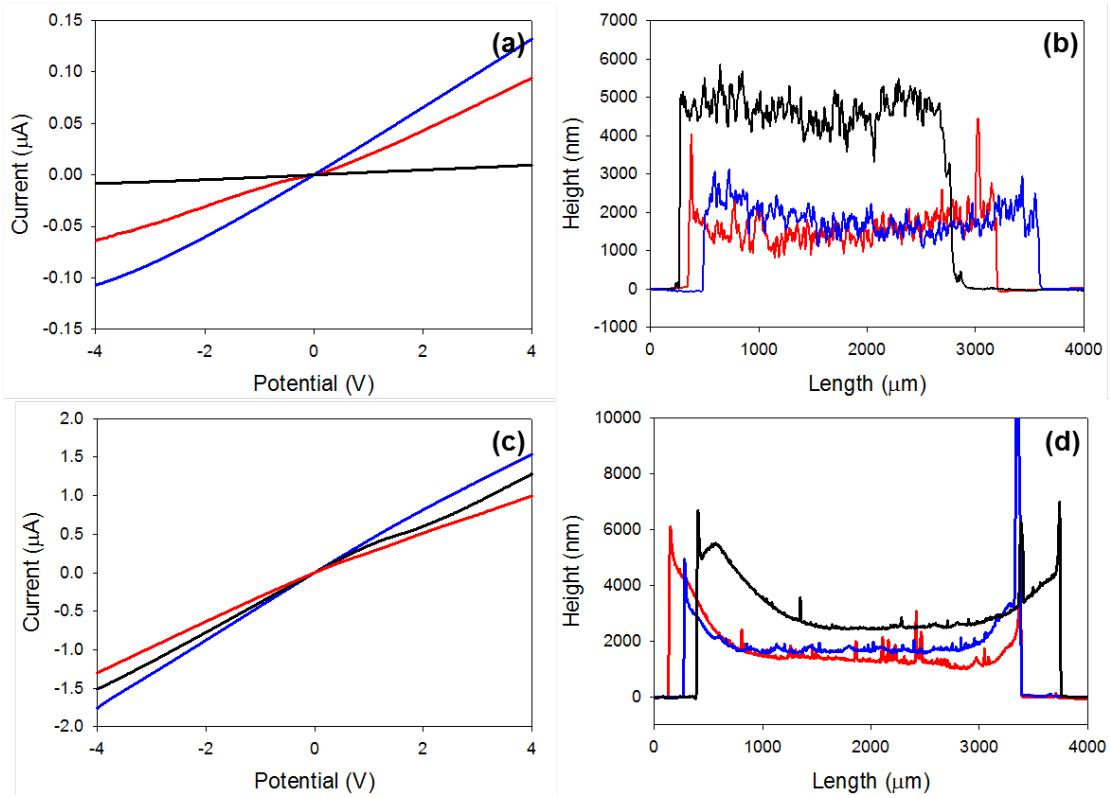

Figure 4.19 Photoresponse of (a) xerogel-**1** (c) dried solution of **1** when irradiated at 365 nm. Profilometry of (b) xerogel-**1** (d) dried solution of **1**. Different coloured data is for different samples. Colours from I-V curves correspond to the same data in the profilometry data.

Focusing on **1**, on irradiating a dried solution in a two electrode cell (2 V) with 365 nm light, the photocurrent increases with time (Fig. 4.20a). On switching off the light, the photocurrent persists for typically 1-8 hours, with the decay shown in Fig. 4.20a being fitted to a single exponential process, with a lifetime of ca. 5300 s. This indicates that the photo-induced conductivity is remarkably long-lived in air. There is variability from sample to sample, presumably due to differences in fibre density and orientation, but the films show lifetimes consistently > 3000 s. Switching the light on and off demonstrated the stability of the films (Fig. 4.20b). Similar behaviour was observed for the xerogel (Fig. 4.20c and d).

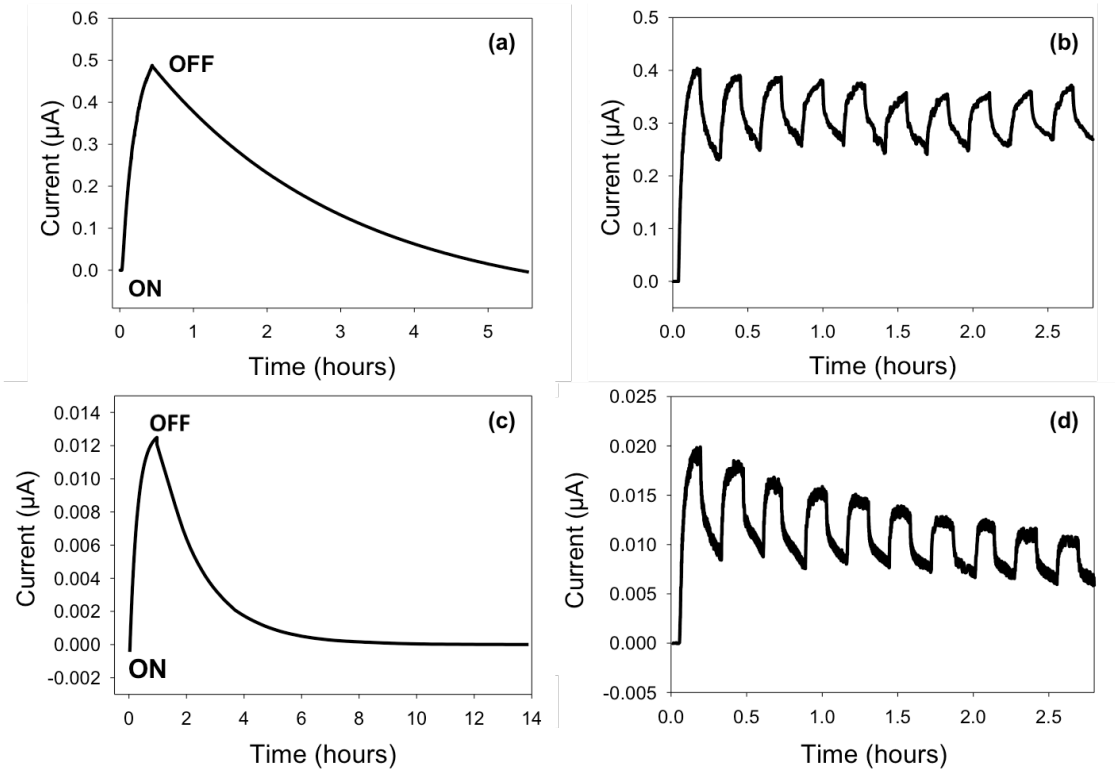

Figure 4.20 (a) Photoresponse for a dried solution of **1**, initially in the dark, then irradiated with 365 nm light, followed by the lamp being turned off. (b) Transient photoresponse for a dried solution of **1** by turning on and off the 365 nm light for multiple cycles. (c) Photoresponse of xerogel-**1** showing the change in conductivity when a 365 nm LED is turned on and off allowing conductivity to return back to off state. (d) Transient photoresponse for xerogel-**1** by turning on and off the 365 nm light for multiple cycles

It was observed that during and after irradiation with 365 nm light, both the xerogel (Fig. 4.21a) and dried solution (Fig. 4.21b) changed colour. The films changed from a red colour to a purple colour on irradiation. This colour change was reversible over several hours. The photos are only shown for xerogel-**1** and dried solution of **1**, but all other PBIs showed the same colour change.

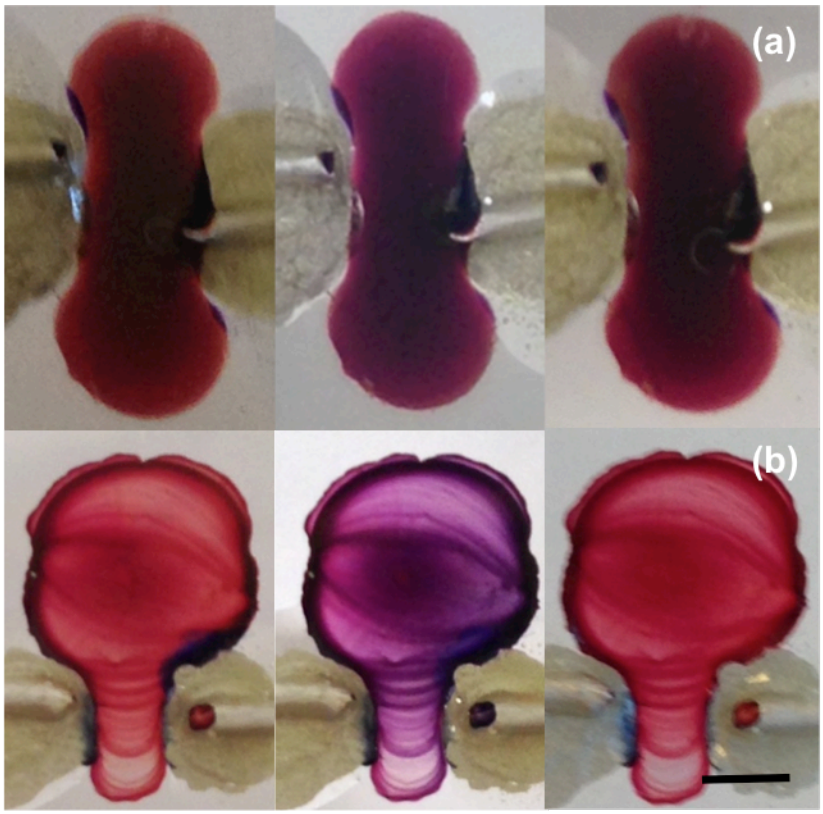

Figure 4.21 Photographs showing the colour of the thin films before irradiation (left), immediately after irradiation (middle) and 18 hours after irradiation (right) for (a) xerogel-**1** and (b) dried solution **1**. The scale bar represents 3 mm for all photographs.

For the xerogel-**1**, the samples were irradiated with 365 nm LED and the UV-Vis-NIR spectrum recorded (data collected by Dr. J. Walsh, University of Liverpool). After irradiation, the formation of a new absorption feature with maxima at 735 nm, 820 nm and 1000 nm (Fig 4.22a) could be observed, in good agreement with data for the formation of the radical anion.[19] Samples were irradiated until these peaks stopped increasing in intensity. This varied from sample to sample. For the dried solution **1**, similar absorptions were observed, albeit with a higher relative intensity, in addition to an increase in the relative intensity of the shoulder at 615 nm (Fig. 4.22b), as expected for the dianion.[20] This correlates with the conductivity of the dried solution being greater than that of the xerogel. For the dried solution **2** (Fig. 4.22d) and xerogel-**2** (Fig. 4.22c), the UV-Vis absorption spectra again show the appearance of these peaks upon irradiation. Only two of the three peaks corresponding to the radical anion can be seen here due to the wavelength range of the spectrometer used. There is little difference seen in the intensity of these peaks between the dried solution and xerogel, which again correlates with the observations

from the conductivity measurements. Spectra for xerogel-**4** (Fig. 4.22e) and dried solution **4** (Fig. 4.22f) again show the peaks for the presence of the radical anion with them being more intense for the dried solution than for the xerogels. This also agrees with the conductivity measurements mentioned earlier. Data for xerogel and dried solution **3** were unable to be collected due to poor film quality. Overall, this data suggests that the more radical anion present in the thin film, the more conductive the sample is.

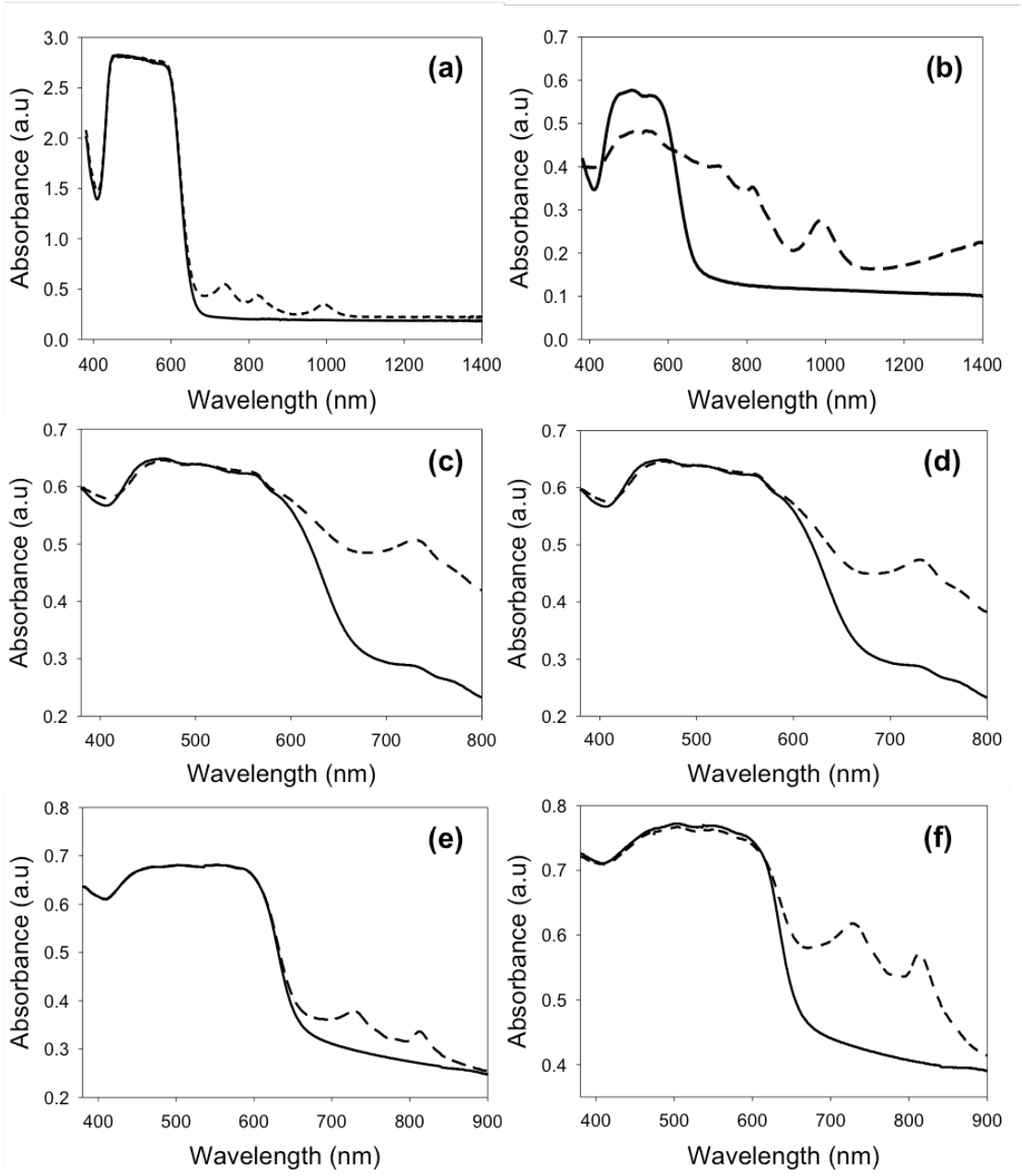

Figure 4.22 UV-Vis-NIR/UV-Vis absorption spectra showing the formation of the radical anion in the film. Data before irradiation (solid lines) and after irradiation (dashed lines) for (a) xerogel-**1**, (b) dried solution **1**, (c) xerogel-**2**, (d) dried solution **2**, (e) xerogel-**4** and (f) dried solution **4**.

It was confirmed that these peaks were characteristic of these species by reduction of **1** in solution using sodium dithionite (Fig. 4.23a).[18] The radical anion is seen with same three distinctive extra peaks and the solution is purple in colour (Fig. 4.23d). The dianion does not have the same peaks as the radical anion but has a more intense peak at 580 nm and a smaller peak at 605 nm and appears pink in solution (Fig. 4.23e). When exposed to air this peak disappears within 25 seconds (Fig. 4.23b) unlike in the film which takes hours. On the basis of these data, we suggest that the higher anion concentration in the dried solution explains the higher conductivity of the dried film over the dried gel. The possible presence of the dianion in the dried solution may also contribute, but the overlap of the spectral features with the ground state and anion prevent definitive assignment.

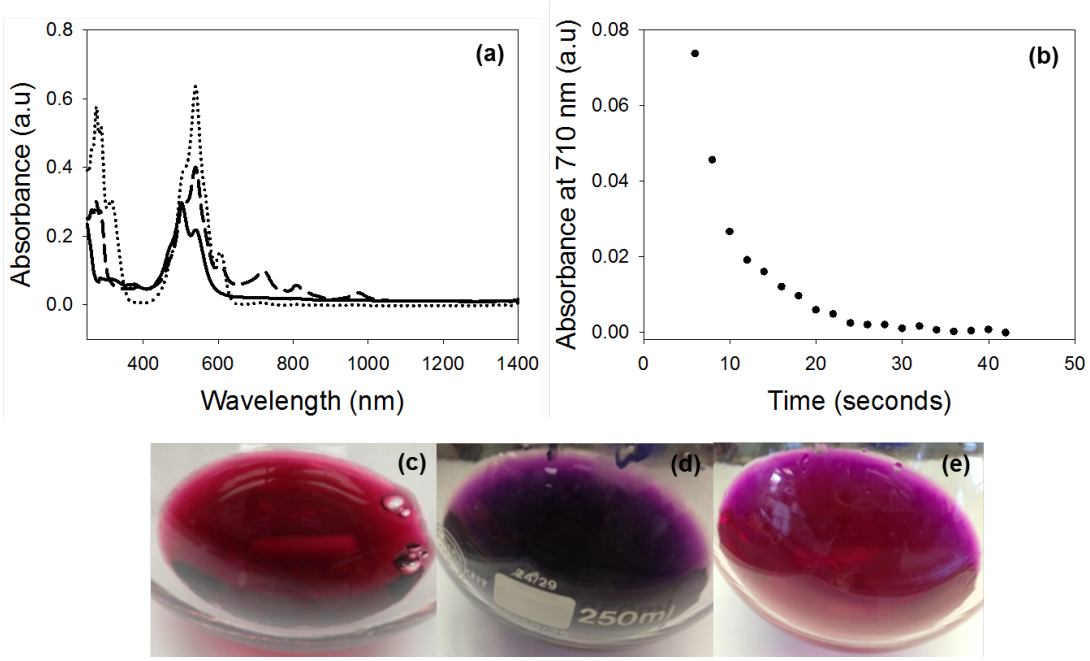

Figure 4.23 (a) UV-Vis showing absorbance of **1** in solution after with various amounts of sodium dithionite added. Solid line represents before sodium dithionite was added (photograph (c)), dashed line is after 20 mg of sodium dithionite was added (photograph (d)) and the dotted line is after 40 mg of sodium dithionite was added (photograph (e)). (b) Change of absorbance in the peak in UV-Vis at 710 nm of the dashed line after being exposed to air.

For the dried films, simultaneously measuring the UV-Vis spectrum and photocurrent after switching off the LED showed that the initial decay was similar in air or under argon (Fig. 4.24 a), and that the conductivity was essentially zero at the point where approximately 20 % of the intensity for the peak at 730 nm remained

(these data were collected by Dr. J. Walsh, University of Liverpool). This is unsurprising; for conductivity a contiguous percolation pathway is required, and hence bulk conductivity is expected to decay before the presence of any conductive species.

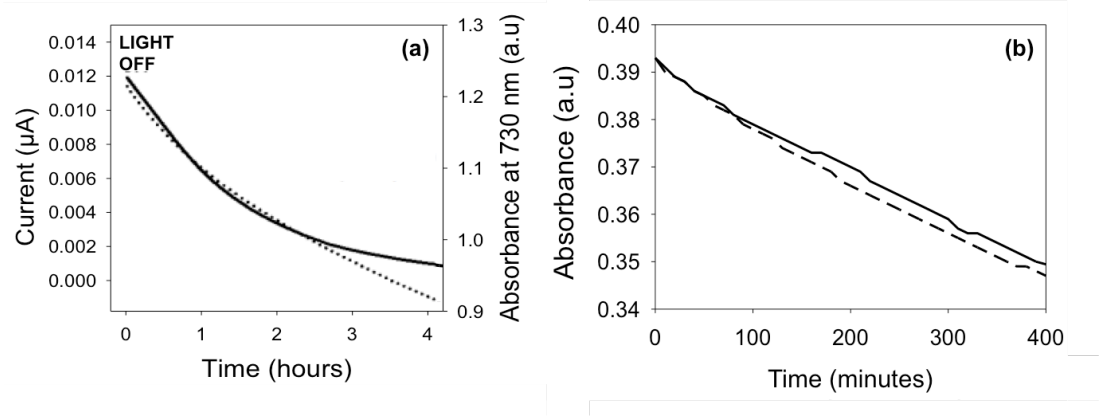

Figure 4.24 (a) Comparison of the rate of decrease in conductivity (b) Change of absorbance at 730 nm with time after the 365 nm LED was turned off of dried solution **1**. The broken line is in air and solid line is under argon.

The slow rate of decay of the photocurrent is surprising. The PBI radical anion in solution can be used as a sensitive probe for O_2.[20, 54] Our materials behave similarly when in solution as shown in Fig. 4.23b, where the radical anion and dianion are quickly oxidised in air. However, when dried as a film, it is clear that the O_2 sensitivity is significantly reduced. Indeed, all of the data in Section 4. 2. 2. are for measurements carried out in air. Under an argon atmosphere, the rate of decrease was similar to that in air; this shows that O_2 has little effect on the recovery of the dried sample (Fig 4.24 b). An issue with many n-type semiconductors is the lack of stability in air. For example, photoconductive PBI-based nanofibers have been shown to be highly sensitive to the presence of O_2, where the photoconductivity was found to be three times higher under argon than under air.[15] This was ascribed to high surface area available due to the morphology and the scavenging ability of O_2. However, in other cases, the morphology can result in a kinetic barrier to the intrusion of water or O_2, for example by using PBIs containing perfluorinated substituents.[55, 56] It has also been reported that aggregation stabilizes the radical anion. When incorporated in a film, the stability of the radical anion to oxygen was found to be higher, taking 20 minutes to be re-oxidized, as opposed to being immediately re-oxidized when in homogeneous solution.[57] This was attributed to

slow diffusion of O_2 into the film. It is likely that our films are behaving similarly, with a slower oxidation time a result of the decreased diffusion rates of O_2 through the films.

Importantly, no changes in the UV-Vis spectra were observed when the samples were irradiated at 450 nm (Fig. 4.25), and hence the lack of photocurrent when irradiated at higher wavelengths can be ascribed to the lack of formation of either radical anion or dianion.

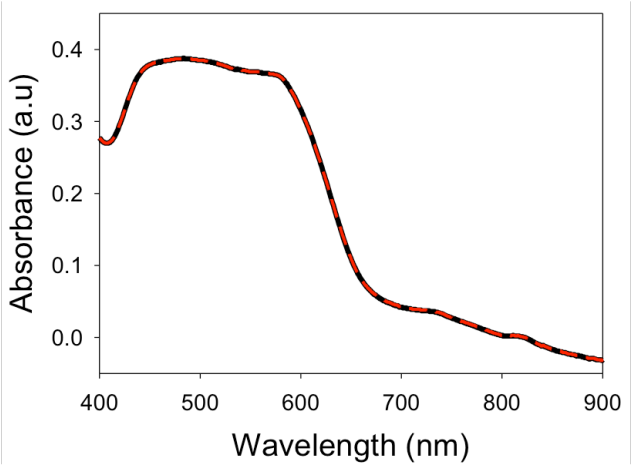

Figure 4.25 UV-Vis spectra showing the absorbance of xerogel **1** in the dark (solid line) and after 45 minutes irradiation under a 465 nm LED (dashed red line)

The correlation between conductivity and the presence of the radical anion is expected. For example, a thin film of a PBI has been shown to form the radical anion by a self-doping mechanism on dehydration in air.[10] A concomitant increase in conductivity was observed. What are perhaps surprising are both the wavelength dependence of the conductivity found here and the O_2 tolerance of the photoconductivity.

As a self-doping mechanism was suggested elsewhere for the formation of the radical anion, this was investigated further.[10] As the perylene becomes negatively charged, the source of the electron was considered. It could be the amino acid breaking down in the UV light, which then donates an electron into the perylene core. If this were to happen, a degradation of the film would likely occur and so a decrease in conductivity over time may be seen. Fig. 4.20b already shows the films

to be recoverable after many cycles of on-off irradiation. This was further tested by placing the film under 365 nm light for many hours and measuring if there was a decrease in current overtime due to a breakdown of the PBIs. Fig. 4.26 shows that the current does not decrease after 3 hours under the UV light. A dried solution of **1** was used in this experiment as it gave the greatest conductivity and so a change in current would be easier to be seen.

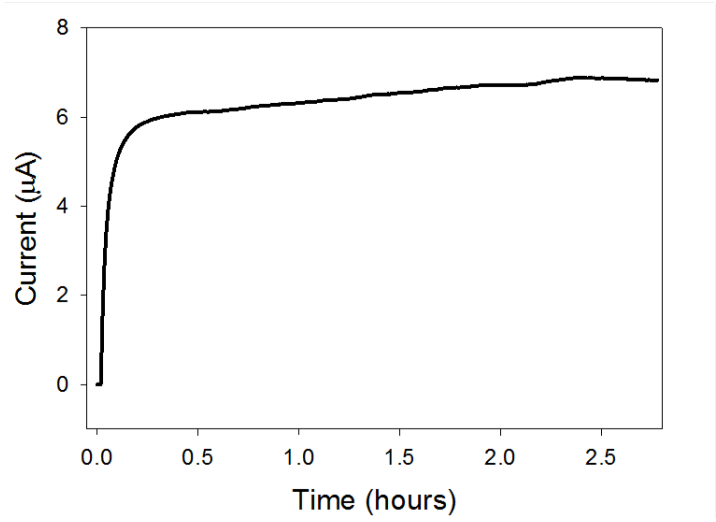

Figure 4.26 Photoresponse graph showing the conductivity of the dried solution of **1** during 3 hours of illumination under 365 nm LED.

The film may have broken down, but not significantly enough to affect the conductivity (as the electron will take the shortest path, some film degradation could still leave a pathway for the current to flow). The sample's conductivity could not be measured under illumination for longer than 3 hours due to instrument limitations and also for safety reasons due to heat produced from the 365 nm LED. ^{1}H nuclear magnetic resonance (NMR) was used to try and probe if there was degradation of the amino acid functionalised PBI. This was done by redissolving the films before and after irradiation in deuterated dimethyl sulfoxide (d_6-DMSO). However, the films were not completely soluble in the d_6-DMSO, or in any deuterated solvent and so spectra were difficult to interpret. Instead, to investigate film breakdown infrared (IR) spectroscopy of the films was used. An IR spectrum of dried solution **1** was recorded before any irradiation. The sample was then irradiated for a total of 3 days. The spectrum was then recorded immediately (Fig. 4.27). There is no change in the spectrum, apart from a new peak at 1520 cm^{-1} that corresponds to the radical anion vibration.[58] This again suggests that film is not breaking down, so is unclear where

the electron is coming from. Solubility and the high absorption co-efficient of these dried samples make them very difficult to analyse by spectroscopy.

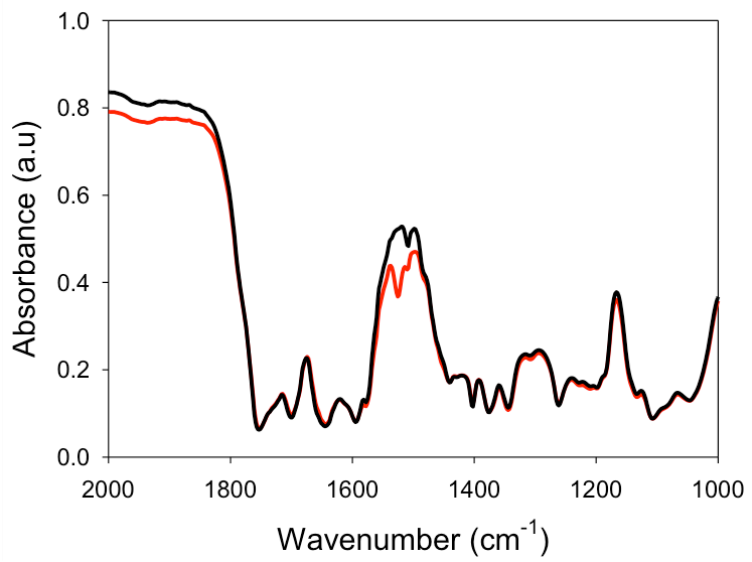

Figure 4.27 FTIR spectrum of dried solution **1** before irradiation (black data) and after irradiation with 365 nm LED for 3 days (red data).

An enhancement in conductivity for a PBI has been found previously on generation of the radical anion using hydrazine vapour.[59] Other groups used diethylamine to increase the conductivity of the PBI fibres.[13] In both these cases, these are strong electron donors, also known as hole scavengers (discussed in more detail in Chapter 5). In this work, no such donor is present (it is also not known what the donor is as discussed above) explaining the greater E_{ebe} here. If the PBI were itself to donate an electron, the simultaneous formation of the radical cation would be expected. The presence of this cation is not clear. Whilst there is significant data available on the radical anion and dianion for a range of PBIs, there is significantly less on the radical cation. Much of the data is contradictory or unclear so direct comparison to our materials is difficult.[60-62] A broad peak above 1200 nm in the UV-Vis spectrum for the dried solution of **1** after illumination with 365 nm LED is observed (Fig. 4.22b). On the basis of the solution phase chemical reduction experiment, this cannot be assigned to the radical anion or dianion (Fig. 4.23a). This feature grows in under UV illumination with a maximum at ~1700 nm, and decays at the same rate as the radical anion. It is possible that the NIR absorption is due to the radical cation, although this would represent a remarkably long-lived charge separated state. Further investigation

could be done using transient absorption spectra (TAS).[63] This would give more information on excited states created and how longed lived UV created species such as the radical anion and cation. Again, the literature on these systems gives different information and is often carried out on highly diluted systems and so would not necessarily be representative of our films, as concentration massively affects PBIs.

As noticed earlier, the dried solutions are more conductive than the xerogels. As the same amount of material is used for each of the experiments, we hypothesise that this is to do with how the fibres are arranged and/or the morphology of the fibres. Sodium hydroxide and GdL were ruled out from causing the differences in conductivity between the samples by looking at other gelators that form worm-like micelles in solution and measuring the conductivity of these samples. Fig 4.28 shows that other gelators are not conductive either as a xerogel or dried solution. The data are very noisy due the sample not being conductive and having no ohmic contact.

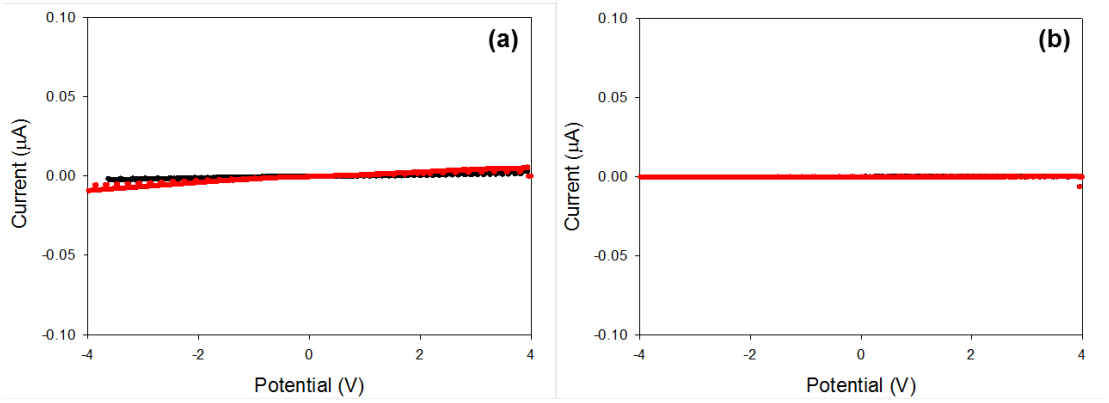

Figure 4.28 Photoresponse of naphthalene diphenylalanine (a) xerogel (b) dried solution. Black data is in the dark and red data is when irradiated using a xenon lamp.

4. 2. 3. Aligned Thin Films

The films were examined more closely by viewing under cross-polarized light under an optical microscope. Cross-polarised light is composed of only light travelling in a north to south direction and an east to west direction. Under cross-polarised light only structures with birefringement (alignment) will show up brightly coloured. For perfectly aligned structures, such as crystals, a Maltese cross is observed. This is due to the two refracted light rays recombining at the back focal plane of the objective; they then interfere and produce a characteristic Maltese cross shape. Xerogel-**1** and

dried solution of **1** will be focused on here to for clarity. Xerogel-**1** and dried solutions of **1** were viewed under cross-polarised light. Fig. 4.29 shows that the two samples look very different. The dried solution of **1** (Fig. 4.29a) shows bright rings whereas xerogel-**1** (Fig. 4.29b) shows very little colour. These microscope images show that the dried solution shows aligned structures, whereas the xerogel does not. These rings seen for the dried solutions could be due to the coffee ring effect.[64] When the sample is deposited onto the glass, the drop sits on the glass with more of the sample in the middle. This results in different evaporation rates and leads to capillary flow. The liquid evaporating from the edge is replaced by liquid from the middle of the drop. The resulting edgeward flow can carry nearly all the dissolved material to the edge and leads to the coffee ring shape. As there are worm-like micelles in solution, these align along edge of the rings. This has been used as method of alignment previously.[65, 66] Samples cast using the mask technique described in Section 4.4 did not show this coffee-ring, as samples were not circular and so dried different.[67] Only samples drop cast showed this alignment.

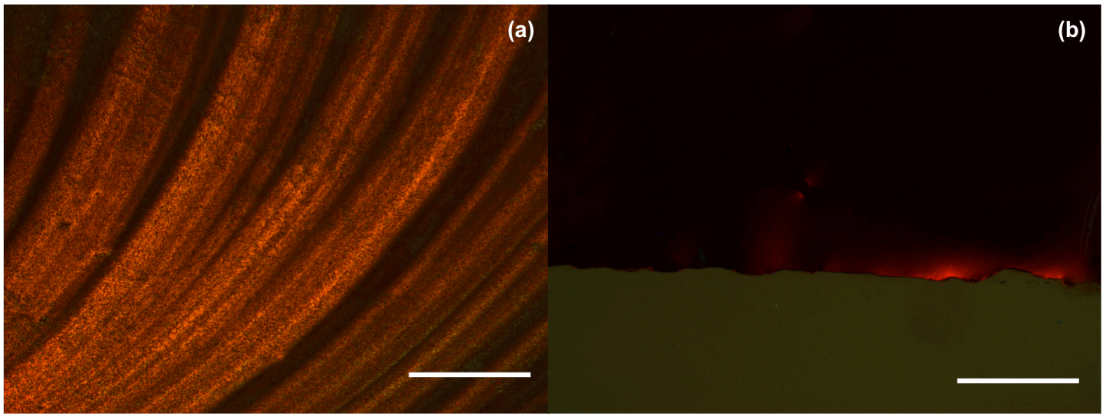

Figure 4.29 Microscope images taken under cross-polarised light of (a) dried solution of **1** and (b) xerogel-**1**. Scale bar represents 50 μm.

These images agree with the SEM images shown in Fig. 4.4 and Fig. 4.8, where the solutions show a greater alignment than the xerogels. A more aligned sample would show increased conductivity as the path the electron has to travel is shorter and so there is less chance of recombination of the charges. To test this, the conductivity was measured with the alignment and against the alignment. This was done by placing silver electrodes either side of the alignment and above and below the alignment (described in detail in Section 4.4). For xerogel-**1**, this was done by

placing electrodes left and right, and top and bottom of the sample. Fig. 4.30a shows the conductivity of xerogel-**1** is very similar in both directions, whereas Fig. 4.30b shows the dried solution has a significantly higher conductivity along the alignment than against. This was highly reproducible. The absolute values of conductivity were slightly different, but the outcome was the same. To quantify this directional dependence on photoresponse, the value at -4 V taken for the measurement against alignment was divided by the value at -4 V for the measurement with alignment. This way, the closer to zero the number is the greater the alignment. This value will be used throughout this Chapter to determine the degree of alignment. For xerogels this was typically around 0.95 and for the dried drop-cast solutions this was around 0.32.

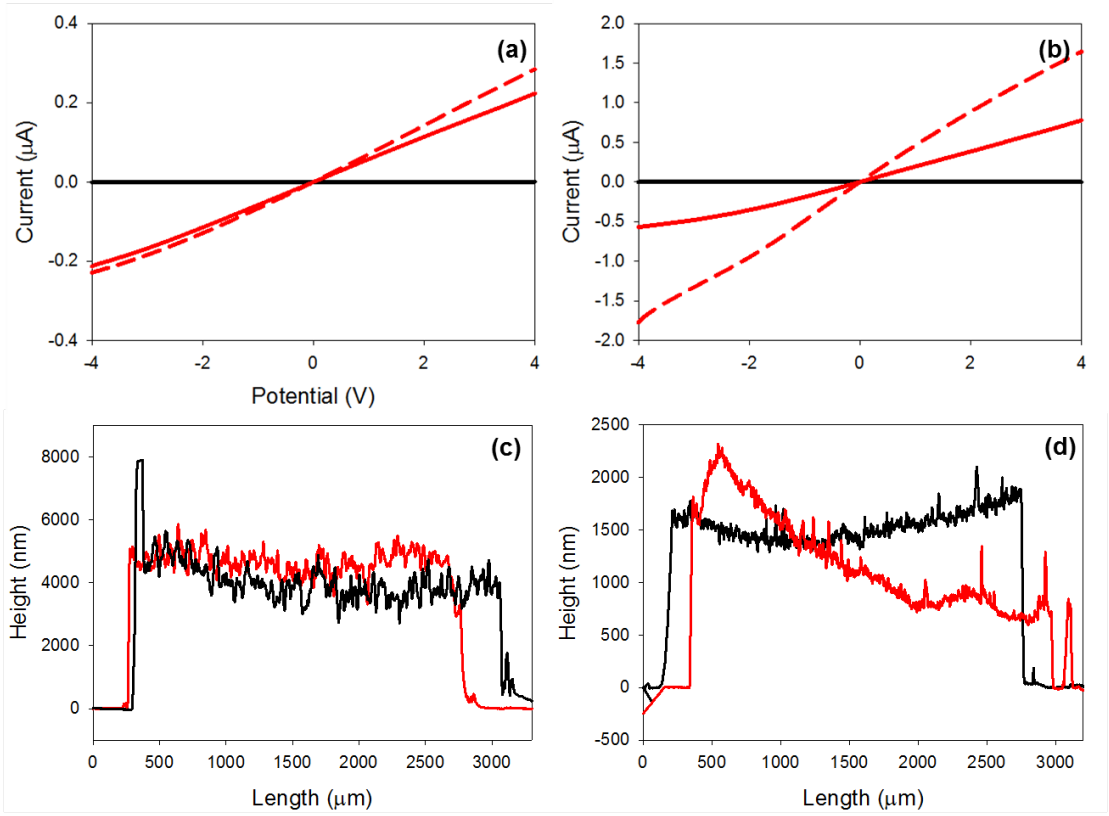

Figure 4.30 Photoconductivity of (a) xerogel-**1**, solid black line is in measured in the dark, dashed red line is measured from left to right and solid red line is measured from top to bottom and (b) dried solution of **1**, solid line is measured in the dark, dashed red line is measured with the alignment and solid read line against the alignment. Profilometry measurements of (c) xerogel-**1**, left to right (red) and top to bottom (black) and (d) dried solution of **1**, black data is with alignment and red data is against alignment.

As the dried solution samples were drop cast as a film first and then a 3 mm x 3 mm section was used for the measurements, concentration effects were investigated. This

was done by preparing many samples and also selecting several sections from the same sample and measuring the conductivity along the alignment. The sample between the electrodes was then removed and redissolved in basic water. The concentration could then be determined by UV-Vis spectrometry by comparing to a calibration curve. The concentration of each of the samples was then plotted against the current at 4 V with and against alignment (Fig. 4.31). This illustrated that the conductivity of the sample was not due to slight variations in concentration. The observed variation in concentration could be due to the rate at which the samples dried down and so how aligned the samples are. The rate at which the samples dry down is due to humidity and temperature. Drying of the samples was done in the open lab at room temperature and so could not be controlled.

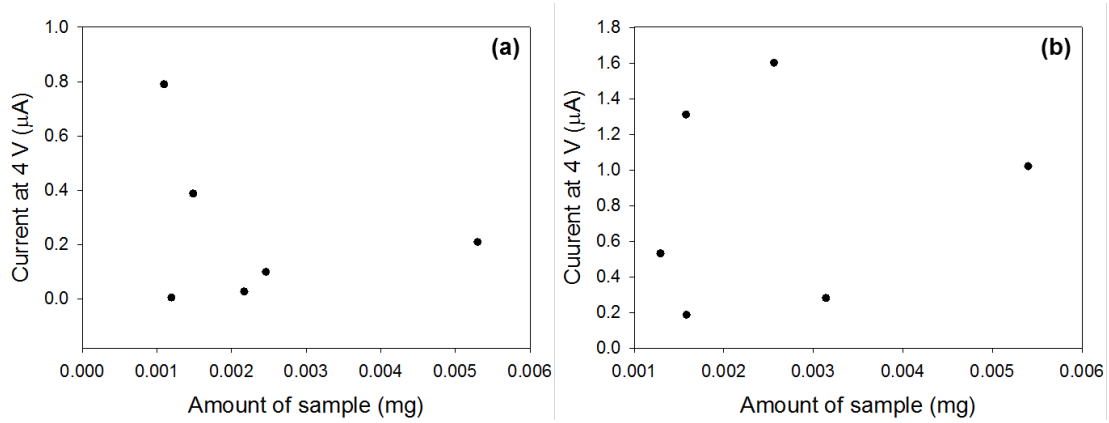

Figure 4.31 Current at 4 V under 365 nm LED compared to the concentration of sample between the silver electrodes for dried solution of **1** (a) against alignment and (b) with alignment.

To further control the concentration and film thickness of the dried solution samples, samples were cast in a mould using sellotape. However, this method removed the coffee-ring effect and the samples showed no directional dependence with a difference in photoresponse of around 0.98 (Fig. 4.32b). This is due to the solution not being spherical and not being able to dry the same as the samples shown in Fig. 4.32a.[67]

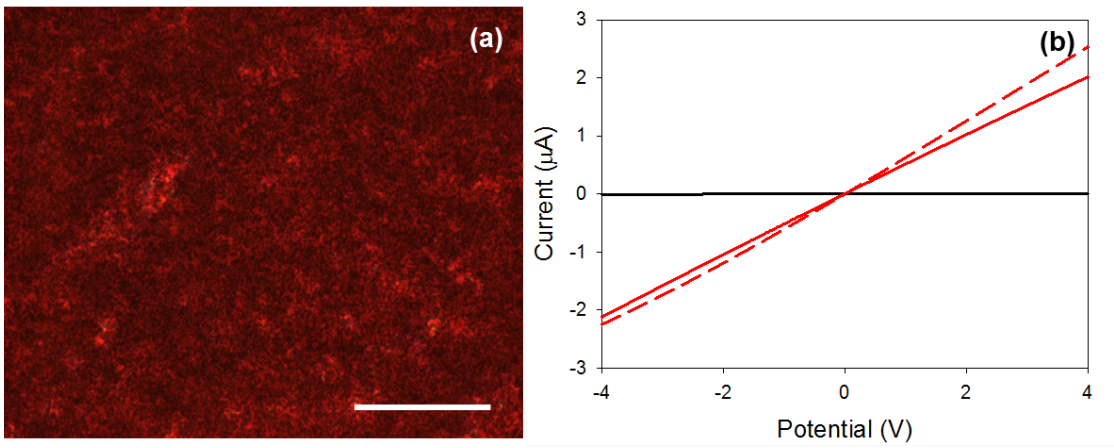

Figure 4.32 (a) Optical microscope image taken under cross-polarised light of a dried solution of **1** using a mask. The scale bar represents 500 nm. (b) Photoresponse of the sample in (a) showing no directional dependence in current. Black data is take in the dark, red data is under 365 nm light. Dashed red data is measurements recorded from left to right of the sample and solid red data recorded from the top to the bottom of the sample.

Anisotropic samples give greater control of the orientation of the fibres and the direction of the conductivity. This is important when designing material to be used in electronic devices. Other methods of alignment were investigated. Potential methods of alignment include shear alignment,[68] spin coating,[69] magnetic alignment,[70] gravitational alignment[71, 72] and doctor blading to name a few. All these methods rely on the solvent in which the material is dissolved evaporating quickly enough to keep the alignment created. As the samples are dissolved in water, this would be difficult to do; changing the solvent would change the morphologies of structures in solution and in the gel.

Spin coating was attempted using solution of **1** at different concentrations and at different rotation speeds. Fig 4.33 shows solutions at 5 mg/mL (Fig 4.33a and b) and 50 mg/mL (Fig. 4.33c and d) both at a rotation speed of 1800 rpm for 30 seconds as examples, but films looked similar at various speeds and time of spin coating. Solutions at 5 and 10 mg/mL did not give a continuous film and did not show any alignment. Solutions at 20 and 50 mg/mL gave a continuous film but when viewed under the optical microscope the samples had started to crystallise (Fig. 4.33d). Hence, these films were not suitable for their photoresponse to be measured. Spin coating may not have been successful due to the glass being hydrophobic and the water being unable to evaporate quickly enough.

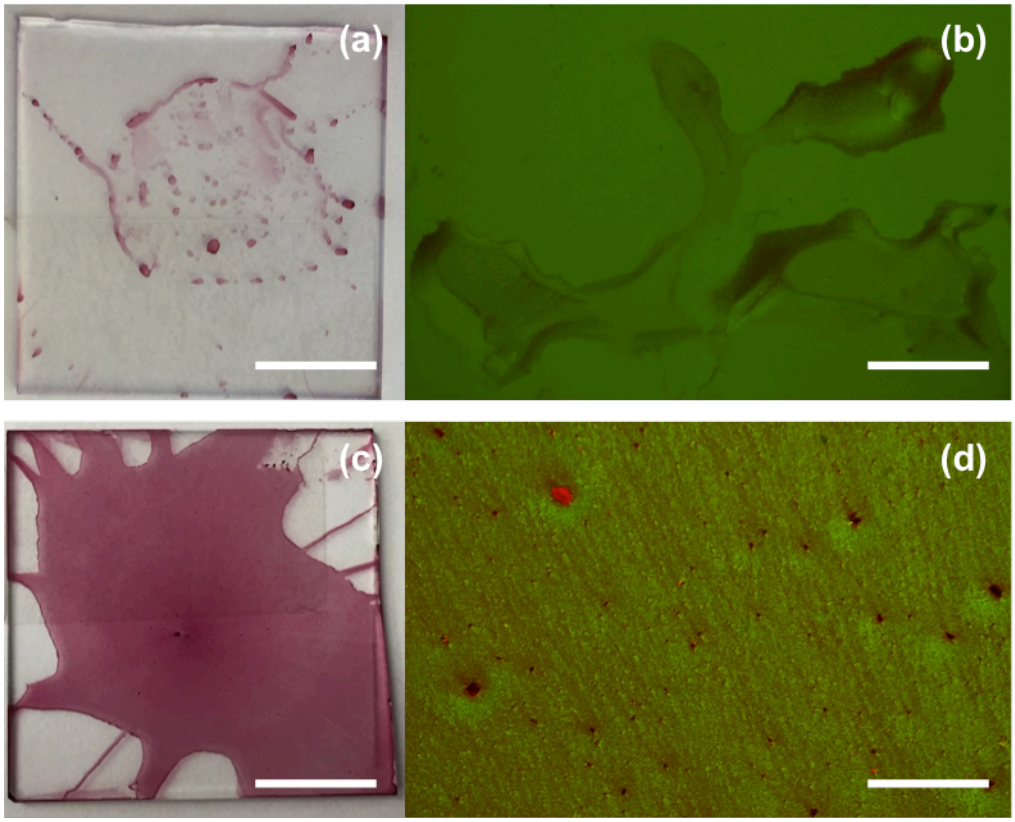

Figure 4.33 Photographs of spin coated films of solution of **1** (a) at 5 mg/mL (c) at 50 mg/mL. Scale car represents 1 cm. Spin coated films microscope images under cross-polarised light (b) at 5 mg/mL and (d) at 50 mg/mL. Scale bar represent 0.5 mm. Spin coating was performed at 1800 rpm for 30 seconds.

The glass surface was made more hydrophilic by rubbing with cotton wool to create a charged surface. Spin coating was tried again, varying the concentration and speed of rotation. The spin coating was performed at up to 10,000 rpm for 60 seconds to try and remove all of the solvent. This time a more homogeneous film was achieved (Fig. 4.34a), but again when examining under cross-polarised light there was no alignment (Fig. 4.34b). This spin coating was performed by Dr. D. Toolan, University of Sheffield. These results illustrated that spin coating of this material in water was not appropriate for aligning the material. Other methods of alignment, doctor blading and gravitational alignment were also attempted, but had the same result as spin coating due to the water not evaporating quickly and the hydrophobicity of the glass.

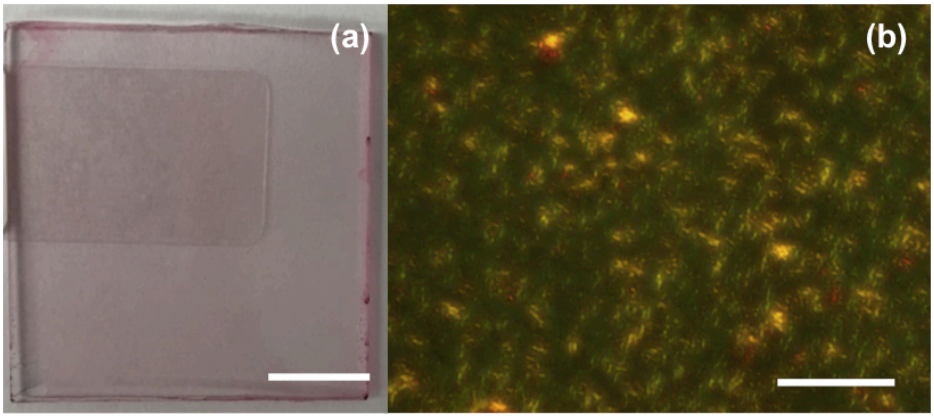

Figure 4.34 (a) Photograph of spin coated solution of **1** at 50 mg/mL at a rotation speed of 10,000 rpm for 60 seconds. Scale bar represents 1 cm. (b) Microscopy image of (a) under cross polarised light. Scale bar represents 50 μm.

Previous work by Wallace et al. demonstrated that worm-like micellar structures could be aligned under a magnetic field.[39] They proposed that the structures align perpendicular to the magnetic field due to the fibres being slightly negatively charged. They were able to do this with solutions and then gel the samples under the magnetic field using GdL. The gels kept their alignment when taken out of the field due to their alignment being locked in by gelation. This alignment was shown by ^{2}H and ^{23}Na NMR (residual sodium from NaOH used in preparation of the solutions), as they associated with the fibres and so showed anisotropic behaviour when the fibres were aligned. This resulted in a splitting of the peaks due to residual quadrupolar coupling of the ^{2}H and ^{23}Na. The amount of splitting is comparative to how aligned the structures are.[73] This method is also useful owing to the fibres themselves cannot be seen using conventional ^{1}H NMR, but the effect on the probes placed in solution, in this case ^{23}Na, associate with the NMR invisible structures can be seen. What happens to the probes can be used to monitor what is happening to the structures.

^{23}Na NMR spectroscopy was performed on solutions of **1** at concentrations ranging from 5 to 50 mg/mL by M. Wallace, University of Liverpool. The data showed splitting in the ^{23}Na peak, which is indicative of alignment of the worm-like fibres in solution (Fig. 4.35). The extent of splitting in the data increases proportionally to the concentration, except for at 50 mg/mL. This could be due to crowding of the material or liquid crystal formation.[74, 75]

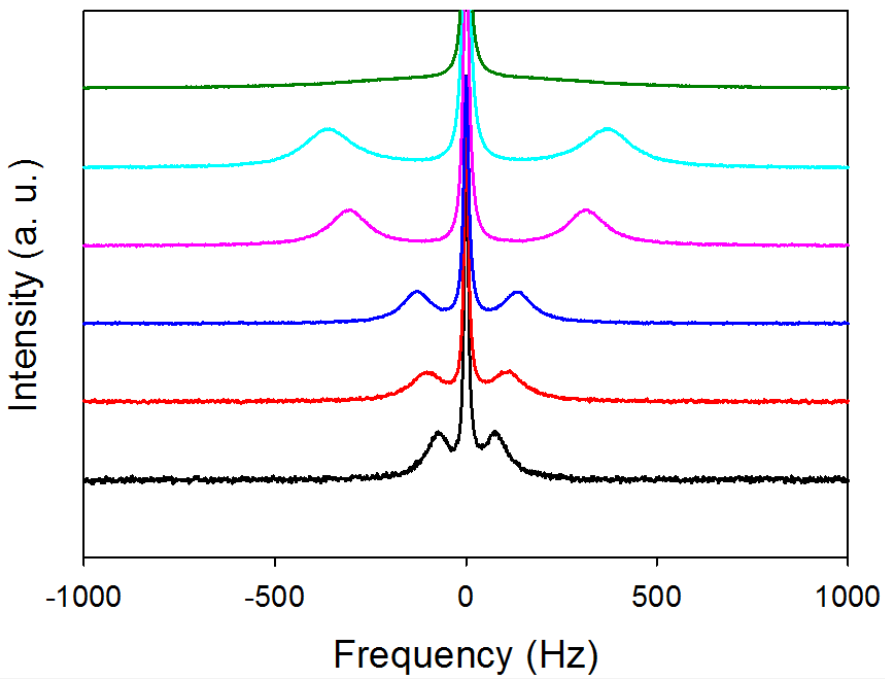

Figure 4.35 ^{23}Na NMR spectra showing splitting of the peak in solutions of **1** after 20 minutes under the magnetic field. Black data is at 5 mg/mL, red data at 10 mg/mL, blue at 20 mg/mL, pink data at 30 mg/mL, light blue data at 40 mg/mL and green data at 50 mg/mL.

This method of alignment was carried out using solutions of **1**, but instead of gelling under the field, they were allowed to dry under the magnetic field. This method allows the alignment of the fibres whilst the water evaporates. These experiments were performed by placing 20 μL of solution onto a glass cover slip, then lowering the slide into a NMR spectrometer and allowing it to dry overnight in the magnetic field with the help of M. Wallace, University of Liverpool. This method is discussed in more detail in Section 4.4. Fig. 4.36 shows optical microscope images under cross-polarised of the solution at different concentrations, dried under the magnetic field. Fig. 4.36 a, b and c show alignment of the sample. Fig. 4.36d at 50 mg/mL seems to show liquid crystalline behaviour at the edge of the sample, this is due to the solution being highly concentrated, this agrees with data shown in Fig. 4.35.

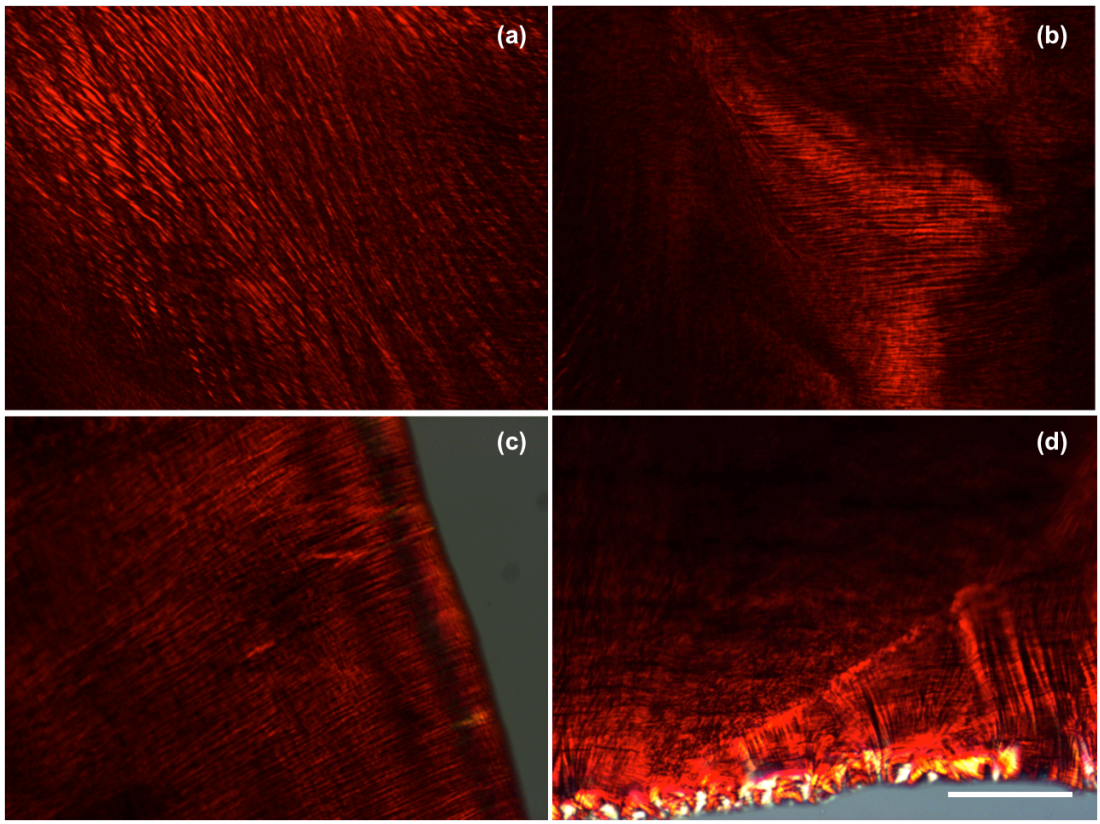

Figure 4.36 Optical microscope images of dried solution of **1** under cross-polarised showing magnetic alignment. Dried solutions from a concentration of (a) 10 mg/mL (b) 20 mg/mL (c) 30 mg/mL and (d) 50 mg/mL. Scale bar represents 50 μm.

SEM images (collected by Dr. T. McDonald, University of Liverpool) of samples dried under a magnetic field also showed this alignment (Fig 4.37c and d) compared to samples not dried in the field (Fig. 4.37a and b). Samples dried out of the field show a more random orientation of the worm like fibres whereas sample dried under the field show a more ordered arrangement.

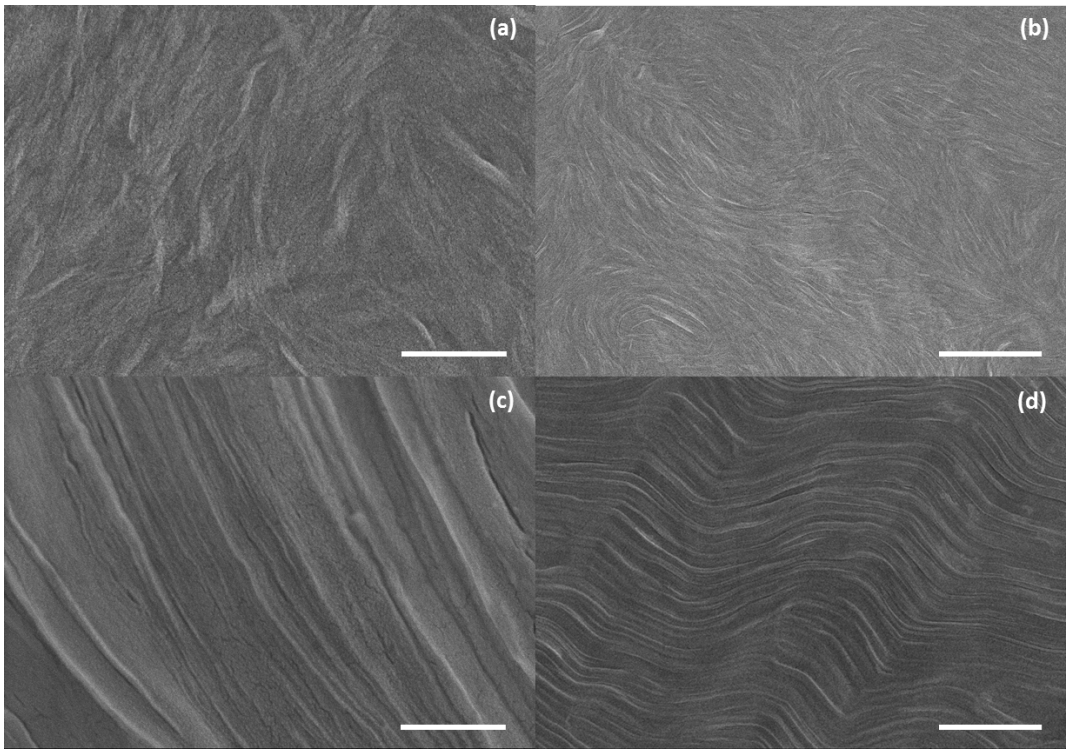

Figure 4.37 SEM images of a 50 mg/mL dried solutions solution (a) and (b) dried away from the magnetic field and, (c) and (d) dried under a magnetic field. Scale bar for (a) and (c) represents 500 nm. Scale bar represents 2.5 μm.

Conductivity measurements were performed as described previously with and against alignment (Fig. 4.38). All samples showed a directional dependence. In the case of a solution at 30 mg/mL (Fig. 4.38c), there is a significant directional dependence. The aligned sample showed a value 0.06 for directional dependence, with measurements against alignment being comparable to that of measurements performed in the dark. The samples gave similar directional dependence at 5 mg/mL (Fig. 4.38a), 10 mg/mL (Fig. 4.38b) and 50 mg/mL (Fig. 4.38d). They all have a directional dependence values between 0.25 – 0.28. They therefore have a better directional dependence value than the coffee-ring samples and so would indicate that the samples are more aligned.

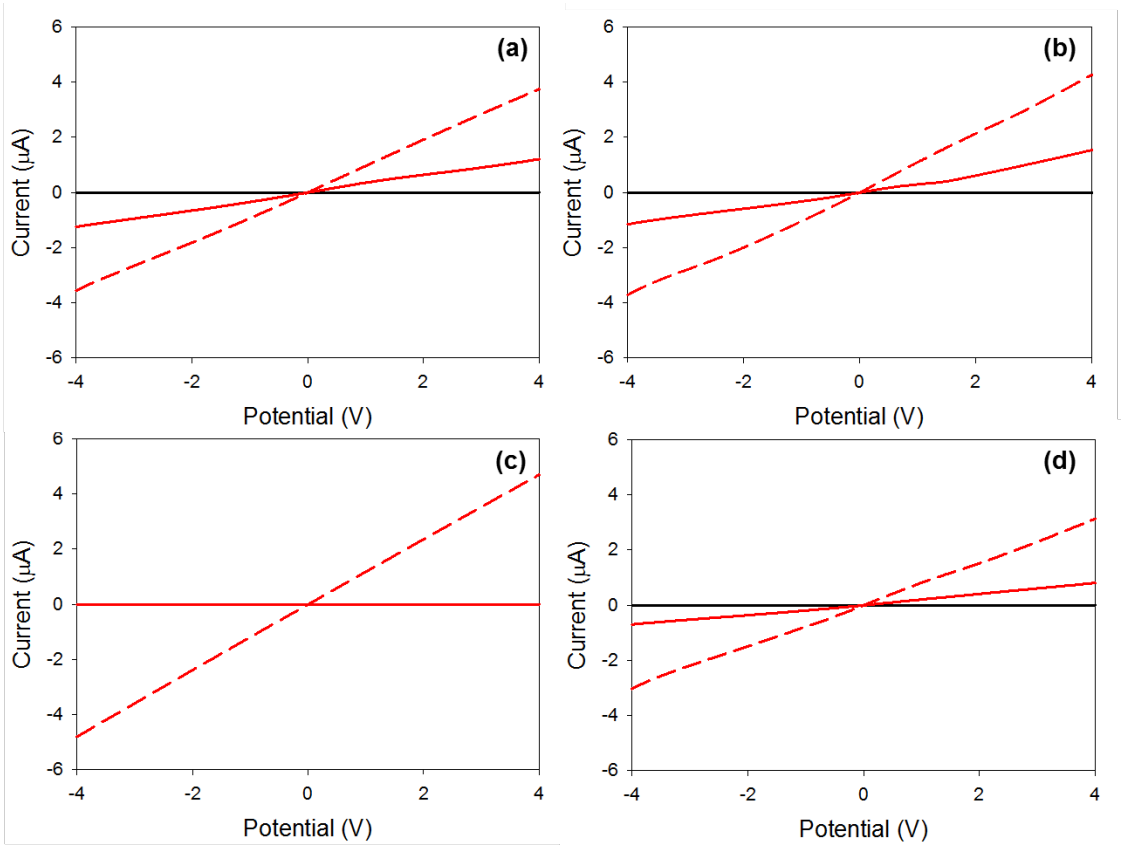

Figure 4.38 Photoresponse of samples dried under a magnetic field of a solution of **1** at (a) 5 mg/mL (b) 10 mg/mL, (c) 30 mg/mL and (d) 50 mg/mL. Black data is in the dark and red data is under 365 nm light. Solid red data is against alignment and red dashed data is with alignment.

Unfortunately, this method of alignment was not always reproducible. Some samples would show no alignment (Fig. 4.39a) or some alignment (Fig. 4.39b). These samples would give less directionally dependent photoresponse measurements (Fig. 4.39c) compared to the very aligned samples (Fig. 4.39d). They also had different absolute current values. This irreproducibility could be due to a number of variables. The strength of the magnet field could be one factor as the strength varied inside the spectrometer. The temperature and humidity of the air could also not be controlled inside the spectrometer and so rate of evaporation would vary. This could also affect the alignment of the material.

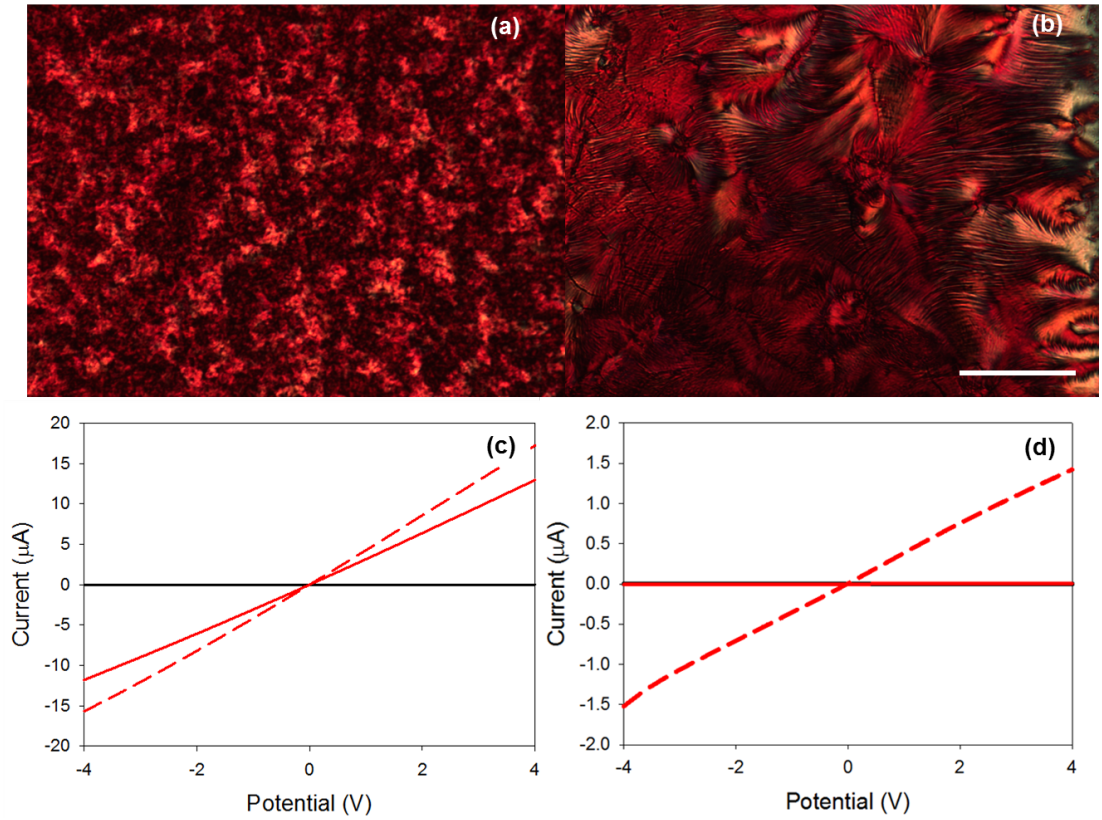

Figure 4.39 (a) and (b) Optical microscope images under cross-polarised light of two different solutions of **1** at 5 mg/mL dried under a magnetic field. Scale bar represents 50 μm. (c) and (d) Photoresponse of the different samples dried under a magnetic field of a solution of **1** at 30 mg/mL on different days. Black data is in the dark and red data is under 365 nm light. Solid red data is against alignment and red dashed data is with alignment.

A more reproducible method of alignment is therefore needed, with less variable parameters. Shear alignment was investigated. Shear happens when you apply stress parallel to a solution. There are several ways of applying shear to a solution; shear flow,[76] mechanical shear,[77] oscillatory shear[78] etc. As worm-like micellar fibres are present in the PBI solutions, if enough shear is applied to the sample then the fibres should align parallel with shear.

To see whether the solutions would shear align, a rheo-optics set-up was used.[79, 80] Here, a rheometer where the bottom plate is glass is used, with a camera and a cross-polarised light source attached used to image the sample. This set up allows us to visually monitor what is happening to the solution under shear. The solution was placed between the two parallel plates on the rheometer and shear applied by rotating the top plate. As the plate rotates, the camera records what is happening. If the

solution is bright then alignment has occurred. When the solution is perfectly aligned, a Maltese cross is visible. The light intensity of the image is proportional to the degree of alignment, as well as the concentration of sample used. This measurement was performed on solutions at 5, 10, 20, 30, 40 and 50 mg/mL of gelator (Fig. 4.40). These measurements were performed with Dr. O. Mykhaylyk, University of Sheffield.

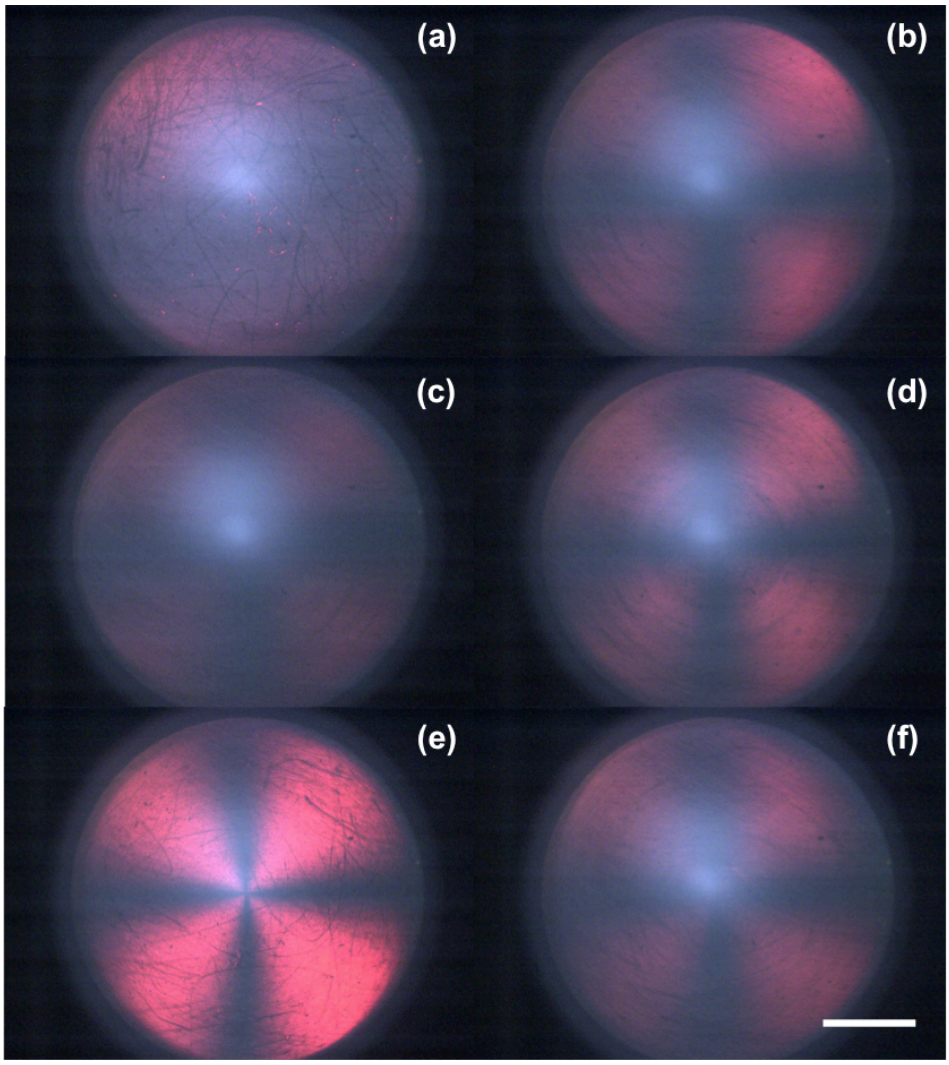

Figure 4.40 Images of solution of **1** under cross-polarised light under 100 s-1 shear using a 25 mm parallel plate with a 0.2 mm gap distance at 25 °C (a) 5 mg/mL, (b) 10 mg/mL, (c) 20 mg/mL, (d) 30 mg/mL, (e) 40 mg/mL and (f) 50 mg/mL. Scale bar represent 5 cm.

When a maximum shear of 100 s^{-1} was applied to the samples for 30 seconds using a 25 mm parallel plate, alignment occurred in all samples. The solution at 5 mg/mL (Fig. 4.40a) showed the least alignment under these conditions, with the dullest picture, whereas the 40 mg/mL (Fig. 4.40e) showed the most alignment with the

brightest, most defined Maltese cross. Less alignment at the lower concentrations could be because there is not enough material in solution for optimum alignment, whereas at 50 mg/mL has more material and may be too crowded.

The shear alignment images can be further analysed and processed using the image analysis software ImageJ. A slice of each image at a 45° angle to the Maltese cross was taken and then combined to produce one image (Fig. 4.41c). The parallel plate applies a different shear rate to each part of the sample (Fig. 4.41a). This is because the outside edge is travelling faster than the middle of the plate, as it has further to travel in order to make one rotation.

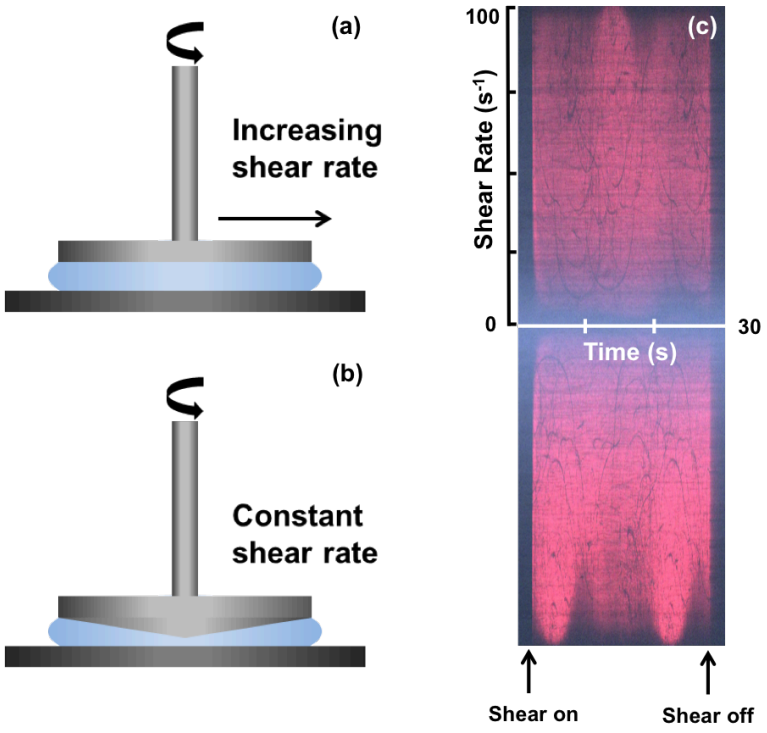

Figure 4.41 Cartoon showing alignment of a solution using (a) parallel plate and (b) using cone and plate geometries on a rheometer. (c) A time sliced image of a solution of **1** at 10 mg/mL under a maximum shear of 100 s^{-1} for 30 seconds.

Hence, on analysing the images as described, the vertical axis is shear rate and the horizontal axis is time. From Fig. 4.41c, it can be seen a shear rate of 10 s^{-1} is needed for alignment as that is where the image is consistently bright. This image also shows that alignment happens very quickly from when shear is applied, but also shows alignment is lost in milliseconds after the shear is stopped. This loss in alignment is

seen more clearly when viewing the images as a video. This quick recovery rules out such alignment method as doctor blading, gravitational alignment and spin coating as the sample recovers quicker than the solvent can evaporate. It also explains why other literature states that alignment of the perylene bisimides is not possible.[81]

The time sliced image shown in Fig 4.41c is for a solution at 10 mg/mL but all concentrations showed very similar results with different intensity of light. To overcome the problem of the solution recovering quickly after shear, it was proposed that the solution could be gelled slowly under a constant shear using a cone and plate geometry shown in Fig. 4.41b. When the shear stopped, the structure would be locked in by gelation and all of the sample would have the same alignment. This method would remove the variables seen for the magnetic alignment as temperature can be set on the rheometer bottom plate, and due to the top plate covering the sample, evaporation of water will be slowed down allowing gelation enough time to occur. By using cone and plate geometry to perform this shear, the viscosity of the sample can be measured, so gelation can be also be monitored. This method could also be used to prepare aligned dried solutions by letting the solution completely dry whilst under shear.

A solution of **1** at a concentration of 10 mg/mL was used in these experiments as it was the lowest concentration that gave a clear Maltese cross (Fig. 4.40). For an aligned dried solution, a piece of glass was sellotaped on to the bottom plate of the rheometer. The solution was placed on the glass and a 25 mm cone geometry was lowered onto the solution so the all the bottom of the geometry was covered. The excess solution was removed. A shear of 10 s^{-1} was applied, as from Fig. 4.41a, this was the lowest shear rate that resulted in alignment. A higher shear was not use to reduce the chance of damaging the film as the film dried. The shear was applied overnight whilst all the water evaporated from the sample. After the solution was dry, the glass could be removed from the rheometer and the sample could be viewed on the microscope under cross-polarised light. Fig. 4.42a shows a photograph where aligned rings of material can be seen. Under cross-polarised light (Fig. 4. 42b, c and d), these aligned rings are clearer and more brightly coloured showing alignment of the material. This method of shear alignment was very reproducible and gave similar images each time performed.

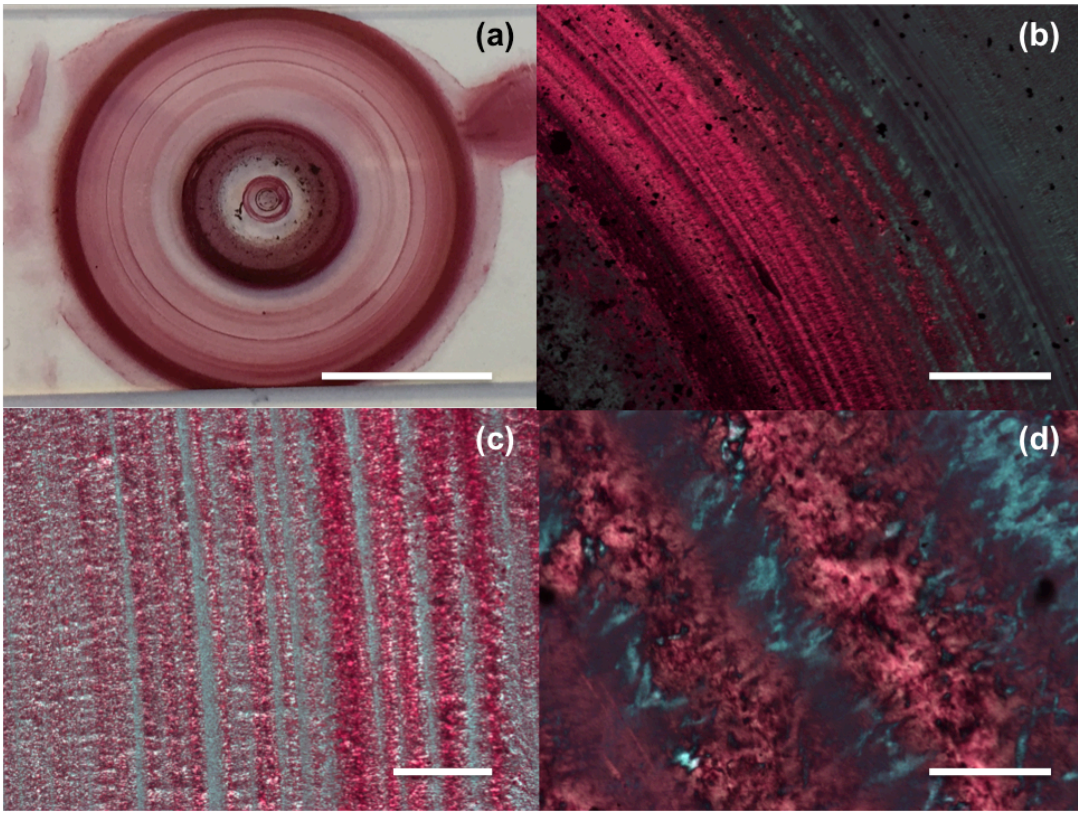

Figure 4.42 (a) Photograph of dried solution of **1** after shearing for 16 hours. Scale bar represents 1 cm. (b)-(d) Optical microscope images of (a) viewed under cross-polarised light. In (b) the scale bar represent 0.5 mm, in (c) the scale represent 0.2 mm and in (d) the scale bar represent 50 μm.

Photoresponse measurements were then performed on these samples as described previously. Fig. 4.43 shows that the sample has a directional dependence of around 0.60. This is lower than seen for both the magnetically aligned and coffee-ring aligned samples, which have an average directional dependence of 0.32 and 0.25 respectively. This method however was found to be much more reproducible and always gave aligned structures, and the same directional dependence value. This is due to there being fewer variables when drying.

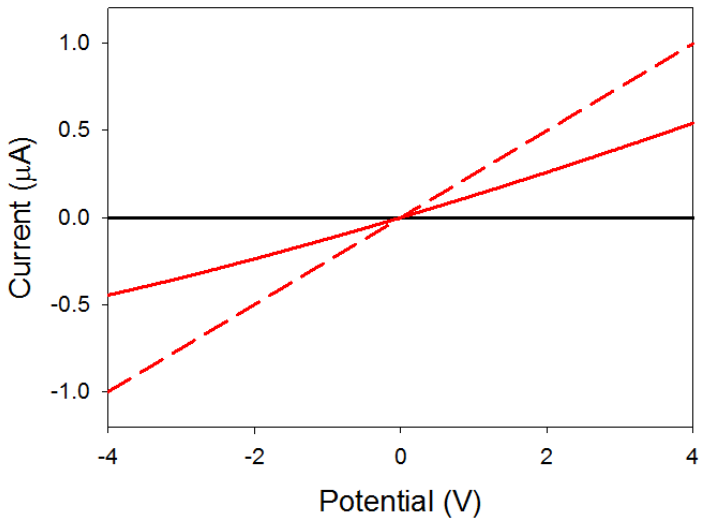

Figure 4.43 Photoresponse of a shear aligned dried solution of **1**. Black data is in the dark and red data is under 365 nm light. Solid red data is against alignment and red dashed data is with alignment.

Due to this slow evaporation of water, is now possible to try and gel the solution under shear. This would result in an aligned gel and therefore would answer whether it was alignment of structures giving a lower photoresponse for the dried gels compared to the solutions, rather than morphology of the fibres.

When lowering the pH of the sample under shear, a few things need to be taken into consideration. The sample needs sufficient time under shear to gel but not too long a time that it disrupts the gel structures. The sample does not need to dry under shear as gelation should lock in any aligned structures formed. The method of gelation is important as shown by Raeburn *et al*. and Draper *et al*., who showed not only does it matter what type of trigger is used (e. g. pH, solvent switch, metal salts etc.) but even within a type of trigger it matter how this is done (e. g. anhydrides, HCl, GdL, hydroquinone etc.).[46, 82-86] The time a trigger takes to form gel can be monitored by pH and rheology. When the pH is below the pK_a of this type of gelator, then a gel is formed.[46] Rheology can be used to see when G′ is approximately an order of magnitude above G″, which is indicative of gelation.[87] The time where both these occur can be used as a rough guide to when gelation has happened. They will however be slightly different to the situation where a constant shear is applied, as a different geometry is used to measure the rheology, and also clearly there is an applied shear. By shearing on the rheometer using the cone and plate geometry, the

viscosity of the samples can also be measured. As gelation occurs, the solution becomes more viscous as the worm-like fibres extend, thicken and lose charge so are able to interact with each other more.[88] As these long fibres align, there should be a viscosity overshoot where viscosity drops.[89] This is seen in polymer solutions as well as when performing viscosity measurements on solutions with worm-like micelles,[42] where upon increasing shear rate the viscosity of the samples drops due to the structures aligning and fibres interact less with each other.[90] As the solution further gels, the viscosity data will have little meaning as the sample is no longer a liquid.

Initially, acetic anhydride was investigated as a pH trigger. This trigger works similarly to GdL by hydrolysing in water to give an acid.[91] Using acetic anhydride resulted in the solution gelling too quickly and the shear made them aggregate (Fig. 4.44a). This was unsuitable for our desired application and so a pH trigger with a longer gelation time was needed. GdL was therefore used as it has a slower gelation time and so gels did not aggregate upon shear (Fig. 4.44b). As described previously, the pH drop was also reproducible and so pH and gelation overtime could be compared as seen in Chapter 3.

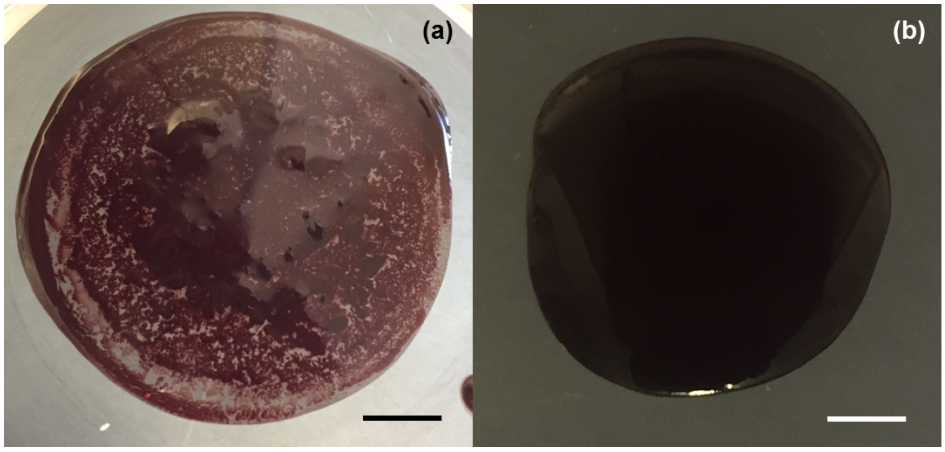

Figure 4.44 Photographs of gels of **1** made at 10 mg/mL prepared on the rheometer plate using (a) acetic anhydride and (b) GdL as triggers. The scale bar represents 1 cm.

When using GdL for gelling under shear, the change in viscosity was measured. Viscosity data is useful as it shows there is a development of structures in solution before any G′ and G″ values can be recorded (Fig 4.45). Fig 4.45 shows that the solution remains roughly the same viscosity as water until 65 minutes when the viscosity rapidly increases. During this time, the solution has reached the first pK_a at

pH 6.7 of the gelator (see Section 4.4 and Fig. 4.49). As pH drops further to the second pK_a at pH 5.4, the viscosity sharply increases as larger structures start to form. At 90 minutes, G′ and G″ start to increase and gelation occurs. In the viscosity data, there is then a decrease in viscosity as the gelling fibres start to align under the shear (the viscosity overshoot). The viscosity then increases again as the gel is developing further until 130 minutes. After 130 minutes, the viscosity data is not reliable due to gelation occurring (viscosity measurements cannot be performed meaningfully on gels). From the gelation time sweep data at around 300 minutes, G′ is an order of magnitude larger than G″ and the pH is 3.6 showing gelation has occurred. From these data, it can be seen that there are larger structures starting to be formed after 60 minutes and gelation has occurred after 300 minutes. Alignment of these structures can be seen in the viscosity data at 130 minutes. This means shear alignment experiments need to be performed for between 130 and 300 minutes.

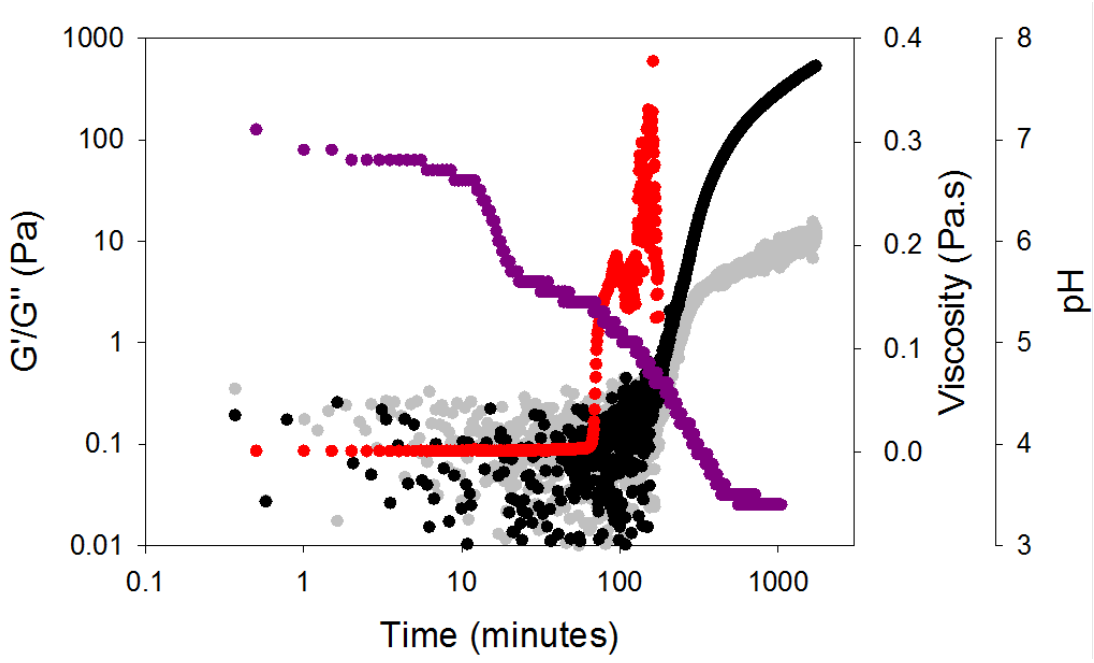

Figure 4.45 Development of G' (black data) and G" (grey data) over time during the gelation of **1** at a strain of 0.5 % and a frequency of 10 rad/s, compared to change in viscosity (red data) and change in pH (purple data) over time.

A shear was therefore applied for samples for between 120 and 180 minutes. When they were sheared for less time than this, then gelation had not occurred and the sample was still liquid (Fig. 4.46a). Applying the shear for longer than 210 minutes resulted in the gel sample being damaged by the shear (Fig. 4.46b).

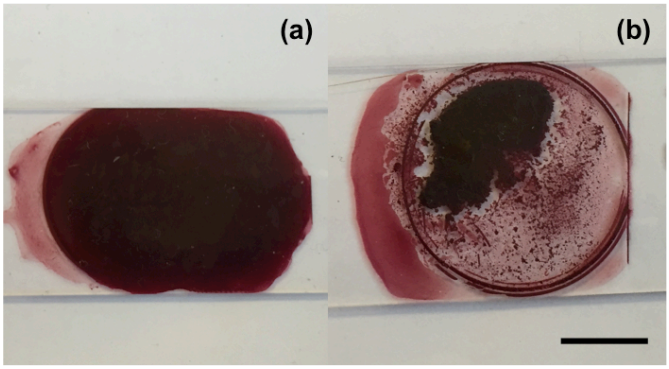

Figure 4.46 Photographs of shear aligned xerogel-**1** after shearing for (a) 1 hour 30 minutes and (b) 4 hours. Scale bar represents 1 cm.

Gels sheared for 150 minutes showed the same ringed pattern as seen with the dried solutions (Fig. 4.47b) but also had denser area of gel in the middle. These samples were allowed to dry in air to give shear aligned xerogels. When viewed under cross-polarised light, they showed aligned structures (Fig. 4.47b to c). This is very different to samples not formed under shear (Fig. 4.29b).

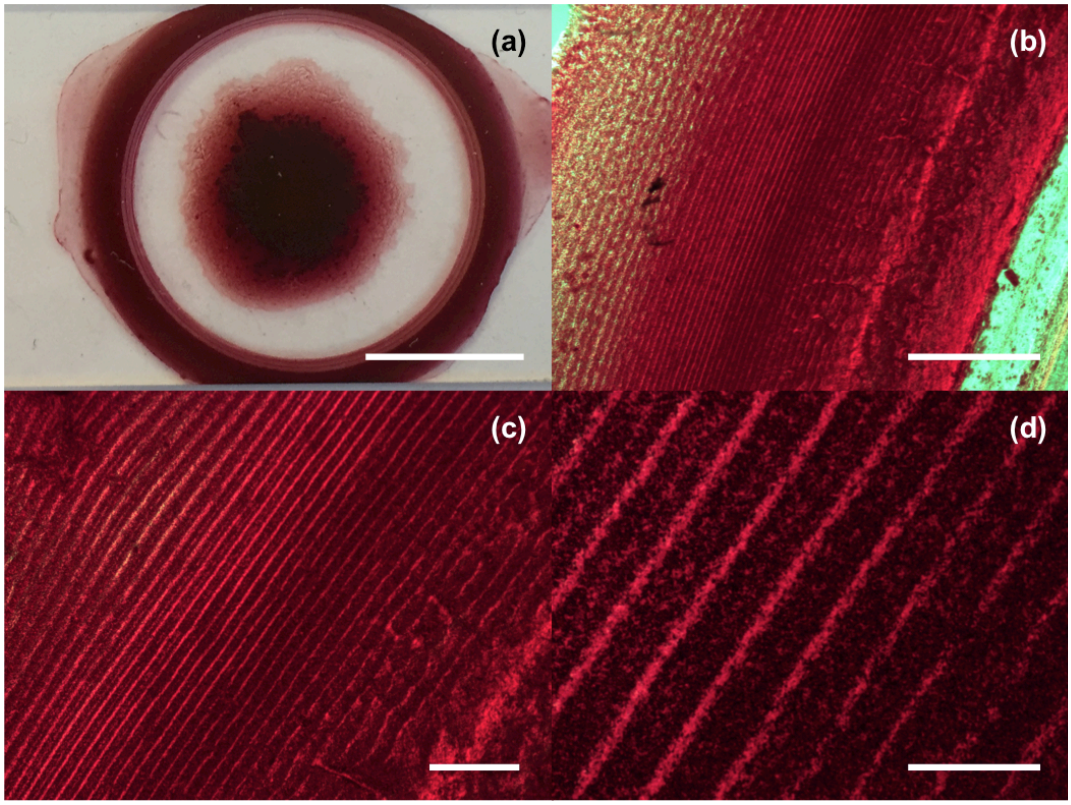

Figure 4.47 (a) Photograph of the edge of the xerogel **1** after shearing for 2 hours. Scale bar represents 1 cm. (b)-(d) Optical microscope images of (a) under cross-polarised light. In (b) the scale bar represent 0.5 mm, in (c) the scale represent 0.2 mm and in (d) scale bar represent 50 μm.

When photoresponse measurements were performed on shear-aligned xerogels, they showed directional dependence (Fig. 4.48a). This again is different to when they are not gelled under shear (Fig. 4.48b). Shear aligned xerogels have a directional dependence of between 0.06 and 0.12, compared to xerogels not gelled under shear which show a directional dependence of 0.95. This method gave very reproducible samples. Not only do shear aligned xerogels show much better directional dependence than non-shear aligned xerogels, but they show a better and more reproducible directional dependence than magnetically aligned, shear aligned and drop-cast dried solutions. This is believed to be due to the fibres being longer than in solution state and so are more able to align, as seen in polymers systems. The absolute conductivity of the shear aligned xerogels remains similar to non-aligned xerogels. This means that alignment of the samples is not why the dried solution is more conductive than the xerogels. Hence, the difference in the photoresponse is due to different fibre morphology or how densely packed the fibres are rather than how aligned the fibres are. This although this needs further work to determine exactly what these morphologies are, as well as film thickness and concentration of material. These factors could contribute to how far the light can penetrate the sample and how much radical anion is generated.

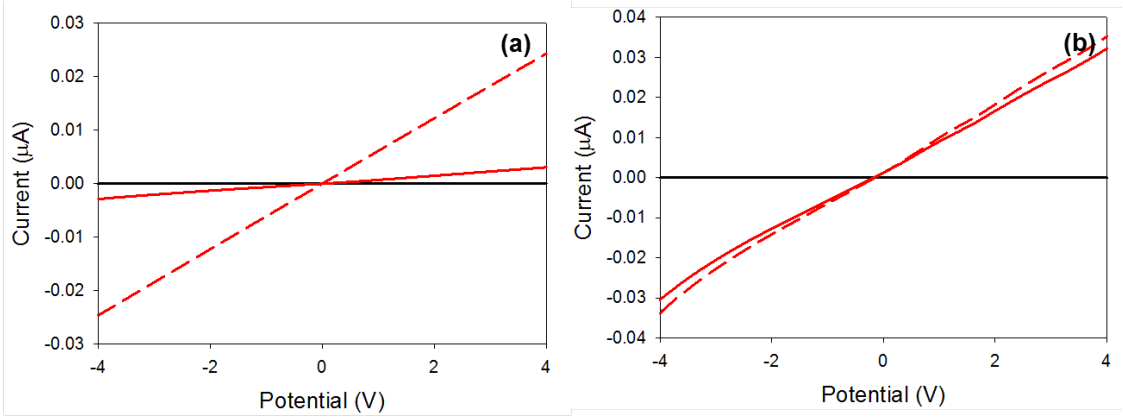

Figure 4.48 Photoresponse of xerogel-**1** at a concentration of 10 mg/mL (a) gelled under shear and (b) not under shear. Black data is in the dark and red data is under 365 nm light. Solid red data is against alignment and red dashed data is with alignment.

4. 3. Conclusions

Four different PBIs functionalised with L-alanine, L-phenylalanine, L-histidine and L-valine were synthesised, all of which formed hydrogels at a gelator concentration of 5 mg/mL. At high pH, each of the gelators forms worm-like micelles in solution. When gels and solutions were dried, they formed films that were photoconductive, apart from gelator-**3** that did not form uniforms films and so measurements could not be carried out. The xerogels and dried solution were conductive due to the formation of a radical anion that was stable in air for many hours. The dried solutions were more conductive than the xerogels. This is thought to be due to a difference in the fibre morphologies at high and low pH. The dried solution also showed directional dependence due to alignment in the sample. Xerogels and dried solutions could be aligned which gave them varying directional dependence depending on which method was used. Alignment under a magnetic field was the best method for alignment in solution, but was not reproducible. Shear of solution showed that solutions aligned very quickly, but then dealigned very quickly after the shear was stopped so methods of alignment such as spin coating and doctor blading are unsuccessful. Gelling under mechanical shear was the best method of alignment for the xerogels, being highly reproducible. This alignment gives a well-defined structure that could be used in electronic devices. If another component were added to the system, such a p-type gelator like 4,4'-stilbene diphenylalanine discussed in Chapter 3, then a well-defined p-n heterojunction could be potentially designed. This will be discussed in Chapter 5.

4. 4. Experimental

4. 4. 1 Synthetic Procedures

Typical Synthesis, [N, N'-di(L-valine)-perylene-3,4:9,10-tetracarboxylic acid bisimide] (4).

In a 100 mL Schlenk flask, 0.79 g (1 mmol) of 3,4:9,10-perylenetetracarboxyldianhydride (PTCDA), 0.47 g (2 mmol) of L-valine and 2.80 g

(20 mmol) of imidazole were added. These were mixed and purged with nitrogen for 10 minutes. The mixture was then heated to 120 °C under nitrogen and left stirring for 5 hours at this temperature. The reaction was then cooled to 90 °C and 3 mL of deionised water was added. The reaction was left for an hour and then cooled to room temperature before filtering to remove unreacted PTCDA. 50 mL of 2 M HCl was then added to lower the pH to between 2 and 3. The acidified mixture was stirred at 60 °C for 4 hours. The precipitate was then collected by suction-filtration and washed thoroughly with acidified water. The dark red solid was dried overnight in a vacuum oven and then freeze dried to remove any remaining water. A typical yield obtained for all PBIs was between 80-90 %.

The same method was used to synthesise [N, N'-di(L-alanine)-perylene-3,4:9,10-tetracarboxylic acid bisimide] (**1**), [N, N'-di(L-histidine)-perylene-3,4:9,10-tetracarboxylic acid bisimide] (**2**), and [N, N'-di(L-phenylalanine)-perylene-3,4:9,10-tetracarboxylic acid bisimide] (**3**).

Around 2 μL of TFA was added to ^{1}H NMR samples of **2**, and ^{13}C NMR samples of **2**, **3** and **4** to improve solubility and visibility in NMR.

1: ^{1}H NMR 400 MHz, (DMSO-d_6, 25 ˚C): δ (ppm) = 12.80 (br, 2H;–OH); 8.29 (d, 4 H); 8.21 (d, 4 H); 5.59 (q, 2 H, J = 7.0 Hz); 1.68 (q, 6 H, J = 7.0 Hz). ^{13}C (100 MHz, DMSO-d_6, 25 ˚C): δ (ppm) = 171.2 (COOH); 161.9 (C=O); 134.2, 133.4, 130.7, 127.8, 123.6, 121.8, 119.2 (perylene core C); 48.6 (CH); 14.4 (CH_2). MALDI-TOF MS: calculated 534.11 Da for $[C_{30}H_{18}N_2O_8]^+$, found 535.3 Da.

2: ^{1}H NMR 400 MHz, (DMSO-d_6 and TFA, 25 ˚C): δ (ppm) = 8.93 (bd, 4 H, J = 8.3); 8.56 (bd, 4 H, 8.3 Hz); 7.47 (s, 4 H); 5.85 (t, 2 H); 3.73 (d, 2 H, J = 15.0 Hz); 3.45 (d, 2 H, J = 15.0 Hz). ^{13}C (100 MHz, DMSO-d_6 and TFA, 25 ˚C): δ (ppm) = 169.7 (COOH); 162.3 (C=O); 133.9, 131.3, 129.9, 128.3, 125.2, 123.9, 121.8 (perylene core C); 52.6 (CH); 23.7 (CH_2). MALDI-TOF MS: calculated 666.15 Da for $[C_{36}H_{22}N_6O_8]^+$, found 665.2 Da.

3: ^{1}H NMR 400 MHz, DMSO-d_6, 25 ˚C): δ (ppm) = 8.3 (d, 4H); 8.1 (d, 4H); 7.3 (d, 4H, J = 7.5 Hz); 7.2 (t, 4H, J = 7.5 Hz); 7.1 (t, 2H, J = 7.5); 5.9 (t, 2H, J = 5.3 Hz);

3.7 (d, 3.5, J = 5.3 Hz); 3.5 (d, 2H, J = 5.3 Hz). ^{13}C (100 MHz, DMSO-d_6 and TFA, 25 ˚C): δ (ppm) = 170.6 (COOH); 162.1 (C=O); 133.6, 130.9, 129.1, 125.0, 123.4, 121.6 (perylene core C); 137.9, 128.2, 127.9, 126.4 (aromatic C); 46.6 (CH); 14.4 (CH_2). MALDI-TOF MS: calculated 686.2 Da for $[C_{42}H_{26}N_2O_8]^+$, found 686.3 Da.

4: ^{1}H NMR 400 MHz, (DMSO-d_6, 25 ˚C): δ (ppm) = 8.50 (d, 4 H, J = 8.2 Hz); 8.37 (d, 4 H, J = 8.2 Hz); 5.20 (d, 2 H, J = 1.3 Hz); 2.75 (qd, 2 H, J = 7.0, J = 1.3 Hz); 1.29 (d, 6 H, J = 7.0 Hz); 0.81 (d, 6 H, J = 7.0 Hz). ^{13}C (100 MHz, DMSO-d_6 and trifluoroacetic acid (TFA), 25 ˚C): δ (ppm) = 170.6 (COOH); 162.3 (C=O); 133.4, 130.9, 127.9, 124.8, 123.3, 121.4, 119.3 (perylene core C); 58.1 (CH); 27.0 (CH_2); 19.1 (CH_3); 19.0 (CH_3). MALDI-TOF MS: calculated 590.17 Da for $[C_{34}H_{26}N_2O_8]^+$, found 590.0 Da.

4. 4. 2 Instruments and Procedures

Nuclear Magnetic Resonance Spectroscopy (NMR)

NMR spectra were recorded using a Bruker DPX-400 spectrometer operating at 400 MHz for ^{1}H NMR and 101 MHz for ^{13}C NMR, in d_6-DMSO or D_2O. TFA was added to some of the samples to increase the solubility as noted above in synthetic procedures.

^{23}Na spectra were recorded by Matthew Wallace at 105.86 MHz (^{23}Na) with 1024 scans, a sweep width of 10 kHz, a 33 us pulse (90 degrees) and a signal acquisition time of 0.3 s, giving a total acquisition time of 6 minutes. All samples were freshly pipetted from the vials into 5 mm NMR tubes and the spectra taken at 298 K, 20 minutes after magnetic field exposure. No significant changes were apparent in the spectra taken after 5 and 90 minutes magnetic field exposure, so structural alignment occurs happens quickly.

Matrix-Assisted Laser Desorption/Ionization Time-of-Flight Mass Spectrometry (MALDI-TOF)

MALDI-TOF mass spectrometry was carried out within the University of Liverpool Biosciences Department using a Waters Micromass M@LDI bench top mass

spectrometer with a-cyano-4-hydroxy-cinnamic acid matrix. A saturated solution of the matrix was made up in 50 % acetonitrile, before applying 2 mL to the target followed by a 2 ml of sample followed by a further 2 mL of matrix. The pulse voltages used was 3400 V and the source voltage used was 16,000 V.

Preparation of LMWG Solutions

The gelator was added to 2 mL of water with an equimolar amount of sodium hydroxide (0.1 M, aqueous) to a concentration of 5 mg/mL. The solution was stirred until all the gelator was dissolved.

Hydrogel Formation

A pH switch method was used to form the hydrogels. Solutions were prepared as above. The solution was then transferred to a vial containing a pre-weighed amount of glucono-δ-lactone (GdL) and shaken gently. The sample was then left to stand overnight to allow gelation to occur. For **1**, 5 mg/mL of GdL was used and for **2**, **3** and **4** 3 mg/mL of GdL was used. For gels formed with acetic anhydride, 3 μL of acetic anhydride was added to solutions prepared as described above.

Preparation of samples on glass slides

Samples were prepared by dropping 20 μL of the LMWG solution onto a glass microscope slide and then leaving overnight to dry in air. Xerogel samples were prepared by forming gels as described above using GdL inside a 1 mL mould. Once gelation had occurred, the gel was then removed from the mould and approximately 0.05 mL of the gel was removed using a scalpel, placed onto a glass microscope slide and allowed to dry in air overnight.

Rheological Measurements

Dynamic rheological and viscosity measurements were performed using an Anton Paar Physica MCR101 and MCR301 rheometer. A cup and vane measuring system was used to perform frequency and strain sweeps. A cone and plate measuring system was used to perform viscosity measurements and gelling under shear. A parallel palate measuring system was used for time sweeps. For frequency and strain tests, 2 mL of the gels were prepared in 7 mL Sterilin vials and left for 24 hours at room temperature before measurements were performed. For viscosity

measurements, samples were prepared at high pH as previously mentioned. For time sweeps and gelling under constant shear, the gels were prepared in a vial and transferred onto the bottom plate. All experiments were performed at 25 °C.

Frequency sweep: Frequency scans were performed from 1 rad/s to 100 rad/s under a strain of 0.5 %. The shear modulus (storage modulus (G′) and loss modulus (G″)) were read at 10 rad/s. These measurements were done within the viscoelastic region were G′ and G″ were independent of strain amplitude.

Strain sweep: Strain scans were performed from 0.1 % to 100 % with a frequency of 10 rad/s. The critical strain was quoted as the point that G′ starts to deviate for linearity and ultimately crosses over the G″, resulting in gel breakdown. From this data, a strain of 0.5 % used for measuring the frequency sweep was in the viscoelastic region.

Viscosity measurements: Viscosity measurements were performed using a 75 mm cone and plate. 1 mL solutions were transferred onto the plate for measurement. The viscosity of each solution was recorded under the rotation shear rate varying from 1 to 100 s^{-1}.

Gelling under shear and shear aligning: Shear aligning experiments were performed using a 25 mm cone geometry. A constant shear rate of 10 s^{-1} was applied to the samples and a viscosity measurement recorded every 30 seconds. For shear aligned solutions these measurements were done for 16 hours. For shear aligned gels this was done for between 2 and 3 hours.

Time sweeps: Time sweeps were performed with a 50 mm plate with a plate gap of 0.8 mm. Tests were performed at an angular frequency of 10 rad s^{-1} and with a strain of 0.5 %. The top plate was flooded with mineral oil to prevent the sample from drying.

Rheo-Optics: Measurements were performed using a RheoOptics- Rheo Micrsocope form Anton Paar at the University of Sheffield. They were performed using a 25 mm parallel plate with a gap distance of 0.2 mm at a maximum shear rate of 100 s^{-1} for

30 seconds. A total of 320 frames were taken at 0.2 seconds per frame. The light source was at a dial of 270 degrees with a gain of 23 and an exposure of 65 ms. These measurements were carried out at the University of Sheffield with Dr. O. Mykhaylyk.

pH Measurements

A FC200 pH probe (HANNA instruments) with a 6 mm x 10 mm conical tip was used for pH measurements. The stated accuracy of the pH measurements is ±0.1. For pH measurement during gelation pH was recorded every minute until a gel was formed. The temperature was maintained at 25 °C during the titration by using a circulating water bath.

"Apparent" pK_a Measurements

A FC200 pH probe (HANNA instruments) with a 6 mm x 10 mm conical tip was used for pH measurements. The stated accuracy of the pH measurements is ±0.1. The pK_a values of the gelators were determined *via* the additions of aliquots of 0.1 M aqueous hydrochloric acid. Measurements were recorded after each addition of HCl and a stable value was reached. To prevent a gel forming, the solutions were gently stirred using a stirrer bar, so keeping the sample a liquid during the "titration" process. The plateaus of the pH indicates the two pK_a of this gelator (Fig. 4.49). Temperature was kept at 25 °C during the titration by using a water bath.

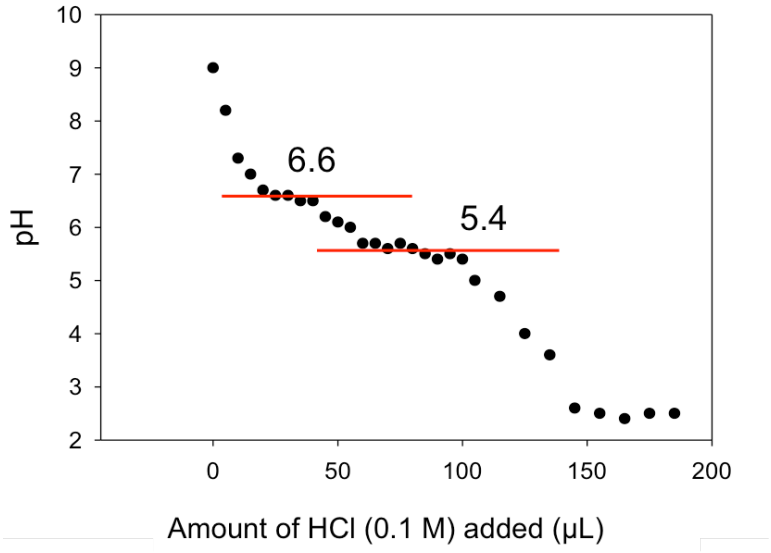

Figure 4.49 Decrease in pH of **1** after addition of HCl (0.1 M). Plateaus show the two pK_as of the gelator.

Scanning Electron Microscopy

SEM images were obtained using a Hitachi S-4800 FE-SEM. Gels and solutions at high pH were deposited onto glass cover slips which were stuck onto aluminium SEM stubs and left to dry for 24 hours. The images were collected by Dr. Tom McDonald.

Powder X-Ray Diffraction (pXRD)

Gel samples were prepared *via* the pH switch method and left to dry completely in air. The samples were ground before being measured. Solution samples were also dried in air and ground before being measured.

Fluorescence Spectroscopy

Fluorescence spectra were collected using a Perkin Elmer Fluorescence Spectrometer LS55. Emission and excitation spectra were recorded in 1.0 cm pathlength cuvettes with slit widths of 2.5 nm and 2.5 nm at a scan rate of 100 nm/min. Emission spectra were collected between 200 nm and 800 nm, exciting at 490 nm and 365 nm. Spectra were recorded at pH 11 and pH 3 at a concentration of 0.05 mg/mL.

Profilometry

Profilometry measurements were carried out using an Ambios XP-200 profilometer. Samples were prepared using a mask, or by cutting the sample with a scalpel to get a clean edge.

UV-Vis-NIR Absorption Measurements

Solution UV-Vis absorption data was measured using a Thermo Scientific Nanodrop 2000/2000c spectrophotometer. The spectrophotometer was used in cuvette mode were samples were prepared in PMMA plastic cuvettes with a pathlength of 1.0 cm. Aqueous samples were prepared at high pH using equimolar amounts of 0.1 M aqueous NaOH solution to gelator and made up to 2 mL with distilled water. A concentration of 5 mg/mL of a gelator was used for aqueous solutions and a dilution series was made for measurements. Gels were made by the pH switch method and pipetting around 100 μL of the solution whilst still liquid into a cuvette. The open cuvette top was then covered and laid on its side whilst it gelled overnight. This formed a thin layer of gel on one side of the cuvette which could be measured.

Solid UV-Vis-NIR absorption data were obtained using a Shimadzu UV-2550 UV−Vis spectrophotometer running the UV Probe software, version 2.34. Spectra were measured either up to 700 or 1400 nm, with scan speed set to medium and using a slit width of 5.0 nm in transmission mode. Samples were prepared as previously mentioned with GdL. This gel was then transferred onto a glass slide and allowed to dry in air overnight in air to form a thin film xerogel.

For solution UV-Vis-NIR measurements samples were prepared in a sealed degassed quartz cuvette with a pathlength of 1 mm.

Thermogravimetric analysis (TGA)

TGA was carried out on a TA Instruments SDT Q600 TGA machine using a constant air flow of 100 mL/min. Samples were heated to 120 ºC with a heating rate 10 ºC/min. The samples were kept at 120 ºC for 20 minutes to remove any water, then ramped to 200 ºC at a heating rate of 10 ºC/min.

Fourier Transformed Infrared Spectroscopy (FTIR)

IR spectra were collected on a Bruker Tensor 27 FTIR spectrometer at a resolution of 2 cm^{-1} with spectral averaging over 64 scans. Measurements were collected using the ATR accessory before and after irradiation of UV light. Samples were irradiated for a total of 3 days.

Optical Microscopy under Cross-Polarised Light

Optical microscope images were collected using a Nikon Eclipse LV100 microscope with a Nikon TU Plan ELWD 50x/0.60 lens attached to an Infinity2-1C camera, with both polariser on. Samples for optical microscopy were prepared on glass microscope slides and allowed to dry for 24 hours before imaging.

Photoconductivity Measurements

Photoconductivity measurements were performed using a Palmsens^3 Potentiostat operating in a two electrode configuration in the absence of a supporting electrolyte. An Applied Photophysics 150 W Xenon arc lamp was used for the 'light' experiments with a spot size of 2 cm^2. A 365 nm LED (LedEngin Inc, LZ1-10U600) with a light source powered by a TTi QL564P power supply operating at 1.0 W was

also used as a light supply. A 10 mL quartz cuvette filled with water was used as an IR filter. Dark experiments were performed in an enclosure in air. Linear sweep measurements were recorded from -4 V to 4 V at a scan rate of 0.05 V/s and a preconditioning step at 0.002 V for 2 seconds. Xerogels were prepared *via* the pH switch method as previously described. Once the gels were formed approximately the same volume of each gel could be placed onto a glass slide between two silver electrodes spaced 3 mm apart. The silver electrodes were made using silver paste which attached copper wires to the glass slide. The gel was then allowed to dry in air overnight to form a xerogels, shown in Fig. 4.50. Epoxy resin glue was placed over the silver electrodes. Again, this was left to dry overnight.

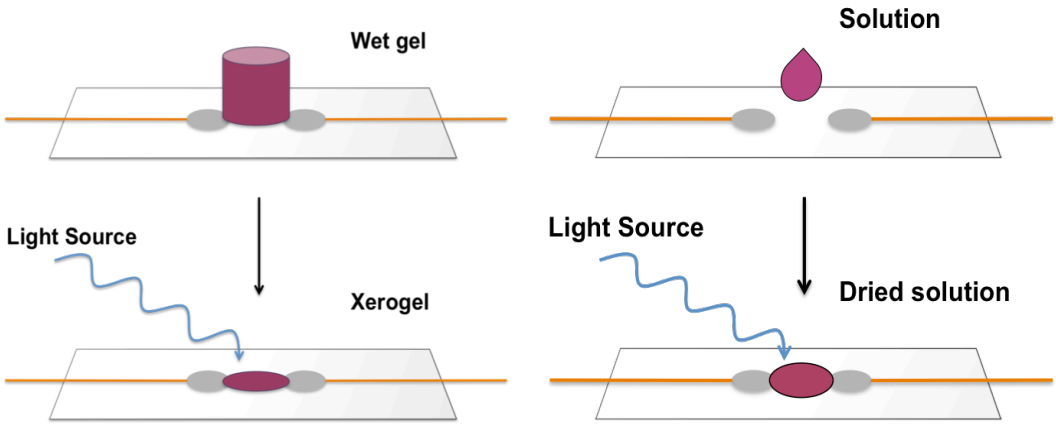

Figure 4.50 Experimental set up for measuring the photoconductivity of xerogels and dried solutions.

The counter and reference electrode clips were connected to one copper wire and the working on the other copper wire to make a two-electrode experiment. Dried solutions at pH 10 were prepared as previously mentioned but placed between the copper wires on the glass slide. For 'on-off' experiments, a cover was placed over the lamp for 'off' and then removed for 'on'.

For directional dependence measurements silver electrodes were placed 3 mm apart with and against the alignment of the samples, this was determined using the optical microscope to place the electrodes. For not aligned samples electrodes were places left and right of the sample and at the top and the bottom of the sample as shown in the Fig. 4.51.

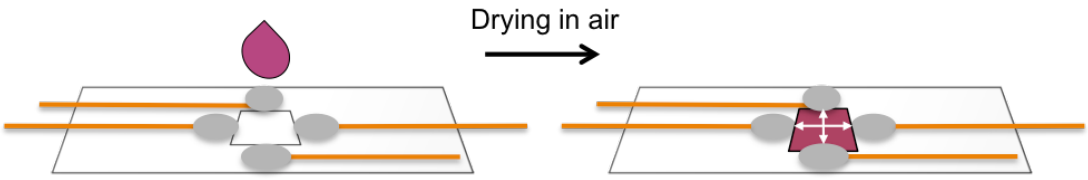

Figure 4.51 Experimental set up of conductivity of aligned samples. Silver electrodes are placed on all sides of the sample. Arrows indicate the direction of the measurement taken.

Wavelength Response Measurements

Samples were prepared on microscope slides between to two silver electrodes as previously mentioned. The light source used was a stabilized 75 W Xenon lamp coupled to a monochromator (OBB Corp., set to 4 nm resolution). Current was measured using a Palmsens[3] potentiostat operating with a two using electrode configuration in the absence of a supporting electrolyte. Measurements were ran at 0.05 V/s for 2000 seconds. The light source was switched on at 100 seconds and the current was allowed to reach a plateau so that a change in current could be recorded. The sample was then put back in the dark and allowed to return to the 'off' state before another measurement was recorded. The intensity of the light at each wavelength was measured using a photodiode so that results could be scaled.

Photochromism

A 365 nm LED with a light source powered by a TTi QL564P power supply operating at 1.0 W was used as the light supply. Samples were placed inside the UV-Vis-NIR spectrometer and the light was placed around 5 cm away from the samples whilst spectra were recorded. The incident light intensity on the sample was measured to be approximately 1 mW/cm^2. Samples were irradiated until intensity of the new peaks plateaued. The lamp was switched of and spectra were taken every minute for the first half an hour, and then 5 minutes until peaks in the spectra had returned to original intensity.

Chemical Reduction of PBIs

Chemical reduction of **1** in solution was carried out by adding sodium dithionite. 40 mL of 0.125 mg/mL of LMGW **1** in pH 10 water were added to a 100 mL round bottom flask and sealed with a subaseal. The solution was degassed with argon for 15 minutes. Sodium dithionite was added in 10 mg portions by carefully removing

the seal and quickly adding it to the solution and replacing the seal whilst under argon. Samples for UV-Vis-NIR were taken by removing 100 µL of solution with a syringe and placed in a sealed degassed quartz cuvette with a pathlength of 1 mm.

Spin Coating

The spin coater used was a Laurell Technologies Corporation WS-650 Series Spin Processor. Spin coating was performed using 50 µL of solution **1** at varies concentrations on glass cut to size. Samples were span at 800-10,000 rpm for 30-60 seconds.

Magnetic Alignment

The superconducting magnet used is a wide bore 9.4 T magnet of a Bruker Avance II spectrometer. The shim stack was removed to widen the effective bore of the magnet and allow the sample to be brought closer to the magnet centre. The cradlein which the samples were placed is a 65 mm diameter plastic lid which is suspended by nylon threads (Fig. 4.52a and b below). A styrofoam insert is used to provide a level base. Glass slides were cut to length and stuck onto the Styrofoam with sticky tape, typically three at a time. 10 uL of PBI-A solution was pipetted and dropped onto slide from height of ca. 2 cm. The sample was lowered down until it rested on the top of the NMR probe (Fig. c below). The samples were left to dry for at least two hours in field. They were in magnet within three minutes of transferring solutions to slides. There was no temperature control so samples were dried at room temperature.

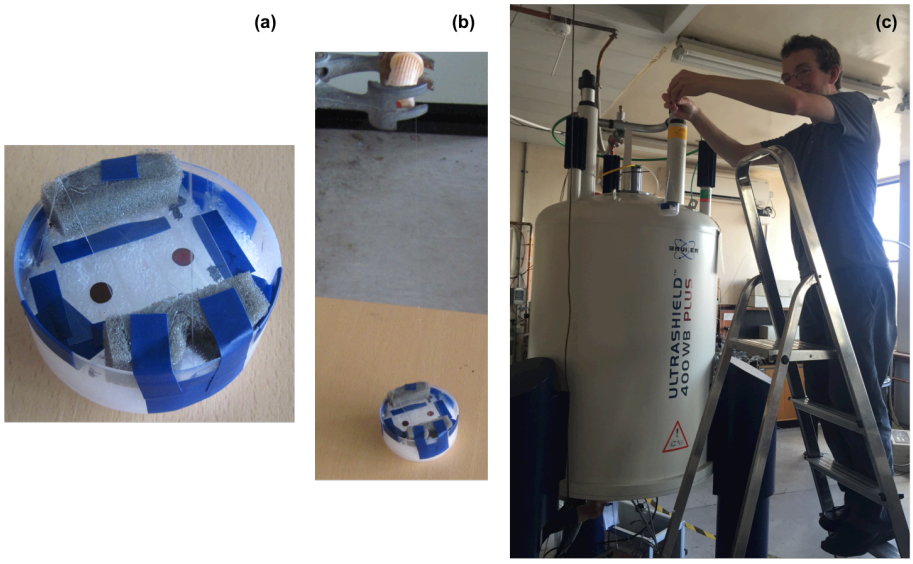

Figure 4.52 Photographs of (a) cradle with samples placed on glass slides. (b) cradle attached to fishing wire (c) cradle being lowered into the spectrometer.

4. 5. References

1. D. Ray, C.-K. Liang, N. D. McClenaghan and D. M. Bassani, *Current Phys. Chem.*, 2011, **1**, 169-180.
2. H. W. Donghang Yan, Baoxun Du, *Introduction to Organic Semiconductor Heterojunctions*, John Wiley & Sons, 2010.
3. S. S. Babu, S. Prasanthkumar and A. Ajayaghosh, *Angew. Chem. Int. Ed.*, 2012, **51**, 1766-1776.
4. I. Gonzalez-Valls and M. Lira-Cantu, *Energy Environ. Sci.*, 2009, **2**, 19-34.
5. C. Li and H. Wonneberger, *Adv. Mater.*, 2012, **24**, 613-636.
6. J. M. Lim, P. Kim, M.-C. Yoon, J. Sung, V. Dehm, Z. Chen, F. Wurthner and D. Kim, *Chem. Sci.*, 2013, **4**, 388-397.
7. D. Görl, X. Zhang and F. Würthner, *Angew. Chem. Int. Ed.*, 2012, **51**, 6328-6348.
8. F. Würthner, V. Stepanenko, Z. Chen, C. R. Saha-Möller, N. Kocher and D. Stalke, *J. Org. Chem.*, 2004, **69**, 7933-7939.
9. W. Jiang, L. Ye, X. Li, C. Xiao, F. Tan, W. Zhao, J. Hou and Z. Wang, *Chem. Commun.*, 2014, **50**, 1024-1026.
10. T. H. Reilly, A. W. Hains, H.-Y. Chen and B. A. Gregg, *Adv. Energy Mater.*, 2012, **2**, 455-460.
11. F. Wurthner, *Chem. Commun.*, 2004, 1564-1579.
12. J. Hu, W. Kuang, K. Deng, W. Zou, Y. Huang, Z. Wei and C. F. J. Faul, *Adv. Func. Mater.*, 2012, **22**, 4149-4158.
13. A. Datar, K. Balakrishnan and L. Zang, *Chem. Commun.*, 2013, **49**, 6894-6896.
14. S. Ghosh, X.-Q. Li, V. Stepanenko and F. Würthner, *Chem. Eur. J.*, 2008, **14**, 11343-11357.
15. Y. Che, H. Huang, M. Xu, C. Zhang, B. R. Bunes, X. Yang and L. Zang, *J. Am. Chem. Soc.*, 2010, **133**, 1087-1091.
16. X. Zhan, Z. a. Tan, E. Zhou, Y. Li, R. Misra, A. Grant, B. Domercq, X.-H. Zhang, Z. An, X. Zhang, S. Barlow, B. Kippelen and S. R. Marder, *J. Mater. Chem.*, 2009, **19**, 5794-5803.
17. A. G. Slater, E. S. Davies, S. P. Argent, W. Lewis, A. J. Blake, J. McMaster and N. R. Champness, *J. Org. Chem.*, 2013, **78**, 2853-2862.
18. E. Shirman, A. Ustinov, N. Ben-Shitrit, H. Weissman, M. A. Iron, R. Cohen and B. Rybtchinski, *J. Phys. Chem. B*, 2008, **112**, 8855-8858.
19. R. O. Marcon and S. Brochsztain, *J. Phys. Chem. A*, 2009, **113**, 1747-1752.
20. L. Zhong, F. Xing, W. Shi, L. Yan, L. Xie and S. Zhu, *ACS Appl. Mater. Interfaces*, 2013, **5**, 3401-3407.
21. H. Marciniak, X.-Q. Li, F. Würthner and S. Lochbrunner, *J. Phys. Chem. A*, 2011, **115**, 648-654.
22. P. K. Sukul, P. K. Singh, S. K. Maji and S. Malik, *J. Mater. Chem. B*, 2013, **1**, 153-156.
23. R. A. Cormier and B. A. Gregg, *J. Phys. Chem. B*, 1997, **101**, 11004-11006.
24. Y. Chen, Y. Feng, J. Gao and M. Bouvet, *J. Colloid Interface Sci.*, 2012, **368**, 387-394.
25. B. A. Gregg, J. Sprague and M. W. Peterson, *J. Phys. Chem. B*, 1997, **101**, 5362-5369.

26. Y. Sun, C. He, K. Sun, Y. Li, H. Dong, Z. Wang and Z. Li, *Langmuir*, 2011, **27**, 11364-11371.
27. K. Balakrishnan, A. Datar, T. Naddo, J. Huang, R. Oitker, M. Yen, J. Zhao and L. Zang, *J. Am. Chem. Soc.*, 2006, **128**, 7390-7398.
28. Y. Huang, J. Hu, W. Kuang, Z. Wei and C. F. J. Faul, *Chem. Commun.*, 2011, **47**, 5554-5556.
29. X.-Q. Li, V. Stepanenko, Z. Chen, P. Prins, L. D. A. Siebbeles and F. Wurthner, *Chem. Commun.*, 2006, 3871-3873.
30. S. Ogi, V. Stepanenko, K. Sugiyasu, M. Takeuchi and F. Würthner, *J. Am. Chem. Soc.*, 2015, **137**, 3300-3307.
31. K. Sugiyasu, S.-i. Kawano, N. Fujita and S. Shinkai, *Chem. Mater.*, 2008, **20**, 2863-2865.
32. S. Roy, D. Kumar Maiti, S. Panigrahi, D. Basak and A. Banerjee, *RSC Adv.*, 2012, **2**, 11053-11060.
33. R. Schmidt, J. H. Oh, Y.-S. Sun, M. Deppisch, A.-M. Krause, K. Radacki, H. Braunschweig, M. Könemann, P. Erk, Z. Bao and F. Würthner, *J. Am. Chem. Soc.*, 2009, **131**, 6215-6228.
34. S. Xu and Z. Wang, *Nano. Res.*, 2011, **4**, 1013-1098.
35. T. Seki, Y. Maruya, K.-i. Nakayama, T. Karatsu, A. Kitamura and S. Yagai, *Chem. Commun.*, 2011, **47**, 12447-12449.
36. A. Laiho, B. M. Smarsly, C. F. J. Faul and O. Ikkala, *Adv. Funct. Mater.*, 2008, **18**, 1890-1897.
37. A. I. Oliva-Avilés, F. Avilés, V. Sosa, A. I. Oliva and F. Gamboa, *Nanotechnology*, 2012, **23**, 465710.
38. T. A. Everett and D. A. Higgins, *Langmuir*, 2009, **25**, 13045-13051.
39. M. Wallace, A. Z. Cardoso, W. J. Frith, J. A. Iggo and D. J. Adams, *Chem. Eur. J.*, 2014, **20**, 16484-16487.
40. W. Tuntiwechapikul, T. Taka, M. Béthencourt, L. Makonkawkeyoon and T. Randall Lee, *Bioorg. Med. Chem. Lett.*, 2006, **16**, 4120-4126.
41. Y. Xu, S. Leng, C. Xue, R. Sun, J. Pan, J. Ford and S. Jin, *Angew. Chem. Int. Ed.*, 2007, **46**, 3896-3899.
42. A. Khatory, F. Kern, F. Lequeux, J. Appell, G. Porte, N. Morie, A. Ott and W. Urbach, *Langmuir*, 1993, **9**, 933-939.
43. L. Chen, T. O. McDonald and D. J. Adams, *RSC Adv.*, 2013, **3**, 8714-8720.
44. L. Chen, G. Pont, K. Morris, G. Lotze, A. Squires, L. C. Serpell and D. J. Adams, *Chem. Commun.*, 2011, **47**, 12071-12073.
45. J. Perdigao, P. Lambrechts, B. Van Meerbeek, G. Vanherle and A. L. B. Lopes, *J. Biomed. Mater. Res.*, 1995, **29**, 1111-1120.
46. D. J. Adams, M. F. Butler, W. J. Frith, M. Kirkland, L. Mullen and P. Sanderson, *Soft Matter*, 2009, **5**, 1856-1862.
47. C. Chassenieux and L. Bouteiller, *Supramolecular Chemistry*, John Wiley & Sons, Ltd, Editon edn., 2012.
48. K. Hyun, M. Wilhelm, C. O. Klein, K. S. Cho, J. G. Nam, K. H. Ahn, S. J. Lee, R. H. Ewoldt and G. H. McKinley, *Prog. Polym. Sci.*, 2011, **36**, 1697-1753.
49. E. R. Draper, K. L. Morris, M. A. Little, J. Raeburn, C. Colquhoun, E. R. Cross, T. O. McDonald, L. C. Serpell and D. J. Adams, *Cryst. Eng. Comm.*, 2015, **17**, 8047-8057.
50. A. O. a. I. Y. S. Akimoto, *J. Phys. Chem. B*, 1997, **101**, 3753-3758.

51. C. Backes, C. D. Schmidt, K. Rosenlehner, F. Hauke, J. N. Coleman and A. Hirsch, *Adv. Mater.*, 2010, **22**, 788-802.
52. J. A. Mikroyannidis, M. M. Stylianakis, M. S. Roy, P. Suresh and G. D. Sharma, *J. Power Sources*, 2009, **194**, 1171-1179.
53. S. G. Louie and M. S. Hybertsen, *Int. J. Quantum Chem.*, 1987, **32**, 31-44.
54. T. H. I. S. Shin, B. Ehrl, D. H. Jang, O. S. Wolfbeis and J. I . Hong., *Anal. Chem.*, 2012, **84**, 9163-9168.
55. B. A. Jones, M. J. Ahrens, M.-H. Yoon, A. Facchetti, T. J. Marks and M. R. Wasielewski, *Angew. Chem. Int. Ed.*, 2004, **43**, 6363-6366.
56. J. H. Oh, S. Liu, Z. Bao, R. Schmidt and F. Würthner, *Appl. Phys. Lett.*, 2007, **91**, 212107.
57. R. O. Marcon and S. Brochsztain, *Langmuir*, 2007, **23**, 11972-11976.
58. Á. J. Jiménez, F. Spänig, M. S. Rodríguez-Morgade, K. Ohkubo, S. Fukuzumi, D. M. Guldi and T. Torres, *Org. Lett.*, 2007, **9**, 2481-2484.
59. Y. Che, A. Datar, X. Yang, T. Naddo, J. Zhao and L. Zang, *J. Am. Chem. Soc.*, 2007, **129**, 6354-6355.
60. R. d. Schmidt, J. H. Oh, Y.-S. Sun, M. Deppisch, A.-M. Krause, K. Radacki, H. Braunschweig, M. Könemann, P. Erk, Z. Bao and F. Würthner, *J. Am. Chem. Soc.*, 2009, **131**, 6215-6228.
61. M. J. Ahrens, M. J. Tauber and M. R. Wasielewski, *J. Org. Chem.*, 2006, **71**, 2107-2114.
62. F. Würthner, A. Sautter, D. Schmid and P. J. A. Weber, *Chem. Eur. J.*, 2001, **7**, 894-902.
63. K. E. Brown, W. A. Salamant, L. E. Shoer, R. M. Young and M. R. Wasielewski, *J. Phys. Chem. Lett.*, 2014, **5**, 2588-2593.
64. R. D. Deegan, O. Bakajin, T. F. Dupont, G. Huber, S. R. Nagel and T. A. Witten, *Nature*, 1997, **389**, 827-829.
65. R. Gebhardt, J.-M. Teulon, J.-L. Pellequer, M. Burghammer, J.-P. Colletier and C. Riekel, *Soft Matter*, 2014, **10**, 5458-5462.
66. R. Sharma, C. Y. Lee, J. H. Choi, K. Chen and M. S. Strano, *Nano Letters*, 2007, **7**, 2693-2700.
67. P. J. Yunker, T. Still, M. A. Lohr and A. G. Yodh, *Nature*, 2011, **476**, 308-311.
68. R. L. Davis, P. M. Chaikin and R. A. Register, *Macromolecules*, 2014, **47**, 5277-5285.
69. D. B. Hall, P. Underhill and J. M. Torkelson, *Polym. Eng. Sci.*, 1998, **38**, 2039-2045.
70. M. E. Tousley, X. Feng, M. Elimelech and C. O. Osuji, *ACS Appl. Mater. Interfaces*, 2014, **6**, 19710-19717.
71. K. M. Baid and A. B. Metzner, *Trans. Soc. Rheo.*, 1977, **21**, 237-260.
72. M. Sanyal, B. Schmidt-Hansberg, M. F. G. Klein, A. Colsmann, C. Munuera, A. Vorobiev, U. Lemmer, W. Schabel, H. Dosch and E. Barrena, *Adv. Energy Mater.*, 2011, **1**, 363-367.
73. M. Wallace, J. A. Iggo and D. J. Adams, *Soft Matter*, 2015, **11**, 7739-7747.
74. J. C. Rowell, W. D. Phillips, L. R. Melby and M. Panar, *J. Chem. Phys.*, 1965, **43**, 3442-3454.
75. J. Lounila and J. Jokisaari, *Prog. Nucl. Mag. Res. Spec.*, 1982, **15**, 249-290.
76. P. LeDuc, C. Haber, G. Bao and D. Wirtz, *Nature*, 1999, **399**, 564-566.
77. G. G. Barclay, S. G. McNamee, C. K. Ober, K. I. Papathomas and D. W. Wang, *J. Polym. Sci. A.*, 1992, **30**, 1845-1853.

78. D. J. Alt, S. D. Hudson, R. O. Garay and K. Fujishiro, *Macromolecules*, 1995, **28**, 1575-1579.
79. O. O. Mykhaylyk, *Soft Matter*, 2010, **6**, 4430-4440.
80. O. O. Mykhaylyk, A. J. Parnell, A. Pryke and J. P. A. Fairclough, *Macromolecules*, 2012, **45**, 5260-5272.
81. D. Franke, M. Vos, M. Antonietti, N. A. J. M. Sommerdijk and C. F. J. Faul, *Chem. Mater.*, 2006, **18**, 1839-1847.
82. L. Chen, K. Morris, A. Laybourn, D. Elias, M. R. Hicks, A. Rodger, L. Serpell and D. J. Adams, *Langmuir*, 2010, **26**, 5232-5242.
83. J. Raeburn, G. Pont, L. Chen, Y. Cesbron, R. Levy and D. J. Adams, *Soft Matter*, 2012, **8**, 1168-1174.
84. J. Raeburn, A. Zamith Cardoso and D. J. Adams, *Chem. Soc. Rev.*, 2013, **42**, 5143-5156.
85. E. K. Johnson, L. Chen, P. S. Kubiak, S. F. McDonald, D. J. Adams and P. J. Cameron, *Chem. Commun.*, 2013, **49**, 8698-8700.
86. E. Draper, l. Mears, A. M. Castilla, S. M. King, T. O. McDonald, R. Akhtar and D. J. Adams, *RSC Adv.*, 2015.
87. P. Terech and R. G. Weiss, *Chem. Rev.*, 1997, **97**, 3133-3160.
88. G. C. Kalur, B. D. Frounfelker, B. H. Cipriano, A. I. Norman and S. R. Raghavan, *Langmuir*, 2005, **21**, 10998-11004.
89. T. I. Burghelea, Z. Starý and H. Münstedt, *J. Non Newton. Fluid Mech.*, 2011, **166**, 1198-1209.
90. F. Lequeux, *Europhys. Lett.*, 1992, **19**, 675.
91. C. A. Bunton and J. H. Fendler, *J. Org. Chem.*, 1965, **30**, 1365-1371.

CHAPTER 5

Self-Sorted Hydrogels Towards Bulk p-n Heterojunctions

5. 1. Introduction

Organic photovoltaic (OPV) devices and other photovoltaic devices work by using p-n heterojunctions.[1] Heterojunctions consist of two semi-conducting materials with different bands gaps.[2] These two different materials are a positively doped material (p), also known as an acceptor, and a negatively doped material (n), also known as a donor. When these are combined, they can be used to convert light energy into a direct current. This happens by light energy exciting an electron in the highest occupied molecular orbital (HOMO) in the n-type material to its lowest unoccupied molecular orbital (LUMO) (Fig. 5.1a).[3] This can be called an exciton, which is considered as an electron hole pair. This electron hole pair is separated by an effective field, which is created by the p-n heterojunction and diffuses across the p type material (Fig. 5.1b). The electron can then cross the junction to the lower energy conductance band of the n-type material, leaving a positive charge or hole in the p-type. This creates a negative charge in the n-type (Fig. 5.1c). As a result, a space charge region is created as charges build up on either side of the junction leading to an electric field as electrons and holes are transported through the materials (Fig. 5.1d) and then are collected at the electrodes (Fig. 5.1e).[4] It should be noted that absorption of a photon can happen in both the p and n-type materials depending on their optical properties.

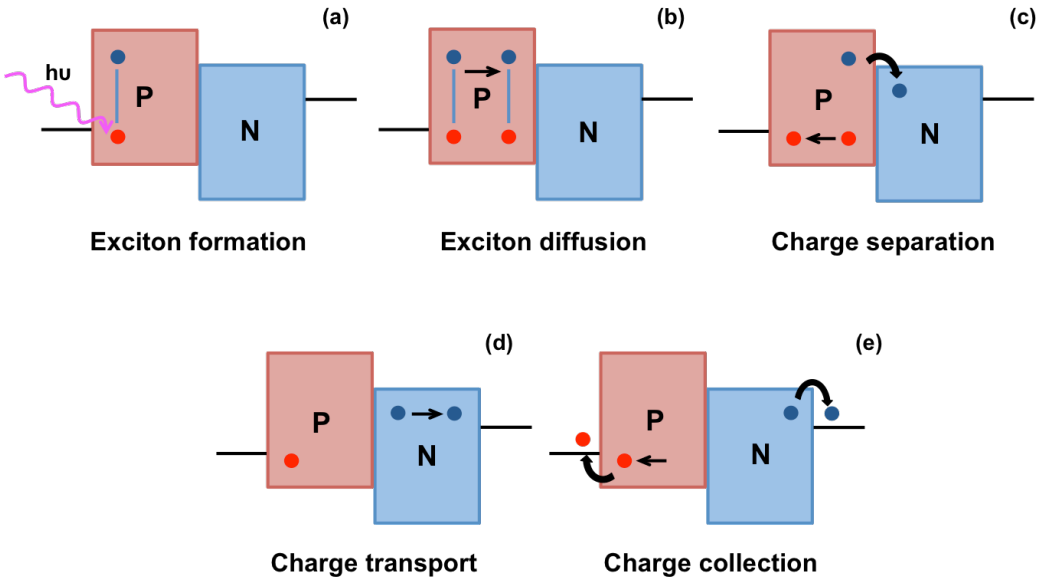

Figure 5.1 A simplified cartoon of a p-n heterojunction showing how a current is generated (a) exciton formation, (b) exciton diffusion, (c) charge separation, (d) charge transport and then (e) charge collection.

OPVs can be classified by what makes up these heterojunctions, the three most common being small molecules, polymers and inorganic-organic hybrids which are made up of polymers or dye molecules with an inorganic semi-conductor.[5] The two p and n materials need to be tuned so that this process can occur easily and efficiently. By tuning the band gap of the material, more light can be used to create the exciton and so light conversion increases. The conduction band in the acceptor material (n-type) needs to be lower than that of the donor material (p-type) so that electrons can cross the heterojunction.[6-8] Electron and holes need to be able to move easily through the materials to the electrodes without recombination and materials should be kept as thin films to give short electron diffusion pathways. Using small molecules and polymers that are conjugated allows electron transfer *via* alternating double bonds.[3, 9, 10]

These p-n heterojunctions can be further classified as flat-heterojunction solar cells, bulk-heterojunctions and dye sensitised solar cells (Fig. 5.2). Flat-heterojunctions are where the p and n materials exist in two separate layers that are deposited onto indium tin oxide (ITO) coated glass and topped with a metal electrode.[11] Bulk-heterojunction solar cells (BHJs) are where a blend of p and n materials is deposited onto the ITO coated glass and again topped with a metal electrode.[12, 13] Dye sensitized solar cells consist of a fluorine-doped tin oxide (FTO) coated with mesoporous inorganic semiconductor such as titanium dioxide and a single layer of dye molecules. This dye layer is then covered in another platinum coated FTO substrate and an electrolyte injected between the two substrates.[13, 14]

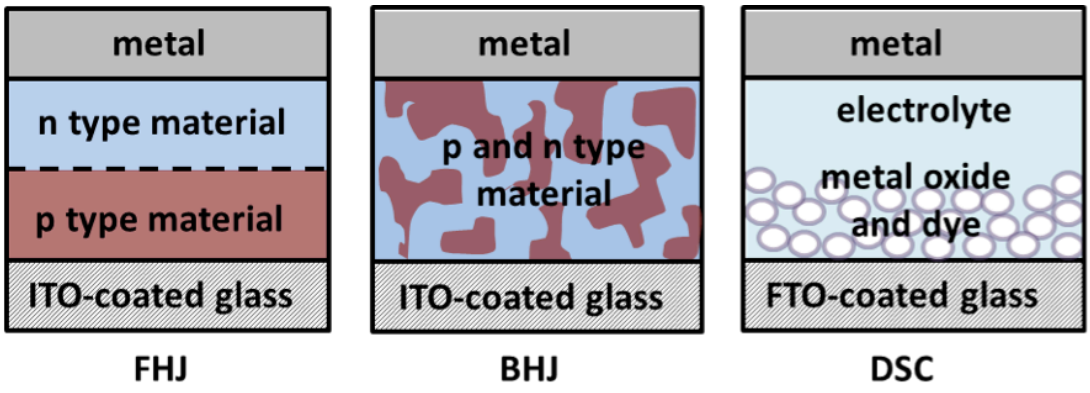

Figure 5.2 Different types of p-n heterojunctions.

Problems with these organic solar cells have been the photo- and chemical stability of the cells and overall efficiency to convert light.[10, 12, 15, 16] Combating these problems can be done a number of ways, such as by tailoring the small molecules or polymers used to make up the p and n-type materials for better charge transfer, charge transport and light harvesting. The use of self-assembly has been used to overcome some of these problems. Self-assembled structures have good HOMO/LUMO overlap due to π-stacking and so increased charge transfer and mobility.[17, 18] Dye based gelator molecules self-assembled so can increase light harvesting by tuning the molecules.[19-21] By using self-sorted systems of multicomponent p- and n-type type gelators, well defined π-stacked fibres could provide a well-defined bulk p-n heterojunction.[22, 23]

As PBIs form long fibres in solution and can gel at low pH as shown in Chapter 4, by using a mixed gelator system with something that could act as a p-type material, such as the stilbene based gelator in Chapter 3, then it could be possible to create a self-assembled p-n heterojunction hydrogel. This could be achieved whereby the two fibres meet in the entangled network.[22] By using GdL for a slow pH switch method with an n-type gelator and p-type gelator both with different pK_as,[24-26] it should be possible to form a multicomponent self-assembled bulk-heterojunction as shown in Chapter 3. These fibres could then interact in different ways. The two different fibres could wrap around each due to hydrophobicity of both fibres, creating a large surface area heterojunction (Fig. 5.3a). Alternatively, fibres could have little interaction with each and so would only have a p-n heterojunction where the two fibres meet (Fig. 5.3b).[22] It has been shown that having the donor and acceptor material too close to each other prevents long range order and efficient electron transfer through the material so the interactions in Fig. 5.3b would be more preferable.[23]

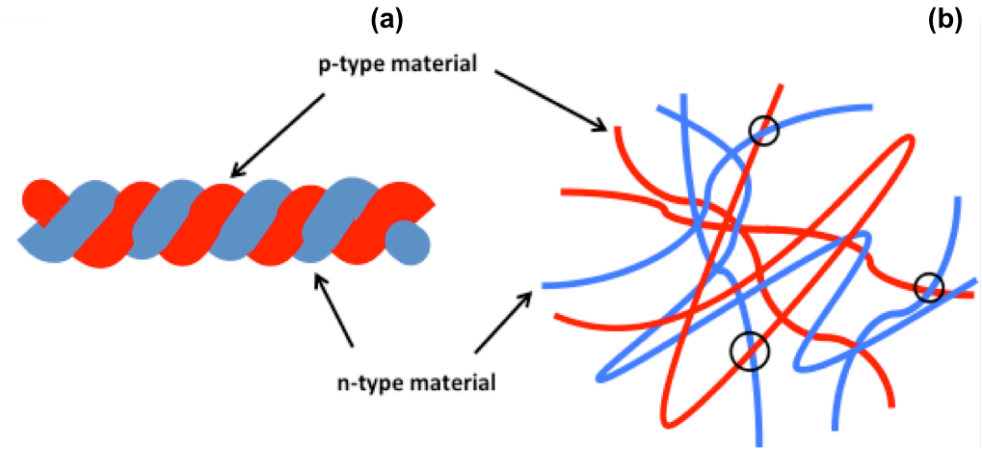

Figure 5.3 Cartoon showing the possible interactions of two self-assembled fibres, (a) shows lots of interaction and (b) little interaction. Where the two fibres meet is a possible p-n heterojunction.

There are many examples of PBIs being used within polymer based gels, but few using low molecular weight gelators (LMWGs).[9, 23, 27, 28] Polymer systems often have poor monodispersity and defects that affect the conducting properties.[23] By using self-assembled small molecules, it is possible to create more monodisperse fibres and good HOMO/LUMO overlap. The few examples using LMWGs are based on organogels, again due to the insolubility of the PBIs. Sugiyasu *et al.* used PBI and thiophene based gelators.[22] They used a heat-cool method to prepare a self-sorted organogel using chloroform. Another organogel based system used by Prasanthkumar et al. used PBI and trithienylenevinylene, again using a heat-cool method for self-assembly.[29] Lu and co-workers used 2,3-dimethyl-5,8-di(thiophen-2-yl)quinoxaline and aminocarbazole units to prepare a donor – acceptor organogelator systems.[30] These non perylene based gels were prepared using tetrahydrofuran (THF), (dimethylsulphoxide) DMSO and dimethylformamide (DMF) and a heat cool method, again demonstrating water solubility is an issue. To increase solubility, large alkyl chains are often used, but these are often attributed to poor performance due to them being insulating.[31] Martin and co-workers co-assembled a perylene bisimide and a π-extended tetrathiafulvalene into a hydrogel using opposing charges on the molecules.[32] They reported these co-assembled structures give long lived separated charge states due to supressed recombination by the structures.

By using a water-soluble PBI gelator (Chapter 4) (Fig. 5.4 (**1**)) and a stilbene-based gelator (Chapter 3) (Fig. 5.4 (**2**)), a pH switch method can be used to form hydrogels. This would allow self-assembly of the two molecules into individual fibres using the slow hydrolysis using GdL. As the two molecules have carboxylic acid groups to improve the solubility in water rather than long alkyl chains this should help improve the performance of the p-n heterojunctions.

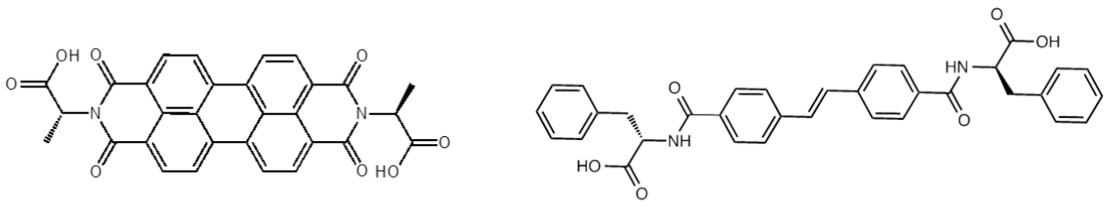

(1) **(2)**

Figure 5.4 Molecular structure of gelator **1** and **2**.

5. 2. Results and Discussion

5. 2. 1. Using hole scavengers

Hole scavengers can also be used to test whether the n-type material can be used within a p-n heterojunction. This is due to the hole scavenger being able to act as an electron donor, and therefore testing whether the n-type material is able to accept an electron which is a crucial property of the n-type material. Hole scavengers have also been used in PBI films to improve the performance of conductive films.[33] They have also been used to reduce the energy needed to cause a response from the sample due to better charge separated states.[34, 35] This would potentially allow less energetic wavelengths to be used, and so be visible light responsive rather than UV responsive, which is needed for OPVs. Hole scavengers work by providing electrons which fill the hole created by the exciton formation. These are most commonly used in H_2 evolution.[36, 37] This prevents recombination of the electron hole pair and so a greater conductivity.[36] It also allows a less energetic wavelength to be used as the exciton created does not to be as physical separated as the hole scavenger prevents recombination of the charges. If hole scavengers work to improve the wavelength

preference and performance of the n-type perylene film, then so would a p-type material.

A film of dried solution of **1** from Chapter 4 was prepared at 5 mg/mL and cast using a mask as described in Section 4. 3. They were prepared on glass small enough to fit a quartz cuvette that could be sealed with a rubber seal. Silver electrodes were placed either side of the thin film and copper wires were attached that were sufficiently long to fit out of the cuvette to be connected to a potentiostat. The sealed cuvette allows the films to be under an atmosphere of a hole scavenger. The film can then be irradiated with different wavelengths of light and the photoresponse measured. The response under air was measured for wavelengths from 365 nm to 628 nm. The film was then placed under an atmosphere of diethylamine, triethylamine, diethanolamine, or triethanolamine and the response under various wavelengths recorded. Different hole scavengers will have different effects on the systems due to the volatility of the hole scavenger, the ability to penetrate the film and the ease of the electron donation to the sample. Fig 5.5 shows the wavelength response under diethylamine (Fig. 5.5a), triethylamine (Fig. 5.5b), diethanolamine (Fig. 5.5c), and triethanolamine (Fig. 5.5d). The response in air was measured at different wavelengths and then the same sample was exposed to the hole scavenger and again response under different wavelength was measured. All samples under a hole scavenger atmosphere show the greatest response at 400 nm. They all allowed a greater current to pass across them, showing that the hole scavenger works.[33]

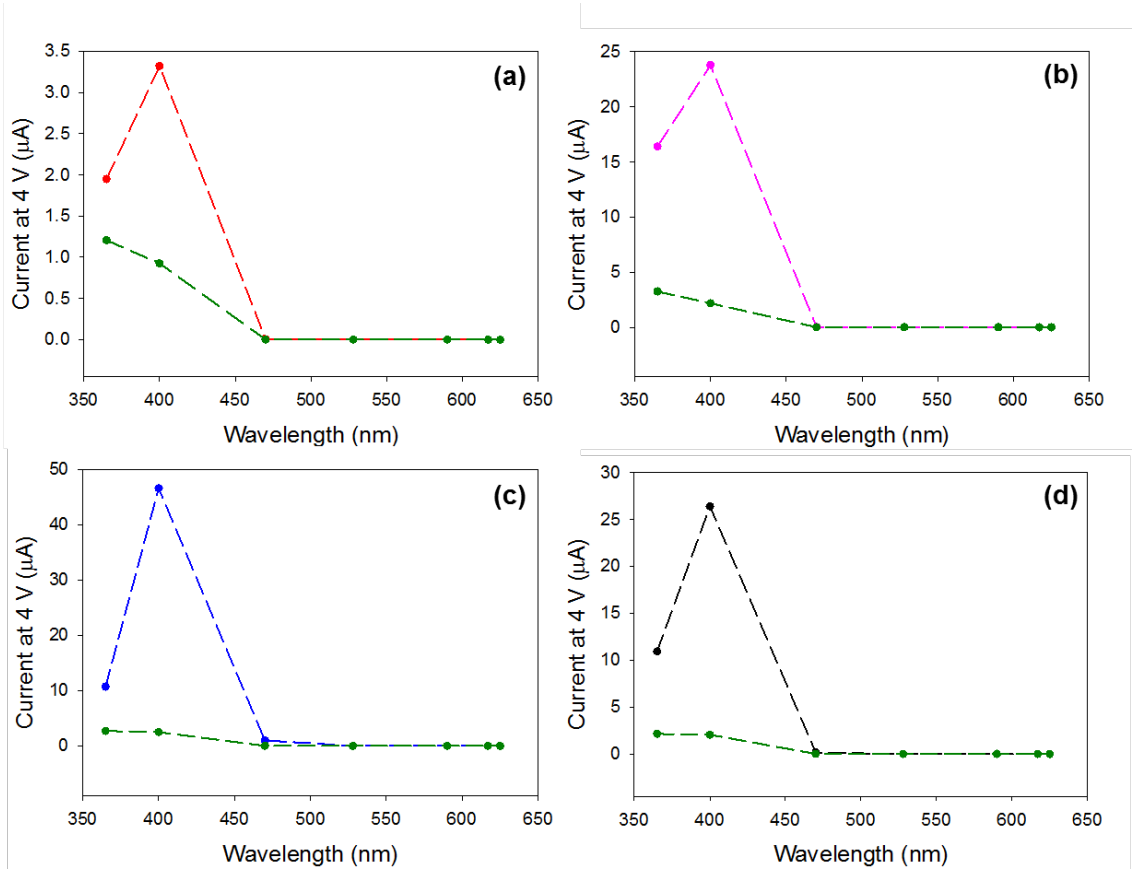

Figure 5.5 Wavelength response of dried solution of **1** under an atmosphere of different hole scavengers compared to the same sample in air (green data), (a) diethylamine, (b) triethylamine. (c) diethanolamine and (d) triethanolamine

When comparing all the data under an atmosphere of the different hole scavengers and in air (Fig. 5.6) the response under different wavelengths was then scaled by the number of photons and then normalised. Ethanolamine gave the greatest response at 400 nm than the other samples, compared to 325 nm under air. Diethanolamine also gives a response at 470 nm, whereas in air the sample gave no response at this wavelength. Triethylamine and triethanolamine gave similar responses to each other and diethylamine gave the smallest response at 400 nm. This is due to the different electron donating properties of the different hole scavengers.[37]

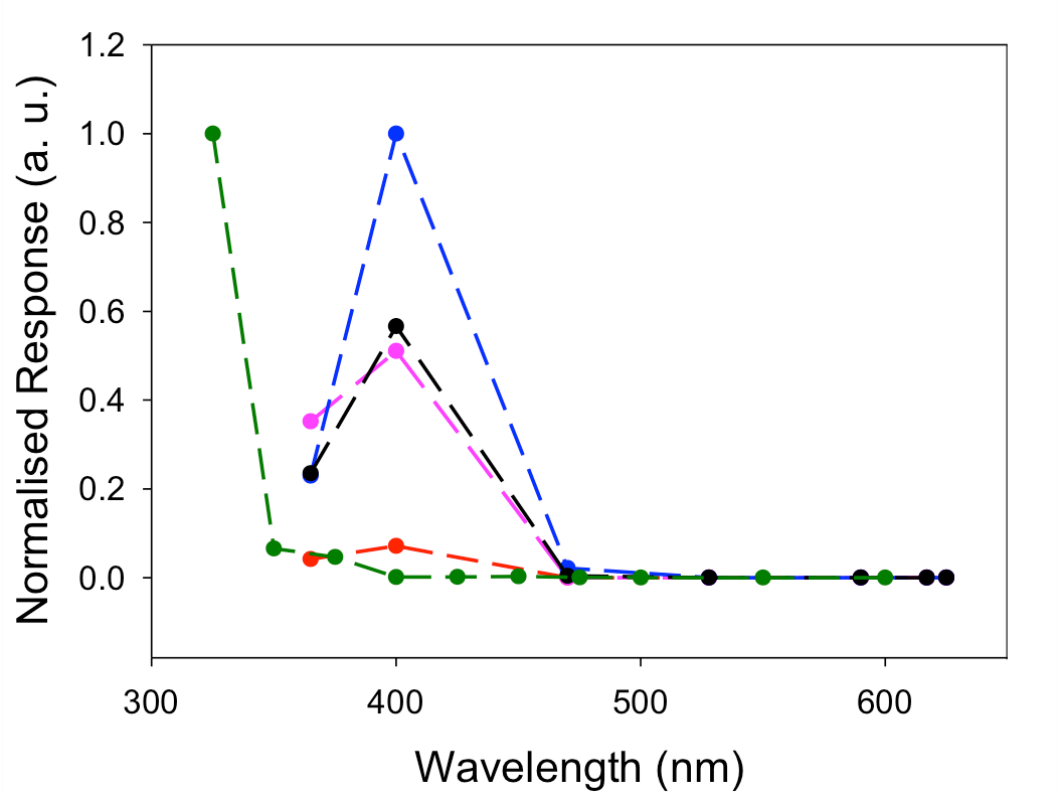

Figure 5.6 Wavelength response of dried solution of **1** under air (green data), diethylamine (red data), triethylamine (pink data) diethanolamine (blue data) and triethanolamine (black data). Data has been scaled to the number of protons and then normalised.

Unlike in Chapter 4, when comparing the wavelength response to the UV-Vis absorption of the dried solution of **1,** the data look more like what is expected (Fig. 5.7). The maximum absorption is more similar to the wavelength giving the largest response. This also is encouraging as it suggests that by using a p-type material, then it would possibly be able to donate an electron into the n-type and so creating a p-n heterojunction. The shift in wavelength preference into the visible region is promising for the use in OPVs.[14] By tailoring the p-type material, the wavelength preference may also be changed.

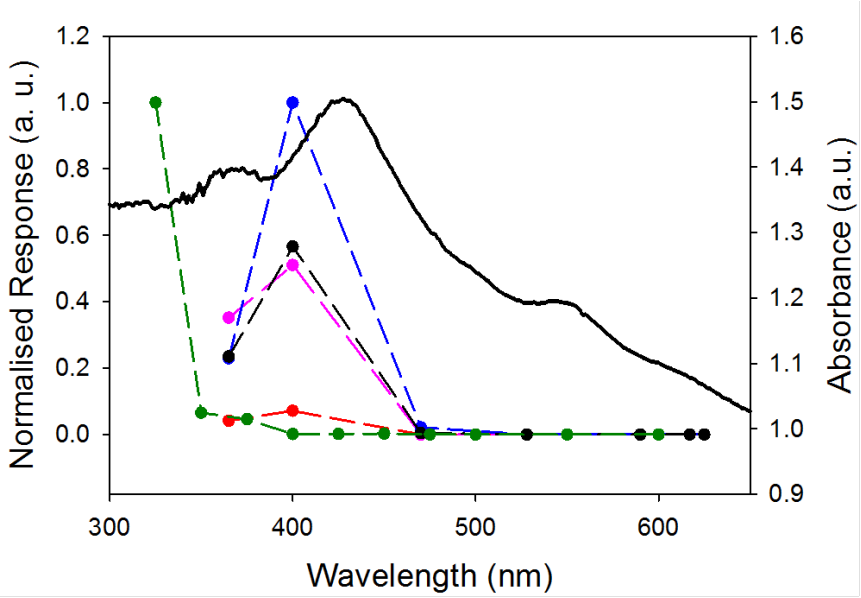

Figure 5.7 Dashed data is the wavelength response of dried solution of **1** under air (green data), diethylamine (red data), triethylamine (pink data) diethanolamine (blue data) and triethanolamine (black data). Solid data is UV-vis absorption spectra of a dried solution of **1**.

After the samples had been exposed under the hole scavenger atmosphere, they were placed back in air. The response under 365 nm was recorded again to check whether the films had been altered by the hole scavenger. Fig. 5.8 shows that the sample gives the same response before and after being placed under an atmosphere of the hole scavenger and then allowed to recover in air.

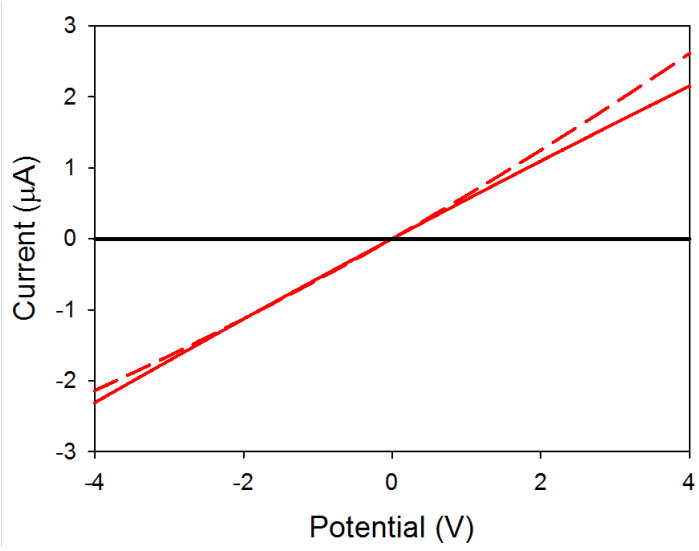

Figure 5.8 Response of a dried solution of **1** to 365 nm LED before the use of triethanolamine (solid red data), after triethanolamine and then allowed to recover in air (dashed red data) and in the dark (black data).

5. 2. 2. Self-sorted p and n-type gelator systems

A solution at high pH of **1** at 10 mg/mL was added in equal volume to a solution of **2** at 10 mg/mL to give a solution of **1** + **2** at a total concentration of 10 mg/mL (5 mg/mL of each gelator). 10 mg/mL of GdL was then added to slowly lower the pH to around 3.8 and left to gel overnight to give a self-supporting gel.[38] Gel-**1**,**2** showed properties typical of LMWGs, which broke at low strain and G′ and G″ being independent of frequency. The gel broke at a strain of 1.5 % strain (Fig. 5.9a). Gel-**1**,**2** had a G′ of ~9000 Pa and G″ of ~ 1200 Pa (Fig 5.9b). Repeat measurements gave similar results.

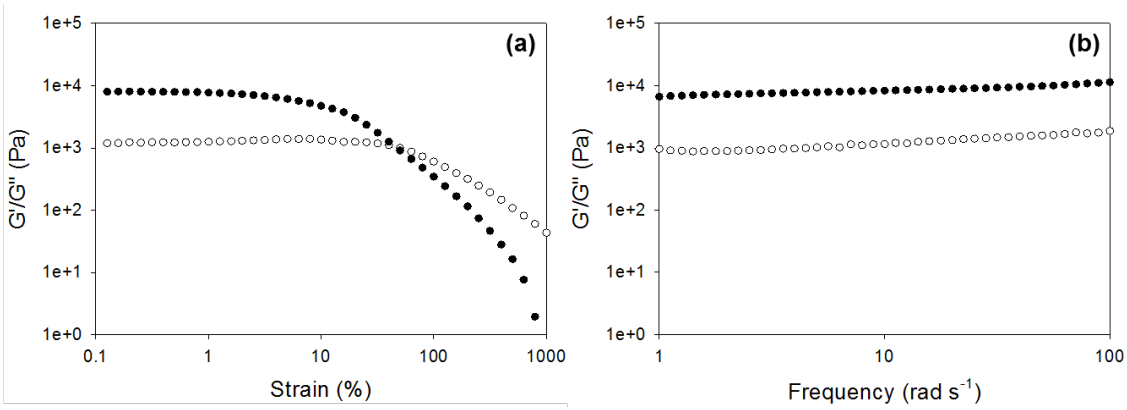

Figure 5.9 Rheology of gel **1**,**2** (a) strain sweep performed at 10 rad/s and (b) frequency sweep performed at 0.5 % strain. Both tests were performed at 25 °C. Full circles represent G' and open circles represent G".

The strength of gel-**1**,**2** differed from gel-**1** and gel-**2** (Fig. 5.10). Gel-**1**,**2** gave a gel with properties stronger than gel-**1** but weaker than gel-**2**. It might be expected that the gel would be dominated by the stronger network. It could also be that the gelators have co-assembled rather than self-assembled, but it is unclear just from rheological properties of the final gels.[24] This difference in gel strength does demonstrate that the networks are influenced by each other. Differences in gel properties may also be due to there being a total of 10 mg/mL rather than 5 mg/mL.

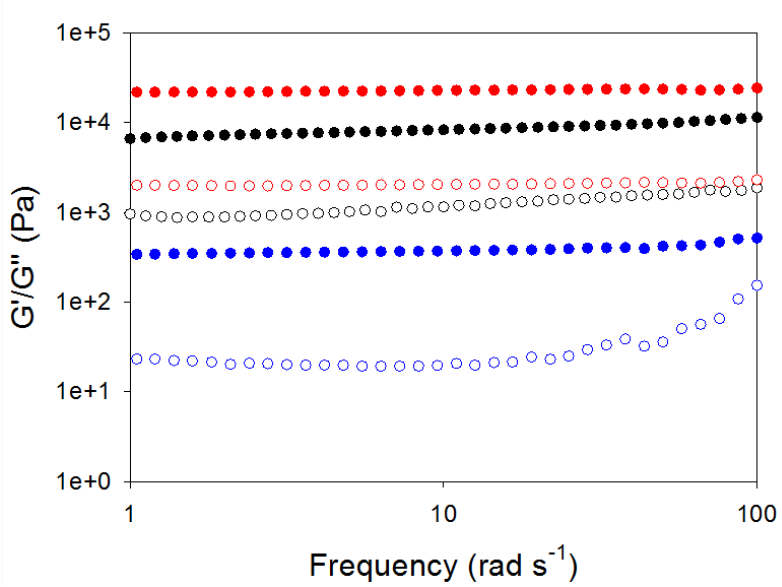

Figure 5.10 Frequency sweeps of gel-**1** (blue data), gel-**2** (red data) and gel-**1**,**2** (black data). Tests were performed at a strain of 0.5 % strain and at 25 °C. Full circles represent G' and open circles represent G".

When looking at all three of these gels under the SEM (images collected by Dr. T. McDonald, University of Liverpool) small differences could be seen in the multicomponent gel (Fig. 5.11a) compared to the single component gels (Fig. 5.11b and c). Gel-**1** seems to have thicker fibres (33 nm ± 10 nm) than gel-**2** (18 nm ± 5 nm). Whereas fibres with different thicknesses can be seen in gel-**1**,**2** (33 nm ± 3 nm and 15 nm ± 4 nm, shown by arrows in Fig. 5.11a), but this is not conclusive and could be due to drying effects.[39] This was also the case in Chapter 3.

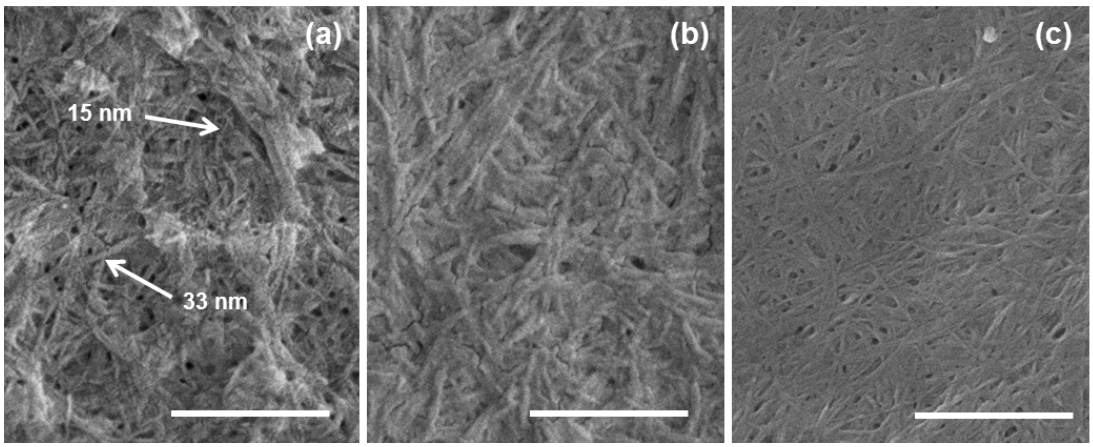

Figure 5.11 SEM images of (a) gel-**1**,**2**, (b) gel-**1** and (c) gel-**2**. Scale bars represent 500 nm.

To further investigate whether the two gelators were self-assembled or co-assembled, the same experiments were carried out as done in Chapter 3. Rheological time sweeps, change in pH and ^{1}H NMR were utilised to investigate this.

Rheology time sweeps and change in pH (Fig. 5.12) during gelation shows that at around 12 minutes there is an increase in G′ and G″ as the pH reaches 6.6. This corresponds to the first pK_a of gelator-**1** shown in Chapter 4. At this point, weak structures must be forming which are not strong enough to form a gel. G′ and G″ further increase when the pH reaches 5.8 after 35 minutes; this is the pK_a of gelator-**2** as shown in Chapter 3. At the point G′ is approximately an order of magnitude larger than G″ and so gelation is occurring.[40] This increase in rheological properties slows down and plateaus until 120 minutes when the pH has reached 5.4. There is then another increase in G′ and G″ until 700 minutes were it plateaus again. Fig. 5.12 shows there are multiple stages in the gelation of **1**,**2**. This could be due to the different gelators assembling at different times.

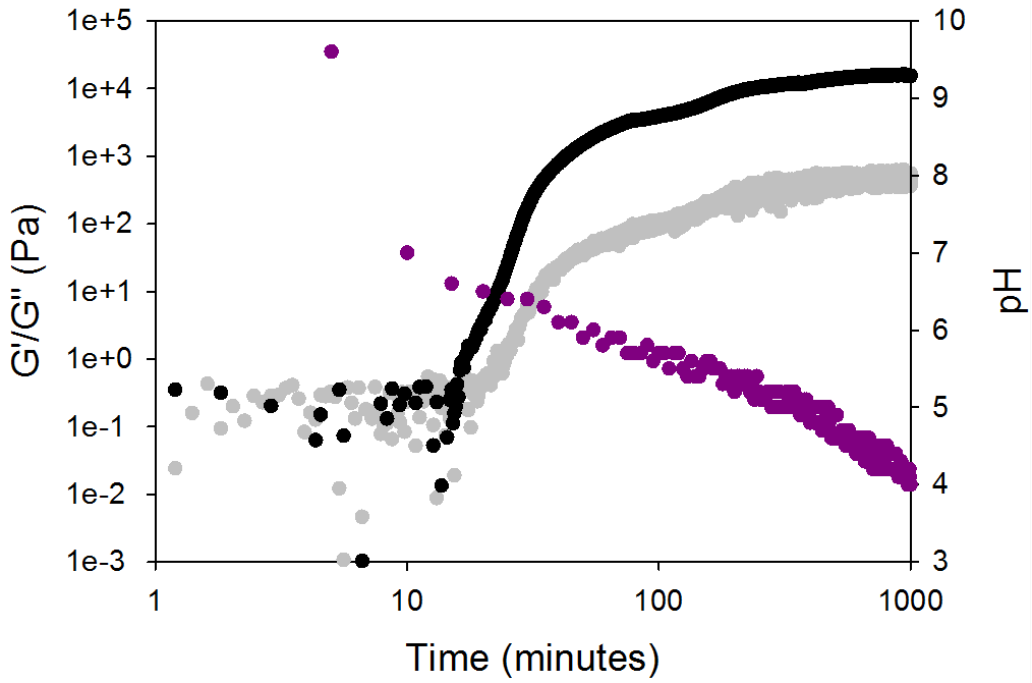

Figure 5.12 Monitoring G' (black data), G" (grey data) and pH (purple data) over time. Time sweeps were performed at a strain of 0.5 %, 10 rad/s and at 25 °C.

When comparing the development of G′ and G″ over time for the different systems (Fig. 5.13), the gelation of gel-**1**,**2** occurs quicker than for that of the single component gels. This may be due to there being more material in solution. The

gelation of gelator **1** is much slower than for **1**,**2** or **2**, but there is an increase in G′ and G″ in gel-**1**,**2** at the time gel-**1** is gelling. This could indicate there are self-sorted, but again this data is not conclusive by itself.

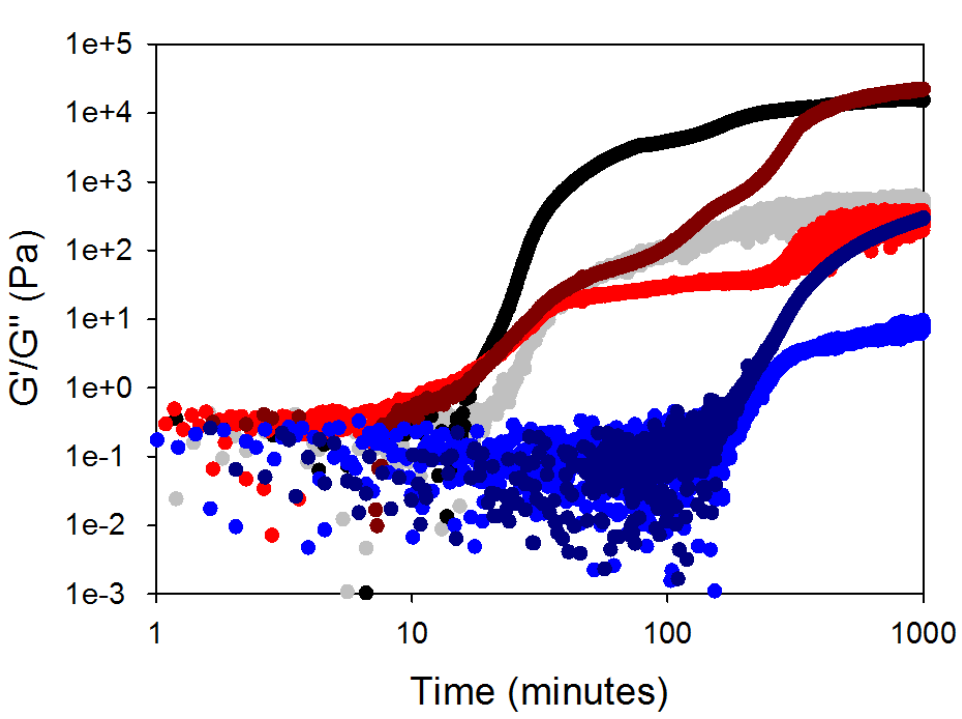

Figure 5.13 Comparison of change in G' and G" over time for gel-**1**,**2** (black data is G' and grey data is G"), gel-**1** (dark blue data is G' and light blue data is G") and gel-**2** (dark red data is G' and red data is G"). Time sweeps were performed at a strain of 0.5 %, 10 rad/s and at 25 °C.

A closer look at change in pH was carried out by small additions of 0.1 M HCl rather than GdL. When using GdL, a plateau is not often seen as the change is pH is quite slow and there is buffering from the systems. If the gelators are self-sorting, then separate plateaus should be seen for each of the gelators.[24] Fig. 5.14a shows that that there are three different plateaus at pH 6.6, 5.8 and 5.4 corresponding to the two pK_as of gelator **1**and the one pK_a for gelator **2**. This becomes more clear when time is plotted on a log scale (Fig. 5.14b).

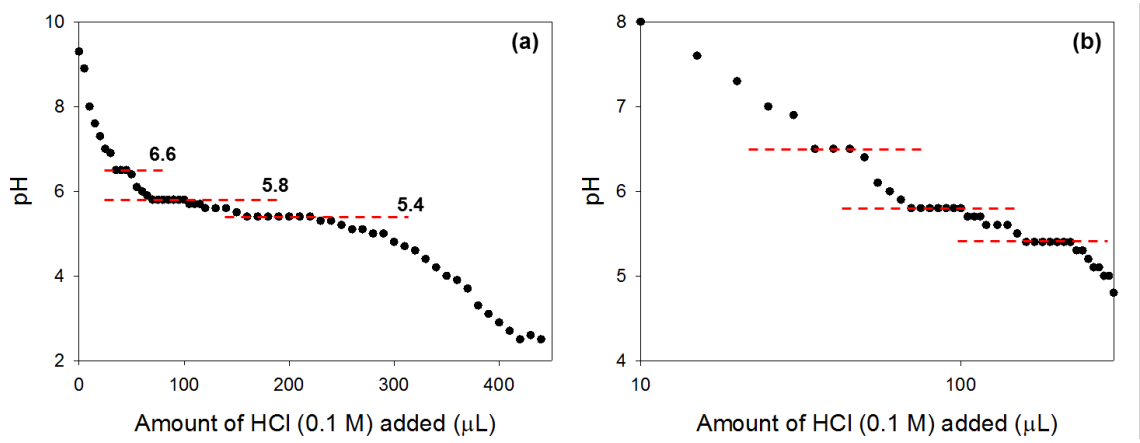

Figure 5.14 Change in pH upon the addition of 0.1 M HCl in a solution of **1**,**2** (a) on a linear scale and (b) on a log time scale. Dashed lines have been added to make the plateaus more clear.

When looking at gelation of gel-**1**,**2** using ^{1}H NMR, the disappearance of peaks corresponding to each gelator can be monitored, (data collected by Edward Eden, University of Liverpool) so the time at which each molecule gels and recorded and compared to pH. Gelator-**1** (Fig. 5.15a) starts to assemble at 40 minutes at a pH of around 6.5 (around the first pK_a of gelator-**1**) and the integral decreases slowly until 250 minutes at a pH of 5.4 (the second pK_a of gelator). After this point there is a larger decrease until 430 minutes and pH 5.0. After 430 minutes, there is a sharp decrease in the integral intensity and so gelation is happening. The integral has almost completely disappeared at 760 minutes and pH 4.3. For gelator-**2**, the intensity of its integral starts to sharply decrease after 75 minutes and at pH 5.8 (the pKa of gelator-**2**) as seen in Fig. 5.15b). The intensity continues to decrease until 420 minutes and pH 3.7.

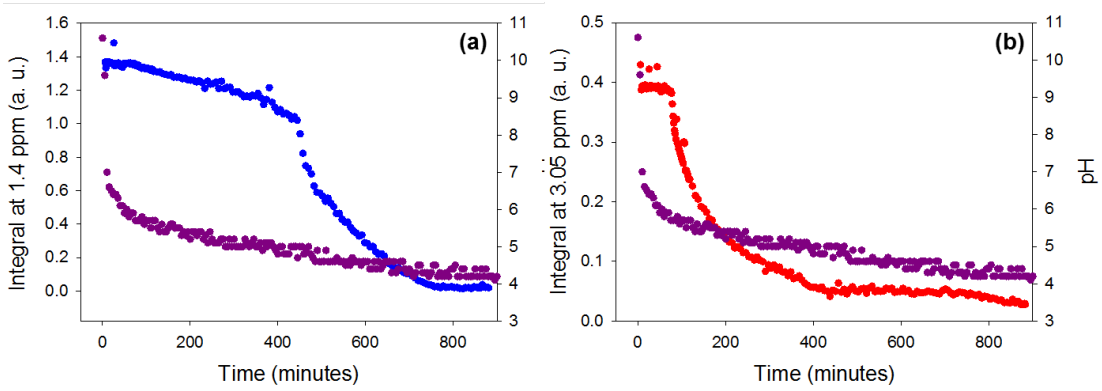

Figure 5.15 Change in intensity of peaks ^{1}H NMR during gelation of **1**,**2** of (a) CH_3 peak at 1.60 ppm from gelator-**1** (blue data) and (b) CH_2 at 3.05 ppm from gelator-**2** (red data) compared to change in pH during gelation of **1**,**2** (purple data).

When comparing the change in the integrals from each gelator on a log time scale (Fig. 5.16), it can be seen that gelator-**1** is starting to assemble before gelator-**2** but does not seem to be gelling. This could be due to the formation of some self-assembled structure which is still NMR visible. Gelator-**2** starts to gel at its pK_a before gelator-**1**. Gelator-**1** then starts to gel after gelator-**2**. This data again suggests that the molecules are self-sorting rather than co-assembling.[24]

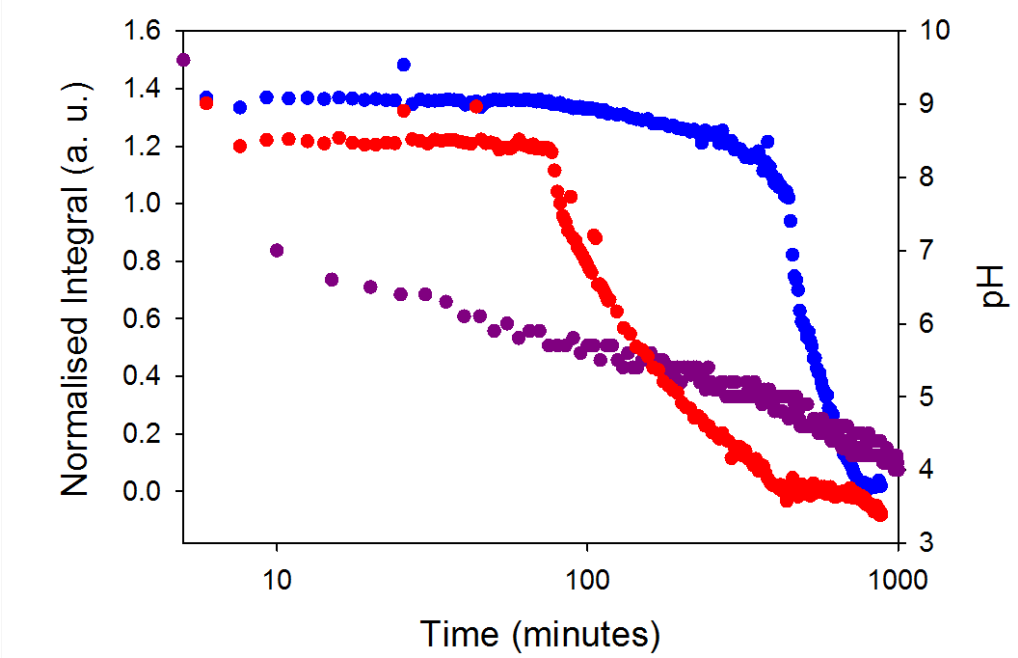

Figure 5.16 Change in intensity of peaks ^{1}H NMR during gelation of **1**,**2** of CH_3 peak at 1.60 ppm from gelator-**1** (blue data) and CH_2 at 3.05 ppm from gelator-**2** (red data) compared to change in pH during gelation of **1**,**2** (purple data).

The assembly of aggregates seen by ^{1}H NMR of gelator-**1** before gelation was occurring was further investigated by measuring the viscosity during gelation. If aggregates are formed, then the solution is expected to become more viscous. Fig. 5.17 shows the solution becomes more viscous before any G′ or G″ can be recorded and so before gelation has occurred. This means that structures are assembling before gelation has occurred and agrees with ^{1}H NMR data for gelator-**1**. This self-assembly could be the formation of the worm-like micelles as seen in Chapter 4. The viscosity overshoot at around 100 minutes also suggests that these systems could be shear aligned as in Chapter 4.

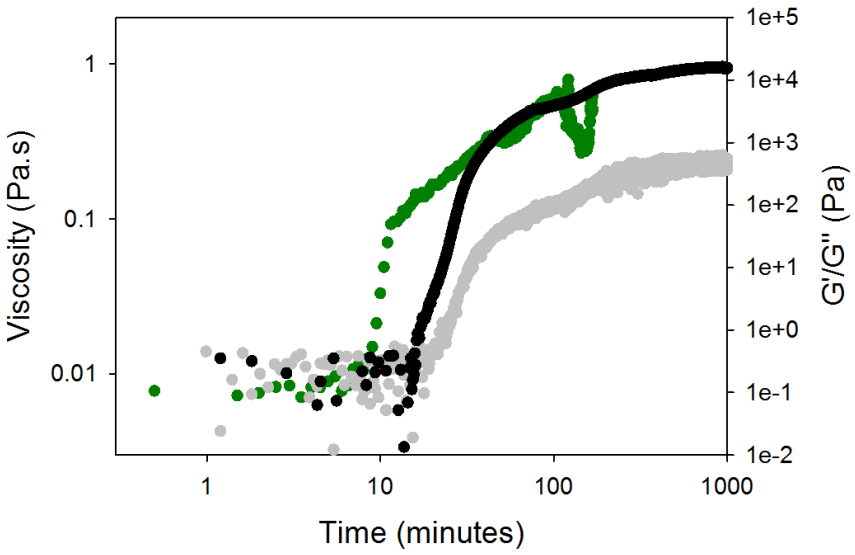

Figure 5.17 Comparison of change in G' and G" over time for gel-**1**,**2** (black data is G' and grey data is G" to change in viscosity (green data) whilst gelling. Time sweeps were performed at a strain of 0.5 %, 10 rad/s and at 25 °C. Viscosity measurements were performed at 5 s^{-1}.

To make sure that the increase in viscosity was due to gelator-**1** rather than gelator-**2** or a co-assembled aggregate of **1** and **2**, the single component systems' viscosity whilst gelling were also compared to the rheology (Fig. 5.18). Fig. 5.18a shows that gelator-**1** assembles before rheology can be measured. The viscosity data for gelator-**2** (Fig. 5.18b) shows an increase at the same point as as G′ and G″ do. This indicates that the increase in viscosity in the gel-**1**,**2** is due to gelator **1** assembling into aggregates before gelling.

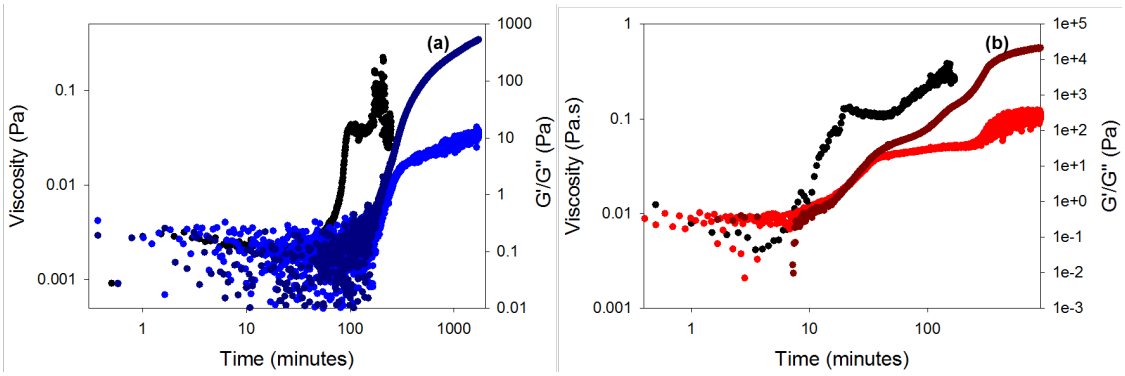

Figure 5.18 Comparison of change in G' and G" over time for gel-**1** (dark blue data is G' and light blue data is G") and gel-**2** (dark red data is G' and red data is G") to the increase in viscosity of the gelling system (black data). Time sweeps were performed at a strain of 0.5 %, 10 rad/s and at 25 °C. Viscosity measurements were performed at 5 s^{-1}.

When all this data is compared and looked at as a whole, it seems to be that the molecules are self-sorting rather than co-assembling (Fig. 5.19). Gelator-**1** assembles into aggregates first at its first pK_a. This does not cause an increase in rheological properties but does increase viscosity and makes them less visible in the ^{1}H NMR. Gelator-**2** assembles at its pK_a and viscosity increases and it rapidly disappears from the ^{1}H NMR as it gels. Gelator-**1** then starts the gel at its second pK_a and then disappears from the ^{1}H NMR and the rheology increases further.

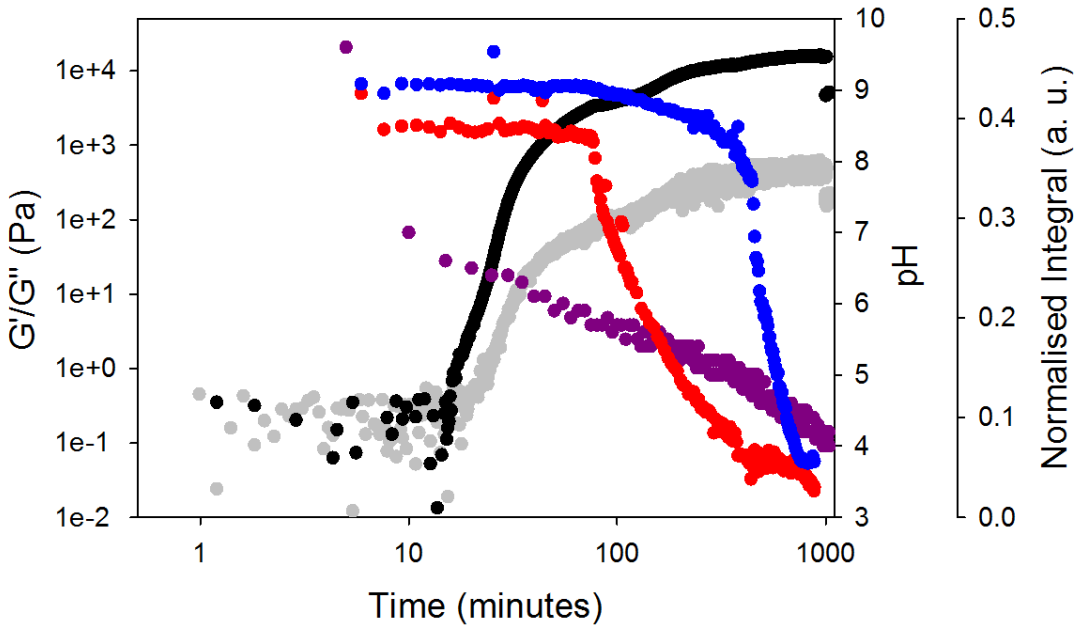

Figure 5.19 Monitoring gelation of **1**,**2** over time. Change in intensity of peaks ^{1}H NMR during gelation of **1**,**2** of CH_3 peak at 1.70 ppm from gelator-**1** (blue data) and CH_2 at 3.05 ppm from gelator-**2** (red data) compared to change in pH during gelation of **1**,**2** (purple data). Change in G' and G" over time for gel-**1**,**2** (black data is G' and grey data is G"), Time sweeps were performed at a strain of 0.5 %, 10 rad/s and at 25 °C.

5. 2. 3. Photoresponse of multi-component system

Solutions and gels were prepared at various ratios of gelator-**1** to gelator-**2**. These were prepared at 1:1, 4:3, 2:1 and 4:1 to see how much of gelator-**2** was needed to change the photoresponse of the films. Thin films were prepared using a mask as done in Section 5. 2. 1. and measured in air. Silver electrodes were placed either side of the sample and attached to a potentiostat using copper wires. The samples were

viewed under SEM (collected by Dr. T. McDonald, University of Liverpool). Fig. 5.11 shows that the gels mixed well and there is not obvious phase separation of the two networks. However for the solutions of **1**,**2**, phase separation occurred upon drying (Fig. 5.20). This shows that the dried solutions would be unsuitable for photoconductivity measurements as the two systems are not interpenetrating and so may not interact with one another.

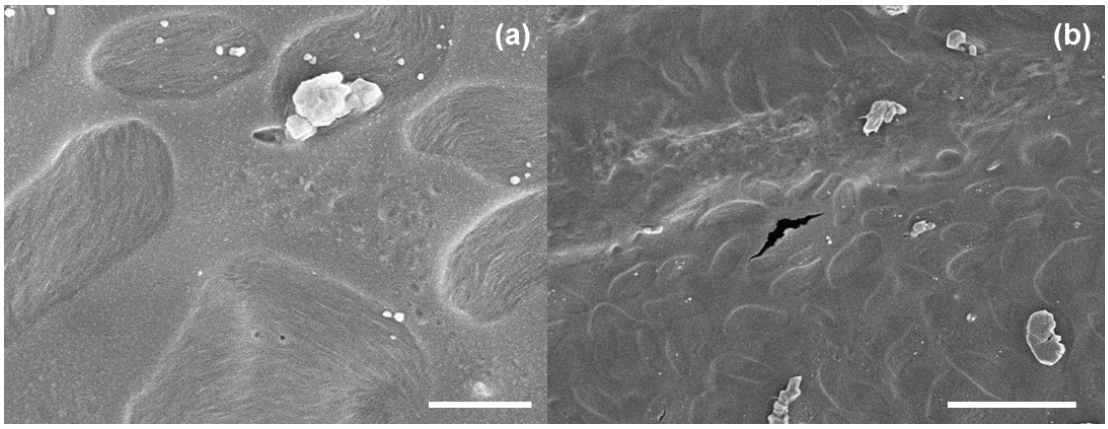

Figure 5.20 SEM images of a mixed solution of **1** and **2** (a) scale bar represents 1 μm and (b) scale bar represents 5 μm.

For each of the ratios of gelator-**1** to gelator-**2** xerogels, the photoresponses were measured (Fig. 5.21). All ratios of gelator-**1** to gelator-**2** now show the greatest response at 400 nm. Ratios of 4:3 and 4:1 show similar responses to each other (Fig. 5.21b and d). They show the greatest response at 400 nm and very little response at 365 nm and at 450 nm and negligible responses at the other wavelengths. The ratio of 2:1 (Fig. 5.21c) again showed the greatest response to 400 nm and a very small response to 365 nm. This sample also showed responses at 450 nm and 470 nm that were larger than the response at 365 nm. The ratio of 1:1 also showed little response at 365 nm and the largest response 400 nm (Fig. 5.21a) but, unlike the other ratios, there is a significant response at 450 nm and a smaller response at 470 nm. The ratio at 1:1 is more visible light responsive than the other ratio samples.

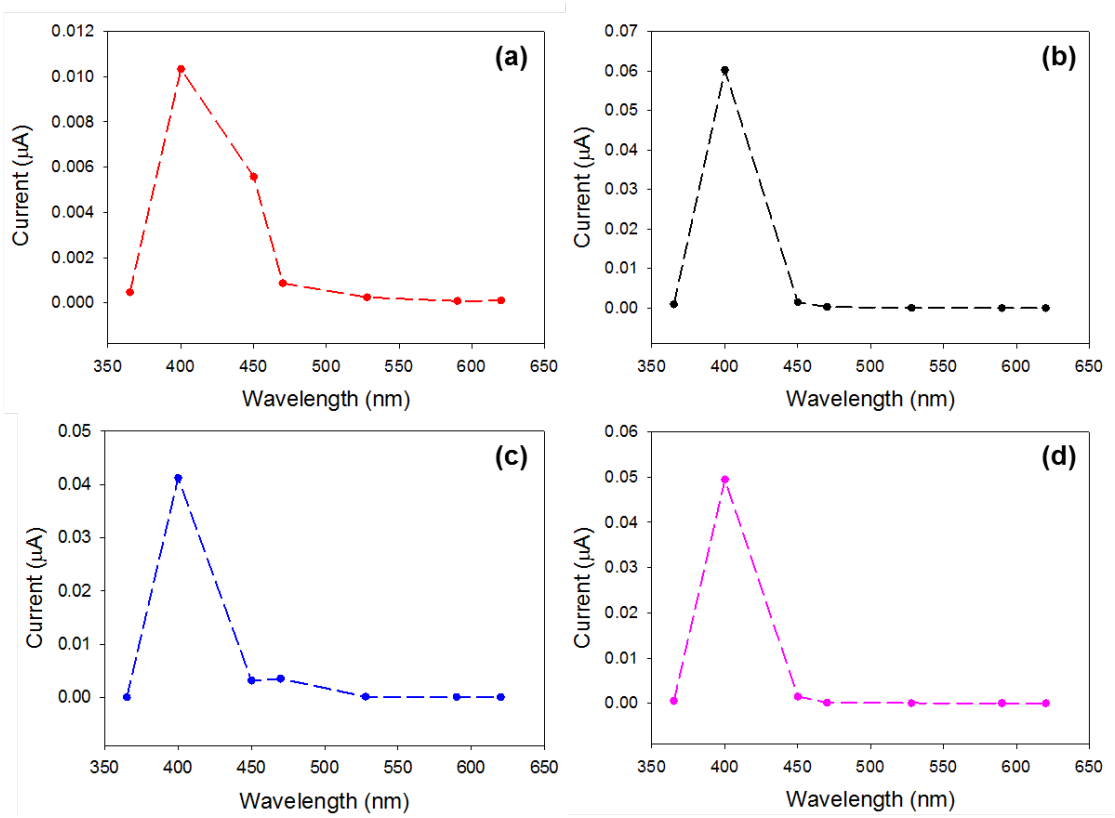

Figure 5.21 Wavelength response of gel-**1**,**2** at different ratios (a) 1:1, (b) 4:3, (c) 2:1 and (d) 4:1.

When comparing all the different ratios to the data for xerogel-**1** (Fig. 5.22), there is a clear change in behaviour of the samples when gelator-**2** is added. Samples with a ratio of 4:3, 2:1 and 4:1 of gelator-**1** to gelator-**2** all show a greater conductivity at 400 nm than the xerogel-**1** at 365 nm. The sample with a ratio of 1:1 of gelator-**1** to gelator-**2** showed the smallest photoresponse but the greatest response at 450 nm and 470 nm. All samples still showed no response to wavelengths ≥528 nm. The samples containing gelator-**2** all showed no response to 365 nm. This is very different to xerogel-**1**, which showed the greatest response to 365 nm. This change in behaviour is also different to when a hole scavenger is added (Fig. 5.5 in Section 5. 2. 1.) which increased the response at 365 nm and 400 nm. The lack of response to 365 nm for the mixed systems is due to gelator-**2** having an absorption peak in its UV-Vis spectrum at 365 nm (Fig. 3.9, Chapter 3) and therefore the light is being absorbed by gelator-**2** and not exciting gelator-**1**. This data shows that gelator-**2** is acting as a p-type material and donating an electron to gelator-**1** the n-type material, although more analysis of this process needs to be done, for example by transient adsorption spectroscopy.

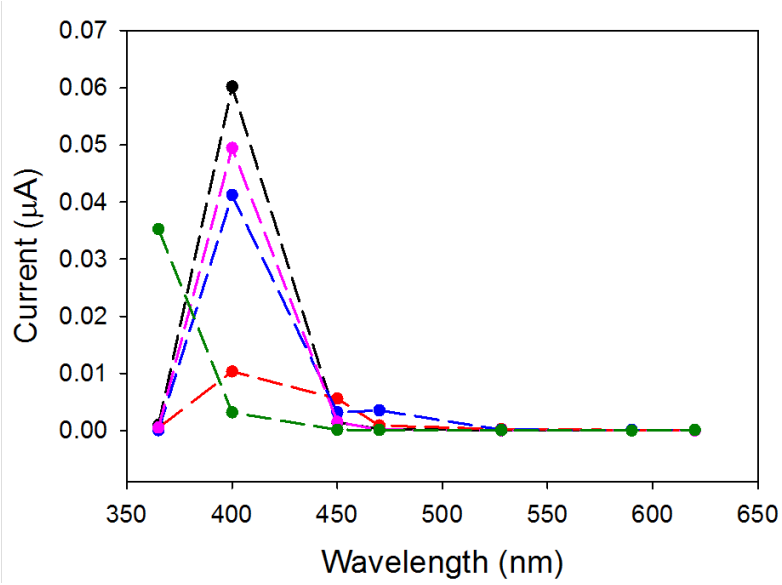

Figure 5.22 Comparison of wavelength response of mixed gelator system of **1** and **2** at a ratio of 1:1 (red data), 4:3 (black data), 2:1 (blue data) and 4:1 (pink data) to xerogel-**1** (green data).

With the mixed system with a ratio of 1:1 of gelator-**1** to gelator-**2** now being visible light responsive, the UV-Vis absorption spectra was recorded. The xerogel-**1**,**2** showed peaks for both gelator-**1** at 450-600 nm and gelator-**2** 300-380 nm (Fig. 5.23a). When xerogel-**1**,**2** was irradiated with 450 nm for 10 minutes, the UV-Vis spectrum showed a new peak at 710 nm (Fig. 5.23b). From Chapter 4 this is the attributed to the radical anion peak in gelator-**1**. Unlike xerogel-**1** this was not formed using 365 nm light but by using 450 nm, showing the photoconductivity is now caused by visible light.

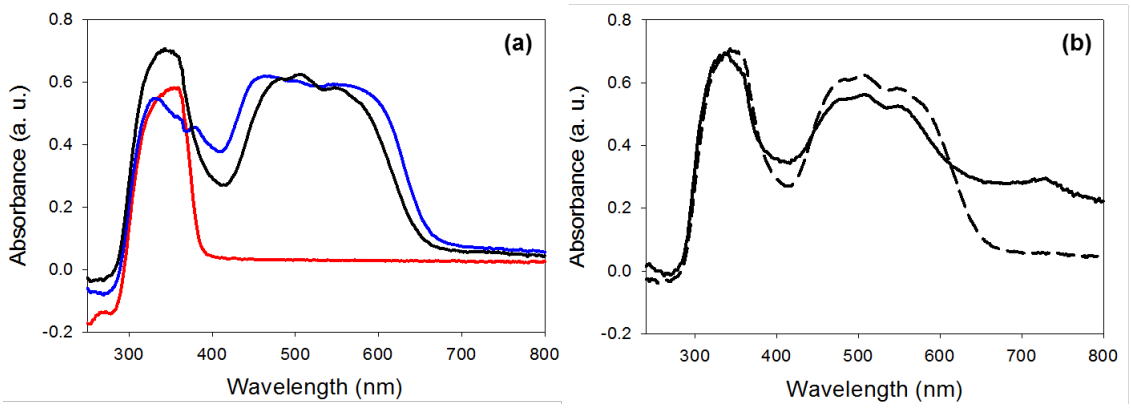

Figure 5.23 UV-Vis absorption spectra of (a) xerogel-**1**,**2** (black data) compared to xerogel-**1** (blue data) and xerogel-**2** (red data). (b) xerogel-**1**,**2** before irradiation (dashed data) and after irradiation with a 450 nm LED (solid data).

5. 3. Conclusions

Hole scavengers can be used to increase the photoconductivity of dried solution of **1** and also change the wavelength preference of the samples from 365 nm to 400 nm. A self-sorted multicomponent gel using a 1:1 mixture of gelator-**1** and gelator-**2** can be formed using the slow hydrolysis of GdL. This was confirmed using ^{1}H NMR, rheological time sweeps, change in pH and change in viscosity over time. The ratio of gelator of gelator-**1** and gelator-**2** was altered and the and dried down to give xerogels with a ratio of 1:1, 4:3, 2:1 and 4:1 of gelator-**1** to gelator-**2**. These mixed systems changed the wavelength preference again from 365 nm to 400 nm, this couls be due to now supressed charge recombination due to the presence of the p-type material. Furthermore, the presence of gelator-**2** made the xerogels unresponsive to 365 nm and more responsive to wavelengths of 450 nm and 470 nm. Xerogel-**1**,**2** at 1:1 forms the radical anion upon irradiation with 450 nm. These results show promising results that gelator-**1** and gelator-**2** can be used for bulk p-n heterojunctions, although more detailed analysis of the process needs to be carried out, for example by transient absorption spectroscopy.

5. 4. Experimental

Preparation of LMWG Solutions

Gelator-**1** was added to 2 mL of water with an equimolar amount of sodium hydroxide (0.1 M, aqueous) to a concentration of 5 mg/mL. The solution was stirred until all the gelator was dissolved. For gelator-**2**, two molar equivalents of sodium hydroxide were used.

Hydrogel Formation

A pH switch method was used to form the hydrogels. Solutions were prepared as above. The solution was then transferred to a vial containing a pre-weighed amount of glucono-δ-lactone (GdL) and shaken gently. The sample was then left to stand overnight to allow gelation to occur. For gelator-**1** and gelator-**2** 5 mg/mL of GdL was used.

For the different ratios of gelator-**1** to gelator-**2**, the amount of gelator-**1** was kept constant (10 mg/mL) and was added to different concentration of gelator-**2**. For 1:1, 1 mL of a 10 mg/mL solution of **1** was added to 1 mL of a 10 mg/mL solution of **2** to give a solution with a total concentration of 10 mg/mL. 10 mg/mL of GdL was then added. For a ratio of 4:3, 1 mL of a 10 mg/mL solution of **1** was added to 1 mL of a 8.75 mg/mL solution of **2** to give a solution with a total concentration of 10 mg/mL. 8.75 mg/mL of GdL was then added. For a ratio of 2:1, 1 mL of a 10 mg/mL solution of **1** was added to 1 mL of a 5 mg/mL solution of **2** to give a a solution with a total concentration of 7.5 mg/mL. 7.5 mg/mL of GdL was then added. For a ratio of 4:1, 1 mL of a 10 mg/mL solution of **1** was added to 1 mL of a 2.5 mg/mLsolution of **2** to give a solution with a total concentration of 6.25 mg/mL. 6.25 mg/mL of GdL was then added.

Preparation of samples on glass slides

Samples were prepared by dropping 20 μL of the LMWG solution on to a glass microscope slide and then left overnight to dry in air. Xerogel samples were prepared by forming gels as described above using GdL inside a 1 mL mould. Once gelation had occurred, the gel was then removed from the mould and approximately 0.05 mL of the gel was removed using a scalpel, placed onto a glass microscope slide and allowed to dry in air overnight. Two silver electrodes spaced 3 mm apart. The silver electrodes were made using silver paste which attached copper wires to the glass slide. The gel was then allowed to dry in air overnight to form a xerogels, shown in Fig. 4.50. Epoxy resin glue was placed over the silver electrodes. Again, this was left to dry overnight.

Photoresponse Measurements

Photoconductivity measurements were performed using an Autolab Potentiostat operating in a two electrode configuration in the absence of a supporting electrolyte. A 365 nm, 400nm, 450 nm, 470 nm, 528 nm, 590 nm and 628 nm LEDs (LedEngin Inc, LZ1-10U600) with a light source powered by a TTi QL564P power supply operating at 3.9 V were used as a light supply. Dark experiments were performed in an enclosure in air. Linear sweep measurements were recorded from -4 V to 4 V at a scan rate of 0.05 V/s and a preconditioning step at 0.002 V for 2 seconds. The

current recorded a 4 V was then used as a value for photoresponse value at each wavelength.

Hole Scavenger Measurements

Samples were prepared on glass slides and copper wires were attached as described above, but the glass was cut small enough to fit into a large quartz cuvette with a pathlength of 1.5 cm and a opening that could be sealed with a B24 rubber seal. The copper wires were pushed through the seal so that it could be attached to the potentiostat and the current measured. The wavelength response was measured in air for each of the wavelengths. 1 mL of the hole scavenger (diethylamine, triethylamine, diethanolamine or triethanolamine) was added to the bottom of the cuvette and the top was sealed. The atmosphere became saturated after 10 minutes and then the sample was irradiated with the LED for 5 minutes and then the current was measured. The sample was then allowed to recover in air for at least 24 hours before the measurement was repeated using a different wavelength.

UV-Vis absorption spectroscopy

Solid UV-Vis absorption data were obtained using a Shimadzu UV-2550 UV−Vis spectrophotometer running the UV Probe software, version 2.34. Spectra were measured either up to 700 or 1400 nm, with scan speed set to medium and using a slit width of 5.0 nm in transmission mode. Samples were prepared as previously mentioned with GdL. This gel was then transferred onto a glass slide and allowed to dry in air overnight in air to form a thin film xerogel.

Scanning Electron Microscopy

SEM images were obtained using a Hitachi S-4800 FE-SEM. Gels and solutions at high pH were deposited onto glass cover slips which were stuck onto aluminium SEM stubs and left to dry for 24 hours. The images were collected by Dr. Tom McDonald.

pH Measurements

A FC200 pH probe (HANNA instruments) with a 6 mm x 10 mm conical tip was used for pH measurements. The stated accuracy of the pH measurements is ±0.1. For pH measurement during gelation pH was recorded every minute until a gel was

formed. The temperature was maintained at 25 °C during the titration by using a circulating water bath. For "apparent" pK_a measurements pH were recorded after each addition of HCl and a stable value was reached. To prevent a gel forming, the solutions were gently stirred using a stirrer bar, so keeping the sample a liquid during the "titration" process. The plateaus of the pH indicates the two pK_a of this gelator. Temperature was kept at 25 °C during the titration by using a water bath.

Rheological Measurements

Dynamic rheological and viscosity measurements were performed using an Anton Paar Physica MCR101 and MCR301 rheometer. A cup and vane measuring system was used to perform frequency and strain sweeps. A cone and plate measuring system was used to perform viscosity measurements and gelling under shear. A parallel palate measuring system was used for time sweeps. For frequency and strain tests, 2 mL of the gels were prepared in 7 mL Sterilin vials and left for 24 hours at room temperature before measurements were performed. For viscosity measurements, samples were prepared at high pH as previously mentioned. For time sweeps and gelling under constant shear, the gels were prepared in a vial and transferred onto the bottom plate. All experiments were performed at 25 °C.

Frequency sweep: Frequency scans were performed from 1 rad/s to 100 rad/s under a strain of 0.5 %. The shear modulus (storage modulus (G′) and loss modulus (G″)) were read at 10 rad/s. These measurements were done within the viscoelastic region were G′ and G″ were independent of strain amplitude.

Strain sweep: Strain scans were performed from 0.1 % to 100 % with a frequency of 10 rad/s. The critical strain was quoted as the point that G′ starts to deviate for linearity and ultimately crosses over the G″, resulting in gel breakdown. From this data, a strain of 0.5 % used for measuring the frequency sweep was in the viscoelastic region.

Viscosity measurements: Viscosity measurements were performed using a 25 mm cone and plate. Around 0.2 mL solutions were transferred onto the plate for measurement after GdL was added. The viscosity of each solution was recorded under the rotation shear rate of 5 s^{-1} during gelation.

Time sweeps: Time sweeps were performed with a 50 mm plate with a plate gap of 0.8 mm. Tests were performed at an angular frequency of 10 rad s^{-1} and with a strain of 0.5 %. The top plate was flooded with mineral oil to prevent the sample from drying.

Nuclear Magnetic Resonance Spectroscopy

For monitoring gelation with time, NMR spectra were recorded on a Bruker DPX-400 spectrometer, operating at 400 MHz for ^{1}H NMR. The gelator solution was mixed with GdL and then directly loaded into an NMR tube to gel. During this time, NMR spectra were collected every 90 seconds for the first 70 acquisitions, and then typically every 5 minutes for the remaining experiment time (typically 14 hours total). The experiments were carried out at 25 °C. For the samples for NMR spectroscopy studies, ethanol (1 μL/mL) was added as an internal standard. A ^{1}H NMR spectrum of the solution was recorded prior to adding GdL to ensure that the ethanol present was accurately known relative to the dipeptides. This ensured any slight variations in weighing were taken into account for each sample. This data was collected by E. Eden, University of Liverpool.

5. 5. References

1. A. Bonfiglio and P. Cosseddu, in *Functional Supramolecular Architectures*, WILEY-VCH Verlag & Co. KGaA, 2011, Chapter 23, pp. 719-740.
2. H. W. Donghang Yan, Baoxun Du, *Introduction to Organic Semiconductor Heterojunctions*, John Wiley & Sons, 2010.
3. S. Günes, H. Neugebauer and N. S. Sariciftci, *Chem. Rev.*, 2007, **107**, 1324-1338.
4. V. Coropceanu, J. Cornil, D. A. da Silva Filho, Y. Olivier, R. Silbey and J.-L. Brédas, *Chem. Rev.*, 2007, **107**, 926-952.
5. A. C. Arias, M. Granström, D. S. Thomas, K. Petritsch and R. H. Friend, *Phys. Rev. B*, 1999, **60**, 1854-1860.
6. A. Ringk, W. S. Christian Roelofs, E. C. P. Smits, C. van der Marel, I. Salzmann, A. Neuhold, G. H. Gelinck, R. Resel, D. M. de Leeuw and P. Strohriegl, *Org. Electron.*, 2013, **14**, 1297-1304.
7. H. T. Black, H. Lin, F. Belanger-Gariepy and D. F. Perepichka, *Farad. Discuss.*, 2014, **174**, 297-312.
8. B. A. Jones, M. J. Ahrens, M.-H. Yoon, A. Facchetti, T. J. Marks and M. R. Wasielewski, *Angew. Chem. Int. Ed.*, 2004, **43**, 6363-6366.

9. D. Ray, C.-K. Liang, N. D. McClenaghan and D. M. Bassani, *Curr. Phys. Chem.*, 2011, **1**, 169-180.
10. B. Maennig, J. Drechsel, D. Gebeyehu, P. Simon, F. Kozlowski, A. Werner, F. Li, S. Grundmann, S. Sonntag, M. Koch, K. Leo, M. Pfeiffer, H. Hoppe, D. Meissner, N. S. Sariciftci, I. Riedel, V. Dyakonov and J. Parisi, *Appl. Phys. A*, 2004, **79**, 1-14.
11. M. Morkel, L. Weinhardt, B. Lohmüller, C. Heske, E. Umbach, W. Riedl, S. Zweigart and F. Karg, *Appl. Phys. Lett.*, 2001, **79**, 4482-4484.
12. Y. Huang, E. J. Kramer, A. J. Heeger and G. C. Bazan, *Chem. Rev.*, 2014, **114**, 7006-7043.
13. M. Grätzel, *J. Photochem. Photobio. C*, 2003, **4**, 145-153.
14. C. Li and H. Wonneberger, *Adv. Mater.*, 2012, **24**, 613-636.
15. M. Grätzel, *Acc. Chem. Res.*, 2009, **42**, 1788-1798.
16. M. A. Green, K. Emery, Y. Hishikawa, W. Warta and E. D. Dunlop, *Prog. Photovoltaics*, 2011, **19**, 565-572.
17. L. Chen, S. Revel, K. Morris and D. J. Adams, *Chem. Commun.*, 2010, **46**, 4267-4269.
18. C. Arantes, M. Scholz, R. Schmidt, V. Dehm, M. L. M. Rocco, A. Schöll, F. Reinert and F. Würthner, *Appl. Phys. A*, 2012, **108**, 629-637.
19. T. M. Figueira-Duarte and K. Müllen, *Chem. Rev.*, 2011, **111**, 7260-7314.
20. D. Görl, X. Zhang and F. Würthner, *Angew. Chem. Inter. Ed.*, 2012, **51**, 6328-6348.
21. P. Osswald and F. Würthner, *Chem. Eur. J.*, 2007, **13**, 7395-7409.
22. K. Sugiyasu, S.-i. Kawano, N. Fujita and S. Shinkai, *Chem. Mater.*, 2008, **20**, 2863-2865.
23. S. S. Babu, S. Prasanthkumar and A. Ajayaghosh, *Angew. Chem. Int. Ed.*, 2012, **51**, 1766-1776.
24. C. Colquhoun, E. R. Draper, E. G. B. Eden, B. N. Cattoz, K. L. Morris, L. Chen, T. O. McDonald, A. E. Terry, P. C. Griffiths, L. C. Serpell and D. J. Adams, *Nanoscale*, 2014, **6**, 13719-13725.
25. K. L. Morris, L. Chen, J. Raeburn, O. R. Sellick, P. Cotanda, A. Paul, P. C. Griffiths, S. M. King, R. K. O'Reilly, L. C. Serpell and D. J. Adams, *Nat. Commun.*, 2013, **4**, 1480.
26. J. Raeburn, B. Alston, J. Kroeger, T. O. McDonald, J. R. Howse, P. J. Cameron and D. J. Adams, *Mater. Horiz.*, 2014, **1**, 241-246.
27. T. Sagawa, S. Yoshikawa and H. Imahori, *J. Phys. Chem. Lett.*, 2010, **1**, 1020-1025.
28. F. Würthner, C. R. Saha-Möller, B. Fimmel, S. Ogi, P. Leowanawat and D. Schmidt, *Chem. Rev.*, 2015, DOI: 10.1021/acs.chemrev.5b00188.
29. S. Prasanthkumar, S. Ghosh, V. C. Nair, A. Saeki, S. Seki and A. Ajayaghosh, *Angew. Chem. Int. Ed.*, 2015, **54**, 946-950.
30. P. Xue, P. Wang, B. Yao, J. Sun, P. Gong, Z. Zhang, C. Qian and R. Lu, *ACS Appl. Mater. Interfaces*, 2014, **6**, 21426-21434.
31. E. Patrick and E. T. Mark, *Appl. Phys. Lett.*, 2011, **98**, 223305.
32. J. López-Andarias, M. J. Rodriguez, C. Atienza, J. L. López, T. Mikie, S. Casado, S. Seki, J. L. Carrascosa and N. Martín, *J. Am. Chem. Soc.*, 2015, **137**, 893-897.
33. Y. Che, A. Datar, X. Yang, T. Naddo, J. Zhao and L. Zang, *J. Am. Chem. Soc.*, 2007, **129**, 6354-6355.

CHAPTER 6

Summary, Conclusions and Future Work

In this Thesis, three different classes of photoresponsive gelators were synthesised, all of which gave very different responses when irradiated with a 365 nm LED. The gelation ability of these new gelators was reported; all gave stable self-supporting hydrogels with varying rheological strength. The effect of irradiation with light on the gels or xerogels, and in solution or as a dried solution was investigated.

In Chapter 2 a coumarin molecule was functionalised with diphenylalanine. This molecule gelled at a concentration of 5 mg/mL using glucuno-δ-lactone (GdL) as a pH gelation trigger. When irradiation with UV light was performed on the bulk gel, dimerisation of the coumarin molecules occurred making the gel opaque, this was monitored by UV-Vis absorption spectrsocopy. Unfortunately, light was unable to penetrate the gel very far and this resulted in the response in the bulk gel not being uniform and so the effect was unable to be measured rheologically. The coumarin was then gelled using an electrochemical method that used hydroquinone to lower the pH on the surface of an electrode. This allowed thin films of gel to be formed rather than bulk gelation. The rheological data showed this method of gelation to be very reproducible. The irradiation of UV light could be achieved uniformly throughout the thin film of gel. The rheological properties of the gel increased upon irradiation due to dimerisation of the coumarin molecules stiffening the fibres. Upon further irradiation, the gel strength continued to increase up till an hour where the increase stopped. This is a highly unusual behaviour. All previous gels described in the literature become weaker or become a solution on irradiation. This post-gelation strengthening of the gel could be used to pattern surfaces for cell growth and differentiation or be used to make microfluidic devices.

A gelator based on a stilbene molecule was reported in Chapter 3. This was functionalised on both sides with a phenylalanine. This molecule was able to form a gel at 5 mg/mL when the pH was lowered from around pH 10 to 3 using GdL. Again bulk irradiation of the gel with UV light proved difficult, so thinner gels needed to be prepared. Gelation of this molecule using electrochemical method was not possible, so gels were formed in moulds to make them thin enough to be uniformly exposed to the light source. When 365 nm LED was used to irradiate the gel, this caused the isomerisation of stilbene moiety from *trans* to *cis,* which led to destruction of the gel. A solution of the stilbene gelator at high pH was also irradiated to form the *cis*, and

when the pH was lowered it did not gel, meaning the *cis*-stilbene was a non-gelator whereas the *trans*-stilbene was. This gel-sol transition was then used to investigate mixed gelator systems. It was hypothesised that if a non-photoisomerisable gelator (a naphthalene-dipeptide) was gelled with the stilbene gelator, then whether the system was self-sorted or co-assembled could be investigated. The assembly of these molecules was monitored using rheology, ^{1}H NMR spectroscopy and changes in pH. From these data, it was concluded that the systems were self-sorted. This is the first time that the presence of two interpenetrated networks has been conclusively proven. This was further shown by removing the stilbene gelator from the system with UV light, leaving the naphthalene gel intact. The rheological data showed that the system with the stilbene removed had the same properties as that of the naphthalene gel by itself, demonstrating the gelation of the stilbene had little influence on the naphthalene gelation. By using a photo mask, parts of the gel could have the stilbene gelator selectively removed. This could be useful in the fabrication of p-n heterojunction to give well-defined interfaces of different materials.

In Chapter 4, perylene bisimide (PBI) gels were formed using a pH switch method. Four different gelators were made with different gel properties, with the phenylalanine functionalised PBI being the most different from the other three. It was also shown that at high pH the gelators were already self-assembled into worm-like micelles. The photoconductive properties of both dried solution and xerogels were then investigated to see whether self-assembly *via* gelation changed the properties of the thin films. The PBI functionalised with phenylalanine did not form uniform films when dried down and so could not be used for this study. It was found that the thin films of both dried solution and xerogels were photoconductive upon irradiation with light <400 nm. This differs to that reported in the literature, and more work on this wavelength needs to be investigated by transient absorption spectroscopy (TAS). The conductivity of these samples arises from the formation of a radical anion, which can be seen by a change in colour and by new peaks in the UV-Vis absorption spectra. This radical anion was stable in air for many hours. The dried solutions were more conductive than the xerogels with the PBI functionalised with alanine being the most conductive. Alignment of the solutions was then investigated as a reason why the solutions were more conductive. It was found that drop casting, magnetic alignment and shear alignment were able to align the

solutions giving them a directional dependence in the conductivity, with magnetic alignment being the best but not the most reproducible. Gels could also be aligned using shear, again giving them a directional dependence in conductivity that could not be achieved when drop cast. When comparing shear-aligned xerogels to shear-aligned solutions, the dried solution still gave a greater conductivity, showing that alignment was not the reason for the difference. Therefore, more work needs to be carried out on these two systems to determine why there are differences in the conductivity. Small angle neutron scattering (SANS) could be used to tell whether the primary fibres of the worm-like micelles are different to that of the gelled fibres, and whether fibre thickness has an effect. The absolute conductivity of these different samples also needs to be carried out using a three-point probe to remove any variable such as sample thickness from the measurements.

In Chapter 5, the perylene films were investigated further as the use as n-type materials and whether the wavelength dependence could be altered. Four different hole scavengers were used which increased the conductivity of all samples by different amounts, depending on which hole scavenger was used. The use of a hole scavenger also changed the wavelength preference from 365 nm to 400 nm. With the use of triethanolamine as a hole scavenger, there was a photoresponse under 470 nm light. These results showed that an electron donating p-type material could be used in the system that would allow a less energetic wavelength to cause a response from the sample. This change in wavelength preference change is more useful when the sample is used in solar cell applications. When mixed with the p-type stilbene gelator from Chapter 3, a mixed p-n system could be made. The assembly of the mixed-gelator was again investigated using ^{1}H NMR spectroscopy, rheology and change in pH. It suggested that the systems were self-sorted rather than co-assembled, but further work could be carried out to determine this conclusively. For example, fluorescence microscope techniques such as confocal microscopy could be used to see whether the fibres were made only of PBIs or stilbenes. Time-resolved fluorescence could also be used to monitor the fluorescence lifetimes of the two molecules to determine whether they are co-assembled. SANS could also be used to determine whether the fibres are self-sorted or co-assembled if the fibres are different enough to each other. The introduction of the p-type materials changed the wavelength preference of the thin films to 400 nm, suggesting that the stilbene has an

effect on the system. Whether these films are acting as p-n heterojunctions could be further investigated using TAS, but the first results seem promising for the use in p-n heterojunction device.

In conclusion, we have used light to induce a range of responses in low molecular weight gels. Many of the described behaviours are novel or are beyond the state of the art and demonstrate that we have a high degree of control and understanding over our systems. The ability to align gels for example is necessary if we are to be able to effectively use these materials for optoelectronic applications. Whilst others have suggested this, few have been able to show how this could be achieved. Future work will therefore exploit this understanding for the use in p-n heterojunctions.